

Determinants of Reperfusion Injury in the Diabetic Heart

Thesis submitted by
Idris John Harding

For the degree of
Doctor of Philosophy
Institute of Cardiovascular Sciences
University College London (UCL)

The Hatter Cardiovascular Institute
Institute of Cardiovascular Sciences
University College London
67 Chenies Mews
London WC1E 6HX

September 2019

DECLARATION

I, Idris John Harding confirm that the work presented in this thesis is my own. Where information has been derived from other sources, I confirm that this has been indicated in the thesis.

Idris John Harding

ABSTRACT

Ischaemic cardiac injury is a leading cause of morbidity and mortality. Recent advances in management of acute cardiac ischaemia have seen early mortality fall and increased survival of myocardial infarction. An increase in prevalence of left ventricular systolic dysfunction and congestive cardiac failure have accompanied increased survival of acute events. Chronic congestive cardiac failure confers high morbidity and late mortality from ischaemic disease. Given the correlation between infarct volume and likelihood of post-infarct heart failure, reduction of infarct size has emerged as an important therapeutic target.

A range of experimental treatments collectively termed “preconditioning” have been shown to reduce vulnerability to experimental myocardial infarction in animals but reproducing these results in human cohorts suffering spontaneous myocardial infarction has proved challenging. One of the explanations advanced for lack of translation has been the high prevalence of diabetes in the human population undergoing myocardial infarction, and a direct interaction between the diabetic state and preconditioning treatments has been proposed. Here, I investigate if animal model of diabetes can be used to predict and overcome failure of preconditioning treatments in the diabetic population.

Using a rat model of type 2 diabetes, alongside rat strains at lower risk of developing diabetes, the impact of blood insulin content and blood glucose content on susceptibility to myocardial infarction and amelioration by preconditioning treatments was quantified. Experimental infarction was induced by temporary coronary occlusion in an *ex vivo* Langendorff preparation; both direct and remote ischaemic preconditioning treatments were studied.

A raised threshold for successful preconditioning in diabetes was confirmed for direct ischaemic preconditioning and identified for the first time in remote ischaemic preconditioning. Relationships between myocardial exposure to glucose and extent of ischaemia-reperfusion injury were described in both diabetic and non-diabetic animals, and the damage attributable to high glucose exposure in non-diabetic hearts rescued by partial blockade of cellular glucose uptake.

IMPACT STATEMENT

Diabetes is a major global health challenge, and diabetic patients continue to experience poor outcomes from diseases for which we have effective treatments in non-diabetic patients. The work reported here builds on earlier findings and confirms that diabetes impairs outcomes in myocardial infarction via inhibition of innate protective mechanisms. After some high-profile setbacks and negative clinical trials, this reaffirms the importance of reperfusion injury in the natural history of ischaemic and diabetic disease.

My work on glucose-mediated exacerbation of reperfusion injury and the pharmacological amelioration of this has already formed the basis of a successful grant application to further investigate this relationship, and a PhD student is already working on the project.

The wider impact unfolding over the years is potentially large, as non-diabetic hyperglycaemia affects large numbers of patients undergoing myocardial infarction and confers significant morbidity. It is currently undertreated and not well understood. International guidelines on treatment, for example, do not distinguish between diabetic and non-diabetic hyperglycaemia but our findings suggest a critical difference between the two. The only intervention subject to large scale clinical trials thus far is insulin, whereas our findings suggest that drugs with exact opposite action on the myocardium may in fact be beneficial.

In the context of a rapidly expanding portfolio of available hypoglycaemic treatments, this work adds to the rationale for trials of acute administration of the novel hypoglycaemics to minimise acute harm from MI, and ultimately to revisit clinical practise and guidelines in this complex area.

On a personal level, the practical and fine motor skills I developed during the experimental work here have undoubtedly helped me in my chosen career as an interventional cardiac electrophysiologist. The analytical skills I employed have helped me assimilate medical and research data in my clinical practise. The understanding of harm conferred by diabetes in ischaemic disease has helped me become a better general cardiologist, more able to address this important problem in an increasingly comorbid patient population.

ACKNOWLEDGEMENTS

I would like to thank my colleagues at the Hatter Cardiovascular Institute, particularly Dr Andrew Hall and Dr Hannah Whittington, for teaching me many of the laboratory techniques involved in this project. Dr Jose Vincencio, Dr Rachel Mogg, Dr Siavash Beikoghli Kalkhoran and Dr Niall Burke also provided important support. A special mention should go to both Dr Rob Bell, my secondary supervisor, who has done his utmost to keep this unwieldy project on track, and to my contemporaries Dr Jack Pickard and Dr Dan Bromage (who both have graduated long since), whose insights helped me cut through the large and often contradictory evidence-base in the area of ischaemia-reperfusion injury.

I am of course extremely grateful to Professor Yellon for the opportunity to undertake this project and for his support in seeing it to a conclusion.

PEER-REVIEWED PUBLICATIONS ARISING FROM THIS WORK

Harding I, Yellon DM, Bell RM. Pharmacological cardioprotection in diabetes. Review. *Diabetes Management*. March 2015.

Whittington HJ, **Harding I**, Stephenson CIM, Bell R, Hausenloy DJ, Mocanu MM, Yellon DM. Cardioprotection in the aging diabetic heart: the loss of protective Akt signalling. *Cardiovasc Res*. 2013 May 30.

ABSTRACTS ARISING FROM THIS WORK

Bell RM, Jasem H, **Harding I**, Almalki A, Arjun S, Yellon DM. High glucose and myocardial ischaemia/reperfusion injury: the role of the sodium/glucose transporter, SGLT1.

Oral presentation at BSCR annual meeting, London, 2016

Harding I, O'Keefe M, Bell RM, Yellon DM. 'Hyperglycaemic exacerbation of myocardial ischaemia/reperfusion injury is mitigated by SGLT inhibition.'

Poster at ESC Congress, London, 2015

Harding I, Bell RM, Yellon DM. 'Efficacy of remote ischaemic preconditioning in diabetic rats.'

Poster at Frontiers in Cardiovascular Biology annual meeting, Barcelona, 2014

Harding I, Whittington HJ, Bell RM, Mocanu MM, Yellon DM. 'Cardioprotection in the aging, diabetic heart: the loss of protective Akt signalling.'

Poster at ESC Working Group on Cellular Biology of the Heart, Varenna, 2013

CONTENTS

Declaration.....	3
Abstract.....	5
Impact statement	8
Acknowledgements.....	10
Peer-reviewed publications arising from this work	12
Abstracts arising from this work	12
Contents	14
Table of figures	18
Table of tables	22
Table of abbreviations.....	24
1. Introduction	29
1.1 Scope	30
1.2 Myocardial ischaemia-reperfusion injury	31
1.3 Diabetes and the myocardium.....	52
1.4 Hyperglycaemia and the myocardium	64
1.5 Research objectives.....	87
2. General methods.....	89
2.1 Introduction	90
2.2 Animals	90
2.3 Diabetes phenotyping.....	94
2.4 Animal morphometry	97

2.5	Ischaemia-reperfusion in the intact heart.....	97
2.6	Modelling remote ischaemic preconditioning.....	115
2.7	Western blot quantification of kinase activation.....	119
2.8	Hypoxia-reoxygenation of isolated cardiomyocytes.....	127
2.9	ROS production on exposure to high glucose	132
2.10	Mitochondrial studies.....	133
3.	Diabetes In UCL's Goto-Kakizaki rat colony.....	141
3.1	Aims and hypotheses	142
3.2	Experimental protocols	143
3.3	Results	143
3.4	Summary of UCL GKR phenotyping studies	164
4.	Inhibition of preconditioning in a rat model of established diabetes.....	165
4.1	Aims and hypotheses	166
4.2	Experimental Protocols.....	166
4.3	Results	166
4.4	Summary of preconditioning studies	195
5.	Glucotoxicity, diabetes and myocardial reperfusion injury.....	197
5.1	Aims and hypotheses	198
5.2	Experimental protocols	199
5.3	Results	199
5.4	Summary of reperfusion glucotoxicity studies	218
6.	Discussions	221

6.1	Structure of discussions	222
6.2	AIM 1: establish and verify models of infarction and direct and remote preconditioning	222
6.3	AIM 2: verify the UCL GK rat as a relevant model of diabetes in which to study myocardial IRI.....	225
6.4	AIM 3: demonstrate impaired cardioprotection in the diabetic model ...	232
6.5	AIM 4: investigate the alterations in RISK signalling that accompany failure of cardioprotection in diabetes.....	236
6.6	AIM 5: investigate if hyperglycaemia exacerbates reperfusion injury and how this differs between diabetic and non-diabetic hearts	239
6.7	AIM 6: investigate the mechanism by which glycaemia exacerbates reperfusion injury in the non-diabetic heart	244
7.	Conclusions and future directions	253
7.1	Conclusions.....	254
7.2	Future directions.....	255
8.	References.....	259

TABLE OF FIGURES

Figure 1.1: Sources of ATP synthesis within the cardiomyocyte.....	33
Figure 1.2: Electron transport chain function	36
Figure 1.3: Contrasting mechanisms for ATP resynthesis in normal versus ischaemic conditions.....	37
Figure 1.4: Reperfusion injury salvage kinase and survival activating factor enhancement pathways	43
Figure 1.5: Biphasic activation of the RISK pathway	47
Figure 1.6: Classical versus revised conceptualisation of the interplay between neural and humoral factors in remote ischaemic conditioning	49
Figure 1.7: Resistance to ischaemic preconditioning in diabetic and non-diabetic rats	61
Figure 1.8: Age and ischaemia-reperfusion injury in the Taconic GKR.....	62
Figure 1.9: Interaction between Toll-like receptor 4 signalling and insulin signalling during physiological stress induces insulin resistance.	68
Figure 1.10: Average blood glucose levels vs inpatient mortality during index admission for acute MI.....	72
Figure 1.11: Results of the DIGAMI trial	80
Figure 2.1: Evolution of glucose intolerance with selective breeding of the Goto Kakizaki rat	92
Figure 2.2: Development of the diabetic phenotype in a typical Goto Kakizaki rat from the Paris colony	93
Figure 2.8: Simplified block diagram showing the basic function of a pump speed control circuit.....	102
Figure 2.9A: Poiseuille's Law and Darcy's Law	103

Figure 2.10: Self-assembled Langendorff constant pressure perfusion rig	104
Figure 2.11: Left ventricular pressure transduction balloon	105
Figure 2.12: Schematic of a Langendorff perfused rat heart	106
Figure 2.13: Pressure trace and parameters derived from left ventricular balloon	107
Figure 2.14: Staining the heart for assessment of infarcted area.....	112
Figure 2.16: Chemical structure of Phlorizin	114
Figure 2.17: Surgical method of inducing rat hindlimb ischaemia	118
Figure 2.18: Example of a standard curve for the Smith protein assay	121
Figure 2.19: Example quantitative Western blot analysis.....	126
Figure 2.20: Custom-built hypoxic chamber.....	131
Figure 2.25: Design of a Clark Oxygen electrode	135
Figure 2.26: Example oximetry trace during mitochondrial respirometry.	139
Figure 3.1: Body weight over time in all three rat strains studied.....	144
Figure 3.2: Fasting blood glucose levels over time in all three rat strains	146
Figure 3.3: Long-term trends in blood glucose levels in all three rat strains ..	148
Figure 3.4: Normal curve for calculation of serum insulin content using Millipore rat insulin assay	151
Figure 3.5: Calculated insulin concentrations using the Millipore rat insulin assay	152
Figure 3.6: Correlation of serum insulin and plasma insulin measurements ..	153
Figure 3.7: Normal curve for calculation of serum insulin content using a Mercodia standard sensitivity rat insulin assay	154

Figure 3.8: Example of calculated insulin concentrations using the Mercodia standard sensitivity rat insulin assay	156
Figure 3.9: Fasting plasma insulin content in two rat strains.....	157
Figure 3.10: Calculation of homeostatic model assessment of insulin resistance statistic and homeostatic model assessment of β cell function	158
Figure 3.11: Insulin responsiveness in two rat strains	159
Figure 3.12: Beta cell function in two rat strains	160
Figure.3.13: Mitochondrial respiration in three rat strains	163
Figure 4.3: Physiological parameters during direct ischaemic preconditioning and <i>ex vivo</i> infarction of Sprague Dawley rat hearts	171
Figure 4.4 (see previous pages): Physiological parameters during ischaemic preconditioning and <i>ex vivo</i> infarction of Goto Kakizaki rat hearts.....	175
Figure 4.5: Reproducibility of infarct size quantification	178
Figure 4.6: Efficacy of direct ischaemic preconditioning in both Sprague Dawley and Goto Kakizaki rat hearts.....	180
Figure 4.7: Physiological parameters during <i>in vivo</i> remote ischaemic preconditioning and <i>ex vivo</i> infarction of Sprague Dawley rat hearts.....	186
Figure 4.8: Physiological parameters during <i>in vivo</i> remote ischaemic preconditioning and <i>ex vivo</i> infarction of Goto Kakizaki rat hearts.....	191
Figure 4.9: Efficacy of remote ischaemic preconditioning in both Sprague Dawley and Goto Kakizaki rat hearts subjected to <i>in vivo</i> remote ischaemic preconditioning followed by <i>ex vivo</i> experimental infarction.....	193
Figure 4.10: Phosphorylation of myocardial Akt in reaction to direct and remote ischaemic preconditioning Goto Kakizaki rat hearts	195

Figure 5.1: Physiological parameters during <i>ex vivo</i> ischaemia and reperfusion with varying concentrations of glucose at reperfusion in Sprague Dawley rat hearts	204
Figure 5.2: Physiological parameters during <i>ex vivo</i> ischaemia and reperfusion with varying concentrations of glucose at reperfusion in Goto Kakizaki rat hearts	208
Figure 5.4: Impact of the SGLT inhibitor Phlorizin on glucose-mediated augmentation of reperfusion injury	212
Figure 5.5: CM-H2DCFDA ROS-sensitive fluorescent dye is appropriately activated by exposure to 100mM H ₂ O ₂	213
Figure 5.6: Detection of ROS in isolated cardiomyocytes after introduction of high glucose medium	214
Figure 5.7: ROS-induced-ROS detection following oxidative stress with two strengths of H ₂ O ₂	215
Figure 5.8: Impact of glucose availability on ROS release in isolated cardiomyocytes at rest and under oxidative stress	215
Figure 5.10: Exposure to glucose during reoxygenation phase of simulated ischaemia-reperfusion in isolated cardiomyocytes	218

TABLE OF TABLES

Table 1.1: Studies examining potency of preconditioning treatments in high glucose vs low glucose conditions.	76
Table 1.2: Studies examining potency of postconditioning treatments in high glucose vs low glucose conditions.	78
Table 2.1: Constituents of modified Krebs Henseleit Buffer	101
Table 2.3: Manipulation of glucose content of Langendorff perfusate whilst maintaining constant osmolality	113
Table 2.4: Preparation of lysis buffer for myocardial tissue samples.....	120
Table 2.5: Preparation of SDS-PAGE gels.....	123
Table 2.6: Preparation of Western blot transfer buffer.....	124
Table 2.7: Membrane blocking and antibody exposure protocol for Akt.....	125
Table 2.8: Base stock solution for rat cardiomyocyte isolation buffers	128
Table 2.9: Rat cardiomyocyte isolation buffers.....	128
Table 2.10: Normoxic bicarbonate buffered solution for stabilisation and reperfusion phases of hypox-reox isolated cardiomyocyte experiments.....	130
Table 2.11: Anoxic bicarbonate buffered solution for simulated ischaemia phase of hypox-reox isolated cardiomyocyte experiments.	130
Table 2.12: Tyrode's buffer for use in confocal microscopy studies of ROS production in isolated cardiomyocytes	133
Table 2.14: Preparation of buffers for use in mitochondrial isolation protocols	134
Table 2.15: Hall's protocol for investigation of ADP-limited, ADP-stimulated, leak and maximal uncoupled respiratory flux through ETC Complex I or Complex II.....	136

Table 3.1: Spontaneous rat mortality in the longitudinal follow-up cohort.....	143
Table 4.1: Morphology and blood glucose content in Sprague Dawley rats used in direct and remote ischaemic preconditioning protocols.....	167
Table 4.2: Morphology and blood glucose content in Goto Kakizaki rats used in direct and remote ischaemic preconditioning protocols	167
Table 4.1: Numerical representation of improving reproducibility of infarct size assessment with increasing assessment experience.....	179
Table 5.1: Baseline characteristics of Goto Kakizaki and Sprague Dawley rats used in variable reperfusion glucose protocols	199

TABLE OF ABBREVIATIONS

ACE	Angiotensin converting enzyme
ADP	Adenosine diphosphate
AMP	Adenosine monophosphate
ATP	Adenosine triphosphate
BCL2	B cell lymphoma-2
BID	BH3 interacting-domain death agonist
BMI	Body mass index
CAD	Coronary artery disease
CAN	Cardiac autonomic neuropathy
CFR	Coronary flow rate
CI95	95% confidence interval
CM	Cardiomyocyte
CP1 & CP2	Chappell-Perry buffers 1 & 2
CRP	C-reactive protein
DevP	Developed pressure
DM	Diabetes mellitus
DM1	Type 1 diabetes mellitus
DM2	Type 2 diabetes mellitus
DR	Death receptor
ERK	Extracellular signal regulated kinase

ETC	Electron transport chain
FAT	Fatty acid translocase
FFA	Free fatty acid
GIK	Glucose, insulin and potassium
GKR	Goto Kakizaki rat
GLUT	Glucose transporter
HG	High glucose
HMGB1	High mobility group B1
IFG	Impaired fasting glucose
IGT	Impaired glucose tolerance
IHD	Ischaemic heart disease
IL	Interleukin
IMM	Inner mitochondrial membrane
IPC	Ischaemic preconditioning
IRS	Insulin receptor substrate
IKB	Inhibitor-KB
IKK	Inhibitor KB kinase
JAK-STAT	Janus kinase / signal transducer and activator of transcription
KME	Potassium, Magnesium and EGTA buffer
LPB	Lipopolysaccharide binding protein
LPS	Lipopolysaccharide

MI	Myocardial infarction
MOMP	Mitochondrial outer membrane permeabilization
NEFA	Non-esterified fatty acid
NF-KB	Nuclear factor-KB
NO	Nitric oxide
NSTEMI	Non-ST-elevation myocardial infarction
OxPhos	Oxidative phosphorylation
PCR	Polymerase chain reaction
PCI	Percutaneous coronary intervention
PI	Propidium iodide
PI3K	Phosphoinositide-3-kinase
PKC	Protein kinase C
RCD	Regulated cell death
RIPC	Remote ischaemic preconditioning
ROS	Reactive oxygen species
SDF-1 α	Stromal derived growth factor-1 α
SDR	Sprague Dawley rat
STAT-3	Signal transducer and activator of transcription-3
STEMI	ST-elevation myocardial infarction
TCA	Tricarboxylic acid
TGF- β	Transforming growth factor- β

TLR-4	Toll-like receptor-4
TNF- α	Tumour necrosis factor alpha
TNFR1	TNF receptor superfamily member 1A
TRAIL	TNF-related apoptosis-inducing ligand
VEGF	Vascular endothelial growth factor
WHO	World Health Organisation
WR	Wistar rat
$\Delta\Psi$	Mitochondrial membrane potential

1. INTRODUCTION

1.1 Scope

Ischaemic heart disease (IHD) and diabetes mellitus (DM) are very common causes of morbidity and mortality. IHD is the leading cause of death worldwide, causing 9.5m deaths in 2016; diabetes now affects 8.5% of the world population with rates of increase on a pandemic trajectory¹. The two problems are interlinked in a complex manner: not only is diabetes a strong risk factor for IHD, it also predicts poor outcomes from the condition². Moreover, IHD and DM share several antecedents including obesity³, insulin resistance^{4,5} and the metabolic syndrome^{6,7}.

These are chronic diseases, and their indolent evolution may pass un-noticed until an acute exacerbation⁸. Therefore, although early detection and intervention are beneficial, we must be realistic that a high proportion of patients with either DM or IHD will present late with an acute complication of the underlying conditions, for example acute myocardial infarction (MI).

MI is a crucible in which we may view the interaction between DM and IHD, as it exemplifies the relationship between the conditions: patients with diabetes are more likely to suffer death and other complications than patients without diabetes in the immediate aftermath of MI⁹⁻¹¹, and the reasons for this remain unclear. This reflects the IHD-DM interaction over the longer term².

Hyperglycaemia (high blood glucose – HG) – a key defining feature of diabetes¹² – also affects patients without diabetes with MI¹³, and predicts early death even more powerfully in this population than in diabetic patients¹⁴⁻¹⁷.

Thus, there are two principal reasons to study the mechanism of impact of DM and blood glucose content on MI:

Firstly, MI remains a high mortality condition in both DM and non-DM patients; better understanding of the acute DM-glucose-MI interaction may lead to treatments which can reduce early mortality for both patients with and without diabetes.

Secondly, understanding the acute interplay may give insights into how diabetes and blood glucose content contribute in the longer-term to raised risk of complications in stable IHD.

1.2 Myocardial ischaemia-reperfusion injury

Human myocardium is vulnerable to ischaemia due to its high metabolic requirements, low capacity for metabolic substrate storage and poor arterial collateralisation^{18,19}. At rest, human myocardium extracts up to 40% of oxygen from afferent blood²⁰; this is by far the highest extraction fraction in the body. As well as extensive mechanisms for matching blood supply to metabolic demand, myocardium possesses a unique ability to switch between metabolic substrates according to supply, and according to the supply of oxygen, as oxygen is used with differing efficiency depending on the metabolic substrate^{18,21}.

Ischaemia, diabetes and non-diabetic HG all involve perturbances to supply of oxygen or metabolic substrates, and all induce functional changes in myocardial metabolism that may initially enable it to better withstand these insults^{22,23}. In the case of acute ischaemia, however, (and possibly also with high blood glucose content and transient high blood insulin content or diabetes) there is a downside to these adaptations in that when the insult comes to an end, restoration of normality may then itself prove harmful²⁴. This is only well-characterised in the case of ischaemia, where restoration of blood supply, typically by some therapeutic intervention, may augment cell damage by a process termed “reperfusion injury”²⁵. In practise this insult – although real - is difficult to demonstrate as distinct from the preceding ischaemic injury, and therefore the catch-all term “ischaemia-reperfusion injury” is often used²⁶.

1.2.1 Myocardial metabolism

The principal metabolically active cell type in the heart is the cardiomyocyte (CM), responsible both for myocardial motion and propagation of the electrical signal that underpins cardiac synchronicity²⁷. Intracellular energy stores are principally in the form of adenosine triphosphate (ATP), which is short-lived and constantly regenerated¹⁸; the process of regenerating ATP accounts for 90% of cardiac oxygen consumption^{21,28}. The chief intracellular fate of ATP is hydrolysis to release energy at the myosin ATPase (76%), sarcolemmal Na⁺/K⁺ATPase (9%) and sarco/endoplasmic reticulum Ca²⁺-ATPase (SERCA – 15%)²⁹.

1.2.2 Sources of ATP

Production of ATP is high yielding and acutely regulated. In health, with liberal oxygen, the main myocardial source of ATP is oxidative phosphorylation (OxPhos) of ADP to ATP by the electron transport chain (ETC), located on the inner mitochondrial membrane (IMM), accounting for 95% of ATP flux. The remaining 5% yields from the citric acid (TCA) cycle. OxPhos is the more efficient ATP source, with respect to both substrate and oxygen consumption^{18,30}.

Generation of acetyl-coA from any substrate feeds into the TCA cycle and eventually OxPhos in the ETC. Acetyl-coA is generated in the IMM from the carbohydrate and fat molecules which are delivered to the CM via blood flow and diffusion through the extracellular space (see Figure 1.1). All processes that generate ATP, except cytosolic glycolysis, require oxygen³¹.

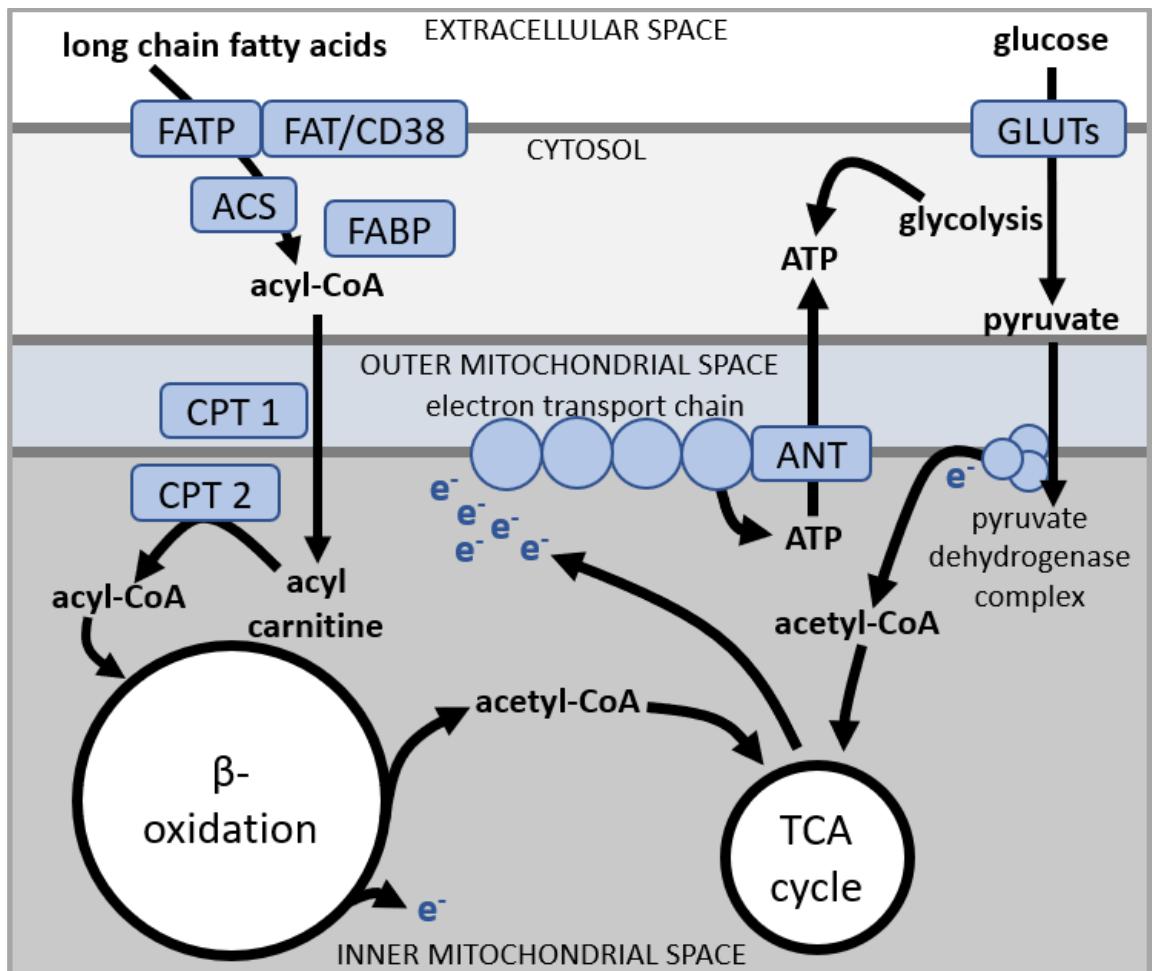


Figure 1.1: Sources of ATP synthesis within the cardiomyocyte. Long chain fatty acids and glucose are taken up via specific receptors on the cell membrane and undergo metabolism in the cell. Fatty acids are taken into the mitochondrion as acyl carnitine via the carnitine shuttle and enter into β -oxidation yielding acetyl-CoA as substrate for the TCA cycle. Glucose is metabolised to pyruvate in the cytosol before being taken up into the inner mitochondrial space as acetyl-CoA and entering directly into the TCA cycle. The TCA cycle yields high numbers of electrons conjugated to carriers, which are then donated into the electron transport chain giving rise to highly efficient production of ATP. FATP = fatty acid triphosphate; FAT = fatty acid translocase; ACS = acyl-CoA synthase; FABP = fatty acid biphosphate; CPT = carnitine acyltransferase. Adapted from Harvey & Ferrier³².

1.2.2.1 Free fatty acid metabolism

Extracellular free fatty acids (FFAs) enter the CM via dedicated transporter proteins in the cell membrane including fatty acid translocase (FAT, or CD36) and are shuttled into the mitochondrion where they are metabolised by oxidation. Each turn of the fatty acid β -oxidation cycle (FFA cycle), liberates acetyl CoA into the TCA cycle also sited in the IMM. The final ATP yield

depends on the length of the initial carbon chain of the FFA fed into the process^{18,30,33}.

1.2.2.2 Glycolysis

Following carbohydrate uptake into the CM by a range of facilitative glucose transporters including the GLUT and SGLT families^{34,35}, sugars are metabolised by cytosolic enzymes in a process that is inefficient in terms of ATP production but requires no oxygen. The endpoint is acetyl-CoA fed into the TCA cycle¹⁸.

1.2.2.3 The citric acid (TCA) cycle

The tricarboxylic acid / citric acid (TCA) cycle of enzymes within the inner mitochondrial space converts the energy of acetyl-CoA into electron-laden hydrogen carrier molecules³².

1.2.2.4 Oxidative phosphorylation (OxPhos)

OxPhos is the final common pathway of oxidative metabolism, in which the electron carriers NADH and FADH₂ produced by other metabolic pathways yield high concentrations of ATP.

The site of OxPhos is the electron transport (ETC), a series of four enzymatic complexes adherent to the IMM, plus an associated ATP synthase (the F₁-F₀ATPase)³⁶. As shown in Figure 1.2, impermeability of the IMM is fundamental, allowing an electrochemical gradient to develop between the inner and outer mitochondrial spaces. The only substances that freely diffuse over the IMM are O₂, CO₂ and H₂O³².

A high energy electron is extracted from NADH at complex I, yielding NAD (free to return to the citric acid cycle) plus a proton (H⁺). Using the small amount of energy liberated by stepping down the electron from a high energy state in NADH to a slightly lower energy state when conjugated to ubiquinone (Q), the free proton is pumped across the IMM into the outer mitochondrial space, generating an electrochemical gradient across the IMM³⁷. This charge is $\Delta\Psi$, the mitochondrial potential, first postulated by Mitchell in 1961³⁸. Q also accepts high energy electrons from FADH₂ via complex II. From Q, electrons are stepped down to complex III, liberating enough energy for more protons

(sourced from complex II's action on FADH₂) to be pumped across the IMM, adding to $\Delta\Psi$. Via cytochrome c the electrons step down once more to complex IV, where they reach their lowest energy state conjugated to O₂ to form H₂O. The proton liberated by complex IV is again translocated over the IMM, augmenting $\Delta\Psi$ ³⁷. The substantial electrochemical gradient thus generated (around -200mV) is enough to propel a proton over the IMM via the F₁-F₀ATPase, driving the phosphorylation of ADP to ATP³⁶.

1.2.2.5 Maintenance of the inner mitochondrial membrane potential

Maintenance of the inner mitochondrial membrane potential, $\Delta\Psi$, requires the IMM to remain impermeable to many key solutes including, most crucially, protons (H⁺). Ingress of protons to the inner mitochondrial space is a highly regulated process and may occur via OxPhos³⁶, via uncoupling proteins (UCPs)³⁹ or following more general permeabilization of mitochondrial membranes⁴⁰. Only if protons enter via OxPhos does $\Delta\Psi$ contribute to generation of ATP.

The physiological function of proton entry via UCPs has yet to be fully elucidated but proton a role in ROS-mediated mitochondrial signalling is considered likely; pathological over-expression of UCPs in the heart is associated with decreasing metabolic efficiency and development of heart failure³⁹.

Whilst UCP-mediated H⁺ entry is common in viable myocardium, less selective permeabilization of the IMM is a feature of cell death, as discussed in Section 1.2.4.5, "Lethal reperfusion injury and mitochondrial permeability". While cells are not subject to lethal injury, IMM permeabilization is suppressed by pro-survival signalling through the B cell lymphoma-2 (BCL2) family of apoptotic regular proteins⁴¹.

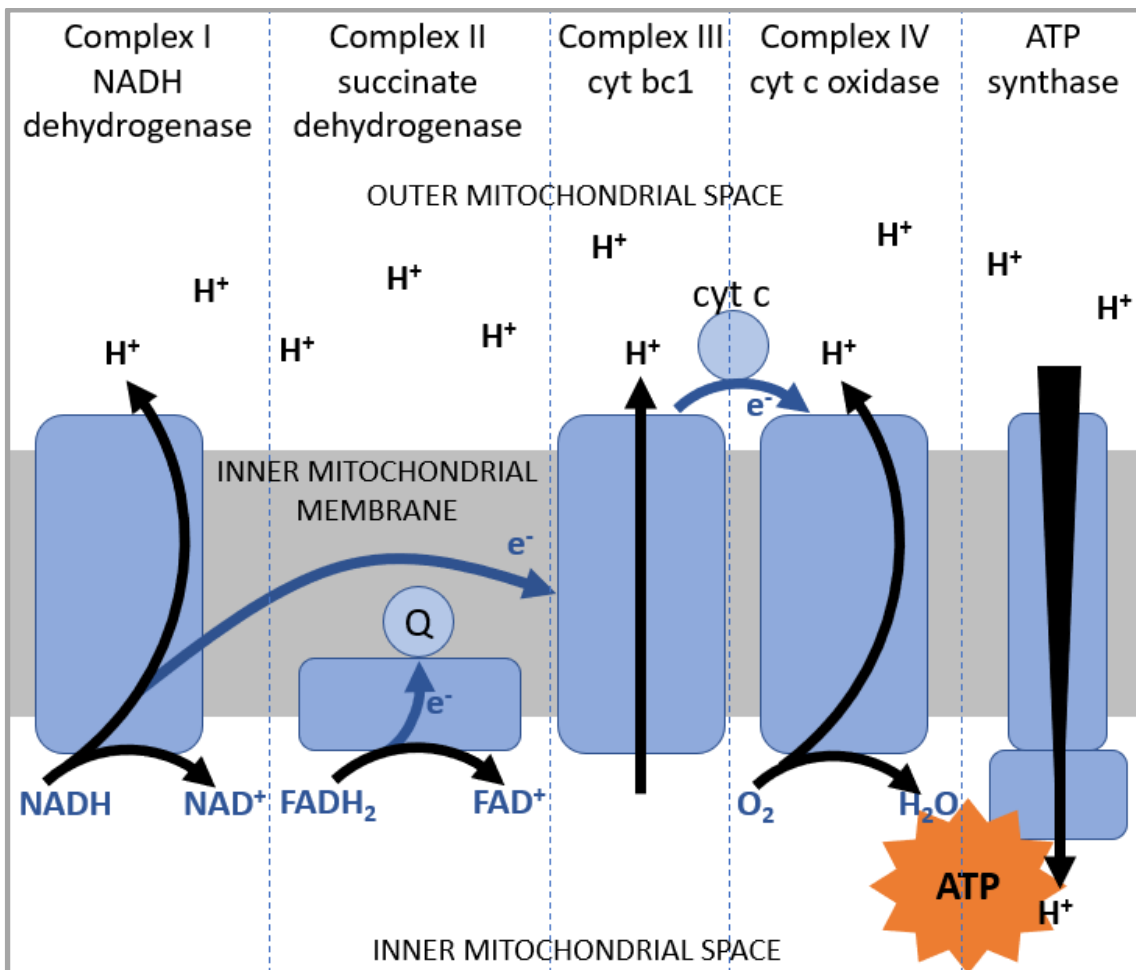


Figure 1.2: Electron transport chain function. Electrons liberated from carriers NADH and $FADH_2$ are progressively stepped down from high energy states releasing energy quanta used to propel H^+ out of the inner mitochondrial space, across the inner mitochondrial membrane. The resulting H^+ electrochemical gradient then drives H^+ ingress over the ATP synthase, catalysing ATP synthesis from ADP and P_i . Cyt: cytochrome; Q: coenzyme Q. Adapted from Harvey and Ferrier³².

1.2.3 Ischaemic injury

Onset of ischaemia heralds reduction of available oxygen, carbohydrate and free fatty acids. From a metabolic perspective, the primary effect of this is reduced ATP formation via OxPhos due to reduced oxygen and substrate availability. This has an immediate effect on myocardial function via reduced ATP hydrolysis and consequent reduced contractile function. Calcium cycling through the sarcoplasmic reticulum is also suppressed and thus Ca^{2+} accumulates in the cytosol leading to ischaemic contracture²⁴. The fall in ATP/ADP ratio and build-up in AMP, inorganic phosphate and cytosolic calcium

activates AMP kinase (AMPK), which in turn upregulates metabolic pathways that can function without oxygen⁴². Thus, glycolysis and glycogenolysis continue, and various glucose uptake channels including GLUT1, GLUT-4 and SGLT1 are upregulated, allowing increased carbohydrate flux through these pathways in absence of oxygen^{43,44}. However, there is reduced transfer of pyruvate from the glycolytic pathways into the mitochondria and thus into the TCA cycle and OxPhos. Under limited oxygen, the fate of pyruvate is to be metabolised by dehydrogenases in the cytosol to lactate, as illustrated in Figure 1.3, causing intracellular pH to drop¹⁸.

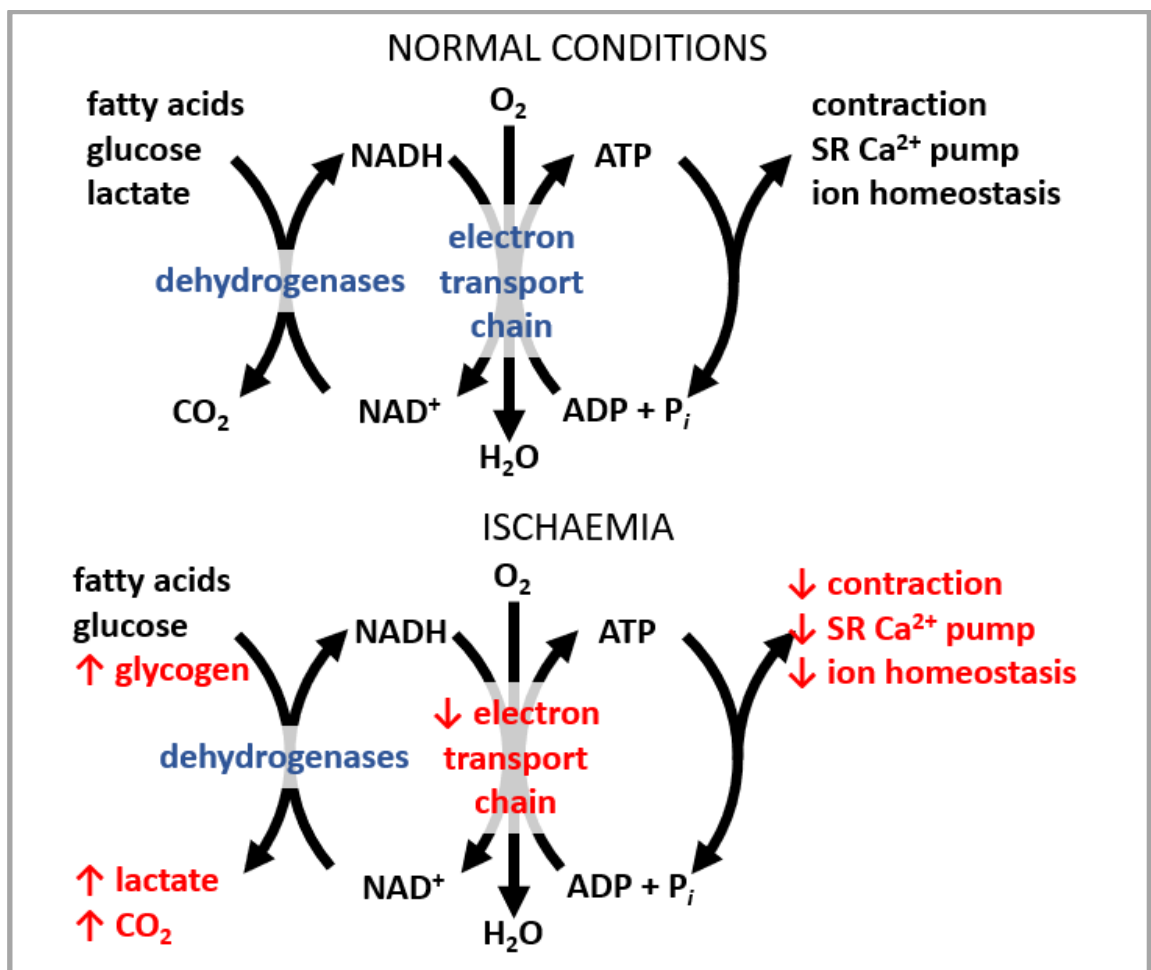


Figure 1.3: Contrasting mechanisms for ATP resynthesis in normal versus ischaemic conditions. Under normal conditions, dehydrogenases metabolise fatty acids, glucose and lactate to reconstitute the electron carrier NADH, which forms ATP via oxidative phosphorylation over the electron transport chain. Under ischaemia, by contrast, NADH is reconstituted by metabolism of substrate to lactate and CO₂, contributing to lowering of intracellular pH, in turn inhibiting vital cell functions including contraction, Ca²⁺ transport and homeostasis of other ions. Adapted from Stanley¹⁸.

As ischaemia persists, falling intracellular pH and ATP depletion worsen and by various perverse mechanisms cause Na⁺, H⁺ and Ca²⁺ accumulation in the cytosol⁴⁵. Eventually despite ATP hydrolysis by the F₁F₀-ATPase⁴⁶ the mitochondrial membrane potential fails and cell death quickly ensues via energetic failure and irrecoverable ionic shifts in a wave that sweeps from endo- to epicardium⁴⁷.

1.2.4 Reperfusion injury

With deep myocardial ischaemia progressing inexorably towards cell death, the stage is set for some dramatic intervention to bring cells back from the brink via restoration of oxygen and metabolic substrate. In the clinical setting of acute myocardial infarction, this is commonly achieved either by spontaneous or pharmacological recanalisation of a thrombosed culprit coronary artery, (“thrombolysis”) or – increasingly – by mechanical intervention to an epicardial coronary vessel accompanied by pharmacological thrombus disruption collectively termed primary percutaneous coronary intervention, or PPCI⁴⁸.

Several pathophysiological processes combine to produce injury at reperfusion. The mechanisms are not fully understood but include oxidative stress⁴⁹, altered calcium metabolism⁵⁰ and rapid correction of intracellular pH⁵¹ followed by an inflammatory response⁵².

It is difficult to dissect out the relative contributions from ischaemic versus reperfusion cell injury. The aftermath of reperfusion at an ultrastructural level provides circumstantial evidence of harm, with rapid mitochondrial swelling, nuclear degranulation and lysis of CMs²⁵. Nonetheless a sceptic would say that this represents rapid clearance of cells mortally wounded during the ischaemic phase, rather than *de novo* injury. The best indirect evidence we have for the existence of reperfusion injury is that therapeutic interventions applied after reperfusion can modulate the burden of cell death⁵³.

1.2.4.1 Metabolism at reperfusion

When liberal oxygen and substrate are supplied to myocardium in deep ischaemia, CM metabolism alters dramatically. Against a background of the shifts that have occurred during ischaemia, these changes may underlie or exacerbate the degree of reperfusion injury²⁴.

1.2.4.2 Osmotic consequences of pH correction

On re-supply of oxygen, mitochondrial oxidative metabolism of both glucose and FFAs restarts, but FFA oxidation dominates. This is due to FFA build-up during ischaemia and suppression of OxPhos by an overactive FFA cycle⁴⁵. Cytosolic glycolysis remains active at a rate that outstrips the TCA cycle and thus harmful lactate production persists so that the cytosol remains acidic compared to the extracellular matrix³⁰.

The resulting cell membrane proton gradient is corrected by activation of the Na^+/H^+ exchanger and $\text{Na}^+/\text{HCO}_3^-$ symporter⁵⁴. This sets up an unopposed inflow of Na^+ , which if unchecked may lead to osmotic cell stretch and rupture. The osmotic gradient is worsened by lactate accumulation during the preceding ischaemia¹⁸.

1.2.4.3 ROS production and the oxygen paradox

Within 10-20secs of the re-supply of oxygen, mitochondria are re-energised and electron flux through the ETC re-initiated⁴⁵. Under physiological conditions, a small electron leakage from the chain is normal, leading to small-scale production of reactive oxygen species (ROS) by mitochondria. Sudden reactivation of mitochondria damaged by preceding ischaemia may, in contrast, lead to large-scale ROS production by electron leakage at complexes I and III⁵⁵. Reactive species then may interact with ETC and other mitochondrial constituents including mitochondrial DNA (mtDNA), leading to self-perpetuating ETC dysfunction, or compromised mtDNA integrity triggering cell death⁵⁶.

Non-mitochondrial sources of ROS are also important at reperfusion. During ischaemia, cytoplasmic xanthine dehydrogenase is converted into xanthine oxidase, which at reperfusion becomes a potent cytoplasmic source of ROS, acting on substrates that have also accumulated during ischaemia⁵⁷. Moreover, cellular defences against oxidative injury (super-oxide dismutase and glutathione peroxidase) are depleted by ischaemia, leaving the cell vulnerable⁵⁸.

1.2.4.4 Intracellular calcium overload

At reperfusion, Na^+ loading of the cell may be worsened by reactivation of ATP-dependent Na^+ pumps including the Na^+/K^+ ATPase. Intracellular Na^+ overload is countered by the $\text{Na}^+/\text{Ca}^{2+}$ exchanger, which extrudes Na^+ in return for

worsening Ca^{2+} accumulation⁵⁹. Cytosolic Ca^{2+} increase leads to sarcoplasmic reticulum (SR) Ca^{2+} overload, as Ca^{2+} is taken up into the SR by SERCA, also reactivated by the presence of ATP⁴⁵. When the SR is grossly overloaded, it spontaneously discharges leading to calcium spikes in the cell and hypercontracture⁵⁴. Threshold for Ca^{2+} release may be lowered by damage to SR constituents during ischaemia.

1.2.4.5 Lethal reperfusion injury and mitochondrial permeability

A wave of cell death advances through the myocardium immediately following reperfusion²⁵; the energy state of the cell at this instant determines the mode of cell death. In the setting of energy depletion, the immediate trigger for cell death is mitochondrial swelling, rupture and energetic failure. Specifically, a voltage-dependent and calcium-dependent channel forms in the inner mitochondrial membrane (IMM), leading to rapid obliteration of the physiological electrochemical potential over the IMM ($\Delta\psi$) with ensuing water ingress, electrolyte loss, mitochondrial swelling and energetic failure⁶⁰. This channel has been termed the mitochondrial permeability transition pore (mPTP)⁶¹.

Even in an energy replete cell, very transient opening of the mPTP can cause cell death. This “flickering” by the mPTP may be insufficient to cause osmotic disruption of the mitochondrion, yet lead to sufficient metabolic uncoupling and ROS production to cause recruitment of pro-apoptotic mediators such as Bax, providing the link between the mPTP and a form of apoptosis⁶².

During ischaemia the mPTP is closed due to acidosis, high intracellular Mg^{2+} and replete intracellular ADP⁶³. At reperfusion, however, rapid shifts in pH, ROS and mitochondrial calcium promote the binding of cyclophilin D to the mPTP, and this binding increases the likelihood of the mPTP opening given sufficient other insults⁶¹. Evidence for the mPTP being the final common pathway of reperfusion cell death comes from the fact that diverse modulators of cell survival, from exogenous drugs, to endogenous autacoids, all impact mPTP opening^{60,64,65}.

1.2.4.6 mPTP-independent cell death

mPTP-driven necrosis is only one of a range of mechanisms by which cells exposed to extreme perturbations in intra- or extracellular environment may trigger cell death. Although death of a cell may occur as a result of overwhelming damage, the majority of cell death events are in fact a coordinated response (“regulated cell death - RCD”). mPTP formation is an example of this; there are many others but not all are relevant to reperfusion injury. All forms of RCD can be described on a spectrum of morphological characteristics from purely apoptotic to purely necrotic; the RCD subroutines most relevant to IRI include intrinsic and extrinsic apoptosis, necroptosis and mPTP-driven necrosis, which has already been discussed.

1.2.4.6.1 Intrinsic apoptosis

Intracellular stressors such as DNA damage, endoplasmic reticulum stress and ROS overload (all common at reperfusion, as outlined above) may activate intrinsic apoptosis at the mitochondrion, resulting in mitochondrial outer membrane permeabilization (MOMP)⁴⁰. Subsequent pro-apoptotic signalling is controlled by the BCL2 family of apoptotic regulators including BAK and BAX, which are also implicated in MOMP itself⁴¹. Caspase-9 (an “initiator caspase”), is a key event downstream of MOMP⁶⁶, as this caspase has among its many substrates other “executioner” caspases (caspases 3, 6, and 7)⁶⁷. Executioner caspases in turn have over 1000 substrates and their action may produce gain or loss of function of these proteins, leading to widespread intracellular changes culminating in cell death⁶⁸.

1.2.4.6.2 Extrinsic apoptosis

A second route to apoptosis (“extrinsic apoptosis”) occurs when the cell stressor triggers proapoptotic signalling via cell surface Death Receptors (DRs). DRs are a subset of the TNF receptor superfamily including TNF receptor 1A, Fas, and TNF-related apoptosis-inducing ligand receptors 1 and 2 (TRAIL-R1 and -R2). Death receptors regulate the function of Caspase-8, which may either directly activate further caspases, or act on the BH3 interacting-domain death agonist (BID), depending on cell type⁶⁹. BID, in turn, results in MOMP via BAX and BAD, as well as releasing inhibition of the executioner caspases resulting in the final apoptotic pathway⁶⁸.

1.2.4.6.3 Necroptosis

DRs are also implicated in necroptosis, a third pathway of regulated cell death. Necroptosis is initiated by specific sequential activation of cell surface DRs, which leads to downstream oligomerisation of mixed lineage kinase domain-like pseudokinase⁷⁰. These activated oligomers may then translocate to the cell membrane and cause permeabilization, which leads to a morphological appearance some way between passive necrosis and active apoptosis, hence the conjugated name⁷¹.

1.2.5 Myocardial survival signalling

A range of interventions have been found to minimise cardiomyocyte death over the short-term. Following any of these interventions, a temporary state of “acute cardioprotection” is induced that appears to reduce susceptibility to a range of normally deleterious insults including ischaemic injury^{72,73}, reperfusion injury⁷⁴ and cytotoxic drugs⁷⁵. Promotion of cellular survival at reperfusion seems to centre on the mitochondrion, particularly prevention of mPTP opening⁷⁶.

mPTP inhibition has been shown experimentally to be the final effector in a cascade of enzymatic signalling that enhances resilience of cardiomyocytes. Following binding by a series of autacoids to cell surface receptors, intracellular signalling cascades are activated which converge on the mPTP. Survival enhancing cascades are diverse, with the two best described being the “reperfusion injury salvage kinase” (RISK) and “survivor activating factor enhancement” (SAFE) pathways, as shown in Figure 1.4 and discussed below:

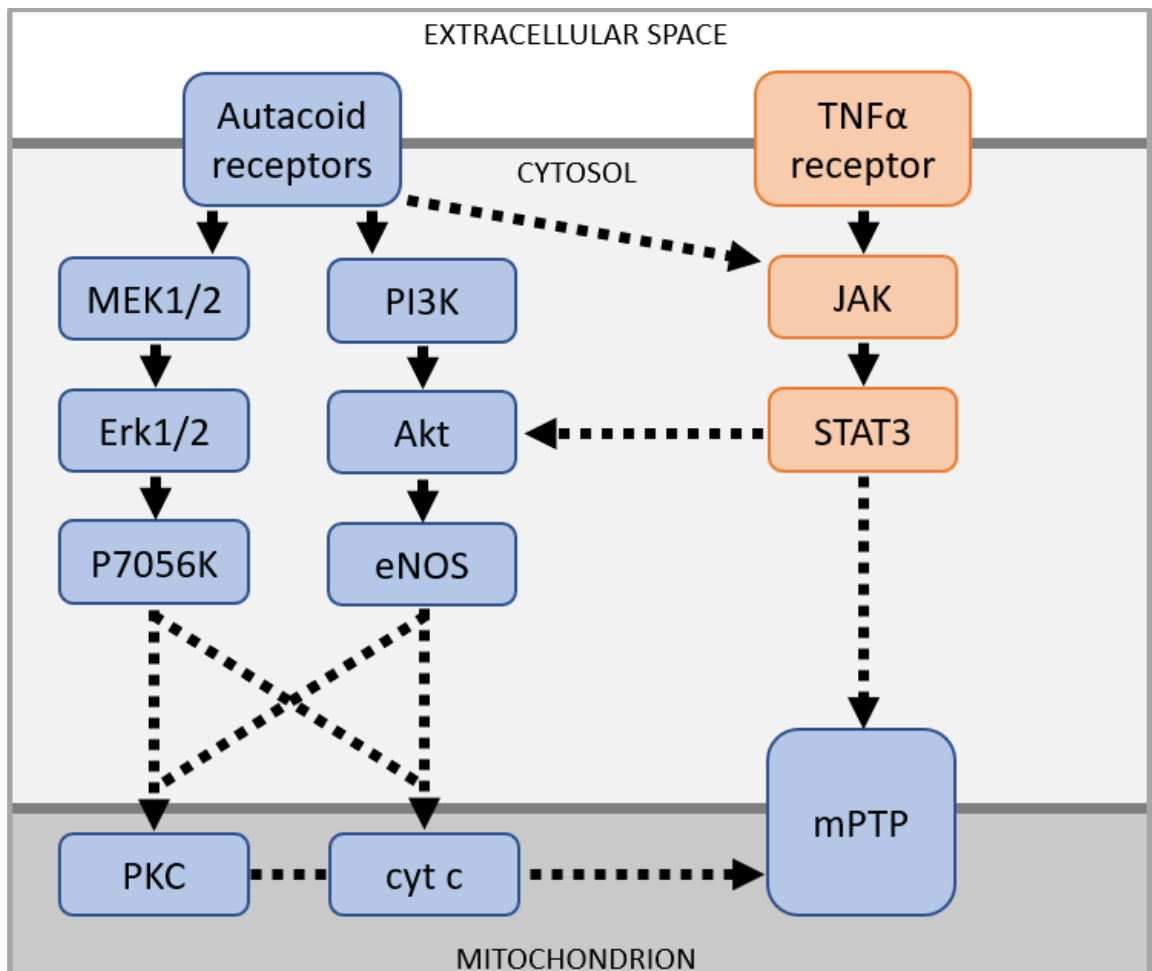


Figure 1.4: Reperfusion injury salvage kinase (RISK - **blue**) and survival activating factor enhancement (SAFE - **orange**) pathways are activated in response to endogenous or exogenous ligands binding to a variety of cardiomyocyte cell surface receptors and converge on the mitochondrion to inhibit mitochondrial permeability transition pore (mPTP) formation. Dotted lines: presumptive pathways.

1.2.5.1 RISK pathway

The reperfusion injury salvage kinase (RISK) pathway was characterised and named by Yellon's group, who observed that acutely cardioprotective interventions such as transforming growth factor- β 1, Atorvastatin and urocortin all act via PI3K-Akt and p42/44 MAPK signalling⁷⁷⁻⁷⁹. The infarct-sparing effects of endogenous substances such as insulin⁸⁰, IGF-1⁸¹, bradykinin⁸² and adenosine^{83,84} have also been shown to depend on RISK signals. Moreover, activation of RISK by pharmacological manipulation at reperfusion consistently produces a 40-50% reduction in cell death⁸⁵.

Downstream targets of RISK are diverse including pro-apoptotic proteins, mitochondrial cytochrome c, protein kinase C and eNOS (as reviewed by Hausenloy and Yellon⁸⁶). Phosphorylation of Bax prevents translocation of this apoptotic trigger protein to the mitochondrion and is associated with reduced mPTP formation and reduced apoptotic cell death^{87,88}.

1.2.5.2 SAFE pathway

The survival activating factor enhancement (SAFE) pathway was described by Lecour after demonstrating that TNF- α elicits an acute cardioprotective response independent of RISK pathway phosphorylation⁸⁹. In place of Akt and p42/44 MAPK phosphorylation, STAT-3 activation was observed, and the cardioprotective effect was blocked by the STAT-3 inhibitor AG490 but not by Akt or MAPK inhibitors, confirming a functionally separate signalling pathway⁸⁹.

RISK and SAFE pathways may be activated together or separately by different protective interventions. Coactivation is evident, for example, for coincident remote ischaemia to elicit a cardioprotective effect (remote preconditioning)⁹⁰, but SAFE pathway activation alone is sufficient for the cardioprotection afforded by intermittent local reperfusion (so-called ischaemic postconditioning)⁹¹. It remains unclear what cross-talk exists between RISK and SAFE pathways beyond the observation that the STAT-3 inhibitor, Stattic, leads to reduced phosphorylation of both STAT-3 and Akt⁹².

RISK and SAFE converge on the mPTP to exert their final pro-survival effect at reperfusion⁹³.

1.2.5.3 Non-mPTP targets of RISK and SAFE

The major burden of cell death at reperfusion is thought to be due to mPTP-associated cellular necrosis⁹⁴; the main effect of pro-survival signalling at reperfusion is therefore by suppression of this mPTP formation^{24,65}. However, other regulated cell death routines may also contribute to the final burden of cell death; RISK and SAFE activation may also modulate these other modes of cell death.

Akt directly impacts the intrinsic apoptotic pathway via phosphorylation of the initiator caspase Caspase-9, thus suppressing its pro-apoptotic activity⁹⁵ and

blocking a key step in the intrinsic apoptotic response to DNA damage, endoplasmic reticulum stress and ROS overload – all common features of reperfusion injury. BAD is also a direct phosphorylation target of Akt in response to upstream pro-survival signals, resulting in increased threshold to MOMP^{96,97}.

The extrinsic apoptotic pathway is also inhibited by Akt-mediated survival signals, as Akt acts on nuclear transcription factors including the FOXO family and p53 to inhibit interaction with target genes. FOXO targets such as Fas ligand⁹⁸ are thus downregulated and less available to trigger extrinsic apoptosis.

Akt has further, indirect effects on apoptosis, mediated by downstream kinases in the RISK cascade, including glycogen synthase kinase-3 β (GSK3 β), which is inactivated by prosurvival signalling upstream of Akt⁹⁹. GSK3 β , in turn, has a wide range of substrates that regulate apoptosis including BCL2 proteins¹⁰⁰. Thus inactivation of GSK by Akt may indirectly inhibit both intrinsic and extrinsic apoptosis¹⁰¹.

Knowledge of the SAFE pathway is less developed than knowledge of RISK and Akt signalling. One area of interplay that has been demonstrated in the heart is that acute activation of JAK-STAT (Janus kinase / signal transducer and activator of transcription) signalling has been shown to inhibit apoptosis via activating BCL2 apoptotic regulators¹⁰². JAK-STAT forms the main SAFE signalling pathway and is best studied in settings of cell proliferation, eg: embryonic and stem cell development and cancer biology. Even from these far removed settings, however, it is clear that the JAK-STAT system enhances cell survival in the face of stressors, via reduced expression of the executioner caspase, Caspase-3¹⁰³. This effect may augment SAFE's cytoprotective effect on IRI.

1.2.5.4 Direct ischaemic preconditioning

Murry *et al* first reported a 25% reduction in infarct size caused by brief sublethal ischaemic episodes prior to a longer, "index" ischaemic event in dogs¹⁰⁴. This was achieved by four five-minute occlusions of the circumflex coronary artery interspersed with five-minute episodes of reperfusion (which they termed "ischaemic preconditioning", or IPC), followed by a 40min occlusion and then four days recovery. Control animals received only the 40min occlusion

and recovery time¹⁰⁴. Numerous studies have reproduced this phenomenon across a range of mammals; the most frequently studied being pig, rat, mouse and rabbit¹⁰⁵. Over 30 years of study, results have remained remarkably constant, with a recent meta-analysis of 503 published studies attributing an average 25% infarct size reduction to the intervention¹⁰⁵.

Initial interpretations hazarded that IPC reduced ischaemic cell death, perhaps by slowing ATP depletion or by improved coronary collateral flow⁷². However, around the turn of the century, two groups, one at the Hatter, showed that IPC recruits PI3K, and that PI3K blockade using Wortmannin during intermittent ischaemia abrogated the efficacy of a preconditioning protocol^{106,107}. This led to conceptualisation of IPC as a “reflex arc” with an afferent, or “trigger” event followed by a memory function and then finally the efferent or “effector” limb of the response. The RISK pathway was thus implicated in the “trigger” phase of IPC but the memory function and effector of protection remained unclear.

Given that the RISK pathway had already been shown to mediate the protection conferred by insulin and other endogenous substances in early reperfusion, Yellon’s group hypothesised that RISK may also be the effector of ischaemic preconditioning. In fact, it proved possible to block the effect of IPC in rat hearts using inhibitors of PI3K or MAPK administered solely during early reperfusion, suggesting that the effector limb of IPC was active at reperfusion, and that RISK was fundamental not just to the trigger phase of protection, but also to the effector phase⁸⁶.

Further confirmation of biphasic activation of RISK was provided by a time course experiment, again in rat, showing peaks in Akt phosphorylation just after a preconditioning protocol (the trigger phase) and again at index reperfusion (the effector phase) in preconditioned hearts, but not in control hearts¹⁰⁸, as shown in Figure 1.5:

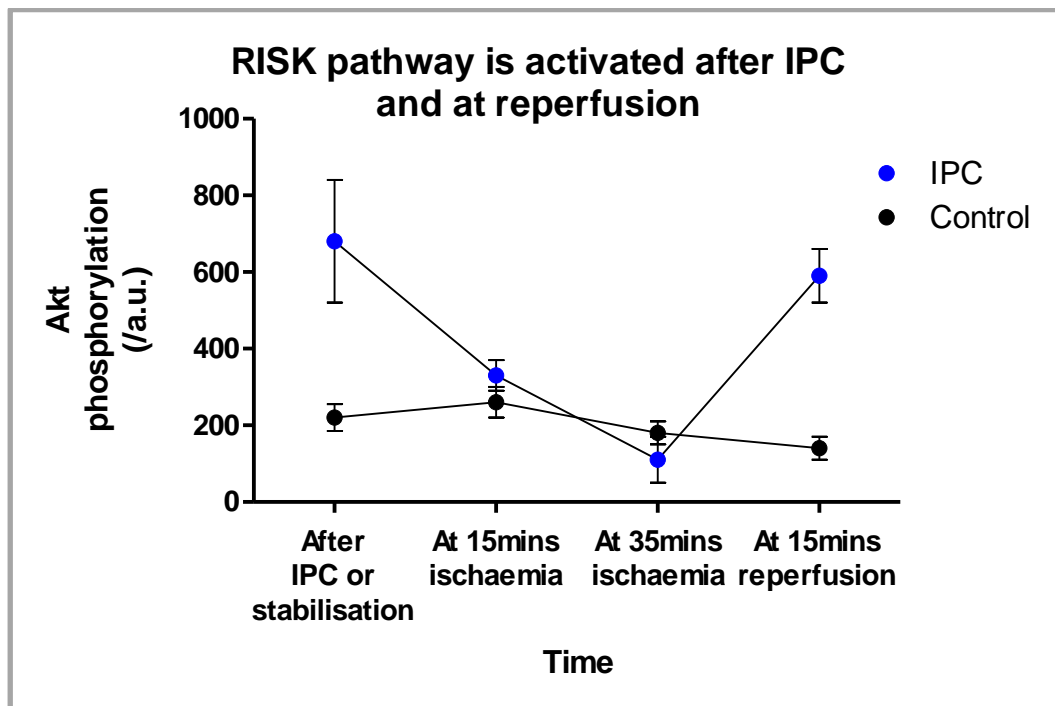


Figure 1.5: Biphasic activation of the RISK pathway after ischaemic preconditioning and again at index reperfusion; IPC = ischaemic preconditioning. Adapted from Tsang *et al*¹⁰⁸.

The trigger phase of IPC has now been extensively investigated with multiple candidate blocking agents, in both isolated rabbit and rat heart. In summary: upstream of RISK, recruitment of cell surface receptors for bradykinin¹⁰⁹, δ 1-opioid¹¹⁰ and adenosine^{111,112} are all implicated and blockade of any one of these is sufficient to prevent the preconditioning effect. Downstream of RISK, the stimulus requires intact mPTP function and can be blocked by Cyclosporin A – an mPTP blocker – given solely during the IPC stimulus¹¹³. PKC ϵ , mitochondrial potassium channels and ROS are also required, and blockers of all these can also abrogate IPC’s protection^{114,115}.

The nature of the “memory” phase of IPC remains mysterious, as does the immediate cause of reactivation of the RISK cascade at the index reperfusion event.

1.2.5.5 Remote ischaemic conditioning

Direct ischaemic preconditioning of the myocardium is a powerful modulator of IRI but requires access to the culprit coronary artery and advanced knowledge of an ischaemic event. Thus, as a clinical treatment it has limited applicability.

Various other acutely protective modalities, some readily translatable into man, have emerged as effective at reducing susceptibility to myocardial IRI, using prior, concomitant or post-reperfusion ischaemia of cardiac or non-cardiac tissue as the conditioning stimulus. Intermittent ischaemia of a remote organ (remote ischaemic conditioning – RIC) prior to (preconditioning – RIPC) or during (perconditioning – RIPerC) index ischaemia of the heart has repeatedly proven to reduce IRI. The RIPC effect was first described by Przyklenk, who applied intermittent occlusion of the circumflex coronary artery in dog, prior to index ischaemia of the territory supplied by the left anterior descending artery. Dogs treated in this way sustained, on average, 10% smaller infarcts than those undergoing index LAD territory ischaemia alone¹¹⁶. A large body of experimental work now exists in small mammals showing a protective effect from prior¹¹⁷ or concomitant¹¹⁸ ischaemia of many different organs on subsequent myocardial IRI, reviewed recently by Bromage¹¹⁹.

The mechanism of RIPC has much in common with that of IPC. Endogenous protective signalling is not unique to the heart: direct IPC is effective in brain¹²⁰, liver¹²¹ and kidney¹²² as well as skeletal muscle¹²³ and skin¹²⁴. The effect is transferrable between organs, with transfer reliant on a thermolabile, hydrophobic moiety between 3.5 and 30kDa in size, which as yet remains unidentified^{125–128}.

Like IPC, RIPC can be conceptualised as a reflex response, with a stimulus, an afferent signalling limb, participation of the central nervous system, an efferent limb and an effector organ. The stimulus is localised ischaemia. In the classic model of RIC, afferent neurones are then activated, relaying the signal to the dorsal motor vagal nucleus (DMVN) in the brainstem, which is seen as the response coordinating centre of the reflex arc. However, elegant experimental work by Jack Pickard at the Hatter has shown, using a factorial study design, that intact vagal supply to the ischaemic tissue is needed to produce the dialyzable humoral factor, which then communicates directly with the heart, as illustrated in Figure 1.6¹²⁸.

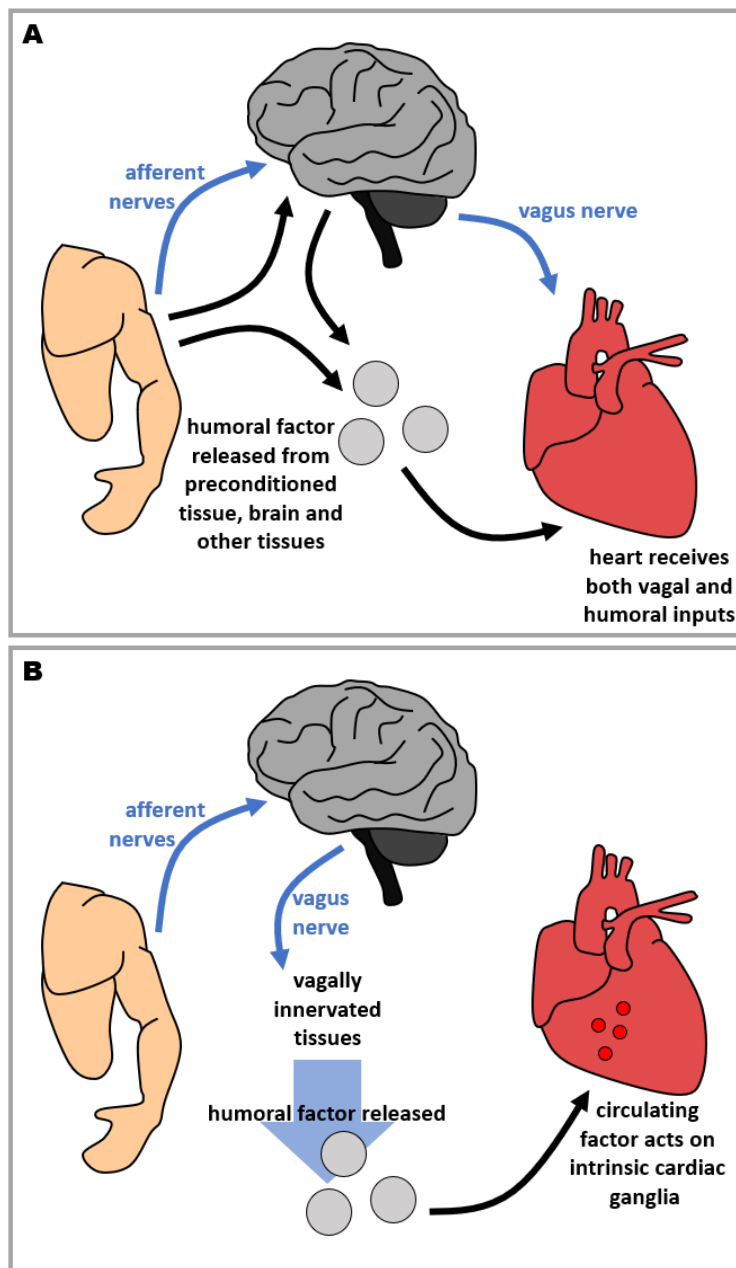


Figure 1.6: Classical (**A**) versus revised (**B**) conceptualisation of the interplay between neural and humoral factors in remote ischaemic conditioning (RIC). In the classical model, afferent nerves and humoral factors act in parallel as the afferent limb of the RIC reflex. Humoral factors also figure in the efferent limb of the reflex along with vagus nerve activation. Pickard showed experimentally however that the afferent limb comprises nerves alone, with the efferent vagus upstream of release of the humoral factors, which only feature in the efferent limb of the RIC reflex, acting directly on intrinsic cardiac ganglia. Adapted from Pickard *et al*¹²⁸.

This recent revision to the RIC concept has rendered much of the previous experiments on RIC mechanism difficult to interpret. RIC can be mimicked by administration of capsaicin, bradykinin or adenosine in distant tissue. However,

experiments implicating any of these substances in the local generation of the RIC signal are outstanding¹²⁹.

Transduction of the RIC signal within the heart has focussed mainly on moieties already implicated in direct IPC. Studies using effluent transfer from preconditioned organs to isolated *ex vivo* heart show that adenosine acts via its A1 receptor on myocardium, which in turn interact with opioid δ and κ receptors^{130,131} to induce a protected state. Stromal derived factor-1 α (SDF α) and bradykinin mimic the RIC response but effluent transfer and target organ blockade experiments, which would locate the site of action in the target organ, are lacking^{132,133}.

The final effector pathway for RIC within the heart is confirmed to involve PI3K¹³⁴ and p42/44 MAPK¹³⁵ by rat and pig experiments in which specific inhibitors given just prior to index reperfusion abrogate the effect of prior RIC. Taken together, these results implicate the RISK pathway as a target organ effector of RIC. Evidence for involvement of the SAFE pathway in RIC has not been forthcoming¹²⁹.

1.2.5.6 Potency of direct vs remote cardioprotection

The mean infarct size reduction reported across all 503 studies included in Wever's 2015 meta-analysis of direct IPC in animals was 24.6%¹⁰⁵. Bromage's systematic review of published animal RIC experiments included just 31 good quality studies with a mean infarct size reduction of 22.2%¹³⁶. Both authors commented that overall study design was poor and quality of reporting suboptimal. Allowing for this, there appears to be little or no reduction in treatment potency when moving from direct to remote ischaemic preconditioning in animal models.

1.2.5.7 Translation of acute cardioprotection

By comparison, the effectiveness of RIC in the clinical setting has been disappointing. A 2015 meta-analysis of clinical RIC studies¹³⁷ included 44 clinical trials reporting on the effectiveness of RIC against three major forms of myocardial IRI: acute MI followed by emergency reperfusion by primary PCI; chronic stable angina / intermittent ischaemia followed by reperfusion with elective PCI; and cardioplegic cardiac arrest and subsequent reperfusion during

on-bypass cardiac surgery. Of these settings, acute MI with early reperfusion by emergency PCI is the closest to the classic animal model of acute IRI used as the setting for most preclinical studies of IRI, thus one would expect the best result in this group.

In fact the largest reductions in biochemical markers of cardiac injury – such as Troponin and CK-MB release from myocardium – were seen in the cardiac surgery trials¹³⁷. Results from RIC used to protect against IRI in PCI are more mixed. The 2015 meta-analysis reports that total CK release is deleteriously affected by RIC in elective PCI¹³⁷ but this may represent random variation given that Troponin release shows a small benefit, and is the more sensitive marker of myocardial necrosis¹³⁸. The effect on Troponin is certainly small, though it does reach statistical significance across the available meta-analyses. All agree that when elective PCI for stable angina is included the benefit to RIC, even on biomarkers, is eroded^{137–139}.

Against this background, three further multicentre randomised controlled trials of RIC reported:

LIPSIA CONDITIONING¹⁴⁰ was a trial of two interventions: 696 patients with STEMI either received PPCI alone or PPCI plus a conditioning intervention. One intervention group received RIC, and another group received RIC plus IPostC. The primary endpoint was infarct size, corrected for area subtended by the infarct artery (termed “myocardial salvage index”) assessed by CMR on the third day of admission. IPostC plus RIC significantly reduced infarct size ($P=0.02$) but RIC alone did not. Interestingly, no IPostC alone group was included, so it is possible that the protective effect was entirely due to IPostC. This explanation is supported by a meta-analysis of 11 IPostC studies suggesting benefit from IPostC alone¹⁴¹.

ERICCA¹⁴² was a trial of RIC during elective coronary bypass surgery, powered to detect reduction in a pooled clinical endpoint of cardiovascular death, nonfatal MI, coronary revascularisation or stroke at 12 months. These were moderate-risk patients (median Euroscore 6) but even so, no statistically significant difference was detected between the RIC and a sham intervention,

both in terms of the primary clinical endpoint, and for secondary endpoints such as biochemical markers of myocardial injury.

White *et al* published a randomised control trial assessing MI size by CMR three to six days after admission with STEMI, in patients randomised to PPCI or PPCI plus RIC with four cycles of five minutes' upper limb ischaemia¹⁴³. In contrast to LIPSIA CONDITIONING, White found a 27% reduction in infarct size, but also found a reduction in myocardial oedema with RIC, which they felt precluded the use of myocardial oedema as a reliable marker to assess the area at risk. Thus, their results were presented as raw infarct size, rather than corrected for the area subtended by the infarct-related artery, which has been common practise since the identification of area-at-risk as a key predictor of infarct size¹⁴⁴. Interestingly, LIPSIA CONDITIONING does not replicate the reduction in myocardial oedema¹⁴⁰.

Thus, the recent picture from clinical trials of RIC remains mixed, in contrast to overwhelmingly positive preclinical studies. Whilst heterogeneity of trial and intervention design probably plays a part¹⁴⁵, there is growing evidence that cardiovascular comorbidities present in human clinical trials subjects but not in healthy young laboratory animals may play a part in blocking RIC. Ageing and type two diabetes, in particular, have been shown to be powerful suppressors of IPC in animal models^{146–148}.

1.3 Diabetes and the myocardium

Long-term data from the Framingham study tell us that patients with diabetes are at roughly double the risk of patients without diabetes for developing heart failure^{149,150}. Once heart failure is established, diabetes significantly increases risk of death and other complications¹⁵¹. Taken together, these observations suggest a direct and toxic effect of diabetes on cardiac function. Given the high prevalence of hypertension, metabolic syndrome and ischaemic disease amongst diabetes sufferers, it is challenging to separate out the direct effects of diabetes on the heart. Whilst accelerated ischaemic heart disease, hypertension and other classical risk factors may account for most of the additional disease burden in DM patients, trial data consistently identify a significant residual risk that is attributable only to diabetes itself¹⁵².

Whilst the epidemiology is complicated by confounding factors from common comorbidities, evidence from human and animal studies suggests mechanisms whereby diabetes may exacerbate the effect of classical risk factors on cardiac muscle structure and function, and its response to intercurrent cardiac ischaemia.

1.3.1 Myocardial metabolism in diabetes

Circulating FFAs and glucose are both increased in diabetes due to reduced hepatic storage¹⁵³. Increased exposure of the heart to circulating FFAs suppresses cardiac glucose metabolism, both directly by causing a shift away from carbohydrate and towards FFA utilisation, and indirectly via reduced function of glucose transporters due to insulin resistance^{154,155}. FFA uptake, storage and oxidation are upregulated, largely under the control of the nuclear transcription factor peroxisome proliferator-activated receptor (PPAR) family^{156,157}. The shift towards fat metabolism is more efficient in terms of ATP production vs substrate usage, but increases oxygen consumption and is deleterious in other ways¹⁵⁸:

FFA storage in the form of triglycerides (TGs) is visible as cellular steatosis, which has been correlated in man with mechanical dysfunction¹⁵⁵. Increased FFA metabolism in turn also increases mitochondrial ROS production from ETC throughput¹⁵⁹, which then has a slew of downstream deleterious effects including mitochondrial DNA damage⁵⁶.

Glucose metabolism is suppressed by up to 40% in the human diabetic myocardium, despite increased availability and uptake of glucose^{155,160}. This results in high levels of intracellular glucose, which may then non-enzymatically glycate cellular components, impeding their function and leading over time to advanced glycation end-product (AGE) formation¹⁶¹. This may have unpredictable downstream effects.

Despite increased production of the proton carriers NADH and FADH₂, flux through the ETC and thus ATP generation via OxPhos is diminished in DM. Two factors are thought to be at play here:

First; under the influence of FFAs, there is an increase in uncoupling proteins (UCPs) in DM, which allow electron flux through the ETC without generation of

ATP. This may account for increased electron leakage and increased mitochondrial ROS production mentioned above¹⁶².

Second; expression and enzymatic activity of ETC components themselves are reduced in diabetic hearts¹⁶³.

Overall, the shift towards FFA oxidation and away from glycolysis and OxPhos increases the metabolic oxygen requirement in the diabetic heart (i.e. decreases cardiac efficiency) by around 86%, potentially increasing vulnerability to ischaemia^{158,164}.

1.3.2 Structural changes hearts of patients with diabetes

The key morphological change in diabetic myocardium is extracellular matrix expansion driven by extracellular fibrosis. This is conserved between human patients with diabetes and animal models¹⁶⁵. Intracellular structural changes are also seen but are less well elucidated.

1.3.2.1 Extracellular fibrosis

Fibrosis may be homogenous “replacement”-type or fibrillar and interstitial in distribution. Whilst it is tempting to ascribe replacement fibrosis to undiagnosed previous myocardial infarction, there is tentative post-mortem evidence that even this extreme fibrotic reaction may occur in diabetes without obstructive IHD¹⁶⁶. More widely accepted is that perivascular and interstitial fibrosis is seen in diabetes due to extracellular accumulation of types I and III collagen, with increased collagen crosslinking attributable to AGE formation and closely linked to increased expression of the receptor for AGE (RAGE)¹⁶⁷.

Homogenous replacement fibrosis is easily identified in man on non-invasive imaging techniques such as cardiac magnetic resonance (CMR) imaging¹⁶⁸. Due to limitations in image resolution, however, identification of frond-like interstitial fibrosis is not yet possible except on histology; CMR techniques can be used to identify extracellular matrix expansion, but not to definitively ascribe it to fibrosis¹⁶⁹. Identifying early fibrosis in man has therefore proven challenging and it is probable that current knowledge under-estimates fibrosis in early diabetic heart disease.

In man, the most convincing evidence of increased fibrillar fibrosis comes from patients with diabetes with impaired systolic function, who necessarily had longstanding and relatively severe heart disease when myocardial biopsies were taken¹⁷⁰. Consequently, it remains uncertain whether heart failure or diabetes is the predominant contributing factor to fibrosis in man. In view of fibrosis having been demonstrated in diabetic animals without overt heart failure¹⁷¹, however, it seems likely that DM on its own does produce fibrosis in man, but that this is significantly exacerbated by development of heart failure later in the course of the disease.

Elaboration of enhanced extracellular matrix requires coordinated action of different cell populations. As the main matrix-producing cells in the myocardium, fibroblasts are critical to the process. Cardiac fibroblasts from diabetic animals consistently produce more collagen and protease inhibitors than non-diabetic controls¹⁷²⁻¹⁷⁴. This activity appears to be under control of angiotensin-2, TGF- β , ROS, and extracellular signal regulated kinase (ERK) signalling¹⁷⁵⁻¹⁷⁸.

1.3.2.2 Intracellular organelles

Within cells, at the ultrastructural level, mitochondria in diabetic CMs have been observed to be smaller and less complex than non-diabetic controls. Although correlations between mitochondrial structure and function are complicated, it is thought that structural changes reflect impaired mitochondrial fusion and decreased fusion protein expression, e.g. mitofusin-2¹⁷⁹. It remains unclear whether structural changes are the cause or effect of altered mitochondrial energetics, though ineffective clearance of damaged mitochondria (i.e. impaired autophagy) probably plays a role¹⁸⁰.

1.3.3 Cardiac function in diabetes

Key functions of the heart are impaired in diabetic subjects. The mechanism of dysfunction is not always clear due to presence of confounders such as hypertension¹⁵⁸, but both clinical and preclinical studies provide robust evidence of impaired diastolic, systolic and electrical function even in early diabetes.

1.3.3.1 Diastolic dysfunction

Echocardiography of well-controlled patients with diabetes without clinical evidence of hypertension or overt heart disease suggests diastolic cardiac

dysfunction in up to 60%¹⁸¹. The absence of detectable diastolic dysfunction in young patients with type 1 diabetes on no medication other than insulin has led to the theory that diastolic dysfunction may relate to metabolic syndrome or diabetes treatments rather than the diabetic state *per se*¹⁸². This hypothesis does not take account of diastolic abnormalities in untreated diabetic animals with a type 1 DM phenotype, and is probably incorrect.

In animal models, reduced diastolic function in DM has been linked to glycation in cardiomyocytes on both structural and functional grounds: Firstly, high glucose promotes cross-linkage of large molecules such as collagen, contributing to myocardial stiffness^{172–174}. Poor active CM relaxation in the diastolic phase has been linked to dysfunction of the calcium sequestration protein SERCA, which in turn has been shown to result from glycation end-product build-up^{183,184}. This is supported by the observation from one study that diastolic function is negatively correlated with HbA1c (a long-term measure of chronic blood glucose content), age and duration of diabetes¹⁸⁵.

1.3.3.2 Systolic dysfunction

Some small observational studies have demonstrated reduced systolic function associated with diabetes^{186,187} in young patients free from other disease. Other studies have reported normal function at rest, but with abnormalities on stress imaging^{188–190}. Where more sensitive assessments such as echocardiographic strain, strain rate and tissue Doppler imaging are used, the likelihood of detecting abnormalities in diabetic patients is increased¹⁹¹.

Persuasively, at the cardiomyocyte level, contractile defects have been related to the effects of glycation products on the ryanodine receptor (RyR) on the sarcoplasmic reticulum^{192,193}. As discussed above, increased intracellular glucose is a characteristic of CMs in diabetes, suggesting a possible causal link between DM and systolic impairment.

1.3.3.3 Electrocardiographic abnormalities

Deranged calcium handling, as described above, and development of cardiac autonomic neuropathy (CAN) both contribute to abnormal electrical activity in the diabetic heart.

Early CAN is characterised by loss of parasympathetic innervation to the heart, with consequent unopposed sympathetic activity. Clinically, this results in raised resting heart rate, reduced heart rate excursion with exercise and abnormal blood pressure response to sleep and orthostasis¹⁹⁴.

Progression of CAN is typified by progressive patchy autonomic denervation in the heart^{195,196}. Adrenergic activity, mediated via cyclic AMP, is a powerful modulator of ionic handling, especially calcium, so that inhomogeneous innervation may result in local electrochemical gradients capable of setting up local re-entry and triggering malignant ventricular arrhythmias¹⁹⁷. In support of this theory, classical markers of inhomogeneous electrical activity on the 12-lead ECG have proven effective predictors of cardiac mortality. Maximal QT interval, QT dispersion and abnormalities of QRS duration all strongly correlate with subsequent risk of death¹⁹⁸. Direct evidence for an underlying arrhythmic mechanism for these deaths is outstanding.

1.3.4 Resilience to ischaemia-reperfusion in diabetes

Compared to patients without diabetes, diabetic patients suffer excess complications following acute infarction events in the heart, brain and peripheral limbs^{199,200}. However, the mechanism of increased complications in the heart remains unclear.

1.3.4.1 Burden of tissue death

There is little consensus in either clinical or preclinical studies on whether hearts from a diabetic host experience more extensive tissue necrosis in response to cardiac ischaemia than hearts from a host without diabetes.

Positron emission tomography and nuclear medicine techniques have been used to compare myocardial scar in patients with diabetes versus patients without diabetes after reperfusion therapy for acute ST-elevation MI. The results conflict, with either no difference²⁰¹ or increased scar size in patients with diabetes^{202,203}. MRI in a mixed population of reperfused and non-reperfused MIs possibly showed larger scar in patients with diabetes, but this study was flawed by conflating diabetes with new-onset hyperglycaemia, so it is not clear what proportion of the study population truly suffered with diabetes prior to admission²⁰⁴.

Biochemical assays to quantify tissue death after reperfused or non-reperfused MI also lack consensus and are confounded by differing release kinetics between patients with, versus patients without, diabetes²⁰⁵. Notwithstanding this caveat, the cohort study EMMACE-2 identified that impaired prognosis of patients with diabetes with prior vascular disease was obviated by correction for blood troponin I as a measure of infarct size²⁰⁶. This is indirect evidence that poor prognosis in MI in patients with diabetes may be due to exacerbation of infarct size. The use of reperfusion therapy is an important confounder in many clinical studies of infarct size. It is well recognised that patients with diabetes tend to gain less from reperfusion than patients without diabetes, with a higher incidence of no reflow²⁰⁷ and other suboptimal results from intervention^{208–210}. This is difficult to control for in the clinical environment where the decision to reperfuse depends on a wide variety of variables²¹¹.

Inflammation Myocardial infarction triggers a reaction characterised by phases of inflammation, proliferation and then maturation, under control of an innate immune response²¹². The innate immune response is activated by necrotic tissue activating alarmin proteins including the protein high mobility group B1 (HMGB1), which is also activated downstream of RAGE in diabetes²¹³. Appropriately regulated inflammation is an essential part of the process whereby infarcted tissue is stabilised mechanically and functionally to form scar in the post-MI heart. This process requires active suppression of the initial inflammatory phase to progress to later phases of healing (proliferation and maturation)²¹⁴. Infiltration of anti-inflammatory cell subsets²¹⁵ and anti-inflammatory signalling from the border-zone of infarction²¹⁶ are both important in moving past the initial pro-inflammatory phase. Failure to suppress the systemically detected inflammatory response one month after MI is associated strongly with adverse prognosis including death and development of heart failure²¹⁷.

Hearts from diabetic animal models consistently exhibit higher markers of inflammation²¹⁸ than from non-diabetic animals, and major pro-inflammatory transcription factors are upregulated^{219–221}. Given the central role played by HMGB1 in both sustaining post-infarct inflammation and in diabetes, it might be supposed that patients with diabetes experience adverse prognosis from MI at

least in part due to dysregulation of the post-infarct inflammatory response. In this paradigm, diabetic patients suffer sustained inflammatory response to infarction, instead of progressing through the proliferation and maturation phases to produce stable myocardial scar in the context of a compensate ventricle. Although this is a compelling theory, there is little direct evidence to support it.

1.3.4.2 Animal models in infarct size studies

Studies of infarct variability in animal models do little to resolve the central question of whether hearts from a host with diabetes are less or more vulnerable. However, they do offer insight into why the question is so difficult to answer.

Many different models of diabetes, and of ischaemia-reperfusion, have been used in study of acute MI in diabetic animals. All have their advantages and drawbacks, and most are valid. A notable – and widely used –exception is the attempt to model diabetes by induction of temporary hyperglycaemia using exogenous glucose, typically administered as an IV or IP injection, or superfused onto cells at high concentration. This strategy is flawed, in that many of the effects of exogenous glucose on cardiac metabolism run counter to the effects of diabetes. For example, impaired intracellular insulin-PI3K-Akt signalling²²², and reduced incretin signalling²²³ are key features of the diabetic heart, but in healthy subjects acute exogenous glucose infusion yields increased insulin-PI3K-Akt transduction, with different effects on incretin signalling depending on the route of glucose administration^{224,225}. Given that both insulin and incretin signalling are crucial to determining extent of IRI, the relevance of exogenous glucose as a model of diabetes in IRI experiments is undermined.

Investigators using *bona fide* models of diabetes differ in their approach to controlling other experimental aspects. A key variable is how long the host animal has been diabetic prior to induction of experimental MI. A typical “acute” model would involve pancreatic ablation with streptozotocin a few weeks prior to infarction^{226–233}, whereas more “chronic” approaches might use animals with an inborn predisposition to diabetes grown for several months^{229,234–240}.

Experiments also vary on ischaemic time, the use of a reperfusion phase and

which metabolic substrates are used in *ex vivo* models of ischaemia. It is not surprising that these very different approaches produce no agreement on the basic question of whether diabetic animals have bigger or smaller infarcts.

In a comprehensive systematic review of ischaemic susceptibility experiments comparing “diabetic” with control animals, the results broke down almost evenly into those indicating excess infarction in diabetes, those showing a protected diabetic state, and those that failed to show a difference either way²⁴¹. It is tempting to look for patterns within the published literature; for example, an association between diabetes duration and infarct size. Whittington herself identified a subset of experiments that seemed to give more consistent results: when an inborn model of diabetes is used, and the heart has access to free fatty acids during index ischaemia-reperfusion, then there is a more consistent suggestion that diabetic hearts sustain more injury than hearts from animals without diabetes^{229,236,242}. However, even within this tiny pool of published data, at least one study finds the opposite, and two show no difference^{238,239}.

It remains unclear whether excess tissue death is a prime driver for impaired prognosis in post-infarct diabetic hearts, and what other diabetes-related factors may modulate the response to ischaemia.

1.3.4.3 Myocardial survival signalling

There is a paucity of data concerning the activity of classical cardioprotective signalling pathways in diabetes, and much conflict between the information that does exist.

Whittington, Tsang and Sivaraman have all undertaken work on myocardial survival signalling in diabetes at the Hatter Cardiovascular Institute, and all have made the link between loss of preconditioning response and reduced signalling through the RISK pathway. There are, however, significant differences in their findings.

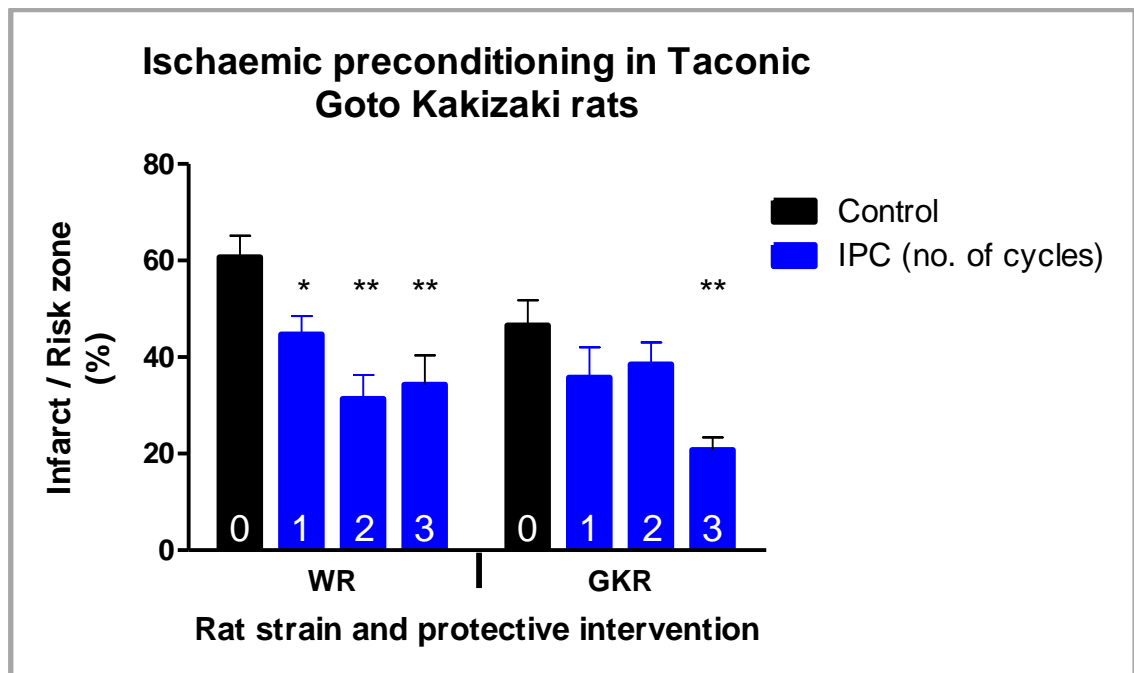


Figure 1.7: Resistance to ischaemic preconditioning in diabetic and non-diabetic rats. A single cycle of IPC is effective at reducing infarct size in non-diabetic WRs, and this effect is maintained with two and three cycles. One and two cycles have no infarct sparing effect in diabetic GKR, however, and only three cycles have an infarct sparing effect in this rat strain. WR: Wistar rat; GKR: Goto Kakizaki rat; IPC: direct ischaemic preconditioning; *: $P < 0.05$ relative to strain-matched control group; **: $P < 0.01$ relative to strain-matched control group. Adapted from Tsang *et al*¹⁴⁷.

Sivaraman describes lower levels of Akt phosphorylation in amputated atrial tissue from diabetic men undergoing elective cardiac surgery²⁴³, whereas Whittington describes higher levels of Phospho-Akt in diabetic than non-diabetic rats²⁴⁴. Tsang and Whittington agree that in diabetic rats there is a failure to acutely increase Akt phosphorylation in response to IPC^{147,244}. Tsang observed this in diabetic rats subjected to ineffective IPC with one or two cycles (Figure 1.7), and Whittington saw the same phenomenon in aged diabetic rats in which IPC failed entirely (Figure 1.8). Of note, Tsang described his animals by weight rather than age, and given the Goto Kakizaki rat's stable weight in adulthood it is difficult to know how old they were, and thus difficult to compare his results with those of Whittington, who showed significant changes in preconditioning success with ageing.

There are two further important areas of agreement between these three investigators:

Firstly, Sivaraman and Tsang agree that a more “intense” ischaemic stimulus is required to elicit a cardioprotective response in diabetes. Sivaraman demonstrated that a longer period of sublethal simulated ischaemia was required in superfused atrial muscle from patients with diabetes to reduce tissue damage by subsequent simulated lethal ischaemia²⁴³. Tsang demonstrated the same “threshold” effect, as diabetic rat hearts required three cycles of IPC to protect against lethal ischaemia whereas rat hearts without diabetes required only one (Figure 1.7).

Secondly, both Tsang and Whittington saw that where IPC remains effective, acute Akt phosphorylation is preserved. Neither investigations, however, had sufficient data on what happens to Akt phosphorylation in non-preconditioned explanted hearts to draw secure conclusions. This is a gap in the existing data.

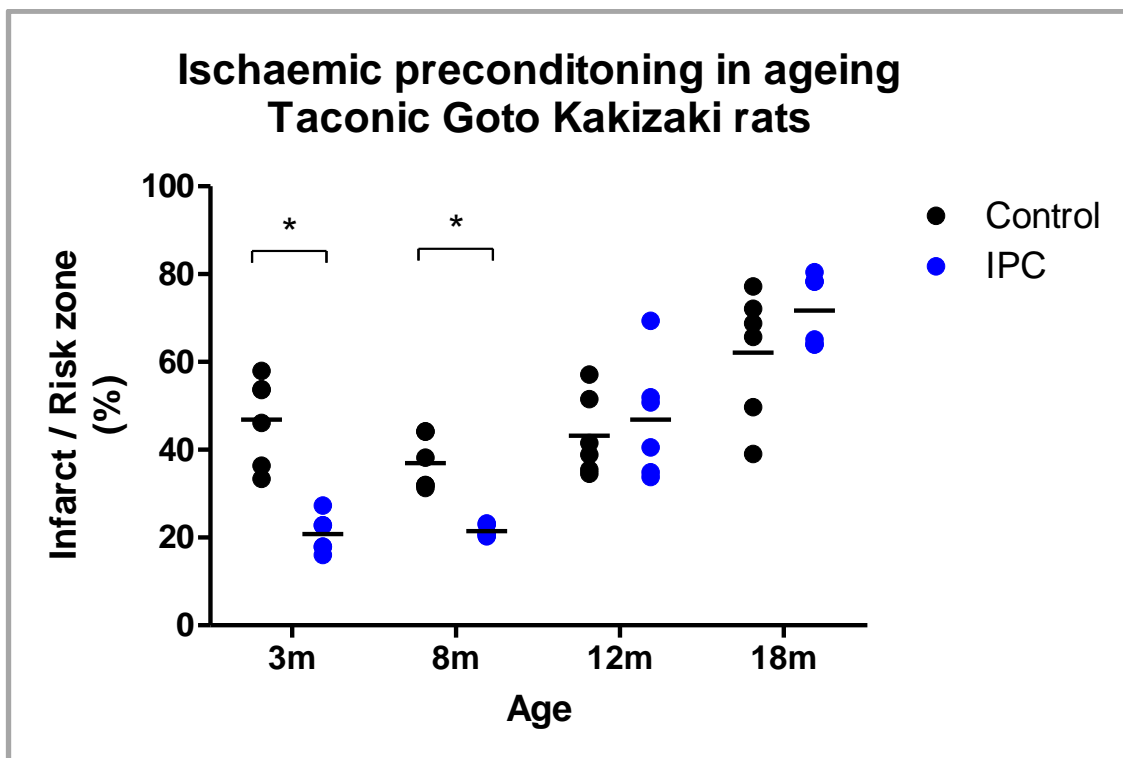


Figure 1.8: Age and ischaemia-reperfusion injury in the Taconic GKR. Whittington found that GKR sourced from Taconic Ltd exhibited increased sensitivity to ischaemia-reperfusion injury, and decreased susceptibility to protection via three cycles of direct ischaemic preconditioning. IPC: ischaemic preconditioning; *: $P < 0.05$. Adapted from Whittington *et al*⁴⁴.

1.3.4.4 Post-infarct remodelling

In contrast to the contradictions surrounding infarct size, there is clear consensus that diabetes promotes adverse remodelling and prognosis following MI regardless of reperfusion strategy. This is reflected in the excess risk of symptomatic heart failure and heart failure complications after MI in diabetes. In one observational study from the pre-thrombolysis era, heart failure affected 26% of diabetic patients with MI versus 16% of patients without diabetes; when the analysis was restricted to patients undergoing second MIs the excess was 50% versus 16%²⁴⁵.

There is thus some epidemiological evidence that the distinction between first and second MI is important, and that serial ischaemic hits are particularly toxic to the diabetic heart.

Adverse cardiac remodelling continues over the long term despite best medical therapy. Patients matched for systolic dysfunction at discharge following a first anterior MI have a far higher chance of readmission with heart failure if they are diabetic (relative risk 2.2)²⁴⁶. This difference persists in a large contemporary cohort matched for a wide range of echocardiographic factors at baseline including LV ejection fraction and end-systolic volume²⁴⁷. In Shah's study, diabetic patients exhibited greater concentric hypertrophy and evidence of raised filling pressures compared to patients without diabetes, suggesting that exacerbation of diastolic dysfunction may drive the difference in late heart failure symptoms.

Disproportionate development of diastolic dysfunction in diabetes after MI is tentatively supported by animal studies. Weeks after experimental infarction *in vivo*, diabetic rats developed excess fibrosis in the infarct border zone, but more significantly also in distant myocardium, compared to non-diabetic controls²⁴⁸. This study did not examine diastolic dysfunction *per se* but increased fibrotic load could reasonably be expected to increase cardiac stiffness.

Counterintuitively, in a rat study that did use echo assessment of diastolic function, most evidence of diastolic dysfunction appeared in diabetic rats that had not undergone MI²⁴⁰. Diabetic rats that underwent MI showed less diastolic compromise, and non-diabetic rats had normal diastolic function. However, the

post-MI echocardiography in this experiment was performed very early, at 24hrs post-MI, and is therefore of dubious relevance as echocardiography certainly predated development of fibrosis in distant myocardium. In addition, echocardiographic measures of diastolic dysfunction are all indirect, and rely on compensatory mechanisms including raised left atrial pressure, to be present.

1.3.5 Diabetes and the myocardium – a summary

The most reproducible findings in diabetic heart are diastolic dysfunction, cardiac fibrosis, altered myocardial energetics and impaired outcomes after ischaemic insults. However, there is little evidence for causative links between altered cardiac function and impaired outcomes; where studies have been carried out into cause and effect – for example on the burden of tissue death – the results are mixed. Partly this is the result of variations in experimental design, but partly it also reflects the lack of therapeutic options for diastolic dysfunction, fibrosis and energetic modulation in the heart; without an effective method for reversing, for example, diastolic failure, it is not possible to show that this is the primary underlying defect.

1.4 Hyperglycaemia and the myocardium

As already discussed, use of hyperglycaemia induced by exogenous glucose as a model of diabetes is over-simplistic and inappropriate (see section 1.3.4.2 - “animal models in infarct size studies”). However, high blood glucose content – as distinct from diabetes - does have effects on the myocardium independent of diabetic state. These effects are worth studying, not least because hyperglycaemia during myocardial infarction predicts higher incidence of post infarct complications. This effect cuts across both diabetic and non-diabetic populations^{15,249–251}.

Transient glycosuria was first identified during acute MI in 1931²⁵²; in more recent studies hyperglycaemia is present in up to half of patients without diabetes undergoing MI and a similar proportion of diabetic patients develop worsening glucose control^{15,250}. Hyperglycaemia during and after myocardial ischaemia predicts poor outcome independently of diabetic status, though interestingly the correlation is much steeper in patients without diabetes^{15,16},

suggesting that diabetic patients may develop a chronic adaptive response to the deleterious effects of hyperglycaemia on myocardium.

1.4.1 Myocardial substrate metabolism during hyperglycaemia

Since early studies in the 1950s, it has been consistently shown that under euglycaemic fasting conditions, the major metabolic substrate for myocardial metabolism is FFAs with only minor contributions from glucose and lactate^{253,254}. In health, however, the myocardium switches to glucose for up to 60% of ATP generation in the postprandial state²⁵⁵.

Evidence for how this switch occurs and the important intermediary signals comes from glycaemic clamp experiments.

1.4.1.1 Glycaemic clamp experiments

In these experiments, differences between arterial and coronary venous blood samples are used to calculate metabolic substrate uptake, typically with radioisotopes used to track fates of glucose, lactate and FFAs.

An early study in dogs²⁵⁶ used a factorial design to examine the effects of clamped hyperglycaemia with and without hyperinsulinaemia, using somatostatin infusion to suppress the normal insulin response to hyperglycaemia induced by glucose infusion. Hyperglycaemia alone had no effect on myocardial glucose uptake but when an appropriate insulinaemic response was permitted, myocardial glucose uptake rose, and plasma FFA levels fell, presumably due to insulin suppression of lipolysis in adipose tissue²⁵⁷. Counteracting the fall in FFAs with an infusion of exogenous FFAs partially suppressed the rise in glucose uptake by myocardium, suggesting that circulating insulin and FFAs are the prime determinants of glucose uptake, rather than glucose availability *per se*²⁵⁶.

FFAs and circulating insulin (rather than glucose availability) also seem to be the prime determinants of glucose uptake in the diabetic heart, as confirmed by a study using positron emission tomography to assess cardiac uptake of 2-[18F]fluoro-2-deoxy-D-glucose²⁵⁸. In type one diabetic patients, Monti *et al* were able to perform hyperglycaemic clamps in the presence or absence of insulin. FFA levels were augmented using intralipid infusion or suppressed with the

niacin derivative acipimox. Myocardial glucose uptake increased with FFA supplementation during hyperinsulinaemia, and with FFA suppression during hypoinsulinaemia. These changes were independent of circulating glucose levels²⁵⁸.

In health, bloodstream content of glucose, insulin and FFAs vary in closely regulated concert. Performing hyperglycaemic clamp experiments without separate manipulation of insulin and FFA leads to an integrated response whereby changing blood glucose content elicits changes in insulin and FFA levels, which then in turn modulate myocardial glucose handling²⁵⁹. Myocardial uptake of glucose increases moderately when blood glucose content is clamped just 3.33mmol/L above baseline fasting levels in healthy men. When the glucose concentration rises to 5.55mmol/L above baseline fasting levels, glucose uptake increases further still. These increases are accompanied by similar increases in lactate uptake and mirrored by profound falls in uptake of FFAs during hyperglycaemia, to less than a third of baseline uptake. Measuring intracellular glycogen and lactate production in the same study showed that the intracellular fate of glucose shifted during hyperglycaemia, with a greater proportion undergoing immediate oxidation on entering cells, suggesting a switch away from FFA metabolism that exceeds the fall in FFA availability²⁵⁹.

1.4.1.2 Stress hyperglycaemia

Glucose clamp experiments, described above, show that the myocardium's ability to switch from FFA to glucose metabolism in the setting of increased glucose availability depends on intact insulin and FFA signalling. Resistance to the effects of insulin impairs this response and decreases metabolic flexibility in the myocardium²⁵⁷.

Loss of the ability to switch metabolic substrate is well-described in the myocardium in diabetes and in chronic animal models of insulin resistance²⁵⁷ but it is less clear how acute changes to insulin sensitivity may impact on minute-to-minute metabolic function in the myocardium. This uncertainty is particularly relevant in stress hyperglycaemia during MI, which is by its very nature a transient phenomenon.

Like the hyperglycaemic clamp, stress hyperglycaemia is characterised by increased glucose in the bloodstream, the chief sources being hepatic gluconeogenesis and glycogenolysis. These processes are under the control of diverse neurohormonal activation, particularly increased activity of the hypothalamic-pituitary-adrenal axis and its chief products cortisol, adrenaline and noradrenaline (reviewed in²⁶⁰). During physiological stress, noradrenaline also increases lipolysis resulting in higher circulating levels of FFAs, whereas during a “pure” hyperglycaemic clamp FFAs tend to decrease, under the influence of the insulin response to hyperglycaemia.

The physiology of stress hyperglycaemia is best typified in sepsis, in which the release of a range of cytokines from diverse sources induces insulin resistance across a range of target cells. TNF- α produced by inflammatory cells, for instance, acts on cells via TLR-4 to block PI3K signalling downstream of the insulin receptor substrate (IRS), inducing peripheral insulin resistance via reduced GLUT-4 translocation²⁶¹ as shown in Figure 1.9:

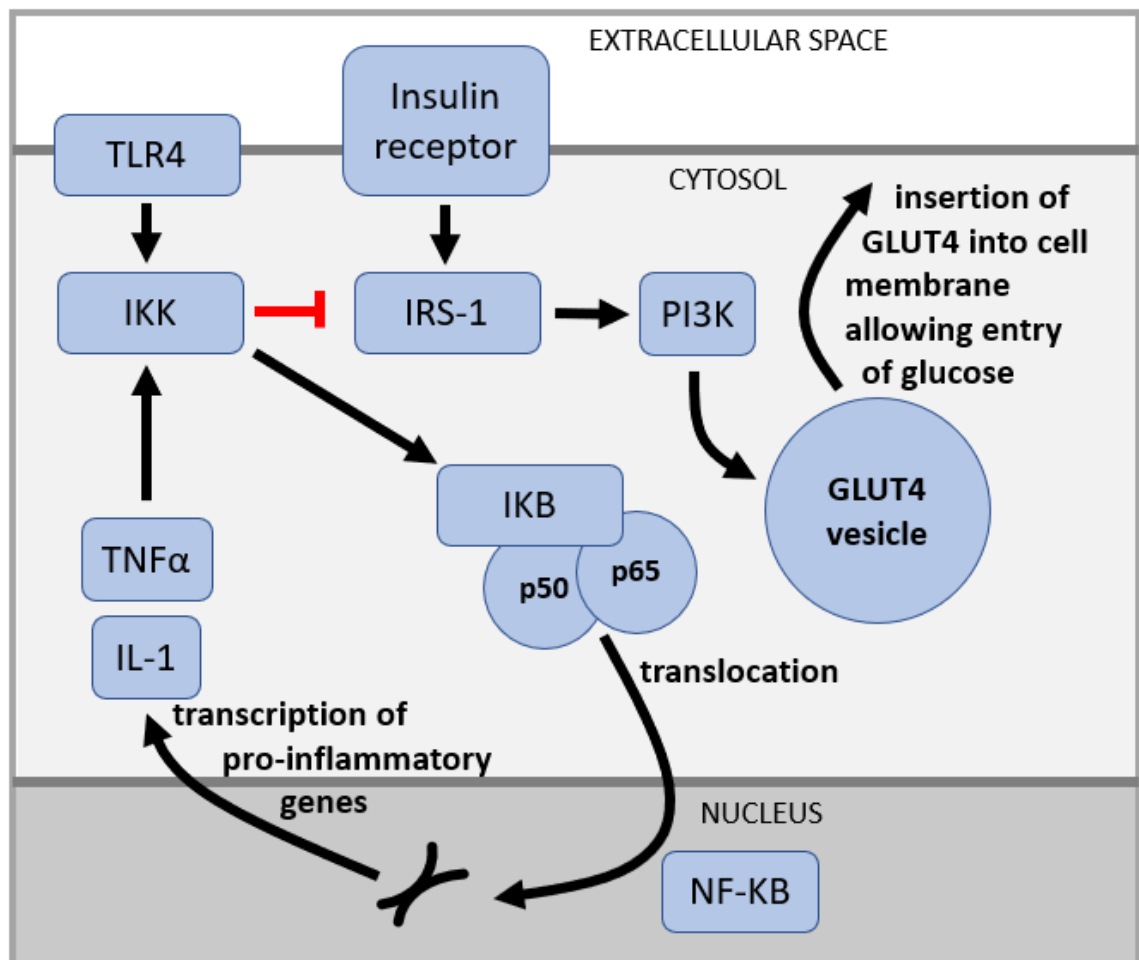


Figure 1.9: Interaction between Toll-like receptor 4 (TLR-4) signalling and insulin signalling during physiological stress induces insulin resistance. Activation of TLR4 causes suppression of IRS-1 signalling via IKK. One of the downstream targets of IRS-1 signalling is the PI3K pathway which transduces the effect of Insulin on the traffic of GLUT4 to the cell membrane. Insulin would usually increase this traffic, however co-activation of TLR4 alongside the Insulin receptor causes suppression of this response. Also downstream of IKK are nuclear transcription factors that upregulate proinflammatory genes including TNF α and IL-1 which then potentiate TLR signalling. GLUT-4: glucose transporter-4; IKB: inhibitor-KB; IKK: inhibitor KB kinase; IRS-1: insulin receptor substrate-1; PI3K: phosphoinosityl-3-kinase. Adapted from Kanety *et al*⁶¹.

1.4.2 Hyperglycaemia and ischaemia-reperfusion injury

It is unknown whether the myocardium itself develops insulin resistance during stress hyperglycaemia, though it certainly does following MI²⁶². Experimental infarction is worsened by activation of TLR-4²⁶³, which is suggestive of a link between insulin resistance and infarct susceptibility.

Hyperglycaemia is a strong risk factor for poor clinical outcomes from ischaemia-reperfusion events both in the heart¹⁶ and in the brain²⁶⁴. This effect cuts across both patients with previously diagnosed diabetes and those without, though there are important differences between these two populations.

1.4.2.1 Blood glucose content predicts early mortality post-MI

Blood glucose content predicts poor outcome from MI consistently across many cohorts studied over the last 40 years, including patients reperfused by thrombolysis²⁶⁵, primary PCI²⁶⁶, and those undergoing no reperfusion therapy^{250,267–269}. Results have not been stratified by STEMI vs NSTEMI, so it remains unclear whether glucose is more harmful in one than the other.

A meta-analysis of studies in the pre-thrombolysis era attributed relative risk of in-hospital death of 3.93 to hyperglycaemia in patients without prior diabetes¹⁵. In the studies pooled for this meta-analysis^{250,270–275}, diabetes was excluded by HbA1c, and hyperglycaemia defined reasonably consistently across studies. Studies with a higher threshold for diagnosing hyperglycaemia tended to identify higher relative risks than those using lower thresholds, which is plausible.

The same meta-analysis identified a relative risk of 1.71 attributable to hyperglycaemia in patients with prior diabetes, or likely prior diabetes based on

HbA1c. Hyperglycaemia was consistently defined in the studies reporting diabetic patients²⁷⁵⁻²⁷⁷ as admission glucose ≥ 10 mmol/L (11mmol/L in one study). The effect of blood glucose content was less strong than in the non-diabetic population examined in the same way; the 95% confidence interval for relative risk crossed the line of identity in each individual study, so that only the pooled relative risk was statistically significant¹⁵.

1.4.2.2 Blood glucose content and other complications of MI

In the absence of reperfusion therapy, hyperglycaemia predicts heart failure and cardiogenic shock on the index admission^{270,272,274,278}. These effects persist when reperfusion therapy is used, and in addition, hyperglycaemia predicts complications²⁷⁹⁻²⁸¹ and failure of reperfusion, including no reflow phenomenon²⁸² and subsequent microvascular obstruction^{204,283,284}.

1.4.2.3 Blood glucose content and burden of tissue death

Observational studies of the relationship between hyperglycaemia and infarct size have significant methodological flaws, but even allowing for this a clear trend has emerged.

All three studies using CMR to evaluate infarct size in a population stratified for hyperglycaemia at admission have reported positive headline associations between infarct size and blood glucose content at admission^{204,283,284}. All three examined only STEMI patients undergoing apparently successful PPCI. Infarct size was reported as proportion of LV tissue mass, with no reference to the concept of an “area at risk”. If anything, this should have made the technique less sensitive, due to variations in coronary anatomy, so the fact that excess tissue death was seen in hyperglycaemic patients suggests the effect is real and large.

However, two of the three studies included low patient numbers (107²⁸⁴ and 93²⁰⁴) and although information on prior diabetic status was collected, results were not stratified by diabetes. These studies provide no information on the relative effects of blood glucose content in the presence vs absence of diabetes, therefore, and it remains possible that the effect seen was only driven by one sub-population or the other.

The largest study, surveying 411 consecutive reperfused STEMI patients²⁸³, was designed to directly compare patients with diabetes and patients without diabetes with and without hyperglycaemia: 88 patients had known diabetes prior to admission, and 323 did not. However, absence of diabetes was not confirmed biochemically, for example with an HbA1c test, so it is possible that some of the “patients without diabetes” were simply undiagnosed. Nonetheless, patterns seen in other – perhaps more rigorous – studies were reproduced, with excess microvascular obstruction, reinfarction and congestive cardiac failure in the diabetic group, suggesting a real difference in glycaemic status between the two groups. The association between hyperglycaemia and larger infarct size seen in earlier studies was also borne out, but with important differences between DM and non-DM populations, which are discussed below.

1.4.2.4 Blood glucose content in patients with and without diabetes

Capes' meta-analysis¹⁵ of studies correlating blood glucose content with outcome from MI hinted at important differences between the effects of hyperglycaemia in patients with diabetes vs patients without diabetes. In summary, the effect of blood glucose content seemed weaker in patients with diabetes, with the relative risk of adverse outcome only reaching statistical significance when all studies were pooled, versus strong signals of harm from small individual studies looking at patients without diabetes.

Studies including patients with diabetes have tended to define hyperglycaemia using higher cut-offs than for patients without diabetes (10-11mmol/L vs 6.7-8.0mmol/L). Of the three studies that have included both DM and non-DM patients^{140,275,278}, only one used the same cut-off of 10mmol/L in both populations²⁷⁸. This was a large observational study including over 3000 patients but, as could be expected, reported a very low prevalence of stress hyperglycaemia in patients without diabetes, as hyperglycaemia was defined very stringently. Such severe hyperglycaemia was, however, a very potent risk factor for poor outcome, conferring a relative risk of 8.82 for congestive cardiac failure or shock²⁷⁸.

It is clear from the remainder of the outcomes studies that even moderate hyperglycaemia in patients without diabetes is sufficient to confer adverse risk. In contrast, Eitel's examination of infarct size stratified by blood glucose content and diabetic status, shows that moderate hyperglycaemia (>7.8mmol/L) is not sufficient to adversely impact patients with diabetes, whereas severe hyperglycaemia (>11.0mmol/L) is²⁸³.

This narrative is given further weight by Kosiborod's authoritative retrospective analysis of inpatient blood glucose content and mortality during 16,871 hospital admissions with MI²⁴⁹. The size and power of this study meant that blood glucose content could be stratified in 0.6mmol/L bands. The resulting curves relating blood glucose content to mortality showed substantial differences between diabetic and non-diabetic patients, confirming earlier suspicions of a weaker (or less steep) effect of hyperglycaemia in diabetes, as shown in Figure 1.10:

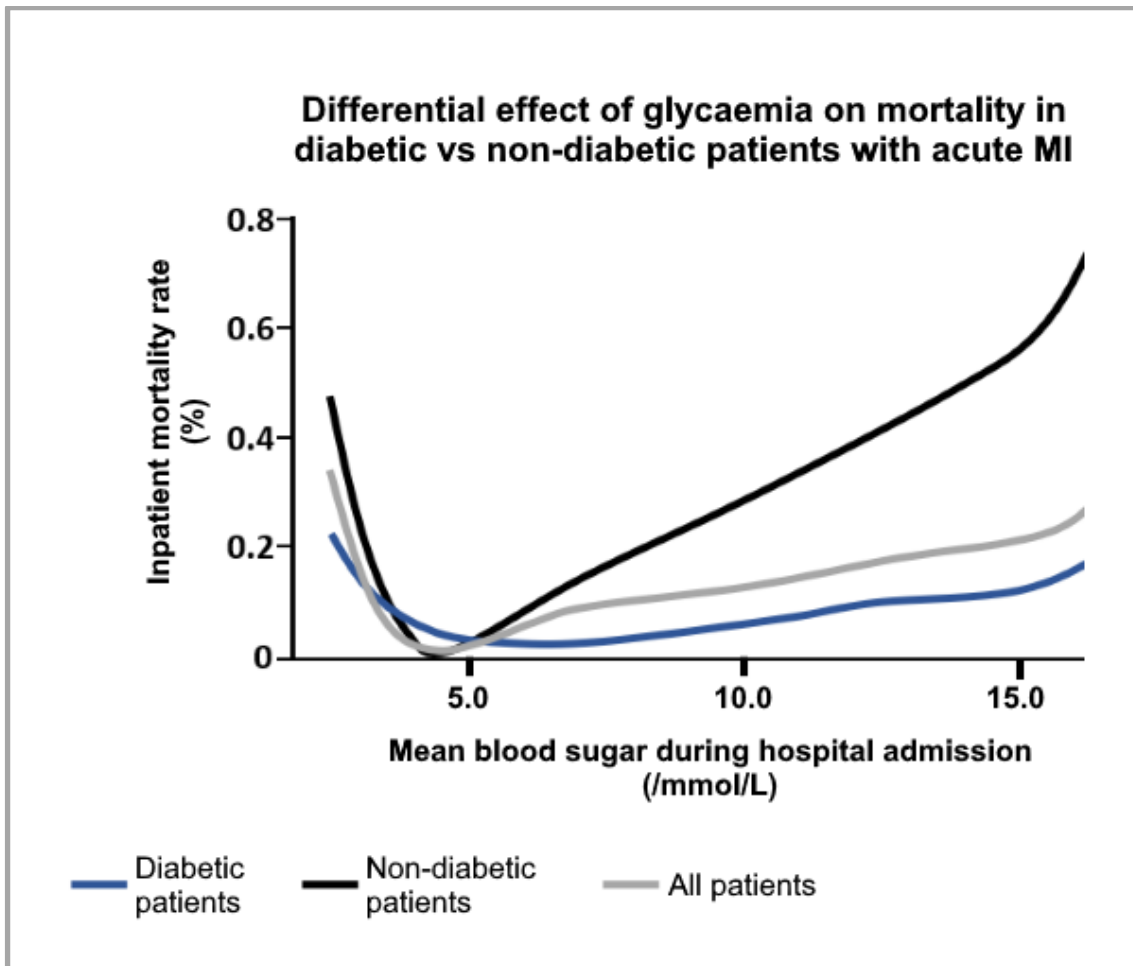


Figure 1.10: Average blood glucose levels vs inpatient mortality during index admission for acute MI. The relationship between blood glucose content and mortality is a J-shaped curve, but significant differences exist between patients with and without diabetes. Nadir inpatient mortality is around 7mmol/L for patients with diabetes but approximately 4.5mmol/L for patients without diabetes. As blood glucose content increases above these levels, there is a steeper increase in mortality for patients without diabetes than those with the condition. Adapted from Kosiborod *et al*⁴⁹.

1.4.2.5 Modulation of ischaemic injury

The best clinical evidence we have is that hyperglycaemia exerts at least some of its deleterious effects during MI by exacerbating tissue vulnerability to infarction. However, due to a lack of studies comparing the effect of high glucose (HG) in reperfused versus non-reperfused MI, we do not know whether excess injury is due to exacerbation of ischaemic or reperfusion cell death.

Studies in animal hearts or isolated cardiomyocytes seem ideally suited to resolving the question of the timing of injury by hyperglycaemia. Studies in whole rat heart have indeed confirmed larger infarct size when IRI occurs during

high glucose induced either by glucose infusion²⁸⁵ or a one-off intraperitoneal injection²⁸⁶. Complementary studies using isolated adult mouse cardiomyocytes again confirmed excess injury, and identified higher levels of oxidative stress in cells subjected to simulated ischaemia-reperfusion perfused in high glucose medium²⁸⁷. However, in all these experiments, HG or normoglycaemia was present throughout pre-ischaemia, ischaemia and reperfusion, so no information was obtained on whether ischaemic or reperfusion injury – or both – was worsened.

1.4.2.6 Evidence for modulation of reperfusion injury

No direct evidence exists linking high glucose availability to increased infarct size specifically in the reperfusion phase of IRI. There is no clinical study demonstrating a greater effect of hyperglycaemia in reperfused MI than MI without reperfusion. However, there is a body of indirect evidence that HG may impair adaptive responses to reperfusion injury.

As discussed above (see section 1.2.5.5 – “Direct ischaemic preconditioning”), preconditioning and preconditioning mimetics exert their protective effect on myocardial survival during the reperfusion phase of injury¹⁰⁸. Experiments in a variety of models of myocardial ischaemia-reperfusion injury have shown that a range of preconditioning interventions are blocked in the presence of high glucose. Similar effects are seen when postconditioning treatments are tested under high glucose conditions. These studies are summarised in Tables 1.1 and 1.2.

The inhibitory effect of high glucose on ischaemic preconditioning may also be present in man. Prodromal angina leading up to MI is reported to be associated with smaller infarct size, and this is interpreted by some to be analogous to preconditioning of the heart by intermittent ischaemia^{288–290}. A study of 549 patients undergoing their first MI in Hiroshima, Japan, suggests that hyperglycaemia abolished the protective effect of prodromal angina²⁹¹. In normoglycaemic patients, prodromal angina associated with a lower risk of 30-day mortality and smaller decreases in LV function, but these differences were absent in patients with blood glucose >11.1mmol/L at admission. This would suggest blockade of clinical ischaemic preconditioning by the presence of hyperglycaemia during MI in man.

Preconditioning and postconditioning both limit infarct size by reducing reperfusion injury, so it follows that if HG blocks pre- and/or postconditioning, then HG is exerting an effect at reperfusion under these circumstances. Indeed, the evidence summarised in Tables 1.1 & 1.2 is secure proof of such an effect. However, this is different from HG having an effect at reperfusion in normal hearts not subjected to any conditioning stimulus. This is a point that is glossed over in much of the conditioning literature: it remains unclear whether conditioning signalling pathways are tonically active in normal hearts and whether the conditioning phenomenon determines infarct size in settings where conditioning stimuli are not specifically invoked. Therefore, although hyperglycaemia inhibits conditioning it is not clear whether this is the mechanism by which HG impacts infarct size in the clinical setting.

Preconditioning treatment	Model of reperfusion	Result	Reference
Remifentanyl 1µmol/L for 20mins	Isolated neonatal rat ventricular cardiomyocytes sIRI	Remifentanyl pretreatment improved cell survival but this effect was reduced by switching from 5.5mmol/L to 25.5mmol/L Glucose medium	292
Ischaemic preconditioning (2x 5/5min cycles)	<i>In vivo</i> mouse LAD occlusion	IPC reduced infarct size in control mice but not in mice preinjected with 2g/kg glucose IP	286
Ischaemic preconditioning (2x 5/5min cycles)	<i>Ex vivo</i> rat LAD occlusion	IPC reduced infarct size in rat hearts perfused with 11mmol/L glucose but increased infarct size in hearts perfused with 22mmol/L glucose	293
Isoflurane 0.5mmol/L for 10mins	Cultured diabetic and non-diabetic human cardiomyocytes sIRI	Isoflurane pretreatment improved cell survival but this effect was abolished by switching from 5mmol/L to 11mmol/L glucose medium.	294
Ischaemic preconditioning (4x 5/5min cycles)	<i>In vivo</i> mouse LAD occlusion	IPC reduced infarct size in control mice but not in mice preinjected with 2g/kg glucose IP	295
Ischaemic preconditioning (1x 5/15min cycle)	<i>In vivo</i> rabbit LAD occlusion	IPC reduced infarct size in control rabbits but not in rabbits infused with 15% glucose IV throughout the protocol	295
Ischaemic preconditioning (4x 5/5min cycles)	<i>In vivo</i> mouse LAD occlusion	IPC reduced infarct size in control mice but not in mice preinjected with 2g/kg glucose IP	296
Ischaemic preconditioning (4x 5/5min cycles)	<i>In vivo</i> dog LAD occlusion	IPC reduced infarct size in control dogs but not in dogs infused with 15% glucose IV during preconditioning only	297
Ischaemic preconditioning (4x 5/5min cycles)	<i>In vivo</i> dog LAD occlusion	IPC reduced infarct size in control dogs but not in dogs infused with 15% glucose IV during preconditioning only	298
Isoflurane 2.1% for 30mins	<i>In vivo</i> rabbit LAD occlusion	Isoflurane reduced infarct size in control rabbits but not in rabbits	299

		infused with 15% glucose IV during preconditioning only	
Isoflurane 1.4% for 30mins	<i>In vivo</i> mouse LAD occlusion	Isoflurane reduced infarct size in control mice but not in mice preinjected with 2g/kg glucose IP	300
Ischaemic preconditioning (1x 5min cycle 24hrs prior to infarction)	<i>In vivo</i> rabbit LAD occlusion	IPC induced second window protection, reducing infarct size in control rabbits, but not in rabbits infused with 50% dextrose IV before and during infarction	226
Isoflurane (dose not stated)	<i>In vivo</i> dog LAD occlusion	Isoflurane reduced infarct size in control dogs but not in dogs infused with 15% dextrose prior to and during isoflurane administration only	301

Table 1.1: Studies examining potency of preconditioning treatments in high glucose vs low glucose conditions.

Postconditioning treatment	Model of reperfusion	Result	Reference
Remifentanyl 1µmol/L for 20mins	Cultured H9c2 cardiomyoblasts	Remifentanyl given at reoxygenation improved cell survival in cells cultured in 5.5mmol/L glucose but not in cells cultured in 25.5mmolL glucose medium	302
Isoflurane 2.1% for 5mins	<i>In vivo</i> rabbit LAD occlusion	Isoflurane given at reperfusion reduced infarct size in control rabbits but not in rabbits infused with 15% glucose IV during ischaemia and early reperfusion	303
Diazoxide 10mg/kg	<i>In vivo</i> rat LAD occlusion	Diazoxide given at reperfusion reduced infarct size in control rats but not in rats infused with 50% dextrose IV throughout the protocol	304
Fasudil 150µg/kg	<i>In vivo</i> rat LAD occlusion	Fasudil given at reperfusion reduced infarct size in control rats but not in rats infused with 50% dextrose IV throughout the protocol	304
Desflurane (dose not stated)	<i>In vivo</i> rat LAD occlusion	Desflurane given at reperfusion reduced infarct size in control rats but not in rats infused with 50% glucose IV prior to and during ischaemia	305
Desflurane (dose not stated)	<i>In vivo</i> rat LAD occlusion	Desflurane given at reperfusion reduced infarct size in control rats but not in rats infused with 50% glucose IV during ischaemia only	305
Sevoflurane (dose not stated)	<i>In vivo</i> rat LAD occlusion	Sevoflurane given at reperfusion reduced infarct size in control rats but not in rats infused with 50%	306

		glucose IV during ischaemia and early reperfusion	
Levosimendan (10µg/kg)	<i>In vivo</i> rat LAD occlusion	Levosimendan given at reperfusion reduced infarct size in control rate but not in rate infused with 50% glucose IV throughout ischaemia and reperfusion	307
Isoflurane 2.1% for 5mins	<i>In vivo</i> rabbit LAD occlusion	Isoflurane given at reperfusion reduced infarct size in control rabbits but not in rabbits infused with 15% glucose IV during ischaemia and early reperfusion	308
Sevoflurane 2.4% for 15mins	Neonatal rat cardiomyocytes sIRI	Sevoflurane given at reoxygenation improved cell survival in cells cultured in low glucose medium (concentration unspecified) but not in cells cultured in 30mmol/L glucose.	309

Table 1.2: Studies examining potency of postconditioning treatments in high glucose vs low glucose conditions.

1.4.3 Hyperglycaemia and myocardial survival signalling

As discussed above, hyperglycaemia is widely reported to block cardioprotective signalling in animal models of myocardial infarct and other myocardial stresses. In addition to the blockade of cardioprotective interventions listed in Tables 1.1 and 1.2, intrinsic cardioprotection mediated by GLP-1 signalling is also negated by high glucose perfusate³¹⁰. Given that most of these cardioprotective interventions are reported to act via RISK signalling, this suggests an inhibitory effect of HG on RISK, but there is no data directly confirming that RISK is suppressed in the non-conditioned heart subjected to HG perfusion.

1.4.4 Hypoglycaemic agents to reduce infarct size

High glucose clearly predicts MI complications and survival, with circumstantial evidence that this may be a causal relationship via modulation of ischaemia-reperfusion injury. Over the last 25 years, various attempts have been made to improve prognosis – and potentially reduce IRI – by manipulating glucose transport around the time of myocardial infarction.

1.4.4.1 Insulin

In addition to potential benefits from reducing hyperglycaemia, insulin also has a direct and glucose-independent effect on IRI, via recruitment of RISK at reperfusion. It thus acts as a conditioning mimetic to reduce reperfusion cell death^{80,311,312}. Clinical interventions with insulin during MI therefore fall into two groups: those aiming to normalise high blood glucose and those in which glucose is given along with insulin and potassium (“GIK infusion”) as a conditioning mimetic.

1.4.4.1.1 Insulin for glucose normalisation

The DIGAMI and DIGAMI-2 trials targeted correction of blood glucose in patients with known diabetes, or glucose >11mmol/L presenting with MI. DIGAMI reported dramatic and early divergence of survival curves (see Figure 1.11) associated with targeting blood glucose 7-11mmol/L by insulin-glucose infusion for at least 24hrs, starting during the hospital admission and by multidose subcutaneous insulin dosing for six months thereafter³¹³.

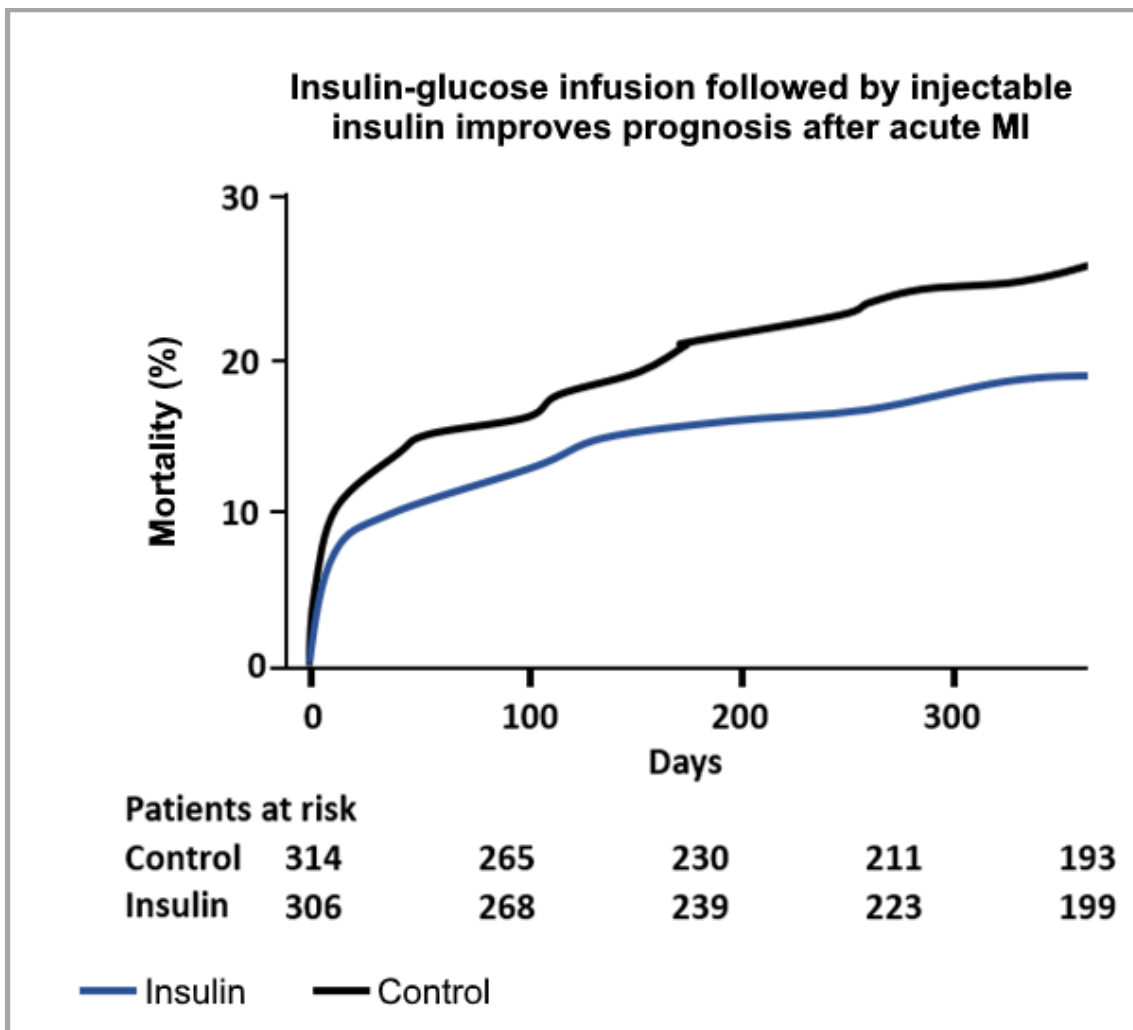


Figure 1.11: Results of the DIGAMI trial showing improved survival following MI associated with early insulin infusion targeting blood glucose 7-11mmol/L and injectable insulin for six months thereafter. Adapted from Malmberg *et al*¹³.

One potential explanation for the very early divergence in survival curves seen in DIGAMI is insulin working to reduce IRI, either via normalising blood glucose or as a direct conditioning agent. This possibility was addressed with a revised trial design; in DIGAMI-2, hyperglycaemic MI patients were randomised to insulin infusion during MI, insulin infusion during MI followed by long-term injectable insulin, or routine care³¹⁴. This second trial reported no difference in primary or secondary outcomes between the treatment groups. Trial design was strikingly similar between DIGAMI and DIGAMI-2 and the failure to reproduce the results of DIGAMI has been much discussed. DIGAMI-2 was, however, grossly under-sized with only 50% power to detect 25% reduction in mortality between treatment groups. Although the inclusion criteria were the same for DIGAMI and DIGAMI-2, patients in DIGAMI-2 had lower glucose readings at

randomisation (mean glucose 12mmol/L vs 15mmol/L), which also may have eroded the therapeutic benefit of glucose normalisation. On the basis of the original DIGAMI results glucose normalisation by insulin infusion remains an important adjunct to routine clinical care in hyperglycaemic MI patients³¹⁵. No distinction is currently drawn in the guidelines between management of peri-infarct hyperglycaemia in patients with vs without diabetes.

1.4.4.1.2 Insulin as a conditioning mimetic

Preclinical evidence is conclusive that supraphysiological concentrations of insulin administered at reperfusion recruits RISK signalling and reduces reperfusion injury. This has been shown both in isolated cardiomyocytes and intact isolated small mammal hearts^{80,311}. *In vivo*, high dose insulin must be accompanied by glucose and potassium (GIK infusion) to avoid hypoglycaemia and hypokalaemia via increased intracellular uptake under the influence of insulin. GIK infusion at reperfusion reduces infarct size *in vivo* in healthy rats³¹⁶.

Evaluation of GIK infusion in the clinical setting has been extensive, beginning in the 1960s. In non-reperfused MI, meta-analysis showed clinical benefit with a statistically significant reduction in in-hospital mortality from 21% to 16%³¹⁷, presumably by modulation of ischaemic injury.

More recent trials have examined efficacy in ameliorating injury in patients undergoing reperfusion, and results have proved mixed. Results of three major clinical trials are given below:

A pilot study (ECLA) tested two GIK preparations, high dose (25% glucose, 50IU soluble insulin, 80mmol KCl) and low dose (10% glucose, 20IU soluble insulin, 40mmol KCl), and found a 66% reduction in early mortality for reperfused MI, when the two intervention arms were pooled and compared to the control arm. This was a small study with a puzzlingly high mortality rate in patients undergoing reperfusion with either thrombolysis or PPCI (12 out of 79 patients died)³¹⁸.

The first large study to recruit only patients undergoing PPCI was the single-centre GIPS study³¹⁹. GIPS tested a high-dose GIK infusion started within 20mins of presentation with MI symptoms, and showed reduction in mortality in

patients without heart failure at presentation; no benefit was seen in patients presenting with heart failure³¹⁹.

The definitive clinical trial of GIK was CREATE-ECLA, in which 20,201 patients with STEMI were randomised across 470 centres to either standard care or standard care plus high dose GIK infusion. Unusually, this study was half of a larger factorial design also testing treatment with the low molecular heparin reviparin vs placebo³²⁰. No significant difference in 30-day mortality was seen between GIK and standard care, either in the study population as a whole, or in prespecified subgroup analysis by admission blood glucose content, heart failure and time from symptom onset. This obviously contradicts the earlier findings of GIPS; notable differences in design between these two large trials include use of PPCI only (in GIPS) vs use of thrombolysis or PPCI (in CREATE-ECLA) as well as timing of the study intervention. In GIPS, the study infusion was commenced 15-20mins after admission and the mean door-to-balloon time was 46mins, implying that the infusion was begun before the reperfusion event in most patients. However, in CREATE-ECLA, 82% of patients only received the study treatment after reperfusion had taken place.

The GIPS investigators then ran a second study (GIPS-II) to address the relatively small size of their initial study subgroup without heart failure. The study intervention was subtly different in this trial, with fixed rate glucose and potassium infusion, but variable rate rapid acting insulin titrated to serum blood glucose³²¹. 889 patients undergoing reperfusion therapy (PPCI, thrombolysis, or thrombolysis with rescue PCI) for STEMI were randomised 1:1 to standard care or study intervention in an open-label design. 30-day mortality was the same in the two groups; the study was terminated early after interim analysis suggested a statistically significant difference was unlikely to be achieved. Precise timing of the study infusion was not reported in this study. In the event, less than 10% of the patients in GIPS-II were treated with thrombolysis or rescue PCI, ruling this out as a reason for failure of the study intervention.

Based on these disappointing trial results, there now exists a consensus that GIK infusion is not beneficial in normoglycaemic patients with MI undergoing reperfusion therapy. However, there are significant gaps in the evidence

supporting this position and the largest trial, CREATE-ECLA, remains difficult to interpret due to late use of GIK infusion in most patients.

1.4.4.2 Glucose uptake modulation

Administration of insulin increases facilitated glucose transport into metabolically active cells, including cardiomyocytes, by activation of IRS1-PI3K signalling and regulated transport of GLUT-4 – facilitative glucose transporters – to the cell surface membrane³²². One potential explanation for the disappointing results of DIGAMI-2 and trials of GIK is that the beneficial effects of insulin on blood glucose content and RISK recruitment is balanced out by harmful effects of acutely increasing intracellular glucose, and triggering increased ROS production at reperfusion. This raises the possibility that reduction (but not complete blockade) of glucose uptake by cardiomyocytes may be beneficial during ischaemia-reperfusion.

1.4.4.2.1 SGLT blockade as a cardioprotective strategy

Facilitative glucose transport is carried out by two families of glucose transport molecules: the GLUTs, as discussed previously, and sodium/glucose cotransporter proteins (SGLTs 1 to 6)³²³. The major physiologically active SGLTs are isoforms 1 and 2, mediating glucose uptake in the gut, and glucose reabsorption from the proximal convoluted tubule, respectively³⁵. The remaining members of the family do not transport glucose, but are implicated in glucose sensing (SGLT3), transport of mannose (SGLT4 & 5) and transport of inositol (SGLT6)³²³.

SGLT inhibitors were developed as hypoglycaemic agents, targeting SGLT1 and SGLT2 to reduce intestinal glucose absorption, and renal glucose resorption from the proximal convoluted tubule. SGLT2 is the more attractive target, responsible for ~97% of renal tubular glucose reabsorption, whereas SGLT1 occurs in the gut and sundry other tissues, and modulation may be associated with unwanted gastrointestinal side effects³²⁴.

Tubular glucose reabsorption is central to the development of hyperglycaemia, as there is no physiological mechanism limiting glucose resorption from the renal tubular filtrate, so that diabetic glycosuria leads to increased glucose

resorption and retention which in turn contributes to spiralling hyperglycaemia – a rare example of biological positive feedback.

Initial clinical trials of SGLT inhibitors focussed on their ability to suppress blood glucose. A range of molecules (e.g.: Dapagliflozin, Canagliflozin and Remogliflozin), proved very effective at improving glycaemic control both *de novo* and as add-on therapy for patients failing on other hypoglycaemic treatments^{325–328}.

US Food and Drug Administration regulations now require cardiovascular outcome safety trials for all new antidiabetes agents³²⁹. Thus, adequately powered cardiovascular outcomes trials have been conducted for all the SGLT inhibitors brought to market; these have reported intriguing patterns of risk reduction.

The EMPA-REG OUTCOME trial³³⁰ randomised 7,020 patients with diabetes and cardiovascular disease (angina, recent MI or stroke) to either Empagliflozin at high or low dose (10mg or 25mg daily) or placebo. Other oral hypoglycaemics were stopped 12 weeks prior to randomisation then reintroduced. Over 2.6 years' median follow-up, cardiovascular death was 38% lower, heart failure hospitalisation 35% lower and all-cause mortality 32% lower in the treated versus the placebo group. These striking outcome reductions occurred despite no reduction in myocardial infarction or stroke, and despite poor achievement of target blood sugars in all three arms of the study. HbA1c did drop slightly in both the control and active arms of the study, but differences in outcome are not explained by differences in glycaemic control. Meta-analysis of large scale macrovascular outcomes studies suggests that the difference in HbA1c seen between treatment groups in EMPA-REG predicts a reduction in major cardiovascular events of around 10%, but that it is insufficient to have an effect on cardiovascular or overall mortality^{331,332}.

CANVAS and CANVAS-Renal were pre-approval and post-approval outcome trials of Canagliflozin. Pooled analysis of these included 10,142 diabetic patients randomised to 100mg or 300mg daily of the drug, or placebo control³³³. Inclusion criteria conferred at least moderate cardiovascular risk, with patients either aged over 30 with established atherosclerotic disease or aged over 50

with two or more major risk factors. Over 2.4 years' median follow-up, a composite endpoint of cardiovascular death, nonfatal MI and nonfatal stroke occurred less in the treated arms than the placebo arm with a hazard ratio of 0.86. No component of the composite endpoint reached statistical significance on its own. The exploratory endpoint of heart failure hospitalization occurred less frequently in the active treatment arm of CANVAS-Renal; analysis was restricted to part of the dataset for these outcomes due to the prior publication of the CANVAS dataset as part of the FDA approval process^{333,334}.

Taken together, EMPA-REG and the CANVAS trials suggest a class effect of SGLT2 inhibitors on cardiovascular mortality and heart failure, but the evidence is not conclusive. EMPA-REG is a stronger trial design than CANVAS, with more straightforward statistical analysis and more clear-cut results. Both trials agree that any improvement in mortality and heart failure occurred without a significant reduction in ischaemic events suggesting improved tolerance to ischaemia-reperfusion, resulting in reduced death and heart failure following MI. Early breaking results of the DECLARE-TIMI 38 outcome trial of Dapagliflozin may support a similar interpretation³³⁵.

Preclinical evidence from experiments in mouse brain suggests that SGLT function during ischaemia-reperfusion events is complex and differs between the ischaemic and reperfusion phases, and between normo- and hyperglycaemia. Brain is better studied than heart in this setting. During cerebral ischaemia, the glucose sensor SGLT3 aids cell survival, and SGLT3 knockdown mice suffer larger cerebral infarcts following irreversible middle cerebral artery occlusion. SGLT1 blockade, contrastingly, has no effect under normoglycaemia, but is deleterious to neurons subjected to oxidative stress under hyperglycaemia^{336–338}.

Translating these insights to the heart is complicated by contradictory evidence regarding SGLT expression in cardiac tissue. It remains unclear to what extent different cardiac cell types express the various SGLT isoforms, and evidence from protein assays conflict with findings from mRNA. In terms of function during IRI, one study reports that a model of chronic myocardial ischaemia induces increased SGLT1 expression, suggesting a role as a glucose scavenger in situations of low supply³³⁹. In support of this, a single well-

designed experiment has shown that continuous treatment with a selective SGLT1 blocker exacerbates infarct size in isolated perfused mouse hearts subjected to ischaemia-reperfusion under normal glucose conditions³⁴⁰.

It remains untested whether acute SGLT inhibition specifically during myocardial reperfusion is beneficial.

1.4.5 Hyperglycaemia and the myocardium – a summary

Hyperglycaemia is a transient phenomenon that may occur on a background of chronically impaired glucose regulation, including diabetes, or without a history of previous metabolic disease. In patients without diabetes, HG is the result of acute physiological stress, and is common in severe illness such as acute MI. Irrespective of the diabetic state, HG confers an adverse prognosis on patients with MI and that effect is stronger in patients without pre-existing diabetes. The weight of evidence from animal studies would suggest that at least part of the deleterious effect of HG is via exacerbation of either ischaemic or reperfusion cell death, though it remains unclear which, and to what extent the effect varies between patients with vs without diabetes, and to what extent the effect may be ameliorable.

Intervention with insulin to reduce complications of MI by acute control of glucose has proved disappointing, and the fact that insulin paradoxically increases intracellular glucose may be relevant. Novel hypoglycaemic agents such as the SGLT inhibitors do not increase intracellular glucose and this may explain why they have shown disproportionate prognostic benefit in patients with ischaemic diseases. Evidence for their mode of action in myocardial reperfusion injury remains outstanding, however.

1.5 Overall hypothesis

With this background in mind, we hypothesised that hearts from patients and animals with diabetes would suffer more cell death in response to a standardised ischaemic insult than hearts from non-diabetics, and that this increased vulnerability could be explained by failure of intrinsic cytoprotective mechanisms due to both the diabetic state and of high blood glucose content.

1.6 Research objectives

This work coalesced into several smaller aims which are outlined below and expanded on in the chapters that follow:

1. To establish and verify rat models of *ex vivo* myocardial infarction, *ex vivo* direct ischaemic preconditioning and *in vivo* remote ischaemic preconditioning. Experiments to achieve this objective are described, along with other general methodologies, in Chapter 2.
2. To verify the relevance of a rat model of diabetes in which to investigate further the interplay between diabetic state, hyperglycaemia and infarct size. Experiments to achieve this objective are described in Chapter 3.
3. To demonstrate that our rat model of diabetes exhibits impaired cardioprotection via direct and remote conditioning. Experiments to achieve this objective are described in Chapter 4.
4. To investigate the alterations in RISK signalling that accompany the expected failure of cardioprotection in our rat model of diabetes. Experiments to achieve this objective are also described in Chapter 4.
5. To investigate to what extent hyperglycaemia exacerbates reperfusion, as opposed to ischaemic, injury, and how this differs between diabetic. Experiments to achieve this objective are described in Chapter 5.
6. To investigate the mechanism by which hyperglycaemia exacerbates reperfusion injury in the non-diabetic heart. Experiments to achieve this objective are also described in Chapter 5.

2. GENERAL METHODS

2.1 Animals

All animal use was in accordance with the United Kingdom Animal Scientific Procedures Act (1986)³⁴¹ under project licence 70/7140. For animals bred at UCL, pups were routinely weaned and sexed at 21 days, and excess female pups euthanased except for those kept for breeding. Males were grown on to adulthood as needed. Access to standard chow and water was *ad libitum* and a standard 12-hour light/dark cycle was used. Environmental temperature was maintained at 21°C.

2.1.1 Sprague Dawley rats

A colony of Sprague Dawley rats is maintained by the Biological Services Unit at University College London, established from founder rats obtained from Harlan Laboratories (Oxon, UK). Male SDRs were obtained aged three months from UCL stock and maintained as a segregated colony within the animal facility until the appropriate age for use in these studies.

SDRs are an outbred white rat, first achieved by crossing Wistar rats to hybrids of laboratory and wild rat stocks. SDRs are the rats most often used in experimental modelling of acute myocardial infarction, despite having variable coronary anatomy, particularly with respect to branching of the left coronary artery³⁴². Variable anatomy may have a knock-on effect on the size of the region subtended by an individual arterial branch and may interfere with attempts to achieve reproducible ischaemic burden by surgical arterial occlusion. The mechanism of this - and correction for it - is discussed in section 2.4.4 ("Regional myocardial ischaemia").

SDRs are also frequently used as a non-diabetic control animal, as they do not exhibit spontaneous features of diabetes over a normal lab rat lifespan. Diabetes may be experimentally induced by complete pharmacological pancreatic ablation using streptozotacin, partial pancreatic ablation using low or chronic dosing of the same drug, or surgical resection of the pancreas³⁴³. Any of these techniques may be used in combination with high fat diet, which augments the phenotype by induction of peripheral insulin resistance. In contrast to other rat strains used here, there are no reports of age or dietary modification alone resulting in overt hyperglycaemia or diabetic complications in

SDRs. Although half will develop diet-induced obesity on a lab chow diet, only after five generations of selective breeding for this feature does this translate into significantly higher basal insulin and glucose levels. Even in these selectively bred F5s, handling of an oral glucose load is still comparable to wild-type controls³⁴⁴. SDRs can therefore be considered at low risk of a spontaneous diabetic phenotype, and thus were chosen as the non-diabetic control animal in these studies, where maintenance of normal insulin metabolism over time is an important feature.

2.1.2 Wistar white rats

Male Wistar rats were obtained aged three months from Charles River Ltd (Margate, UK) and kept in house at the UCL Biological Services Unit until being used. Once at UCL they were kept in the same conditions as the other strains.

WRs are an outbred strain of white rat, first bred at the Wistar Institute in 1906 for biological and medical research. Like Sprague Dawley rats, they have low potential for spontaneous development of diabetes or hyperglycaemia, but may be subject to pharmacological or surgical intervention to reproduce aspects of the condition. Unlike SDRs, selective breeding over many generations has produced an overtly hyperglycaemic and diabetic substrain³⁴⁵: the Goto Kakizaki rat, described below.

2.1.3 Goto Kakizaki rats

Founder rats were obtained from Taconic Ltd (Denmark) in the mid-1990s and used to establish a breeding colony of GKR rats at UCL. Breeding and husbandry arrangements were similar to those for SDRs kept in the same facility, save for the need to house GKR rats fewer per cage due to aggressive behaviour in older animals.

2.1.3.1 Origins of the Goto Kakizaki rat

The inbred GKR strain was produced from outbred Wistar rats at Tohoku University by Goto et al. From a wild type WR colony, selective breeding of normal WRs over 35 generations produced an overtly hyperglycaemic population. Individuals with the poorest tolerance to an oral glucose load were selected for breeding; individuals whose glucose tolerance fell outside the “normal range” were excluded. It is not clear what is meant by the “normal

range”, but the implication in near contemporary publications is that normal distribution curves were constructed for each inbred generation, and outliers excluded³⁴⁶. Fasting glucose was seen to gradually deteriorate over the breeding programme, with clear-cut glucose intolerance after five generations:

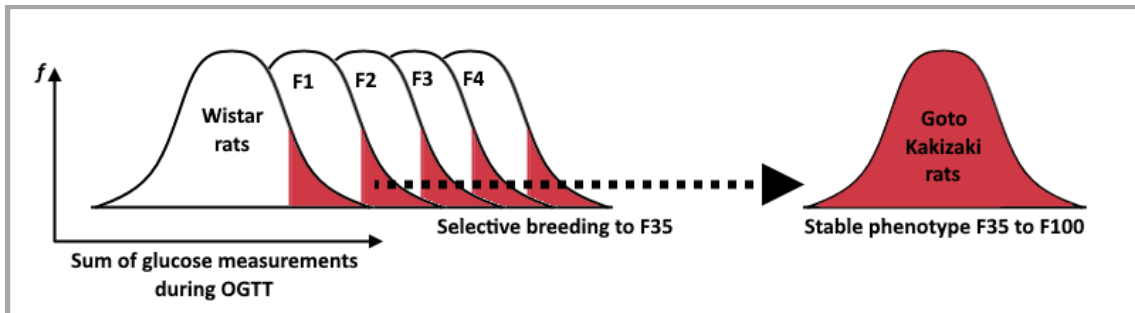


Figure 2.1: Evolution of glucose intolerance with selective breeding of the Goto Kakizaki rat. Red area: hyperglycaemic outliers compared to wild type Wistar rat population. Adapted from Portha *et al*³⁴⁵.

Glucose tolerance statistics have been subsequently reported to be stable across over 100 generations in colonies in Paris, Dallas, Stockholm, Cardiff, Coimbra, Tampa, Kuwait and Shanghai.

2.1.3.2 Phenotype of the Goto Kakizaki rat

The GKR is not an analogue of either human type 1 or type 2 diabetes mellitus, but a model that reproduces some salient features of the conditions. The Paris colony is the best described in the literature and provides much of the basis for the acceptance of the model, though little has been published from other colonies to demonstrate consistency. A primary event in development of hyperglycaemia seems to be defective recruitment of pancreatic beta cells from the precursor pool, leading to reduced beta cell mass and reduced glucose-induced-insulin release from early *in utero*. During this “prediabetic” phase there is increased peripheral sensitivity to insulin and increased peripheral glucose utilisation rate during euglycaemic clamp experiments. Overt hyperglycaemia manifests soon after weaning at 28 days and thereafter the phenotype resembles increasingly the human diabetic phenotype, with deteriorating glucose tolerance and basal hyperglycaemia, underpinned by progressive failure of insulin secretion in early adult life.

Interestingly, later in life insulin levels are maintained and in this GKR differ from their non-diabetic Wistar controls³⁴⁷. However, despite maintained insulin secretion, there is an age-related deterioration in insulin action, due to increasing peripheral insulin resistance. This is thought to be linked to reduced expression of the glucose transporters GLUT2, GLUT-4 and insulin receptors³⁴⁸. Late in life, GKRs develop many of the late diabetic complications seen in man³⁴⁶.

A summary of the Paris GKR phenotype is illustrated in Figure 2.2.

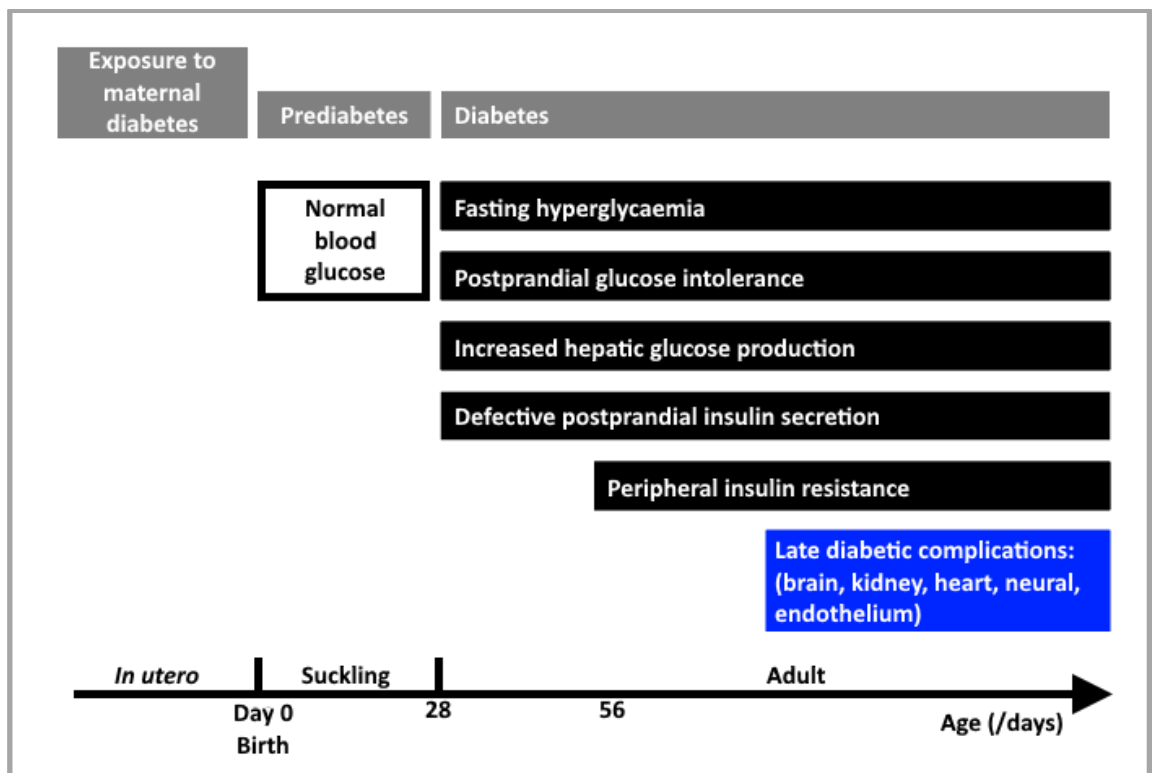


Figure 2.2: Development of the diabetic phenotype in a typical Goto Kakizaki rat from the Paris colony showing a prediabetic phase up to 28 days old followed by overt features of clinical diabetes and then complications from late adulthood. Adapted from Portha *et al*³⁴⁵.

However good a phenotypic match the adult GKR is for altered glucose handling and defective insulin signalling in human diabetes, the underlying cause is different, and it may impact differently on other, non-insulin signalling pathways. Little is known, for instance, about incretin signalling in the adult GKR. This is a limitation of the model that maybe relevant to cardiac survival signalling.

2.2 Diabetes phenotyping

Due to restrictions on the project licence we operated under we only had access to blood tests undertaken in the fasting state and could not undertake more than two blood tests in 24 hours in conscious animals. This prevented glucose tolerance testing, as the only route open to us was performing the tests in anaesthetised animals as part of a terminal procedure. Anaesthetising animals for repeated blood tests affects glucose handling³⁴⁹. We were therefore limited to conducting single blood tests in fasted animals.

2.2.1 Animal phlebotomy

Animals were fasted, with continued access to water, from 4pm the previous day prior to phlebotomy being carried out at 8am. This prolonged fasting was then common practice at UCL Biological Services Unit for fasted procedures and occurred under the guidance of staff veterinary officers and also external inspections. The practice of prolonged fasts has since been reviewed. All fasted experiments conducted previously at the Hatter and cited elsewhere in this work were carried out with similar fasting durations.

After weighing, brief heating to 38°C in a thermostat controlled heat-box was used to induce vasodilation, following which either manual restraint or a purpose-built rat restrainer was used and the lateral tail vein punctured using a butterfly needle with the tubing cut away to minimise dead space. We attempted the technique with different gauges of needle before choosing a 23 gauge as the best compromise between rate of flow and ease of cannulation of the tail vein.

We also attempted venous sampling without prior heating, to minimise stress to the animal, and thus minimise acute cortisol release and alterations to glucose handling caused by this³⁵⁰. Sampling from unheated animals proved uncomplicated in SDRs and WRs of all ages. However, blood sampling in GKR was more technically challenging even with heat-induced vasodilation, and without this manoeuvre proved unfeasible, even after submerging the tails in water at 42°C to cause local vasodilatation. Out of 12 GKRs attempted, sufficient blood sampling (0.5ml) was achieved in only four without heating, versus 10 with heating. In SDRs and WRs we consistently achieved success in

more than 9/10 animals after the initial learning curve, with or without heating. We decided to continue heating all animals prior to phlebotomy for consistency, therefore.

The difference in tail structure between GKR and other strains was obvious macroscopically, with the GKRs having bulkier tails and veins buried deeper. This was particularly pronounced in older animals. The soft tissues of the tail were coarser with a grittier texture when punctured by the phlebotomy needle, suggesting increased fibrous tissue deposition within the tail.

All procedures were in accordance with local standard operating protocols. The procedure was terminated at the first sign of any animal distress or after two unsuccessful attempts at phlebotomy due to the risk of venous collapse and subsequent tail necrosis.

2.2.2 Fasting blood glucose and HbA1c quantification

Drops of whole venous blood were analysed for glucose content at source using the Accu-check blood glucose meter system (Roche, UK) and for glycated haemoglobin using the A1Cnow+ system (Bayer, UK) both calibrated as per manufacturers' instructions.

2.2.2.1 Utility of glycated haemoglobin (HbA1c) measurements

Non-enzymatic interaction between biological molecules and glucose circulating in the non-cellular fraction of blood occurs slowly over time³⁵¹. In the case of the interaction between glucose and haemoglobin, the rate of reaction is unregulated, and influenced principally by glucose concentration and stoichiometry of interaction between circulating glucose and the haemoglobin molecule. Over time, therefore, accumulation of the products of this reaction can be related back to the concentration of circulating glucose. HbA1c assays quantify glycated haemoglobin as a proportion of total haemoglobin, and thus give an indirect assessment of blood glucose concentration over lifetime of the currently circulating Hb molecules³⁵².

The gold standard method for HbA1c quantification is High Performance Liquid Chromatography, which exploits the difference in electrochemical properties

between Hb and HbA1c to discriminate between the two forms. The A1CNow+ system we elected to use is validated against HPLC³⁵³.

2.2.2.2 Limitations of glycated haemoglobin measurements

Interference with veracity of HbA1c measurements comes in two forms: firstly, there is a short list of factors that perturb the relationship between real and measured HbA1c values by distorting assay performance. These essentially are technical factors and vary with the precise assay used. Persistence of foetal haemoglobin, other Hb variant isoforms and high levels of carbamylated Hb molecules found in patients with renal failure are the most important of these abnormalities³⁵⁴.

Secondly, there is a heterogeneous and less well elucidated set of factors that disturb the relationship between HbA1c accumulation and the level of circulating blood glucose. Heterogeneity of haemoglobin structures may also lead to this second type of error by affecting the pharmacodynamics of the glycation reaction.

Although principally dependent on the concentration of glucose over time, the stoichiometry of HbA1c accumulation is also influenced by haemoglobin content, the number of circulating erythrocytes, and mean corpuscular haemoglobin³⁵⁵. Less easily measured and corrected for, glucose permeability of the erythrocyte membrane, erythrocyte turnover and lifespan also affect the relationship³⁵⁴. Heterogeneity of erythrocyte longevity even within the normal variability seen in man is now recognised as sufficient to perturb HbA1c measurements³⁵⁶. Radioisotope studies in rat have shown RBC longevity to be similar between juvenile SDRs and juvenile WRs, confirming that this factor should have no bearing on comparisons between our rat strains³⁵⁷.

During serial testing of HbA1c in individual adult humans, many of the above factors can safely assumed to be constant. However, in a new-born rat these are not valid assumptions. Working from first principles, the persistence of foetal haemoglobin and the rapid expansion of both blood volume and erythrocyte number during rapid growth must have implications for the ability of an HbA1c measurement to accurately reflect the mean blood glucose over the lifetime of a

typical erythrocyte in the peripheral circulation, and a key stage in our study is therefore to demonstrate utility of HbA1c measurements in this setting.

2.2.3 Preparation of plasma

Venous blood was collected into vials containing 1.8mg K₂EDTA per ml blood, mixed and underwent centrifugation for 10mins at 1300 RCF. Supernatant plasma was aspirated as 15µL aliquots and stored at -60°C.

2.2.4 Preparation of serum

Venous blood was collected into vials containing no anticoagulant and left to coagulate at room temperature for 45mins before centrifugation at 1300 RCF for 15mins. The supernatant serum was stored at -60°C as 15µL aliquots.

2.2.5 Blood insulin quantification

Three commercial ELISA kits were used for serum and plasma insulin quantification: first the Millipore Rat / Mouse Insulin 96 Well Plate Assay (Cat. # EZRMI-13K) was used but some samples proved to have insulin concentrations below the lower bound of reproducibility for the assay. Therefore, assays from Merckodia were trialled in both standard (product #10-1250-01) and ultra-sensitive (product #10-1251-01) forms.

Optimisation of the methodology of blood insulin quantification is described in Chapter 3: "Testing for evidence of diabetes in UCL's Goto Kakizaki Rat colony".

2.3 Animal morphometry

Animals were weighed prior to phlebotomy, and prior to use in terminal experiments. Terminal weight was used to calculate the lethal or sublethal dose of Pentobarbitone required.

Explanted hearts were weighed following use in Langendorff isolated heart perfusion experiments, prior to freezing.

2.4 Ischaemia-reperfusion in the intact heart

The method of *ex vivo* perfusion of the mammalian heart used here was first described by Oscar Langendorff in 1895, as a modification to a method for

isolated frog heart perfusion described by Carl Ludwig in 1866³⁵⁸. Langendorff's original description utilised cat, rabbit and dog hearts, but small mammals such as rat and mouse hearts are now more commonly used in what is now universally referred to as the Langendorff method. Very few modifications to the original method have been made over the intervening 120 years and Langendorff's central observation that prompt supply of physiological perfusate down the coronary arteries of an explanted and apparently lifeless mammalian heart could effect immediate resuscitation, has remained key. The heart remains intact, with perfusate supplied via a cannula inserted into the aortic root, forcing the aortic valve closed by hydrostatic pressure, directing flow down the coronary arteries. Where modifications have been made, they have generally been to simplify the operation, for example the move away from whole blood perfusion, or to correct for some of the biggest physiological perturbances attendant on removing the heart from the body.

The key advantage of the Langendorff model to our work, and the reason it has been central has been key to many experimental advances across pharmacology and physiology, is that it allows rapid throughput of experiments with reproducible results. Moreover, externalisation of the heart allows easy surgical intervention on the heart, as well as access for recording a wide range of physiological data including electrocardiographic, functional and histological outcomes.

These key advantages do come at a price, in that explanting the heart and working on it outside the live body introduces confounders such as cardiac denervation, temperature perturbances and absence of a circulatory afterload on either ventricle. These limitations, and the methods employed to mitigate and control for them, are discussed below.

2.4.1 Rat euthanasia

The first stage of surgical euthanasia by heart explanation is the induction of deep anaesthesia to prevent pain and suffering by the animal. In studies of myocardial survival, there is an additional reason to prevent stress, as activation of the adrenocortical axis and other stress pathways^{22,359,360} have been shown to elicit tissue survival responses, and could therefore interfere with

experimental outcomes. Animals were therefore acclimatised to handling during routine husbandry tasks, and care taken to perform euthanasia quickly.

Choice of euthanasia method is not straightforward for these experiments and numerous options are available but none without problems. Inhaled volatile anaesthetics require complex delivery equipment and have potential to activate cardioprotective signalling³⁶¹. Physical methods of euthanasia such as decapitation have the advantage of being quick, but there may be a delay between death and heart explant (the importance of this is discussed below) and the method may induce a vagal outpouring, which can induce a cardioprotective state³⁶². Opiate overdose is an effective method, but is known to induce protective pathways within the heart³⁶³. Barbiturates provoke deep anaesthesia quickly but there is a narrow therapeutic range for these drugs and anaesthesia can quickly progress to respiratory arrest and death, depriving the heart of oxygenated blood and resulting in inadvertent ischaemic preconditioning.

Notwithstanding dosing problems, sodium pentobarbital is the preferred anaesthetic for induction of terminal anaesthesia in non-recovery experiments, as it can be administered quickly and safely via the intraperitoneal route with good systemic absorption. Moreover, animals anaesthetised with pentobarbital seem to exhibit larger modulation of infarct size in response to protective interventions than is the case when other anaesthetics are used. This suggests that pentobarbital neither protects the myocardium itself, nor interferes with the signalling pathways used by other protective treatments^{364,365}. The range of interventions tested under pentobarbital anaesthesia includes ischaemic preconditioning, remote ischaemic preconditioning³⁶⁶, ischaemic postconditioning and also treatment with preconditioning mimetic drugs³⁶⁷.

Rats were therefore restrained and anaesthetised with 55mg/kg pentobarbital via the intraperitoneal route, placed in a clean box away from other animals and noise sources, and observed regularly for level of alertness and signs of distress. Further pentobarbital was given where needed but, in the majority, a single dose was sufficient to sedate the animal to the point where hindlimb and corneal reflexes were extinguished, and surgical euthanasia could take place painlessly.

2.4.2 Heart explantation

The surgical technique for heart explantation is well-described. With the animal in the supine position, a rooftop incision is made to the upper abdomen using scissors; the diaphragm is cut and the anterior chest wall incised along the anterior axillary lines towards the forelimbs. Lifting the flail portion of the chest wall away results in a clamshell thoracotomy exposing the mediastinal structures and pleural cavities. The heart is manually anteflexed and the pedicle comprising the aorta, caval veins and pulmonary vessels is transected in one cut. The heart is placed promptly into an ice-cold bath of the perfusate used on the Langendorff rig and transferred promptly to the rig. Immediate cooling causes cardiac arrest and prevents the development of ischaemic damage within the heart. Prompt initiation of retrograde perfusion on the Langendorff rig prevents inadvertent activation of protective signalling pathways within the myocardium, which could pervert experimental results^{368,369}. This is the reason for avoiding euthanasia or surgical methods that introduce delays between cessation of native coronary perfusion and initiation of extracorporeal perfusion on the retrograde perfusion rig.

2.4.3 Retrograde cardiac perfusion

The heart was mounted on a custom-machined cannula approximately 2.5mm internal diameter, connected to a flow of warmed modified Krebs-Henseleit Buffer (mKHB), which was made up daily as per Table 2.1, maintained at constant temperature by a thermostatically controlled water jacket apparatus, and bubbled with a 95% O₂ / 5% CO₂ Carbogen mixture (BOC, UK) to achieve pH 7.40±0.05 and pO₂>50kPa. Appropriate perfusate temperature, pH and O₂ content was confirmed with a blood gas analyser just prior to anaesthetising the rat, and every half hour during the perfusion.

Constituent	Molecular weight	Concentration (/mmol/L)
NaCl	58.44	118
NaHCO ₃	84.01	25
D-glucose	180.2	11
KCl	74.55	4.7
MgSO ₄ .7H ₂ O	246.5	1.22
KH ₂ PO ₄	136.1	1.21

CaCl ₂ ·2H ₂ O	147	1.84
--------------------------------------	-----	------

Table 2.1: Constituents of modified Krebs Henseleit Buffer (mKHB) used as perfusate for Langendorff retrograde heart perfusions.

mKHB is supplied at a pressure approximating physiological aortic pressure into the aortic root, which is sutured tightly onto the cannula using two loops of 3-0 calibre cotton sutures. The pressure of perfusate forces the three leaflets of the aortic valve downwards, so that they close together. The only potential exit for mKHB arriving in the cannula at pressure is down one of the two murine coronary arteries.

The positioning of the aorta on the cannula and the positioning of the securing sutures are vitally important: if the aortic stump is too short or the cannula placed too low within the aortic root, then either the cannula or the securing sutures may obstruct one or both coronary ostia, leading to fixed high resistance to flow at the start of the coronary vessel, and low pressure in the vessel beyond this obstruction. This may inadvertently induce a low-flow ischaemia model, either regionally or throughout the whole heart.

Conversely, if the aortic stump is too long, or the sutures placed too high, the weight of the heart may cause the aorta to tear, or small leaks may develop around the top of the aorta as aortic geometry is distended. Either of these problems leads to a low resistance route for the mKHB to take, and perfusion of the coronary arteries is therefore compromised.

The clue to inappropriate cannula position is a coronary flow rate that falls outside the expected range for the setup being used.

2.4.3.1 Perfusate supply at constant pressure

Langendorff's original model used an elevated reservoir of perfusate (he used blood) to ensure constant perfusion pressure at the coronary ostia. Use of a large bore tube to deliver perfusate from the reservoir to the cannula ensured minimal resistance in the circuit before this point, as per Poiseuille's Law (Figure 2.9A), and therefore perfusate reached the coronary ostia at a pressure related solely to the reservoir height. Elevation of the reservoir could be adjusted to achieve physiological pressure for the species of heart under study.

In contemporary labs, the constant pressure effect is achieved either by elevating the perfusate reservoir and minimising circuit resistance (as *per* Langendorff) or by employing a pressure sensor at the level of the aortic cannula, feeding back to an electronic pump controller set to deliver a control voltage to a pump controlling the delivery of perfusate. Our lab has both setups. Figure 2.8 is a block diagram illustrating the function of the electronic feedback module used in our setup to control a Gilson Minipuls 3 peristaltic pump:

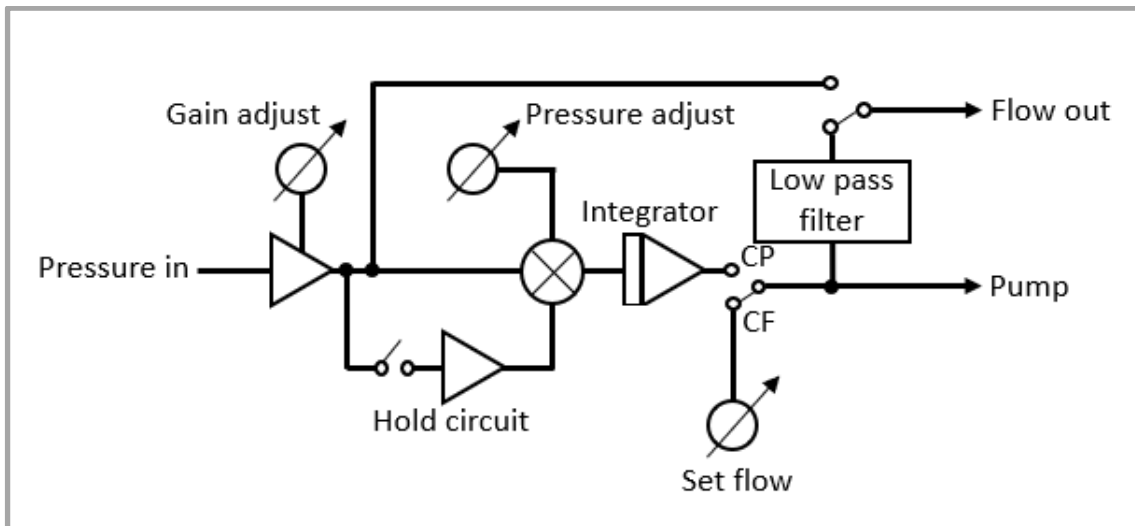


Figure 2.8: Simplified block diagram showing the basic function of a pump speed control circuit allowing constant flow (CF) or constant pressure (CP) control of perfusate flow. Activating the hold circuit results in a feedback loop to maintain constant pressure via adjusting the pump speed control voltage according to the sensed pressure voltage input. Sensitivity to changes in sensed pressure can be adjusted via the “gain adjust” variable resistor, whereas the “pressure adjust” variable resistor sets the target pressure.

2.4.3.2 Perfusate supply at constant flow rate

A third possibility for control of perfusate delivery to the coronaries was proposed by Katz. Figure 2.8 represents a situation where flow is manipulated to maintain a constant pressure in the presence of unknown resistance within the circuit. Katz proposed turning this on its head to deliver perfusate at constant flow, to measure pressure at the coronary ostia and use this to calculate resistance within the coronary arteries using Darcy’s Law (Figure 2.9B). The main application of this method was in studying the actions of vasoactive drugs on the coronary bed³⁷⁰. It has limited application in the study of ischaemia-reperfusion, except perhaps in the reperfusion phase of a regional ischaemia model to reveal abnormalities of vascular tone distant to the culprit artery, as discussed below.

$$\mathbf{A} \quad \text{Flow} = \frac{\pi \times \text{Driving pressure} \times r^4}{8 \times \text{Viscosity} \times \text{Length}}$$
$$\mathbf{B} \quad \text{Flow} = \frac{\text{Driving pressure}}{\text{Vascular resistance}}$$

Figure 2.9A: Poiseuille's Law. This illustrates the sensitivity of perfusate flow to the radius (r) of the transmitting vessel. For systems driven by constant pressure generated by elevating the perfusate reservoir, therefore, large bore tubing must be employed to minimise resistance in the circuit. **B:** Darcy's Law. In a constant flow system, the pressure drop across the coronary bed can be measured and used to calculate coronary vascular resistance.

2.4.4 Practical lab setups

We employed two varieties of constant pressure Langendorff retrograde perfusion rigs. In both, perfusate delivery was controlled by pumps driven by a variable voltage output STH pump controller (ADInstruments, Oxon, UK) set up as illustrated in Figure 2.8. One setup was bespoke, assembled from heat jacketed glass tubing, which was thermostatically controlled via a heat pump mounted under the desk. Trial and error showed the optimum temperature for heat jacket fluid to be 40°C. The heat jacketing surrounded the perfusate reservoir and included two heat exchangers on the route from the reservoir to a heat jacketed bubble-trap, under which was mounted the Langendorff perfusion cannula. Between the cannula and the bubble trap was a side branch for an electronic pressure sensor that fed back to the SGH pump controller. This setup is illustrated in Figure 2.10.

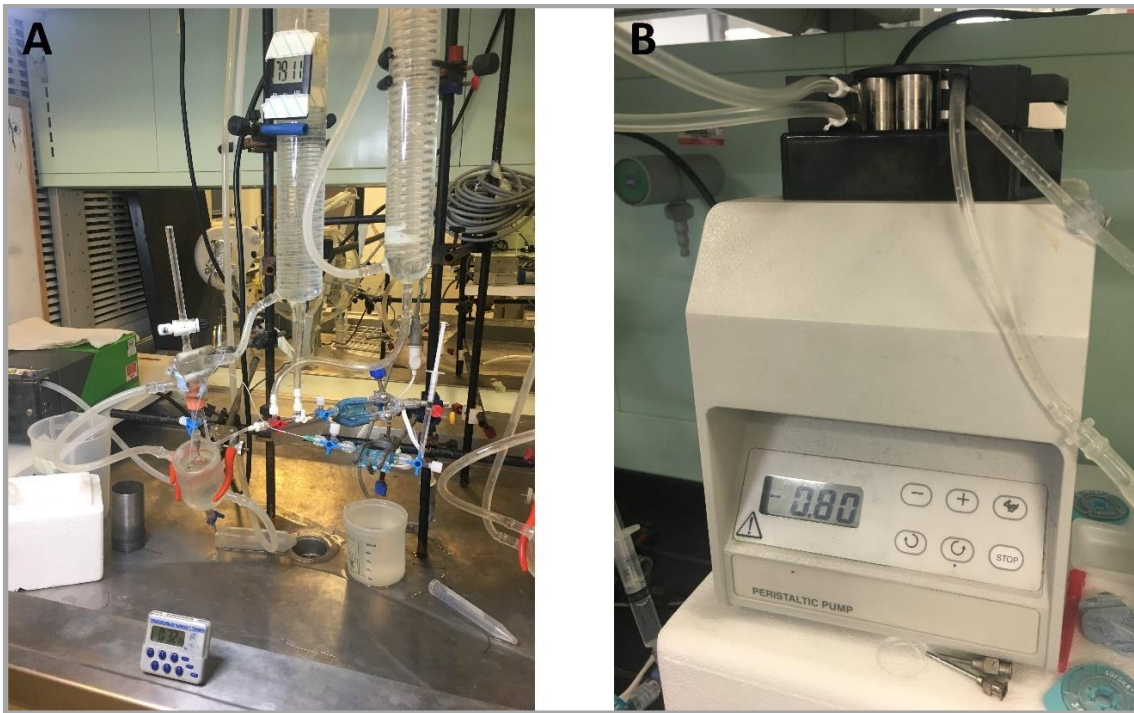


Figure 2.10: Self-assembled Langendorff constant pressure perfusion rig (**A**) driven by a Gilson Minipuls pump (**B**).

A second lab setup was a self-contained proprietary Langendorff rig (ADInstruments, Oxon, UK) contained within a cylindrical water bath with built-in thermostatically controlled heat pump. The component parts were similar to the *ad hoc* preparation, but with plastic rather than glass tubing and with proprietary machined parts and joints. The bubble trap, mount for the cannula and cannular were built into the assembly. The Minipuls was the only part of the perfusate supply circuit outside the water bath.

2.4.5 Physiological monitoring

After the heart was secured on either rig, the perfusate flow was quickly turned up to a rate that generated a perfusion pressure of 70mmHg, and the pump controller set to deliver a variable voltage to the pump to maintain this pressure. The left atrium was then removed, revealing the mitral valve, and a 1-2mm cut made into the pulmonary artery to allow introduction of a calibrated thermocouple into the right ventricular outflow tract (RVOT). The thermocouple connected via a Bioamp channel to Labchart recording software (ADInstruments, Oxon, UK).

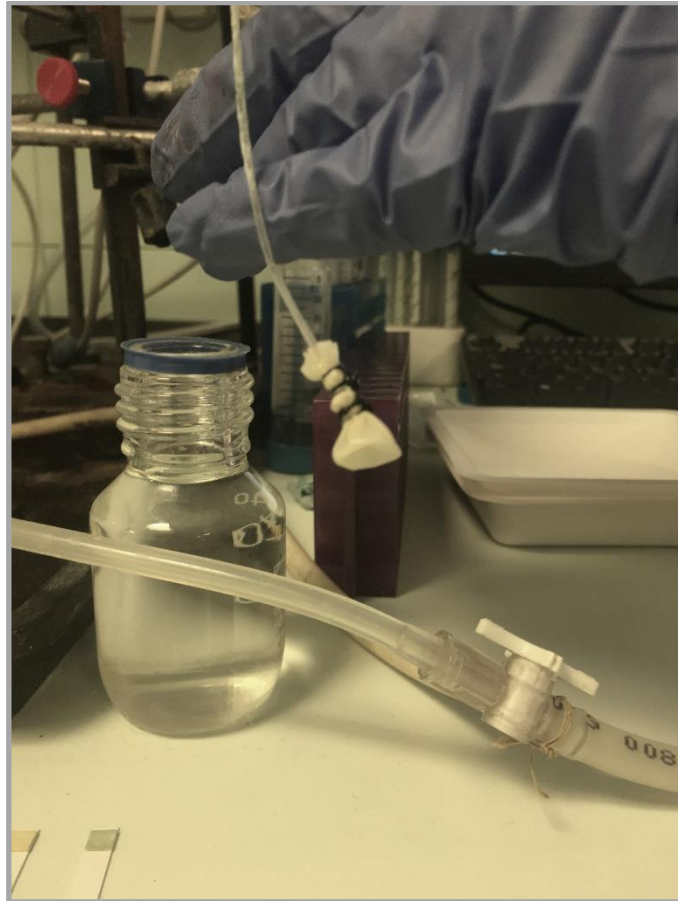


Figure 2.11: Left ventricular pressure transduction balloon. This is fashioned from a condom tip cut to size and tied onto 1.5mm bore plastic tubing. This is then connected to a 2ml syringe and filled with distilled water to distend the left ventricle of the isolated heart, allowing us to mimic LVEDP and also transduce work done by the heart via a pressure sensor connected to the circuit.

A 3ml volume balloon, as shown in Figure 2.11, was advanced through the left atriotomy and mitral valve into the left ventricle, where it was gently distended by the injection of water. Pressure within the balloon was transduced via a second pressure sensor and Bioamp channel to Labchart recording software (ADI instruments, Oxon, UK), yielding a left ventricular pressure trace. The final preparation of a hanging heart is shown in Figure 2.12.

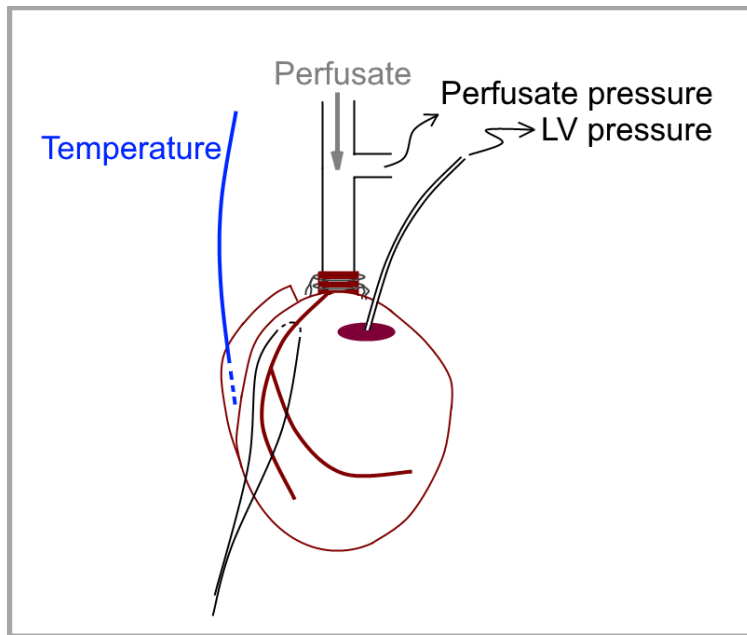


Figure 2.12: Schematic of a Langendorff perfused rat heart. The temperature probe is sited in the right ventricular outflow tract (RVOT), while the left atrium has been removed and a balloon introduced through the mitral valve into the left ventricle to transduce LV pressure and derived statistics. The left coronary artery has been encircled by a suture passed under it. The whole heart is suspended by the aortic root being tightly sutured to the bottom of a metal cannula, through which perfusate is supplied. A side-branch on the cannula allows constant monitoring of the perfusion pressure, which feeds back to the pump driving the perfusate and regulates the flow. The tube extending from the LV balloon is also connected to a pressure sensor, and syringe to allow further inflation of the balloon to maintain left ventricular end diastolic pressure (LVEDP) to be maintained during stabilisation.

2.4.6 Physiological control and stabilisation

The controlled variables on a constant pressure Langendorff perfusion with an LV balloon are coronary perfusion pressure, heart temperature, and LV distension, which is reflected in the left ventricular end diastolic pressure (LVEDP) derived from the LV pressure trace transduced from the LV balloon (see figure 2.13). Distension of the LV balloon was adjusted up to 10 minutes into the perfusion to give a baseline LVEDP of 5-10mmHg, which is considered physiological, leading to appropriate LV developed pressure and therefore appropriate LV work as per the Frank Starling law of the heart³⁷¹ .

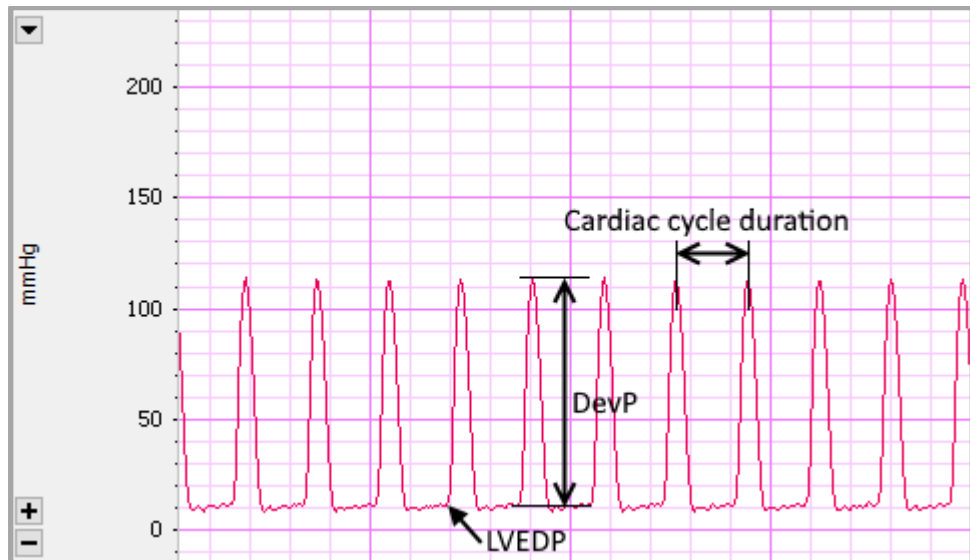


Figure 2.13: Pressure trace and parameters derived from left ventricular balloon. LVEDP: Left ventricular end diastolic pressure; DevP: Developed pressure; heart rate is time divided by cardiac cycle duration.

Cardiac temperature is influenced by temperature of the perfusate, coronary flow rate, plus any extraneous heat sources. From the moment the heart was first perfused on the rig, we aimed to keep the heart temperature well within the target range, aiming for far stricter control than $37 \pm 0.5^\circ\text{C}$ allowed by published Langendorff standards. Even small variations in temperature have been shown to influence infarct size, and larger temperature excursions may activate protective signalling pathways^{372–374}. We achieved this by close monitoring of data from the thermocouple placed in the RVOT. Minor temperature changes were corrected by raising or lowering a heat jacket around the heart. More significant heating was achieved by placing filament lamps next to the hanging heart, and longer-term trends in temperature were addressed by adjusting the temperature of the heat jacketing or water bath around the perfusate supply rig.

2.4.7 Induction of myocardial ischaemia

Following a stabilisation or pre-treatment phase of perfusion, one of two methods may be used to induce ischaemia in the isolated heart. The choice here is between global versus regional myocardial ischaemia and both have their merits.

2.4.7.1 Global myocardial ischaemia model

Global myocardial ischaemia is induced simply by turning off the perfusate supply, rendering the entire isolated heart ischaemic. This has the advantages of being extremely simple, reproducible and very well characterised. It is probably the model most commonly used to study ischaemia-reperfusion injury *ex vivo* in the literature, with a large historical evidence base.

The drawbacks are mainly theoretical; strictly speaking it is a model of bradycardic cardiac arrest, as this is virtually always the rhythm induced in hearts subjected to global ischaemia in this way. Global ischaemia and bradycardic arrest introduces yet another level of abstraction away from the situation of localised myocardial ischaemia in man that we are trying to model.

Most crucially, however, using global ischaemia means that there is no remote continually perfused myocardium in the model. Remote myocardium is increasingly recognised to play an important part in localised ischaemia-reperfusion injury, and is the source of many signalling moieties that underpin post-infarct remodelling after myocardial infarction³⁷⁵. This is particularly relevant for any study of diabetes, as the changes seen in remote diabetic myocardium post-infarct are different from those seen in non-diabetic myocardium²⁴⁸.

We therefore elected to use a more clinically relevant model of regional myocardial ischaemia in our studies.

2.4.7.2 Regional myocardial ischaemia model

During the stabilisation phase of Langendorff perfusion, described above, a 3-0 silk suture was used to under-run the left coronary artery within the thickness of the myocardium. Over 9/10 SDR and WRs have a single main left coronary artery supplying 50% of left ventricular myocardium³⁷⁶; occlusion of this artery results in ischaemia of approximately 50% of left ventricular myocardium, therefore. At the allotted time, regional myocardial ischaemia was induced by tightening the suture around the artery and securing the tension on the suture with a snare.

Successful arterial occlusion was verified by a sudden increase in coronary vascular resistance, and consequent 30% or more drop in coronary pressure and LV developed pressure. The anterior LV wall was also observed to become pale and oedematous.³⁷⁷. The sudden drop in perfusate flow was accompanied by a prompt tendency for the measured temperature of the perfused heart to drop. This was anticipated and counteracted by raising the heat jacket around the heart, and insulating material was placed above the heart to keep the temperature in the target range.

2.4.8 Reperfusion

Reperfusion is an important stage of both the global and regional myocardial ischaemia models of acute myocardial infarction. From a practical viewpoint, reperfusion allows washout of ruptured cellular contents, including the dehydrogenase enzymes on which our infarct size quantification technique relies. In simple terms, it is only the washout of oxidising enzymes from infarcted tissue that allows a colour contrast to develop with exposure to 2,3,5-triphenyl-2H-tetrazolium chloride. See section 2.5.10 (“staining and quantification”) for further details.

Reperfusion is also vital for the development of the reperfusion phase of ischaemia reperfusion injury. The temporal relationship between reperfusion and injury is conclusively demonstrated by electron microscopy documenting a wave of ultrastructural destruction at restoration of perfusate flow⁹⁴.

Preconditioning treatments have been demonstrated to exert their protective effect on this phase of injury¹⁰⁸, and therefore to omit reperfusion from our experiments would negate our investigations into the efficacy of IPC.

After 35mins regional ischaemia the LCA ligature was loosened and the anterior LV wall was reperfused, which was confirmed by partial recovery of myocardial colour, coronary flow rate and developed pressure. Reperfusion then continued for a further 60 minutes.

Until recently, studies of IRI included a minimum of 120 minutes reperfusion, however work by our group has demonstrated no significant reduction in injury with only an hour’s reperfusion²⁴⁴.

2.4.9 Direct ischaemic preconditioning

Hearts undergoing Langendorff perfusion in these studies were either assigned to control perfusion, or to receive direct ischaemic preconditioning. Direct ischaemic preconditioning is described in detail in Chapter 1 (“Background”). The original description of direct ischaemic preconditioning applied preconditioning ischaemia to only the region of the heart later subjected to lethal (“index”) ischaemia³⁷⁸, however more recent studies at the Hatter have used whole organ ischaemia during the preconditioning treatment. Following the description of remote ischaemic preconditioning, where non-lethal ischaemia in one coronary bed protects against subsequent ischaemic injury in myocardial tissue supplied by another artery¹¹⁶, it could be argued that subjecting the whole organ to the preconditioning treatment is invoking a mixture of remote and direct preconditioning. However, this method of experimental preconditioning is widely used across different research groups including ours.

Ischaemic preconditioning can be invoked in a healthy isolated heart by any interruption to perfusion lasting over three minutes, followed by reperfusion of at least one minute^{379,380}. However, a threshold effect exists in diabetic hearts such that brief or non-repetitious episodes of non-lethal ischaemia fail to induce protection in diabetic hearts. Increasing the number of short ischaemic insults restores the potency of IPC in diabetes¹⁴⁷.

We aimed to induce a preconditioned state using either one or three five-minute interruptions of whole heart perfusion simply by turning off a three-way tap above the aortic cannula to cause recirculation of the mKHB perfusate. Flow was interrupted at five-minute intervals. Myocardial temperature was maintained by anticipating the inevitable drop and positioning a heated water jacket, filament lamps and insulating materials appropriately.

2.4.10 Staining and quantification

Following the reperfusion phase of Langendorff perfusion, the LV balloon and temperature probe were removed from the heart and the LCA permanently occluded by tight knotting of the suture around it. The heart and cannula were removed from the Langendorff rig and 1– 2ml Evans’ blue dye 0.25% in aqueous solution was injected down the cannula, staining the substance of the myocardium in the areas not supplied by the occluded LCA. Excess dye was

wiped and gently washed off, and the heart removed from the cannula and weighed. It was then wrapped to stop dehydration of the external surface, and frozen overnight.

The following day, the heart was stained according to an established protocol to identify viable and non-viable tissue. The most basal part of the potential infarct was located by the knot occluding the LCA. The volume of the heart apical to the knot was divided into five short axis slices, and bathed in 0.1% 2,3,5-triphenyltetrazolium chloride (TTC) in aqueous solution for 15mins at 38°C, with gentle shaking every five minutes. TTC in solution reacts with dehydrogenases in viable cells, causing the viable myocardium to develop a deep red colour. In necrotic areas subject to reperfusion, dehydrogenases have been depleted by washout and thus TTC remains white, creating a contrast between the viable and dead tissue. Viable tissue previously stained by the injection of Evans' blue remains a deep blue colour, unaffected by TTC.

The three colours were then intensified by a minimum of an hour's incubation at room temperature in 10% neutral buffered formalin and hearts assigned a random 4 digit number to blind subsequent analysis.

Following this, slices were compressed gently *en face* between two glass plates, and their basal surfaces scanned into a digital bitmap file at 600 dots per inch using a flatbed scanner.

The cumulative effect of the colouring steps was to give a tricolour appearance at this stage, illustrated in Figure 2.14. The three colours represented tissue never at risk of infarction (blue); tissue deprived of blood flow by LCA occlusion but that had survived (red); and necrotic tissue (white).

The three coloured areas were outlined using colorimetric analysis and their areas calculated. The ratio of area at risk (white plus red) to total myocardial cross-sectional area was used to validate experiments, as it is established that area at risk predicts infarct size. Hearts where the area at risk fell outside the predetermined range 40-75% were excluded from results.

The primary outcome of this technique was the infarcted cross-sectional area (white) expressed as a proportion of the at risk (white plus red) cross-sectional area:

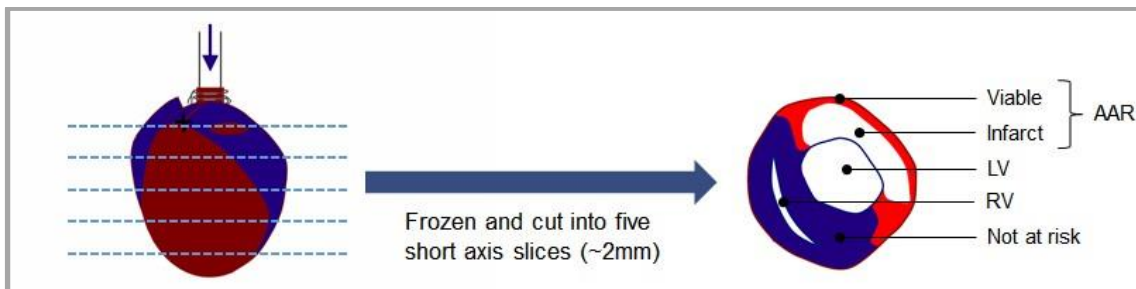


Figure 2.14: Staining the heart. The left coronary artery (LCA) is tied off and 0.25% Evans blue dye injected into the rest of the heart via the still-patent right coronary artery. The heart below the knot occluding the LCA is sliced into five slices, which are incubated in TTC to cause a colour change of the non-blue tissue (see text). Viewed *en face*, each slice now comprises three regions: white (infarct), red (viable and supplied by the LCA) and blue (not supplied by the LCA). This allows calculation of the main experimental endpoint, which is the Infarct / Area At Risk (AAR), or white / [white + red]

2.4.11 Varying conditions during reperfusion

To investigate the effects of various changes to conditions during reperfusion, modifications were made to the perfusion buffer. Recipes were as follows.

2.4.11.1 Variable glucose

Modified Krebs-Henseleit buffer (mKHB) was prepared with various concentrations of D-glucose. Osmolality was maintained constant across different solutions using D-mannitol, a hexose sugar with a molecular weight very similar to glucose (182.2 vs 180). D-mannitol participates in energy metabolism only in fungi and the parasitic organism *Eimeria tenella*; it is not an energy substrate for mammalian cells³⁸¹.

[D-Glucose] (/mmol/L)	[D-Mannitol] (/mmol/L)
5	28.00
11	22.00
16.5	16.50
22	11.00
33	0.00

Table 2.3: Manipulation of glucose content of Langendorff perfusate whilst maintaining constant osmolality by the addition of D-Mannitol.

2.4.11.2 Blockade of basal glucose uptake

To confirm the effects of variable glucose during reperfusion, we sought to reduce glucose entry into metabolically active myocardial cells during reperfusion. Glucose uptake our *ex vivo* Langendorff cardiac perfusion model with mKHB is entirely passive, as the system lacks insulin and other anabolic hormones, which may augment substrate uptake *in vivo*. Interestingly, replacement of these hormones via the use of whole blood as a perfusion medium does not significantly augment the availability of high energy phosphates in the perfused heart, suggesting that stimulated glucose uptake via the insulin-responsive facilitative glucose transporter GLUT-4 is not required for cardiac metabolism in the isolated heart³⁸².

Facilitative glucose transporters other than GLUT-4 may be involved in Langendorff glucose transport, however. GLUT1 is significantly expressed in heart, is implicated in a significant component of basal cardiac glucose uptake and could be an attractive target for us to block³⁸³. There is no shortage of pharmacological GLUT1 blockers, but most – for example the theophyllines – have well-documented cardiovascular effects and could be expected to interfere with our experimental endpoint by off-target effects³⁸⁴. An exception to this is the barbiturate family but use of these drugs in our experiments would be confounded by use of barbiturate anaesthesia during rat euthanasia.

The sodium-dependent glucose transporters (SGLTs) are a family of sugar transport proteins and members of the family (SGLT1 and 2) have been implicated in basal glucose transport in the myocardium³⁵. SGLT1 is highly expressed in both human and murine myocardium, and blockade during

ischaemia has been shown to worsen the extent of ischaemic injury, presumably by reducing glucose flux to the ischaemic and post-ischaemic myocardium, effectively prolonging the ischaemic insult³⁴⁰. Channel function during reperfusion alone has not been studied. Selective blockers of the SGLT2 isoform are in clinical use to prevent glucose reabsorption in the kidney and thus control hyperglycaemia in diabetes³⁸⁵.

Phlorizin is a non-selective reversible competitive antagonist to glucose uptake by SGLT1 and SGLT2. Chemically it is a phenol glycoside, with an exposed sugar residue (Figure 2.16) that interacts with the sugar binding site of the SGLTs in place of D-glucose³⁸⁶. There also exist separate Phlorizin binding domains (PBDs) in the SGLT family; binding at these sites induces extensive conformational change in SGLT molecules, preventing glucose binding and contributing further to the antagonism of glucose uptake³⁸⁷.

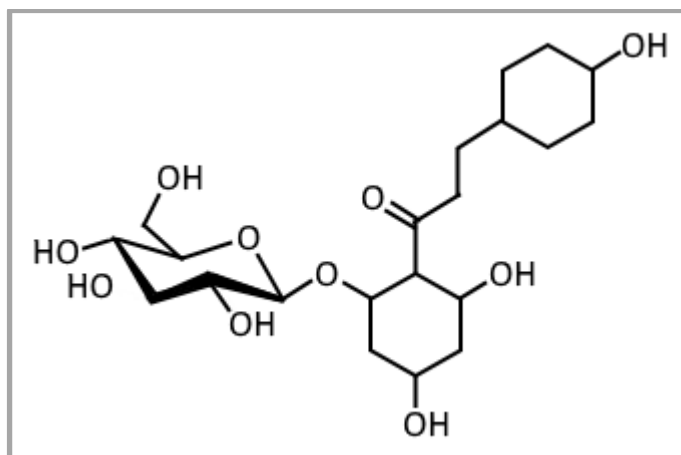


Figure 2.16: Chemical structure of Phlorizin, a phenol glycoside non-selective competitive antagonist to glucose uptake via the SGLT family of glucose transporters. Adapted from Frasc *et al*³⁸⁶.

Our hypothesis was that partially blocking glucose uptake during reperfusion would prevent or reduce the sudden burst of reactive oxygen species production triggered by abrupt restoration of metabolic substrate, and potentially exacerbated by exposure to high glucose³⁸⁸. We did not therefore want to block the entirety, or even most of glucose uptake, but just reduce it slightly. SGLT-mediated glucose transport, therefore, seemed an ideal target, as SGLT1 contributes significantly but not overwhelmingly to myocardial glucose uptake,

and Phlorizin has already been shown to be effective in reducing glucose uptake in the heart^{340,389}.

Most studies of Phlorizin in the isolated heart have used doses in the millimolar range. However, the IC₅₀s for Phlorizin with respect to SGLT1 and SGLT2 function are only 60nM and 439nM respectively^{390,391}. Using doses several orders of magnitude higher than this risks off-target and non-specific effects. We chose a dose in the low micromolar range for our experiments. 6.6mg of Phlorizin (Abcam, UK) was reconstituted in 150µL dimethyl sulfoxide (DMSO) which was added to 5L of mKHB perfusate for use in Langendorff experiments. 150µL of DMSO vehicle was added to control perfusate.

2.5 Modelling remote ischaemic preconditioning

We sought to investigate whether the increased threshold to ischaemic preconditioning in diabetic animals also affects the more clinically relevant phenomenon of remote ischaemic conditioning (RIC).

RIC was originally described as ischaemia of one coronary bed protecting a neighbouring coronary bed from subsequent ischaemia-reperfusion injury¹¹⁶. It is now recognised that non-lethal ischaemia of one vascular bed may protect many distant vascular beds from subsequent, coincident or even prior lethal IRI (RIPC, RIPerC and RIPostC respectively). For clinical translation, however, RIC has come to refer to non-lethal ischaemia applied to skeletal muscle in a limb to protect against a concurrent or later ischaemic insult to an inaccessible visceral organ. The reasons for concentrating on limb skeletal muscle are obvious: short bursts of ischaemia can be induced by simple tightening of a ligature or sphygmomanometer cuff. This simple intervention has been tested in clinical trials targeting protection of kidney³⁹², brain and spinal cord³⁹³, as well as extensive attempts to protect the heart from STEMI^{118,394}, planned cardiac surgery^{395–398} and elective PCI³⁹⁹. Results in clinical trials have been neutral, in contrast to the significant benefit seen in animal studies, possibly related to poor understanding of the RIC stimulus¹¹⁹.

2.5.1 Preparation of the animal for remote ischaemia

Induction of limb ischaemia in animals requires general anaesthesia, to immobilise the subject and also to prevent pain, suffering and activation of preconditioning pathways via a stress response^{22,359,360}. Much the same considerations are present in choice of anaesthetic as for anaesthesia prior to heart explantation, with the obvious addition that any method that rapidly results in death is unsuitable. The choice is essentially between different pharmacological methods and as with heart explantation protocols, the barbiturates have much to recommend them in that they do not induce a cardioprotective state^{364,365} and achieve deep anaesthesia quickly. The main drawback is the potential for respiratory depression, but this can be countered by sustaining the animal on a mandatory volume small animal ventilator.

We therefore administered sodium pentobarbital 20mg/kg intraperitoneally (slightly less than half the dose used in terminal protocols) and observed the same precautions to avoid animal distress. Once hindlimb and corneal reflexes were absent, but whilst the animal was still seen to make respiratory effort, he was placed supine, secured in place on a thermostatically controlled pad and the trachea intubated using the outer tubing from a 1¼" 14G SurFlash intravenous catheter (Terumo Medical Incorporation, NJ). The trachea was transilluminated to guide intubation, and large angled forceps used to retract the tongue and enable visualisation of the vocal cords.

The endotracheal tube was attached to a small animal ventilator (Harvard Instruments) set to deliver 2.5ml O₂ at 80 cycles per minute. Tube position was confirmed by bubbling the exhaust through 1cm depth of redistilled water, which also provided quasi-physiological peak end expiratory pressure and reduced work of breathing for the animal. Further pentobarbital was administered in 1-5mcg doses in the rare event of coughing or other signs of light anaesthesia.

2.5.2 Physiological monitoring

ECG electrodes were attached to monitor three lead ECG and heart rate. A thermocouple temperature probe was inserted 5mm into the anus connected to a digital display. Rectal temperature was maintained at 37±0.5°C by adjusting the thermostatically controlled heating mat and deploying filament lamps for additional warming or fans for cooling. We found that by pre-heating the mat to

38.5°C then switching it off for a period, and achieving prompt tracheal intubation prior to respiratory arrest, endogenous temperature regulation was maintained and minimal external adjustments were needed in most cases. Target heart rate was 350-500 based on observations in conscious male SDRs⁴⁰⁰. Arrhythmias were noted from the ECG. Heart rate and temperature were recorded every 10mins.

2.5.3 Hindlimb ischaemia

A choice of methods is available for inducing hindlimb ischaemia in rat. Fidelity to the RIC intervention in man is best achieved using a miniature sphygmomanometer cuff inflated to suprasystolic pressure and this has been recently used at the Hatter in mouse. However, a recent meta-analysis by Bromage identified variable RIC methodology and lack of understanding of the RIC stimulus as a possible factor contributing to failure of translation into man¹¹⁹. Given that the sphygmomanometer cuff method involves compressing a significant proportion of the proximal rat limb, it is potentially associated with significant non-ischaemic effects including barotrauma to soft tissues and non-specific neuronal stimulation, particularly small fibre nociceptors¹²⁸; considering the need for a specific intervention producing limb ischaemia and little else, we discounted this method.

Surgical methods have been employed to render one or both hindlimbs ischaemic by placing a clip on one or both femoral arteries in the pelvic region⁴⁰¹. We adapted this method to operate via a minimal incision in the femoral region where the femoral artery is superficial to muscle, thus minimising tissue trauma and thus also minimising afferent nociceptive neuronal activity, which may augment the preconditioned state¹²⁸.

2.5.3.1 Surgical method

In all animals undergoing both RIC and sham protocols, a single 7mm oblique skin incision was made and blunt dissection carried out down to the superficial fascia of underlying muscles. The superficial femoral artery was visualised, and further careful blunt dissection carried out towards the retroperitoneum to reveal the bifurcation of the common femoral artery (CFA). 3-4mm proximal to the bifurcation, a 4-5mm section of artery was carefully freed from underlying structures by blunt dissection.

With practice, the above could be performed in roughly five minutes, giving ample time between stabilising the animal on the ventilator, and commencing RIC or sham continuous limb perfusion at 10mins.

After 10 minutes ventilation the animal was assigned to either sham or RIC. Sham animals were simply ventilated until 40 minutes had passed, whereas a 10g vessel clip (#15911, World Precision Instruments, USA) was applied to the free portion of the RIC animals' right femoral artery for five minutes. Up to three cycles of five minutes limb ischaemia and five minutes reperfusion were delivered thus.

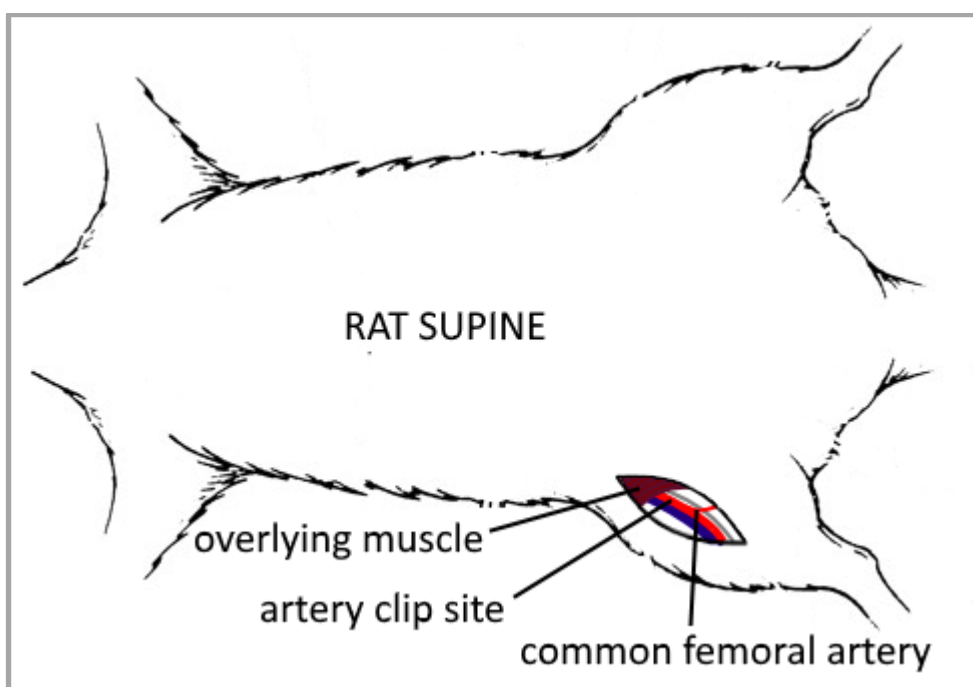


Figure 2.17: Surgical method of inducing rat hindlimb ischaemia. With the animal in the prone position, under general anaesthesia a femoral incision and blunt dissection allows exposure of the femoral bundle. This allows an artery clip to be placed, temporarily obstructing flow of blood to the right hindlimb.

Limb ischaemia was verified by loss of pulsation of distal vessels, which were visible in the surgical field, and colour change both of surgically exposed muscle and of the foot pad. Colour changes in the foot pad followed a classic ischaemic-hyperaemic pattern from pink (normal), to blueish-grey (ischaemic), to bright red (hyperaemia during early reperfusion).

2.5.4 Subsequent experimental infarction

After 40mins of RIC or sham continuous limb perfusion, depth of anaesthesia was verified and the heart explanted into iced mKHB as for other experimental infarctions. The heart was transferred onto a primed Langendorff rig, the usual monitoring equipment inserted, and a snare run under the LCA to prepare for occlusion as previously described. Hearts were stabilised for 10mins prior to occlusion of the LCA by tightening the snare; subsequent regional infarction, reperfusion, processing and analysis was as for other experimentally infarcted hearts.

2.6 Western blot quantification of kinase activation

To investigate the role of classical ischaemic preconditioning signalling in the modulation of infarct size in diabetic hearts, samples were taken for Western blotting. Blots of phosphorylated and non-phosphorylated forms of the key proteins in the preconditioning cascade were prepared and quantitatively analysed to give a measure of the degree of activation of the cascade, i.e. the proportion of each protein existing in its phosphorylated form.

2.6.1 Preparation of ventricular lysates

There is conflicting data concerning whether the classical IPC signalling pathway, RISK, is activated in diabetes or not. Differences in sampling timepoints may account for this discrepancy. This is discussed fully elsewhere. In brief: conflict exists between data collected shortly after animal euthanasia, which show increasing activation of the pathway with animal age, versus data collected after preconditioning stimuli, which suggest a failure of preconditioning in animals with established diabetes^{147,244}.

We sought to address the discrepancy by processing samples collected as soon as practicable after death, and after either preconditioning or control *ex vivo* Langendorff perfusion.

Animals were euthanased as for other terminal procedures and the heart explanted. The organ was promptly mounted on a Langendorff perfusion rig perfusing at constant flow 10mls/min. For baseline samples the heart was only perfused briefly until the effluent ran clear. This was important to remove blood

from the coronary vasculature and cardiac chambers, as erythrocytes contain many of the same MAPK cascades implicated in myocardial preconditioning signalling, and could contaminate Western blot results⁴⁰².

To prepare control and preconditioned samples of myocardium, hearts were secured on a Langendorff rig and perfused at constant pressure as per section 2.5.3 (“retrograde cardiac perfusion”).

Ventricular tissue was harvested by slicing the perfused hearts beneath the atrioventricular groove and instantaneous cooling in a freeze clamp under liquid N₂ and stored at -80°C.

Tissue lysates were prepared on ice from 10mg frozen tissue samples per 100µl freshly prepared tissue lysis buffer by mechanical disruption with pestle and mortar followed by sonication. Lysis buffer was made up according to the recipe in Table 2.4:

Constituent	Final concentration
Tris pH 6.8	100mmol/L
NaCl	300mmol/L
NP ₄ O	0.5%
EDTA	10µL/ml
HALT protease inhibitor(Thermo Fisher Scientific, USA)	10µL/ml
COMPLETE protease inhibitor(Roche, UK)	10µL/ml
pH to 7.4 with NaOH 1M	

Table 2.4: Preparation of lysis buffer for myocardial tissue samples (credit: Dr A Hall)

Following homogenisation, samples were centrifuged for 10min at 10,000rpm at 4°C to remove unsuspended tissue detritus. The protein-rich supernatant was then frozen at -20°C.

2.6.2 Equalisation of protein content

Aliquots of tissue lysates were passively warmed to room temperature and 10µl samples added to a 50:1 mixture of bicinchoninic acid (BCA) and CuSO₄.

Protein concentration determined by the colour change of the Smith assay,

which was carried out in a 96 well plate format at 40°C. Colour change was detected on an Omega Flurostar plate reader reading absorbency at $\lambda=562\text{nm}$.

The Smith assay relies on two stages of chemical interactions: Cu^{2+} ions within the BCA/ CuSO_4 mixture are reduced to Cu^+ in the presence of protein, specifically cysteine/cystine, tyrosine, and tryptophan side chains. This reaction happens more rapidly at 37-60°C. The colour change is caused as bicinchoninic acid subsequently chelates the newly formed Cu^+ ions. The resulting compound avidly absorbs light at $\lambda=562\text{nm}$ making the assay suitable for automated reading, as the availability of Cu^+ ions is in direct proportion to the concentration of protein in the original sample.

A normal curve was constructed for each run of the Smith assay, using known bovine serum albumin standard solutions; an example is shown in Figure 2.18. The equation of the normal curve was derived using the linear regression function in GraphPad Prism (GraphPad, USA). All samples and standards were run in duplicate.

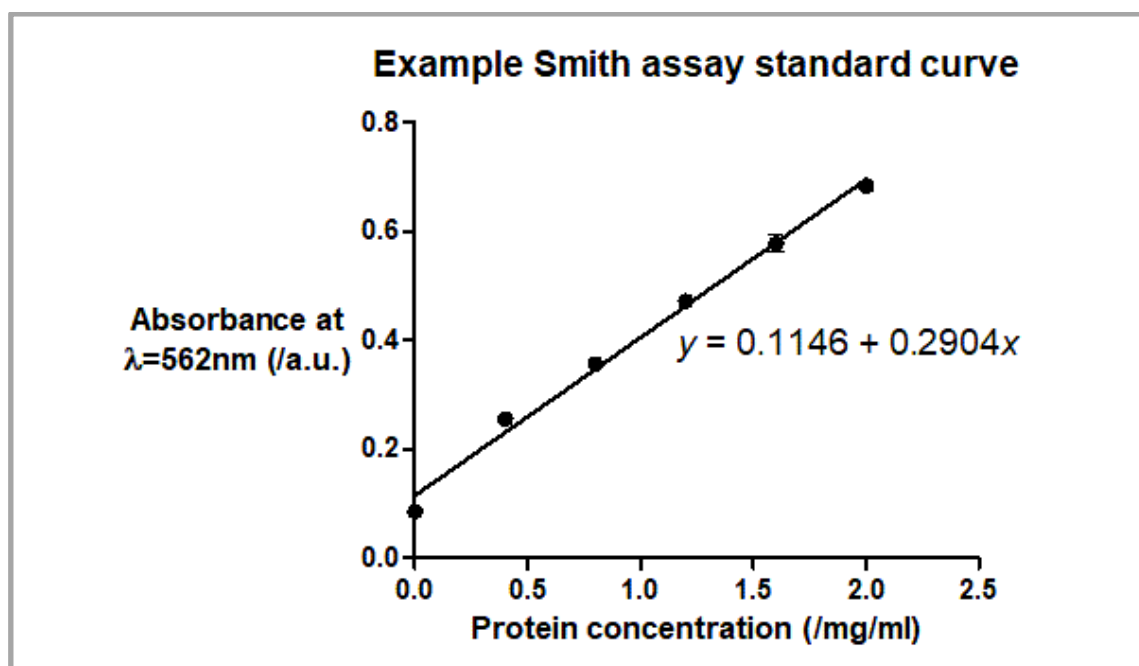


Figure 2.18: Example of a standard curve for the Smith protein content assay, prepared using standard samples of known concentrations of bovine serum albumin. The line of best fit shows direct correlation of known vs measured albumin concentration, as quantified by absorbance.

Using the results of the Smith assay, ventricular tissue lysates were diluted to equivalency for protein concentration using redistilled water, then diluted 1:1 with Laemmli's lysis buffer (Sigma, UK) to ensure even charge distribution throughout the homogenate. 6-mercaptoethanol was added at 5% of the final sample volume to aid denaturing. Samples were then heated to 98°C for 10mins to denature then centrifuged at 8000 rpm for 5 mins and kept on ice.

2.6.3 Protein gel electrophoresis

Proteins were separated via sodium dodecyl sulphate polyacrylamide gel electrophoresis (SDS-PAGE). Separation of proteins by molecular weight in a polyacrylamide gel with sodium dodecyl sulphate was first described by Shapiro in 1967⁴⁰³. The presence of SDS denatures multimeric proteins so that they all have similar charge to mass ratios; a charge applied across the polyacrylamide gel then causes migration of proteins in direct proportion to their mass alone. The proportion of polyacrylamide in the gel determines the size of pores within the gel, which in turn influences the resistance to travel by proteins. Therefore, gel strength and current applied can be tailored to separate proteins within a range of masses of interest. 15% gels are ideal for resolving proteins in the range 12-45 kDa, and 8% gels for molecules 50-200 kDa.

Our SDS-PAGE gels were prepared freshly prior to use according to standard published recipes given in Table 2.5. TEMED and APS were added immediately prior to use.

Constituent	15 % resolving gels (x2)	8% resolving gels (x2)	Stacking gel
1M Tris-HCl (pH 8.8)	3.75ml	3.75ml	N/A
1M Tris-HCl (pH 6.8)	N/A	N/A	0.625ml
30% Acrylamide	5ml	3.44ml	0.75ml
Water	1.092ml	2.795ml	3.456ml
10% SDS	100µl	100µl	50µl
Add the following immediately prior to use			
TEMED	7.5µl	7.5µl	7.5µl
10% Ammonium Persulphate	75µl	75µl	75µl

Table 2.5: Preparation of SDS-PAGE gels (Credit: Dr A Hall)

Gels were prepared using the Mini Protean III system (BioRad, UK). This system requires approximately 3.5mls of running gel solution, topped with 50% isopropanol to ensure a level surface. Once set, the isopropanol is removed and the stacking gel constructed on top of the resolving gel using a plastic comb to

form loading wells. A molecular weight marker ladder (BioRad, UK) was loaded in the first lane of each gel and protein samples in all other wells. 180-200V was applied across the gel until the molecular weight marker ladder indicated sufficient separation of the molecular weights being studied.

2.6.4 Transfer of proteins to a membrane support

Transfer of proteins from the delicate resolving gels onto a more resilient membrane is essential to allow exposure to antibodies and subsequent detection of proteins. Membranes used include nitrous cellulose, polyvinylidene fluoride (PVDF) and nylon, and methods for transferring from gel to membrane include diffusion, vacuum and wet and semi-dry electrotransfer⁴⁰⁴. We used semi-dry electrotransfer onto a PVDF support (Amersham, UK).

Transfer buffer was freshly made according to the recipe in Table 2.6. The innate hydrophobicity of the PVDF membranes was countered by soaking in methanol, then they were equilibrated in transfer buffer. Resolving gels were placed onto the PVDF membranes in a semi-dry transfer cell (BioRad, UK) between layers of blotting paper wetted in transfer buffer, creating a paper-PVDF-gel-paper sandwich. Air bubbles were pressed out and the cell was sealed. Transfer was achieved by applying 10V at 1A for two gels or 1.5A for four gels, for 45mins.

Constituent	Final concentration
Tris-base	25mmol/L
Glycine	0.19mmol/L
Methanol	20% v/v

Table 2.6: Preparation of Western blot transfer buffer (Credit: Dr A Hall)

2.6.5 Membrane blocking and antibody application

To prevent non-specific binding of antibody to protein, exposed antigen was blocked by submerging in 5% skimmed milk reconstituted with PBS-Tween tablets (Sigma, UK). Made-up PBS contained 10mM phosphate buffer, 2.7mM KCl, 137mM NaCl and to this was added 0.1% Tween 20 (Sigma, UK). 5% BSA was substituted for the milk component when phospho-proteins were under study, as the milk phospho-protein casein would potentially allow non-specific binding of phospho-protein antibodies. Loading controls and incubation steps

were tailored to the molecular weight (MW) of the protein of interest and performance of each specific protein-antibody interaction. The basic starting protocol is outlined in Table 2.7. Loading control proteins included α -actin (MW: 42kDa), α -tubulin (MW: 50kDa) or VDAC1 (MW: 31kDa).

Step	Solution	Time
Block	5 % Milk	Overnight at 4°C
Wash	PBS-Tween	3 x 10 min at room temp
1° antibody	5% Milk + 1° antibody (1:1000)	3 hrs at room temp
Wash	PBS-Tween	3 x 10 min at room temp
L/C antibody	5% Milk + 1° antibody to loading control (1:10000)	45mins at room temp
Wash	PBS-Tween	3 x 10 min at room temp
2° antibody	5% Milk + 2° antibody (1:10k)	1 hr at room temp
Wash	PBS-Tween	3 x 10 min at room temp
Enhanced chemiluminescence reagent (Amersham, UK)		3 min at room temp

Table 2.7: Membrane blocking and antibody exposure protocol for Akt. Timings were modified for different protein-antibody pairings for optimum performance as determined by trial and error. Milk was substituted with BSA for blotting of Phospho-proteins. Loading controls were tailored to the molecular weight of the protein of interest and the separation of molecular weights on the molecular weight ladder.

2.6.6 Protein detection by enhanced chemiluminescence

The proprietary secondary antibody used was conjugated to a horse radish peroxidase (HRP) enzyme, which is a strong catalyst of oxidising reactions involving H_2O_2 . The enhanced chemiluminescence (ECL) substrate is supplied in two parts, one containing H_2O_2 and the other its substrate, luminol. After mixing and adding to the HRP on the surface of the blotted PVDF, luminol is oxidised by H_2O_2 in the presence of HRP to form 3-aminophthalate. The reaction emits light at $\lambda=428nm$. Various compounds can be added to enhance light emission and thus aid detection, but the principal remains that HRP is only present where secondary antibody had attached to primary which is in turn attached to the protein of interest on the PVDF. Light emission therefore occurs only at the site of a protein of interest, and at an intensity that is proportional to the concentration of protein at that site.

In practise, membranes were bathed in freshly prepared ECL mixture for three minutes, then wrapped in Sarin wrap and secured into an X-ray film cassette (Kodak, UK) and transferred to a photographic darkroom. Hyperfilm ECL high performance chemiluminescence film (GE Healthcare, UK) was exposed to the cassette; exposure time was determined by trial and error to optimise protein band appearance and intensity. The chemiluminescence film was developed and fixed using standard photographic developer and fixative chemicals (Kodak, UK). Membranes were aligned with the films and the positions of the various molecular markers transcribed onto the film for reference.

2.6.7 Total and phosphorylated band quantification

Films were digitised on a flatbed scanner against a white background. ImageJ software (NIH, US) was used to quantify the density of the protein of interest, and this was corrected for the density of the loading control band protein run in the same lane and exposed from the same blot.

For quantification of Phospho-protein as a proportion of total protein, the Phospho-protein and total protein bands were corrected for their individual loading controls, and then the Phospho- band divided into the total protein band, as illustrated in Figure 2.19.

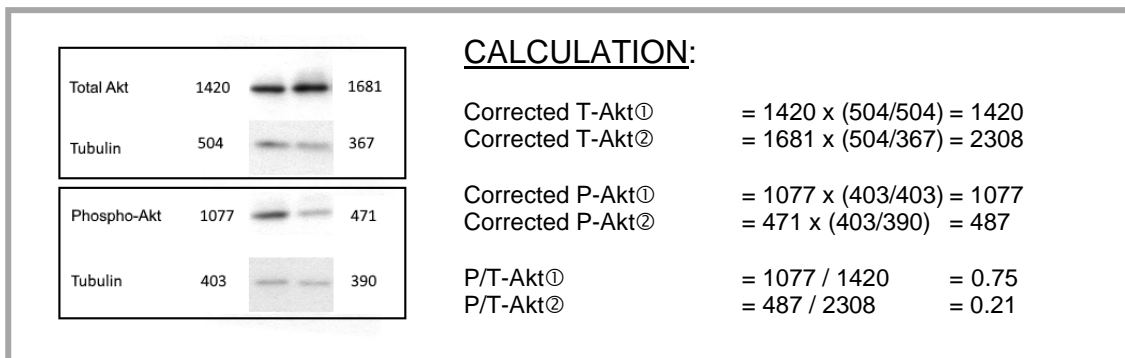


Figure 2.19: Example quantitative Western blot analysis. Phospho-Akt (P-Akt) and Total-Akt (T-Akt) bands are corrected for Tubulin loading control by dividing the quantitative densitometry readout for the P-Akt or T-Akt by a ratio of the corresponding Tubulin loading band to the maximally dense Tubulin loading band, as this reflects relative channel loading. The resulting corrected T-Akt and P-Akt are then divided into one another to give a readout of the proportion of T-Akt that is phosphorylated.

2.7 Hypoxia-reoxygenation of isolated cardiomyocytes

A second model of ischaemia-reperfusion was used to confirm findings in the whole heart Langendorff perfusion. Use of an isolated cardiomyocyte model enabled us to study the cardiomyocyte cell type on its own, and to establish whether cardioprotection requires integrated cell-cell signalling or can be effective in a single cell type. Straightforward drug studies can be undertaken to investigate signalling mechanisms underlying phenomena seen in the whole organ model.

Isolation of cardiomyocytes was originally described in 1976⁴⁰⁵ and is now used as a first step in many biochemical studies. Performed well, the technique produces a population of differentiated cardiac cells which may then be easily subjected to various conditions including, for our purposes, simulated ischaemia-reperfusion injury (sIRI, or more correctly “hypoxia-reoxygenation injury”) and oxidative stress. The mainstay of producing the cells is enzymatic digestion of the cardiac extracellular matrix to liberate them, followed by plating and stabilisation in an appropriate maintenance medium.

2.7.1 Preparation of isolated rat cardiomyocytes

Two practical techniques for liberating cardiomyocytes are available: the more straightforward approach is concomitant enzymatic and mechanical disruption of the ventricular architecture. However, a refinement to the technique sees enzymatic digestion performed on a Langendorff rig prior to mechanical disruption of the ventricles. According to experience in our group, the staged technique seems to improve cellular yield, and given the easy availability of Langendorff equipment in our lab, we opted to use this.

This method has been refined from published variants by our colleague at the Hatter, Dr Andrew Hall, whose work is duly acknowledged.

Animals were euthanased by heart explantation as per section 2.5.1 (“rat euthanasia”) and mounted on a sterile constant flow Langendorff rig perfused at 10mls/min. A sequence of five perfusate solutions were prepared and used to digest the heart, as per tables 2.8 and 2.9. All buffer constituents were sourced from Sigma Aldrich (UK).

Salt	Final conc. (mmol/L)	Amount per 500ml	Amount per 1L	Amount per 2L
NaCl	130	3.79g	7.59g	15.18g
KCl	5.4	0.2g	0.4g	0.8g
MgCl ₂	1.4	0.066g	0.133g	0.266g
Na ₂ HPO ₄	0.4	0.028g	0.057g	0.114g
HEPES	4.2	0.5g	1.0g	2.0g
pH to 7.3 at 37°C				
Glucose	10	0.9g	1.8g	3.6g
Taurine	20	1.25g	2.5g	5g
Creatine	10	0.655g	1.31g	2.62g

Table 2.8: Base stock solution for rat cardiomyocyte isolation buffers (credit: Dr A Hall).

Sol ⁿ	Function	Additional solute	Amount per 50ml of base solution
1	Clear heart of blood	750µmol/L CaCl ₂	37.5µl of 1mol/L CaCl ₂
2	Hypocalcaemic cardiac arrest	100µmol/L EGTA	2mg of EGTA
3	Enzymatic digestion	100µmol/L CaCl ₂ 0.5mg/ml Collagenase	40µl of 100mmol/L CaCl ₂ 18mg Collagenase
4	Reintroduce calcium	0.5mmol/L CaCl ₂	10µl of 1mol/L CaCl ₂
5	Reintroduce calcium	1mol/L CaCl ₂	20µl of 1mol/L CaCl ₂

Table 2.9: Rat cardiomyocyte isolation buffers (credit: Dr A Hall)

All solutions are warmed to 37°C and pH corrected to 7.3 by titration of 1M NaOH. The explanted heart is perfused with solution 1 for four minutes to clear blood and stabilise the heart function. Solution 2 is then substituted and perfused for four minutes during which contraction arrests due to chelation of calcium by ethylene glycol-bis(β-aminoethyl ether)-N,N,N',N'-tetraacetic acid (EGTA). Solution 3 is then substituted and after giving sufficient time for washout of EGTA, is recirculated. This is the start of the enzymatic digestion

phase. After 8-10 minutes, judged by the changing texture of the heart, the ventricles are amputated into further Solution 3, and cut into ~2mm pieces with scissors, the first stage of physical digestion. The solution is then bubbled with Oxygen and further disrupted by repeated gentle suction into a Pasteur pipette.

The supernatant solution is now periodically checked for liberated cell content under light microscopy. Highly cellular supernatant is pipetted off and further mechanical disruption of the residual intact tissue undertaken until sufficient cells have been liberated. The residual supernatant is sieved through gauze and the collected supernatants containing liberated cells allowed to settle for 10 minutes. A cellular pellet forms and is resuspended in 20mls of Solution 4 to begin reintroduction of Calcium, which was depleted during introduction of EGTA. Again, cellular tissue precipitates, and is resuspended in 20mls Solution 5 with physiological Calcium concentration, allowing intact electromechanical coupling to resume.

2.7.2 Cardiomyocyte culture

Standard cardiomyocyte culture conditions common in our lab were used⁴⁰⁶. Isolated cardiomyocytes were resuspended in plating medium (Medium-199; Sigma, UK) supplemented with 2 mg/ml bovine serum albumin, 0.66 mg/ml creatine, 0.66 mg/ml taurine, 0.32 mg/ml carnitine, 50 U/ml penicillin, 5 µg/ml streptomycin (Calbiochem, Nottingham, UK). The cell suspension was pipetted onto a 22mm glass cover slip (VWR, UK) pre-coated with Lamin (1mg/ml in Dulbecco's sterile Phosphate Buffered Saline). After an hour to adhere at 37°C, 95%O₂/5%CO₂ and 90% humidity, cells were washed with further plating medium, then left overnight to incubate in 1ml plating medium before use in one of the following experimental protocols.

2.7.3 Simulated ischaemia-reperfusion

During myocardial ischaemia-reperfusion in the intact heart, cardiomyocytes are subject to falling extracellular pH, reduced oxygen tension and reduced energy flux. Failure of oxidative metabolism and ion pumps results in extracellular accumulation of lactate and potassium²⁴. This can be modelled in isolated cells by substituting the usual glucose and oxygen-rich culture medium with an acidic medium containing less glucose and oxygen and high levels of lactate and potassium. This approach is widely used to model ischaemia-reperfusion and is

referred to as simulated ischaemia-reperfusion (sIRI) or the hypoxia-reoxygenation (“hypox-reox”) model. It has been widely employed by our group and others to investigate various aspects of cardioprotection, preconditioning and resilience to ischaemia-reperfusion^{406,407}.

Normoxic and hypoxic buffers are prepared to the recipes in Tables 2.10 and 2.11 respectively, based on published protocols⁵⁴ modified for use in our group.

Substrate	Final conc. (mM)	Amount per L	Amount per 500ml	Amount per 250ml	Amount per 100ml
Glucose	10	1.8	0.9	0.45	0.18
NaCl	118	6.8	3.4	1.7	0.68
KCl	2.6	0.193	0.0965	0.0483	0.0193
KH ₂ PO ₄	1.2	0.163	0.0815	0.0408	0.0163
MgSO ₄	1.2	0.295	0.1475	0.0738	0.0295
NaHCO ₃	22	1.8	0.9	0.45	0.18
CaCl ₂ (1M Stock)	1.0	1ml	0.5ml	0.25ml	0.1ml

Table 2.10: Normoxic bicarbonate buffered solution for stabilisation and reperfusion phases of a hypox-reox isolated cardiomyocyte experiment. This is gassed with 95%O₂/5%CO₂ to a pH of 7.4 at 37°C (credit: Dr A Hall).

Substrate	Final conc. (mM)	Amount per L	Amount per 500ml	Amount per 250ml	Amount per 100ml
NaCl	127.8	7.4g	3.7g	1.85g	0.74g
KCl	14.8	1.1g	0.55g	0.275g	0.11g
KH ₂ PO ₄	1.2	0.163g	0.0815g	0.0408g	0.0163g
MgSO ₄	1.2	0.295g	0.1475g	0.0738g	0.0295g
NaHCO ₃	2.2	0.184g	0.092g	0.046g	0.0184g
CaCl ₂ (1M Stock)	1.0	1ml	0.5ml	0.25ml	0.1ml
Na lactate	10	1.7ml	0.85ml	0.425ml	0.17ml

Table 2.11: Anoxic bicarbonate buffered solution for simulated ischaemia phase of a hypox-reox isolated cardiomyocyte experiments. This is gassed with 5% CO₂-95% N₂ to a pH of 6.4 at 37°C (credit: Dr A Hall).

2.7.3.1 A practical simulated ischaemia-reperfusion protocol

After stabilisation overnight in supplemented M-199 cell culture medium (section 2.6.2 “cardiomyocyte culture”), cells were washed and placed in anoxic medium (Table 2.11). The cells were placed in an airtight custom-built hypoxic chamber (Figure 2.21) which was then filled with 5% CO₂-95% N₂ until just over atmospheric pressure and sealed.



Figure 2.20: Custom-built hypoxic chamber. Plated cardiomyocytes are placed in the chamber, which is then gassed with positive pressure 5% CO₂-95% N₂ and sealed. The cardiomyocytes are thus exposed to a near-zero Oxygen tension environment, which along with the provision of hypoxic buffer (described in the text) is a well-validated model of tissue ischaemia.

The hypoxic chamber was then placed in our standard atmospherically-controlled incubator for the duration of the hypoxic phase of the experiment. At simulated reperfusion, cells were removed from the hypoxic chamber, washed and placed in normoxic medium (table 2.6). Cells were maintained in standard incubator conditions (37°C, 95%O₂/5%CO₂ and 90% humidity) for the simulated reoxygenation period. 3 µM propidium iodide was added for 10 minutes (see section 2.6.5 “cardiomyocyte survival assay”) for the cardiomyocyte survival assay.

Control cells were incubated in normoxic medium, kept in standard incubator conditions (37°C, 95%O₂/5%CO₂ and 90% humidity) throughout, with washes

and fresh medium containing propidium iodide to correspond to simulated reperfusion.

2.7.4 Varying conditions during simulated reperfusion

Durations of simulated ischaemia and reperfusion were varied during optimisation of this experimental protocol. Reperfusion was conducted with exposure to variable glucose concentration. This was achieved by substituting the glucose in the normoxic buffer recipe (table 2.10) with a glucose-mannitol mixture (Table 2.3) to ensure consistent osmolality across reperfusion.

In experiments examining the effect of blocking cellular uptake of Phlorizin 3 μ M dissolved in DMSO, or DMSO vehicle alone was added to reperfusion buffer. See section 2.5.12.2 (“blockade of basal glucose uptake”) for further details.

2.7.5 Cardiomyocyte survival assay

After the time allotted for simulated reperfusion, the percentage of cells stained with propidium iodide (PI) was determined using a Nikon Eclipse TE200 fluorescent microscope to calculate the percentage cell death in each treatment group. For each treatment group 80 cells were counted, taken from four randomly-selected fields of view.

2.8 ROS production on exposure to high glucose

To investigate the mechanism underlying variable cardiomyocyte survival from IRI with variable glucose during reperfusion, we subjected isolated cardiomyocytes to different conditions of glucose, both in a steady state and after stress induced by reactive oxygen species and measured ROS production.

Isolated cardiomyocytes were prepared as per sections 2.8.1-2, washed, and transferred into Tyrode’s buffer, prepared as per the recipe in Table 2.12:

Solute	Final Conc (/mmol/L)	Amount per 50ml	Amount per 250ml
NaCl	137	400mg	2g
KCl	5.4	20mg	100mg
MgCl ₂	0.4m	4 μ l of 1mol/L	20 μ l of 1mol/L
CaCl ₂	1	50 μ l of 1mol/L	250 μ l of 1mol/L
Glucose	10	90mg	450mg

HEPES	10	119mg	595mg
-------	----	-------	-------

Table 2.12:

Tyrode's buffer for use in confocal microscopy studies of ROS production in isolated cardiomyocytes (credit: Dr A Hall).

Cardiomyocytes were loaded with the fluorescent ROS indicator CM-H2DCFDA at a concentration of 10 μ M for 30mins and then stabilised in standard Tyrode's without dye for a further 30mins. Thereafter standard Tyrode's buffer was substituted with Tyrode's in which the D-Glucose component was replaced with D-Glucose and D-Mannitol to produce solutions with varying Glucose content but consistent osmolality (prepared as per Table 2.3). Cells were incubated at 37°C, 95%O₂/5%CO₂ and 90% humidity throughout. Various timescale experiments were undertaken to find the optimal time for imaging ROS and these are presented in the results section, Chapter 5, "Effects of glucose on the response to reperfusion injury in a diabetic and a non-diabetic model".

2.8.1 ROS imaging

CM-H2DCFDA is a widely-used ROS-sensitive dye emitting light at $\lambda=527\text{nm}$ in response to an excitation at $\lambda=495\text{nm}$ ⁴⁰⁸. Five cells per timepoint per experimental run were imaged with a Zeiss 510 CLSM confocal microscope equipped with 40x oil immersion objective lens (Plan-Apochromat, NA 1.3) using an Argon laser for excitation. Images were saved (one cell per image) and analysed using ImageJ software (NIH) to calculate Corrected Total Cellular Fluorescence (CTCF) on the green channel.

2.9 Mitochondrial studies

Mitochondrial function is central to resilience to ischaemia-reperfusion injury. The propensity for the mitochondrial permeability transition pore to open is a key determinant of cell survival during reperfusion⁷⁶. Mitochondria are also key intracellular sites of ROS generation; ROS are key mediators of IRI, and may trigger cell death or indeed may activate the final common pathway of the preconditioning response to protect against reperfusion cell death^{409–411}.

Pharmacological uncoupling of mitochondrial respiration has been linked to induction of a preconditioned state⁴¹². Mitochondria from hearts with impaired insulin signalling have been shown to have abnormalities including uncoupled

respiration. We hypothesised that changes in uncoupled respiration in our rats' hearts may underlie their changing vulnerability to myocardial IRI. We therefore studied mitochondrial respiration in various states of coupled and uncoupled respiration.

2.9.1 Rat euthanasia

Animals were killed by heart explantation under anaesthesia as described.

2.9.2 Mitochondrial isolation

Mitochondria were isolated from ventricular tissue via an adaptation of the differential centrifugation method described originally by Palmer in the 1970s⁴¹³. Hearts were explanted into Chappel-Perry buffers (CP1 and CP2), prepared as per Table 2.14. Blood was removed by rinsing, the tissue was weighed, diced with scissors and homogenized in a dounce tissue homogeniser, in 1ml CP1 buffer per 100mg ventricular tissue. 15 dounce strokes were needed to homogenise the tissue before it was incubated in an Eppendorf tube with Trypsin 100µL/ml for 10mins. The homogenate was combined with an equal volume of CP2 buffer and re-homogenised in the dounce. Differential centrifugation was used to separate out the mitochondrial fraction with spins at 1000g for 10mins and 5200g for 10mins before resuspension of the pellets in fresh CP2 buffer and a further spin at 5200g for 10mins⁴¹⁴.

Constituent	Chappel-Perry buffer 1 (CP1)	Chappel-Perry buffer 2 (CP2)	"KME" buffer
KCL	100mmol/L	100mmol/L	100mmol/L
MOPS	50mmol/L	50mmol/L	50mmol/L
MgSO ₄	5mmol/L	5mmol/L	5mmol/L
EGTA	1mmol/L	1mmol/L	1mmol/L
ATP	1mmol/L	1mmol/L	-
Fatty acid free bovine serum albumin	-	2mg/ml	-
pH to 7.4 with 1M KOH			

Table 2.14: Preparation of buffers for use in mitochondrial isolation protocols (Credit: Dr A Hall)

Finally, the pellets of mitochondria were resuspended in 200 μ L KME buffer.

A Smith protein assay was then performed, and concentrations equalised across samples to 5 μ g/ μ L as per the method in section 2.6.2 (“equalisation of protein content”).

2.9.3 Mitochondrial respirometry setup

Mitochondrial respiration was assessed by measuring the rate of Oxygen depletion from mitochondrion-rich buffer under controlled conditions. Oxygen was detected via polarography using a Clark oxygen electrode⁴¹⁵ mounted in a thermostatically controlled chamber with continuous agitation of the mitochondrial medium by a magnetic stirrer, to equalise Oxygen tension throughout the volume.

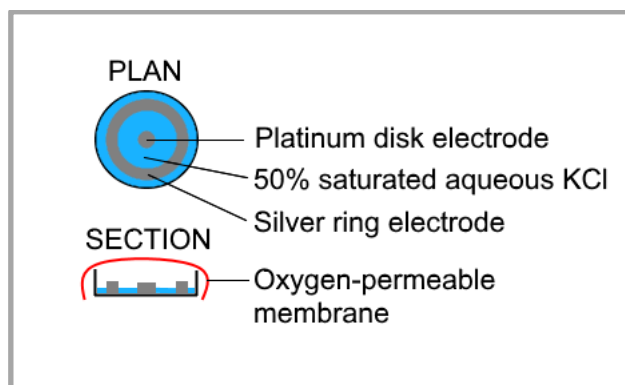


Figure 2.25: Design of a Clark Oxygen electrode⁴¹⁵. This allows detection of Oxygen tension via a small voltage applied across the electrode, which causes Oxygen to be reduced at the cathode and Silver to be oxidised at the anode. The current thus induced increases steadily until the Oxygen supply limits further increase. The plateau current thus reflects the available Oxygen concentration at the cathode.

A Clark Oxygen electrode comprises a Silver anode and Platinum cathode suspended in an electrolyte, as shown in Figure 2.25. A small voltage (approximately 700mV) applied across the electrodes causes Oxygen to be reduced at the cathode and Silver to be oxidised at the anode. Thus, a current is induced and increases steadily, until such a time as Oxygen supply limits further increase. The plateau current therefore reflects the available Oxygen content. In our setup, the Platinum cathode is bathed in 50% saturated KCl (17.5g of anhydrous salt in 100ml redistilled H₂O) covered by an Oxygen-permeable membrane and enclosed within a thermostatically controlled unit

(Oxytherm, Hansatech Instruments, UK). The electrode is linked to a computer interface for continuous graphing of Oxygen tension. Electrode calibration is checked before each use with Mito 5 buffer (described below) equilibrated with atmospheric oxygen at 25°C, which should read approximately 2000mV calibrated to 253.2nmol/L of O₂. Oxygen is then scavenged by addition of excess sodium sulphite (Na₂SO₃) after which the correctly prepared Clarke electrode should approximate zero.

2.9.4 Respirometry protocol

70µL of mitochondria suspended in KME buffer were added to 230µL Miro 5 buffer (EGTA 0.5mmol/L, MgCl₂.6H₂O 3mmol/L, K-lactobionate 60mmol/L, Taurine 20mmol/L, KH₂PO₄ 10mmol/L, HEPES 20mmol/L, Sucrose 110mmol/L, fatty acid free BSA 1g/L, pH 7.0 with KOH 1M) and allowed to equilibrate at 25°C.

After achieving a steady state of Oxygen tension, substrates for either electron transport chain (ETC) Complex I or Complex II were added to stimulate transport through the ETC in the absence of ADP (so-called ADP-limited respiration), as described by Pravdic⁴¹⁶ and modified by Hall⁴¹⁴. After reaching steady state respiration, indicated by unchanging rate-of-change on the graph of Oxygen tension, serial additions of substrates and blockers were made as per Hall's protocol, shown in Table 2.15:

Respiration state	Complex I	Complex II
ADP-limited (state 2)	Glutamate 10mmol/L Malate 10mmol/L Na pyruvate 10mmol/L	Succinate 5mmol/L Rotenone 1µmol/L
ADP-stimulated (state 3)	ADP 250µmol/L	
Leak only	Oligomycin 250µmol/L	
Uncoupled	Serial FCCP 1µmol/L additions until maximal rate	
Nil (background O ₂ loss)	Antimycin A 5µmol/L	

Table 2.15: Hall's protocol for investigation of ADP-limited, ADP-stimulated, leak and maximal uncoupled respiratory flux through ETC Complex I or Complex II

2.9.4.1 ADP-limited respiration (state 2)

At the start of the protocol, there is low-rate electron flux through the ETC, with electrons entering via either NADH dehydrogenase (Complex I) or Coenzyme Q (Complex II) as determined by the electron donors provided. Glutamate, Malate and Pyruvate supply electrons via NADH to Complex I, and Succinate is reduced to Fumarate by Complex II. When Complex II was under study, Complex I inhibitor Rotenone was added to prevent residual NADH donating electrons via Complex I.

2.9.4.2 ADP-stimulated respiration (state 3)

After addition of ADP, F_1-F_0 ATP synthase imports protons across the mitochondrial membrane, phosphorylating ADP to ATP with the liberated energy. The proton gradient activates Cytochrome bc₁ (Complex III), Cytochrome c and Cytochrome c oxidase (Complex IV) thus achieving maximal electron flux through the ETC coupled to ATP generation. O₂ is consumed at a maximal coupled rate as Complex IV reduces O₂ to H₂O.

2.9.4.3 “Leak” respiration

Oligomycin is a macrolide antibiotic that binds to the F_0 portion of the ATP synthase molecule, preventing proton flux. After administration of Oligomycin the only residual electrochemical gradient across the inner mitochondrial membrane is due to proton leak; only minimal (“leak”) transport of protons is therefore possible via Complexes III and IV, and the flux of electrons via the ETC therefore falls to a rate that reflects the degree of residual proton leak across the IMM. This is so-called leak respiration.

2.9.4.4 Uncoupled respiration

Addition of the ionophore carbonyl cyanide p-(trifluoromethoxy)-phenyl-hydrozone (FCCP) allows free transport of ions across the IMM and therefore dissipates the electrochemical gradient. This renders the F_1-F_0 ATP synthase inactive due to dissipation of the proton gradient, but protons are now present at high concentration in the inner mitochondrial space, so Complexes III and IV have access to ample protons as substrate for electron transfer. Electron flux through the chain therefore reaches maximal uncoupled rate and Oxygen is consumed rapidly to form H₂O at Complex IV.

2.9.4.5 Measuring background O₂ loss

Antimycin A is a metabolic poison that binds cytochrome C reductase to inhibit the oxidation of ubiquinone and disrupt the Q cycle of enzyme turnover. This in turn blocks both the flux of protons through Complex IV and stops Complex IV accepting electrons from further up the ETC. Flux through the ETC therefore halts and no longer contributes to Oxygen loss in our model. Any subsequent decrease in O₂ tension is due to non-ETC mechanisms. This rate is minimal and is used to correct for environmental O₂ loss during the experiments.

Figure 2.26 shows a representative O₂ trace generated from an Oxytherm datafile imported into GraphPad Prism, and illustrates the calculations performed to derive experimental results.

2.9.5 Respirometry interpretation

The Oxytherm instrument generates a datafile with Oxygen tension and rate of change of Oxygen tension over time recorded every second. For each phase of the respirometry protocol the steady state rate of change of Oxygen was recorded. For the uncoupled phase, FCCP was given repeatedly until no change was seen in the slope of the O₂ tension graph (two doses in the example trace in Figure 2.26) indicating maximal uncoupling. The steady state slope after the last dose of FCCP was taken as the maximal uncoupled respiration rate. An increase in Oxygen tension was characteristically seen after the addition of Antimycin A. The slope of the line was measured once steady state was reached after this increase, characteristically there was a level trace or slight decline in O₂ at this point. The gradient with Antimycin A was the background O₂ loss and this slope was subtracted from other slopes during the same experimental run, to adjust for environmental O₂ loss.

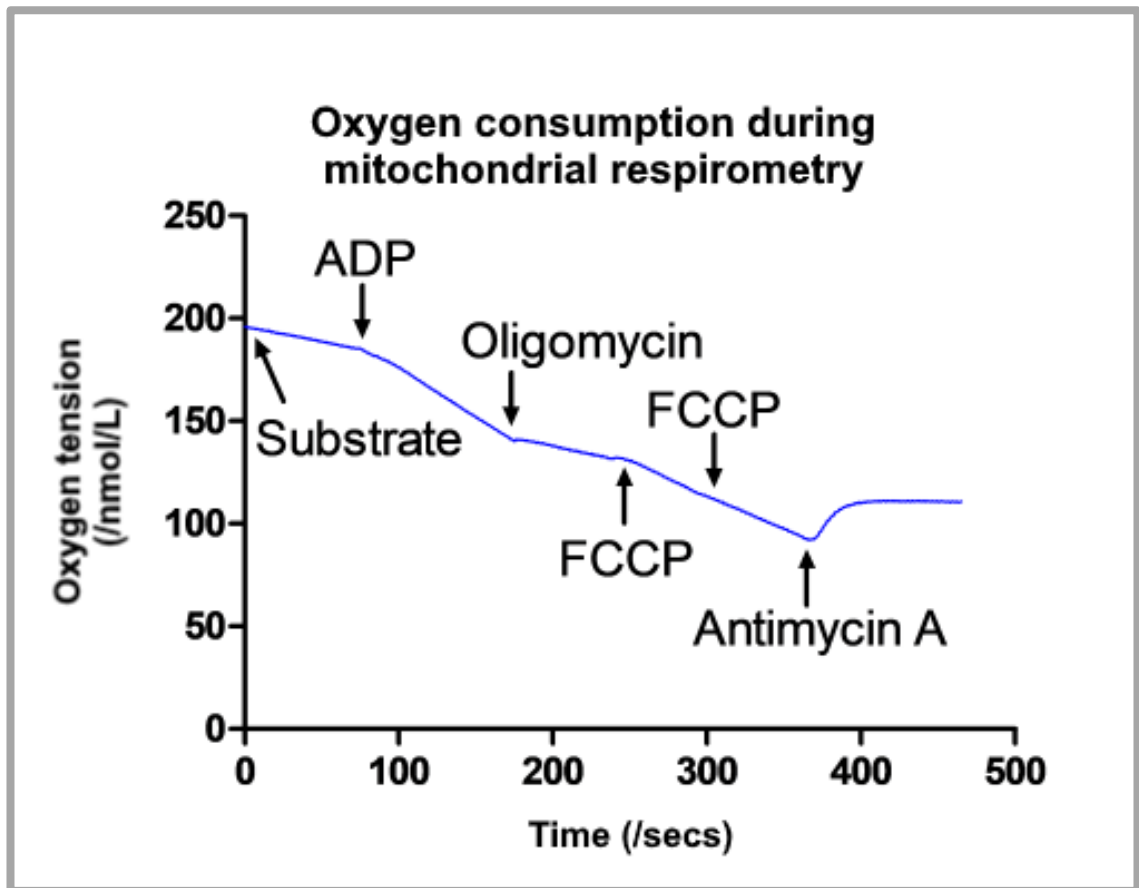


Figure 2.26: Example oximetry trace during mitochondrial respirometry. Addition of substrates to either Complex I or Complex II of the Electron Transport chain initiates ADP-limited (state 2) respiration, consuming Oxygen. The rate of respiration is reflected by the slope of the graph, determined by the rate of Oxygen consumption. Addition of ADP leads to ADP-stimulated (state 3) respiration. Oligomycin binds with the F_0 portion of the ATP synthase molecule, preventing proton flux and leaving only residual electrochemical gradient across the inner mitochondrial membrane is due to proton leak, the so-called “leak” respiration rate. The ionophore FCCP allows free transport of ions across the IMM and therefore dissipates the electrochemical gradient. Electron flux through the chain therefore reaches maximal uncoupled rate as protons are now plentiful in the inner mitochondrial space. FCCP is added several times until maximal rate of Oxygen consumption is reached. The addition of Antimycin A inhibits the final step of the ETC, thus rendering the entire chain inactive. Any further Oxygen loss represents Oxygen loss from the system, and can be used to correct all the other measured rates for environmental loss of Oxygen.

3. TESTING FOR EVIDENCE OF DIABETES IN UCL'S GOTO-KAKIZAKI RAT COLONY

3.1 Aims and hypotheses

We require a diabetic animal model in which to study myocardial ischaemia-reperfusion injury. This work aims to establish:

1. Whether DM remains present in the UCL GK colony;
2. Whether glucose handling remains impaired in similar fashion to man and to other GKR colonies;
3. Whether the diabetic phenotype in the adult animal changes over time, and if it does, whether there is an optimal age when the phenotype has relevance to the phenotype of a diabetic patient likely to suffer an MI (i.e. established diabetes);
4. What age-related defects in myocardial mitochondrial function exist in the GKR as compared to wild-type controls.

We hypothesise that UCL-GKRs will exhibit changes similar to the metabolic defects seen in other GKR colonies³⁴⁷. Compared to wild-type Sprague Dawley rats and Wistar rats, in UCL-GKR we expect hyperglycaemia from adolescence onwards, followed by late development of insulin resistance. We also expect significant growth retardation in the UCL-GKR compared to non-diabetic rat strains, as reported in other colonies.

We hypothesise more marked age-related changes in mitochondrial function in the GKR than in comparator rat strains.

3.2 Results

3.2.1 Cohort size and tracking

In total, 20 GKR, 15 SDR and 15 WR were included in the weight and diabetes development study longitudinal cohort. We attempted to track weight gain and changes to blood parameters in individual animals, but this failed due to problems with enduring labelling of individual animals. We attempted to track animals via tail tagging but these tags rubbed off, and then via their cage locations, and whilst this was possible for larger animals (all Wistar) that were individually caged, this was not successful for smaller animals housed up to three per cage as per animal husbandry standard operating protocols at UCL. Moreover, we found that even individually caged animals lost their non-statutory cage labelling during moving rooms in the animal house.

3.2.2 Survival

We also attempted to construct survival curves for each rat strain to illustrate the longevity of each strain. However, this was hampered by very low spontaneous mortality within the strains, compared to the rate at which they were used in non-recovery experiments. In total, throughout longitudinal follow-up of this cohort, five GKs died spontaneously, versus 1 SDR and 1 WR. All other participating animals were euthanised during other experimental protocols during this work. Nonetheless, crude mortality rates per month can be calculated as shown in table 3.1, although these are not very meaningful due to the significant cohort attrition caused by using animals in non-recovery experiments.

Rat Strain	Sprague Dawley	Wistar	Goto Kakizaki
Individuals followed from 3 months	15	15	20
Mean length of follow-up	9.0 months	9.6 months	9.2 months
Total spontaneous deaths	1	1	5
Crude spontaneous mortality rate	0.74% per month	0.69% per month	3% per month

Table 3.1: Spontaneous rat mortality in the longitudinal follow-up cohort.

3.2.3 General health

Two Goto Kakizaki rats were euthanased after developing obvious palpable tumours, versus no SDRs and one Wistar. Other deaths were spontaneous and not preceded by observable ill health. GKR developed clinically obvious cataract after age eight months. GKR tended to consume more water than Wistar or SDRs.

3.2.4 Body weight

All 50 animals (20 GKR, 15 SDR, 15 WR) included in the longitudinal follow-up study were weighed once or more. Body weight over time is shown in Figure 3.1.

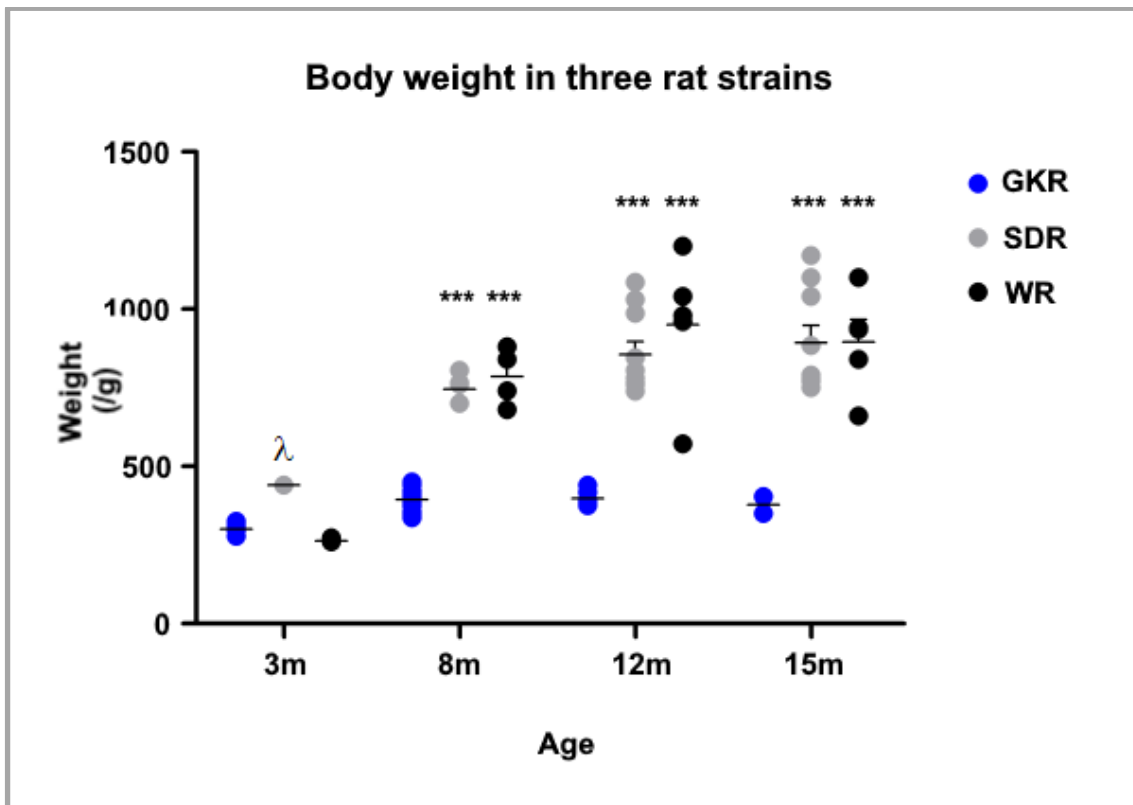


Figure 3.1: Body weight over time in all three rat strains studied. At 3 months, WRs are significantly lighter than SDRs, with a trend towards being lighter than GKRs. SDRs and WRs put on weight up to the age of 12 months at which point the weights of both these strains stabilised. There was no statistically significant difference between the weights of SDRs and WRs at 8, 12 or 15m. GKRs followed a different pattern of weight gain, adding a comparatively small amount of weight from 3 to 8 months age and therefore being significantly lighter than both SDRs and WR at 8m age. GKRs' weight remains stable from 12 months onwards. GK: Goto Kakizaki, SDR: Sprague Dawley, WR: Wistar, m: months, g: grams; ***: $p < 0.001$ vs age-matched GKR group; λ : $p < 0.05$ vs age-matched WR group.

At 3 months, WRs are significantly lighter than SDRs ($263\pm 2\text{g}$ vs $440\pm 0\text{g}$; $P<0.05$), with a trend towards being lighter than GKR (s) ($301\pm 7\text{g}$; $P=\text{NS}$). SDRs and WRs put on weight up to the age of 12 months ($746\pm 20\text{g}$ increasing to $856\pm 41\text{g}$ and $785\pm 45\text{g}$ increasing to $895\pm 161\text{g}$, respectively) at which point the weights of both these strains stabilised. There was no statistically significant difference between the weights of SDRs and WRs at 8, 12 or 15m. GKRs followed a different pattern of weight gain, adding a comparatively small amount of weight from 3 to 8 months age ($301\pm 7\text{g}$ increasing to $395\pm 6\text{g}$; $P<0.0001$) and therefore being significantly lighter than both SDRs and WR at 8m age ($395\pm 6\text{g}$ vs $746\pm 20\text{g}$ and $785\pm 45\text{g}$; $P<0.001$ for both comparisons). GKRs' weight remains stable from 12 months onwards ($399\pm 10\text{g}$ at 12 months, $378\pm 28\text{g}$ at 15 months; $P=\text{NS}$ for both in comparison to 8 month weight).

Analysis of the spread of weights reveals that weights of the GKRs is highly consistent (standard deviations 19g, 28g, 25g and 37g at 4 respective ages) compared to the weights of SDRs, which diverged over time (standard deviations 0g at 3m, versus 46g, 128g and 166g at 8, 12 and 15m respectively). WR weights also varied more with age (standard deviations 5g at 3m, then 91g, 161g and 232g at 8, 12 and 15m).

In summary: Wistar rats were slightly lighter than the other two strains at the first weighing at 3 months old. All three strains then put on weight up to 8 months of age, but GKRs accumulated significantly less weight than the other two strains. From 8 months, GKRs' weight then remained stable, whereas SDR and WR weight increased further to 12 months before stabilising. From 8 months onwards, the spread of weights observed in both SDR and WR groups was larger than the spread in the GKR group.

3.2.5 Fasting blood glucose

All 50 animals (20 GK, 15 SDR, 15 WR) included in the longitudinal follow-up study had fasting blood glucose measured once or more. In total, 84 blood glucose measurements were taken, i.e. an average of 1.7 per animal. Fasting blood glucose content at the four sampling ages is shown in Figure 3.2:

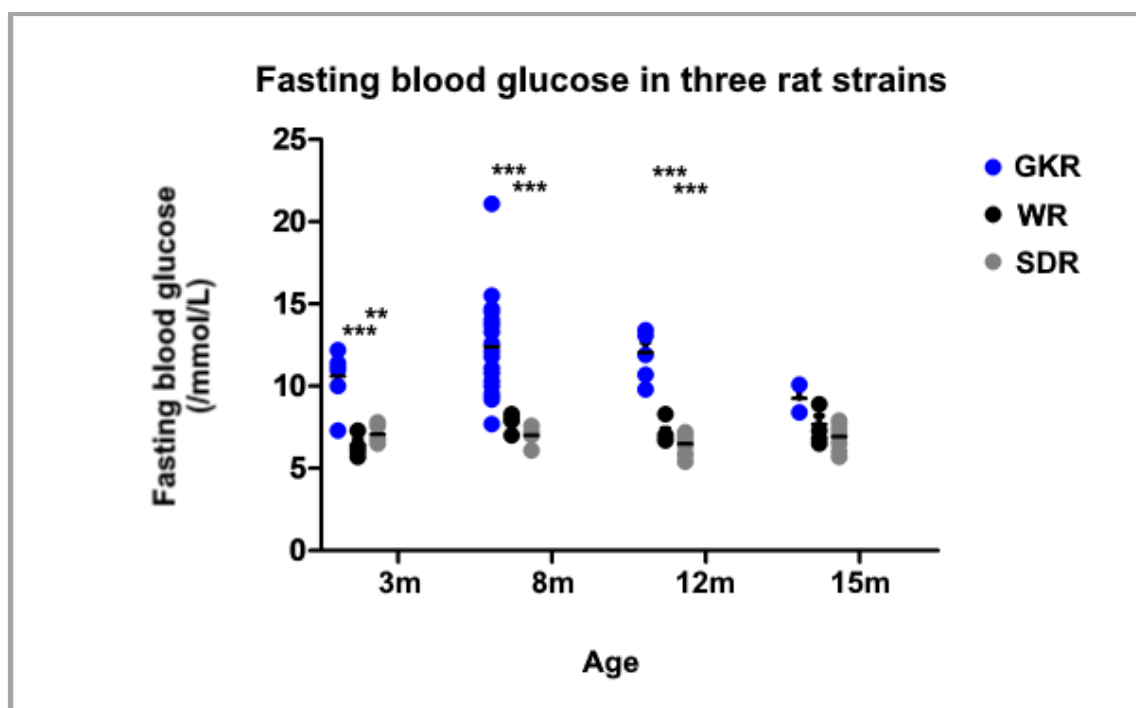


Figure 3.2: Fasting blood glucose levels over time in all three rat strains studied. GKRs' fasting glucose was significantly higher than fasting glucose in WRs at all ages except 15 months. GKRs' fasting glucose was also significantly higher than fasting glucose in SDRs at all ages except 15 months. At all ages, WRs and SDRs had similar fasting glucose levels. Neither GK, SDR nor WR fasting glucose changed significantly with age. GK: Goto Kakizaki, SDR: Sprague Dawley, WR: Wistar, m: months, mmol/L: millimoles per litre, **: $P < 0.01$ vs age-matched GKR group, ***: $P < 0.001$ vs age-matched GKR group. Number (n) per group is 6-20.

GKRs' fasting glucose was significantly higher than fasting glucose in WRs at all ages except 15 months (10.61 ± 1.51 mmol/L vs 6.45 ± 0.69 mmol/L at 3m, 12.38 ± 2.96 mmol/L vs 7.82 ± 0.57 mmol/L at 8m, 12.05 ± 0.53 mmol/L vs 7.10 ± 0.68 mmol/L at 12m, $P < 0.001$ for each comparison; 9.25 ± 1.20 mmol/L vs 7.68 ± 1.15 mmol/L, $P = \text{NS}$ at 15m). GKRs' fasting glucose was also significantly higher than fasting glucose in SDRs at all ages except 15 months (10.61 ± 1.51 mmol/L vs 7.08 ± 0.58 mmol/L at 3m, 12.38 ± 2.96 mmol/L vs 7.02 ± 0.56 mmol/L at 8m, 12.05 ± 0.53 mmol/L vs 6.49 ± 0.61 mmol/L at 12m,

$P < 0.01$, $P < 0.001$ and $P < 0.001$ respectively; $9.25 \pm 1.20 \text{ mmol/L}$ vs $6.92 \pm 0.75 \text{ mmol/L}$, $P = \text{NS}$ at 15m).

At all ages, WRs and SDRs had similar fasting glucose levels ($6.45 \pm 0.69 \text{ mmol/L}$ vs $7.08 \pm 0.58 \text{ mmol/L}$ at 3m, $7.83 \pm 0.57 \text{ mmol/L}$ vs $7.02 \pm 0.56 \text{ mmol/L}$ at 8m, $7.10 \pm 0.68 \text{ mmol/L}$ vs $6.49 \pm 0.61 \text{ mmol/L}$ at 12m, $7.68 \pm 1.15 \text{ mmol/L}$ vs $6.92 \pm 0.75 \text{ mmol/L}$ at 15m; $P = \text{NS}$ for each comparison).

Neither GK, SDR nor WR fasting glucose changed significantly with age ($P = \text{NS}$ for all comparisons).

In summary: GKR exhibited high fasting blood glucose content compared to both other strains at all ages except 15 months, and at no age were SDRs distinguishable from WRs on the basis of fasting blood glucose content. Fasting blood glucose content did not alter with age in any strain.

3.2.6 Glycated haemoglobin

All 50 animals (20 GK, 15 SDR, 15 WR) included in the longitudinal follow-up study had blood drawn for glycated haemoglobin analysis. In total, 76 glycated haemoglobin measurements were taken, i.e. an average of 1.5 per animal. Glycated haemoglobin at the four sampling ages is shown in Figure 3.3:

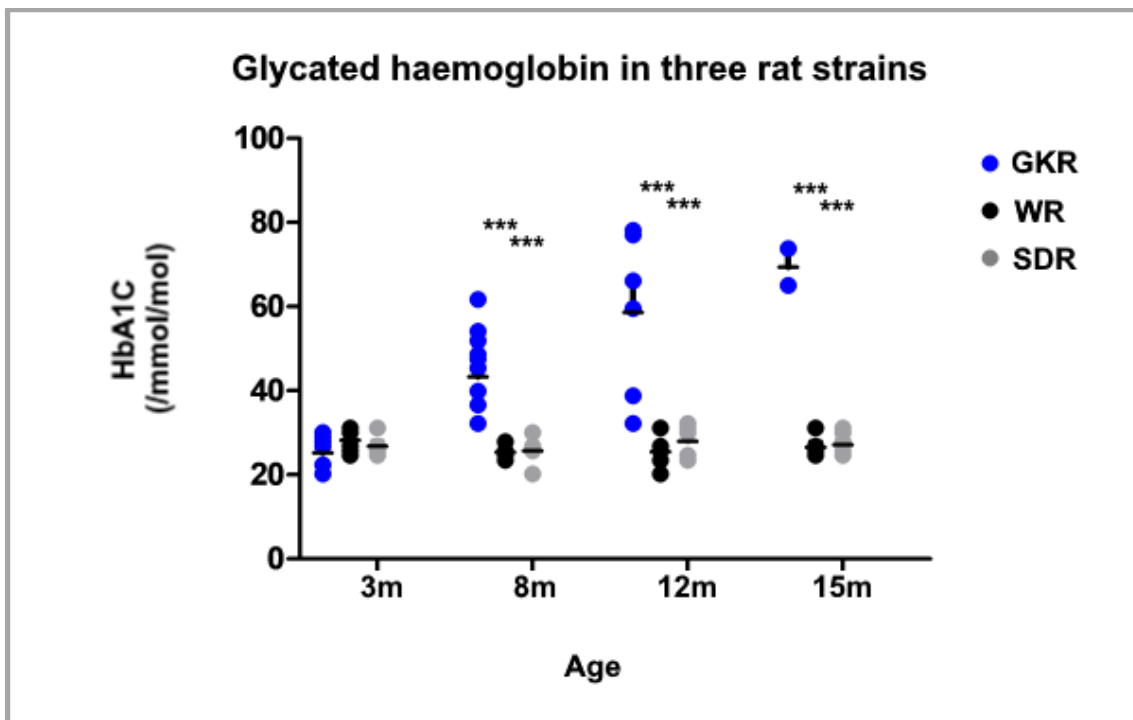


Figure 3.3: Long-term trends in blood glucose levels in all three rat strains studied. Haemoglobin glycation (an indirect measure of long-term trend in blood glucose content) was present at a low baseline level in all three strains. In the WR and SDR it remained at this low level at all ages, and no distinction was present between these two strains. GKR developed significantly higher levels than their own baseline, and the age-matched values of the other strains, by 8 months age. This elevated glycation persisted in GKR throughout all subsequent measurements. GK: Goto Kakizaki, SDR: Sprague Dawley, WR: Wistar, m: months, HbA1c (mmol/mol): millimoles of glycated haemoglobin (HbA1c) per mole of non-glycated haemoglobin. ***: $P < 0.001$ vs age-matched GKR group.

Glycated haemoglobin was present at the same low level in all strains at 3 months age (GKR 25.21 ± 4.18 mmol/mol, WR 28.23 ± 2.90 mmol/mol, SDR 26.78 ± 2.56 mmol/mol; $P = \text{NS}$ for all comparisons).

Levels of glycated haemoglobin rose significantly between 3 months and 8 months in the GKR strain (from 25.21 ± 4.18 mmol/mol to 43.26 ± 9.77 mmol/mol; $P < 0.05$) and then remained static ($43.26 \pm$ mmol/mol at 8m, 58.65 ± 19.32 mmol/mol at 12m, 69.40 ± 6.18 at 15m; $P = \text{NS}$ for all comparisons). This was markedly different from trends in blood glucose content in the SDR and WR strains, which stayed at a low level, indistinguishable from the baseline level at 3 months age in both strains throughout life (WR: 28.23 ± 2.91 mmol/mol at 3m, 25.41 ± 1.87 mmol/mol at 8m, 25.46 ± 4.05 mmol/mol at 12m, 26.56 ± 2.72 mmol/mol at 15m, $P = \text{NS}$ for all comparisons; SDR:

26.78±2.56mmol/mol at 3m, 25.68±3.54mmol/mol at 8m, 27.99±3.80 at 12m, 27.14±2.94 at 15m, P=NS for all comparisons).

At no age was haemoglobin glycation distinguishable between WRs and SDRs (P=NS for comparisons at all ages).

At all ages 8 months and over, haemoglobin glycation in GKR was significantly higher than in WRs (43.26±9.77mmol/mol vs 25.41±1.87mmol/mol at 8m, 58.65±19.32mmol/mol vs 25.36±4.05mmol/mol at 12m, 69.40±6.18 vs 26.56±2.72mmol/mol at 15m; P<0.001 for each). Likewise, at all ages 8 months and over, haemoglobin glycation in GKR was significantly higher than in SDRs (43.26±9.77mmol/mol vs 25.68±3.54mmol/mol at 8m, 58.65±19.32mmol/mol vs 27.99±3.80mmol/mol at 12m, 69.40±6.18 vs 27.14±2.94mmol/mol at 15m; P<0.001 for each).

At no age did haemoglobin glycation differ between SDRs and WRs (26.78±2.56mmol/mol vs 28.23±2.91mmol/mol at 3m, 25.68±3.54mmol/mol vs 25.41±1.87mmol/mol at 8m, 27.99±3.80mmol/mol vs 25.46±4.05mmol/mol at 12m, 27.14±2.94mmol/mol vs 26.56±2.72mol/mol at 15m; P=NS for each comparison).

In summary: haemoglobin glycation was present at a low baseline level in all three strains. In the WR and SDR it remained at this low level at all ages, and no distinction was present between these two strains. GKRs developed significantly higher levels than their own baseline, and the age-matched values of the other strains, by 8 months age. This elevated glycation persisted in GKRs throughout all subsequent measurements.

3.2.7 Blood insulin levels

We attempted to measure blood insulin levels in the fed state, however local animal license conditions would have required performing tail vein phlebotomy without prior vasodilation by brief exposure to 38°C in a heat box. The reason for this was concern about the safety and welfare of animals being heated in the fed state, as overheating in the fed state – although very unlikely during the brief heating we employed – could induce vomiting, which would be not only unnecessary suffering for them, but also potentially injurious to their health via respiratory aspiration of vomitus. Phlebotomy in non-heated 3-month SDRs was

feasible, and we achieved some viable blood samples with this technique, however phlebotomy in older animals, and particularly in GKR, was very technically challenging due to apparent venosclerosis and deposition of excess connective tissue within the tail with age. The preparation of plasma required a fixed volume of whole venous blood from the animal and we fixed this early on to 0.5ml, ensuring a fixed concentration of the anticoagulation K_2EDTA . Despite developing significant expertise in rat phlebotomy over the course of this project, we could not reliably achieve 0.5ml of venous blood using our tail phlebotomy technique without prior vasodilation by heating. All insulin measurements, therefore, were conducted in vasodilated, and therefore starved, animals.

3.2.7.1 Insulin assay selection

An ELISA assay for insulin was selected on the basis of recent publications by other groups working in a similar area, easy availability and reported efficacy and reproducibility at the levels of blood insulin content we expected to find based on other reports of insulin levels in the GKR⁴¹⁷, together with compatibility with our optical assay reading equipment⁴¹⁸. The Millipore Rat / Mouse Insulin 96 Well Plate Assay requires optical absorbance to be measured at $\lambda=450\text{nm}$ and $\lambda 590\text{nm}$. The numerical difference in absorbance is then calculated and plotted against the insulin concentration for control samples containing known concentrations of rat insulin. A line of best fit is derived from the known points, and this is used to derive an equation for the relationship between the assay readout (Y-axis) and insulin concentrations (X-axis). This equation is then solved to yield the insulin concentrations present in unknown samples, in our case, aliquots of rat serum. The only guidance given in the assay documentation and references is that the best fit equation is “a 4- or 5-parameter logistic equation”. The resulting normal curve for the first run of the Millipore assay, together with the polynomial equation derived is presented in Figure 3.4:

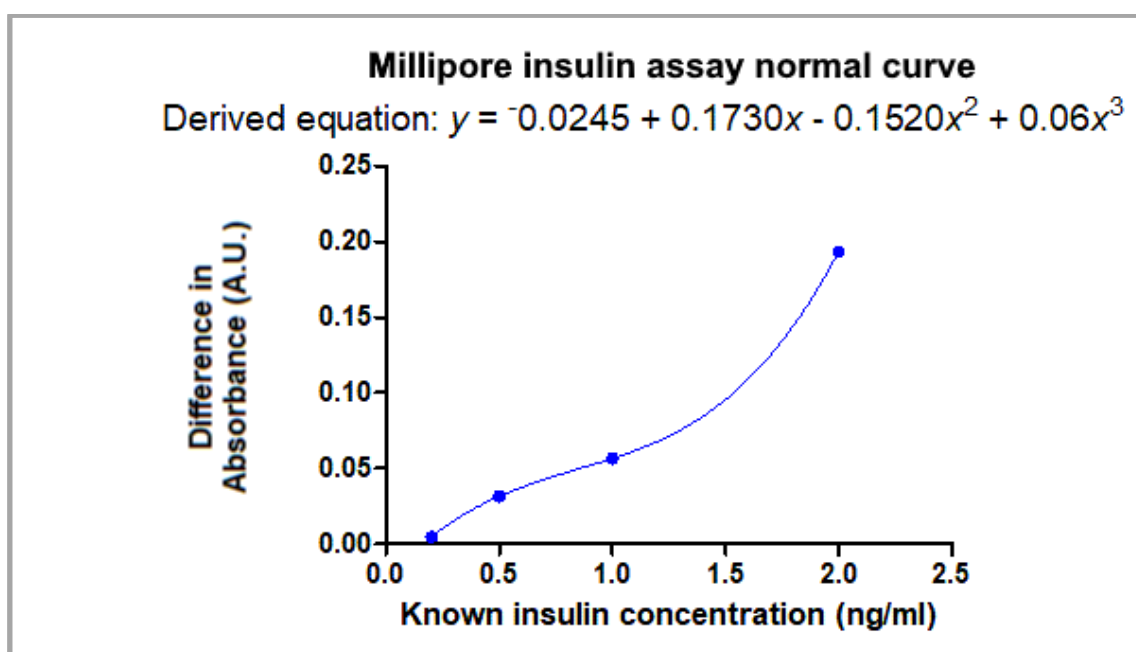


Figure 3.4: Normal curve for calculation of serum insulin content using Millipore rat insulin assay, Cat. # EZRMI-13K. A.U: arbitrary units.

The polynomial equation was then used to calculate the value of x (insulin concentration) that would yield the measured difference in absorbance for each unknown sample. This was carried out using polynomial solving by iteration in MS Excel, yielding successful solutions in 13/15 unknown samples in the first run. During the first run of this assay a problem became apparent, in that some of the experimental samples from GKR, prepared as serum, had levels of insulin present that were below not only the theoretical cut-off for reproducibility of the assay (0.1 ng/ml), but also well below the point of the lowest concentration standard supplied with the assay, and so outside the range for which we could be confident that the equation linking absorbance characteristics to insulin concentration held correct. An example of this is shown in Figure 3.5, in which a sample of successful equation solutions for unknown insulin concentrations are plotted against the standard curve:

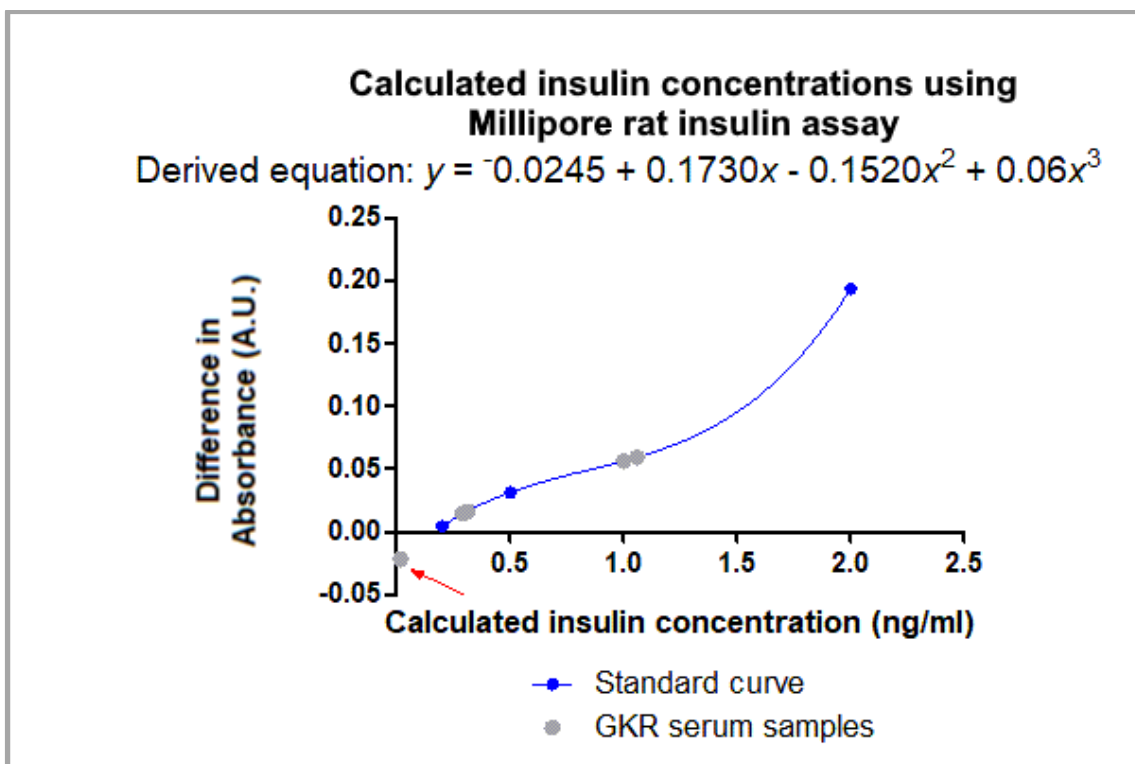


Figure 3.5: Calculated insulin concentrations using the Millipore rat insulin assay. Red arrow indicates sample with insulin concentration outside the validated range for this assay. A.U.: arbitrary units. Each point is the mean of four experimental runs.

Of note, all successful equation solutions lie on the line of the equation curve, implying that solving the polynomial has been successful and not thrown out

inappropriate results, for example negative or imaginary numbers. The arrowed calculated insulin concentration (\leftarrow), however, lies outside the range covered by the known standard insulin samples, and therefore is outside the range we can be confident that the equation holds good for. Quite aside from this, the calculated insulin concentration illustrated by the arrowed point (0.018ng/ml) is below the limit of sensitivity for this assay (0.05ng/ml) when using a sample volume of 5 μ l.

Clearly, we needed an alternative insulin assay with a lower sensitivity cut-off, and a lower concentration standard curve, or to move to a technique yielding higher concentrations of insulin.

We had chosen to measure serum insulin rather than plasma mainly for the convenience of sample preparation. Aware that most published literature reports plasma insulin levels, we performed a second run of the Millipore assay using aliquots of plasma and serum taken at the same time from the same animals (a combination of GKR and WR). The results are given in Figure 3.6:

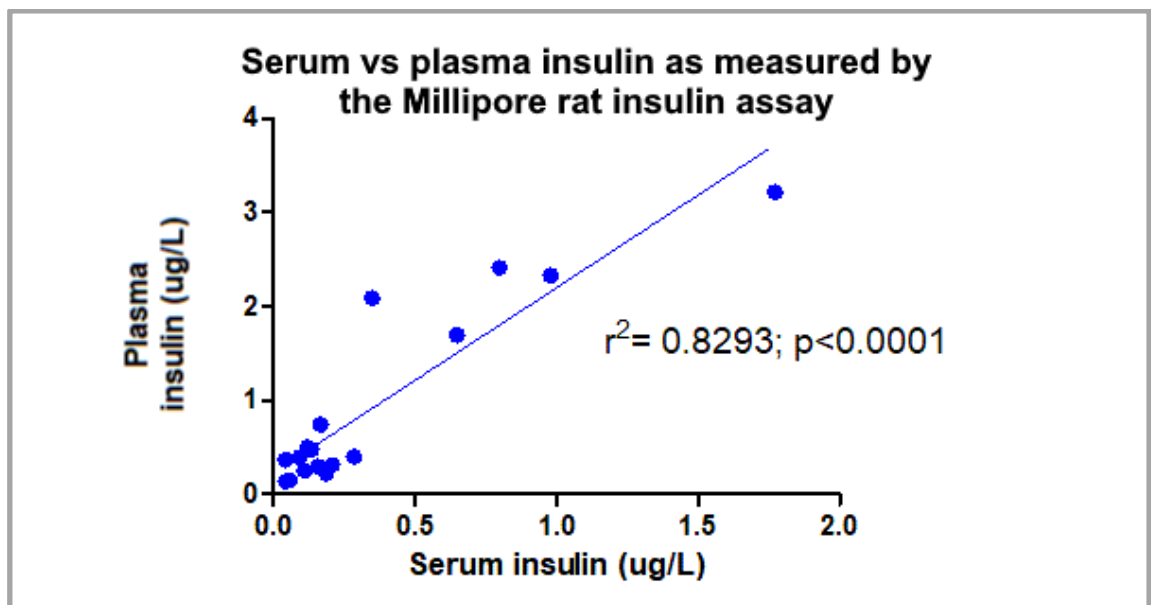


Figure 3.6: Correlation of serum insulin and plasma insulin measurements in the same animals. This illustrates a strong correlation and also that plasma insulin is consistently measured higher than serum insulin. Each point is the mean of $n=4$ experimental runs for an individual rat.

Two things are noticeable on this plot: first that there is a strong correlation between insulin measured in plasma, and insulin measured in serum from the

same animal. Second, that the plasma insulin is consistently measured higher than the serum insulin: all 7 measured plasma levels plotted here are higher than their corresponding serum measurements. Comparison of the two measures with a paired t-test confirms that plasma measurements are significantly higher across the group.

To avoid encroaching on the lower limit of sensitivity of the assay, therefore, we switched to measuring plasma insulin instead of serum. We also took advice from another group working in the area⁴¹⁹ and changed the assay for subsequent measurements. On advice, we selected a rat insulin ELISA produced by Merckodia, Sweden, as this is produced in both standard (product #10-1250-01) and ultra-sensitive (product #10-1251-01) versions, covering insulin contents 0.15-5.5µg/L and 0.02-1.0µg/L respectively, therefore in combination more than capable of measuring reliably over the full range of results we had observed so far.

Methodology for the Merckodia assay was different from the Millipore, with only a single measure of optical density at $\lambda=450\text{nm}$ required. Again, a normal curve was constructed for each experimental run, and an example of this is shown in Figure 3.7:

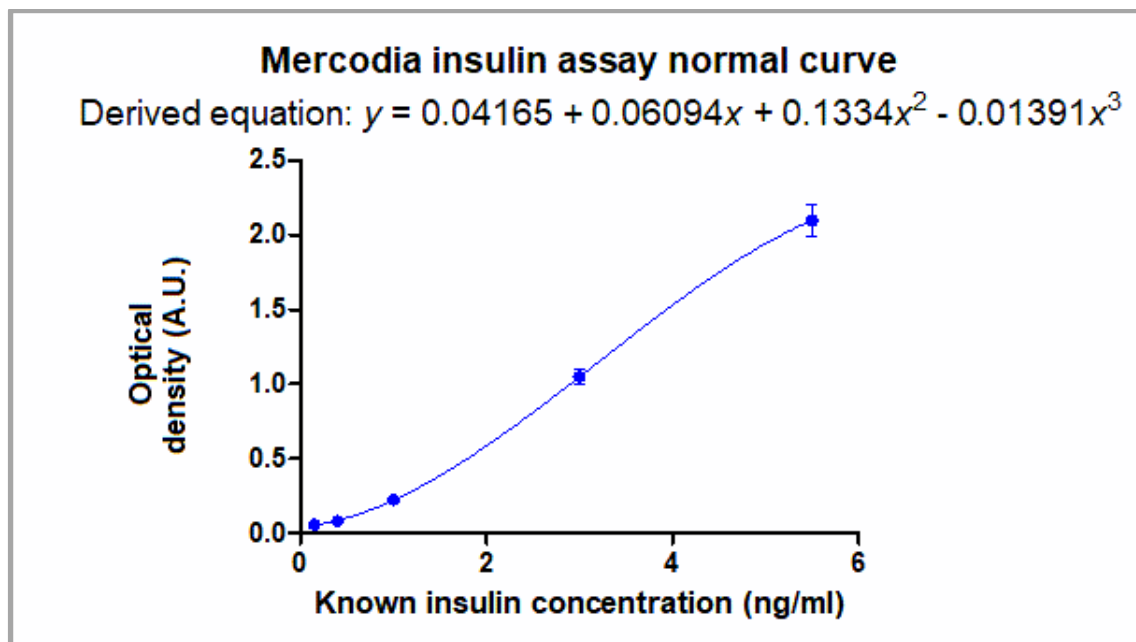


Figure 3.7: Normal curve for calculation of serum insulin content using a Merckodia standard sensitivity rat insulin assay, Cat #10-1250-10. A.U: arbitrary units. Error bars (where shown) show S.E.M but these are minimal hence omitted for most points; each point is the mean of four experimental runs.

The advantages of this assay for our application are shown on this standard curve: the normal curve covers a broader range, allowing a broader range of unknown insulin concentrations to be calculated from the resulting curve and equation. Moreover, the normal curve extends closer to an insulin concentration of 0 (down to 0.15ng/ml rather than 0.2ng/ml) and there is a closer bunching of the supplied insulin standards towards the very bottom of the scale, giving a more accurate derivation of the equation of the curve in this region, so that lower insulin concentrations are more likely to be estimated with greater accuracy with this, rather than the Millipore, assay.

As before, Microsoft Excel's iterative polynomial solving function was used to solve the equation of the standard curve for each value of y (the measured optical density), to yield the corresponding value of x (the unknown insulin concentration). An example of how these values fell on the standard curve in the first experimental run using the Mercodia assay is shown in Figure 3.8.

Of note, 11/11 of the calculated measurements fall exactly on the standard curve line, suggesting that the equation derived for the line is slightly more accurate than the Millipore assay. Comparing Figure 2.7 with the corresponding figure for the Millipore (Figure 2.4) reveals that the equation describing the Millipore line is very marginally less accurate. The switch to measuring plasma insulin has also paid off, with 100% of the calculated insulin concentrations (on this experimental run at least) above the detection limit of the Mercodia assay:

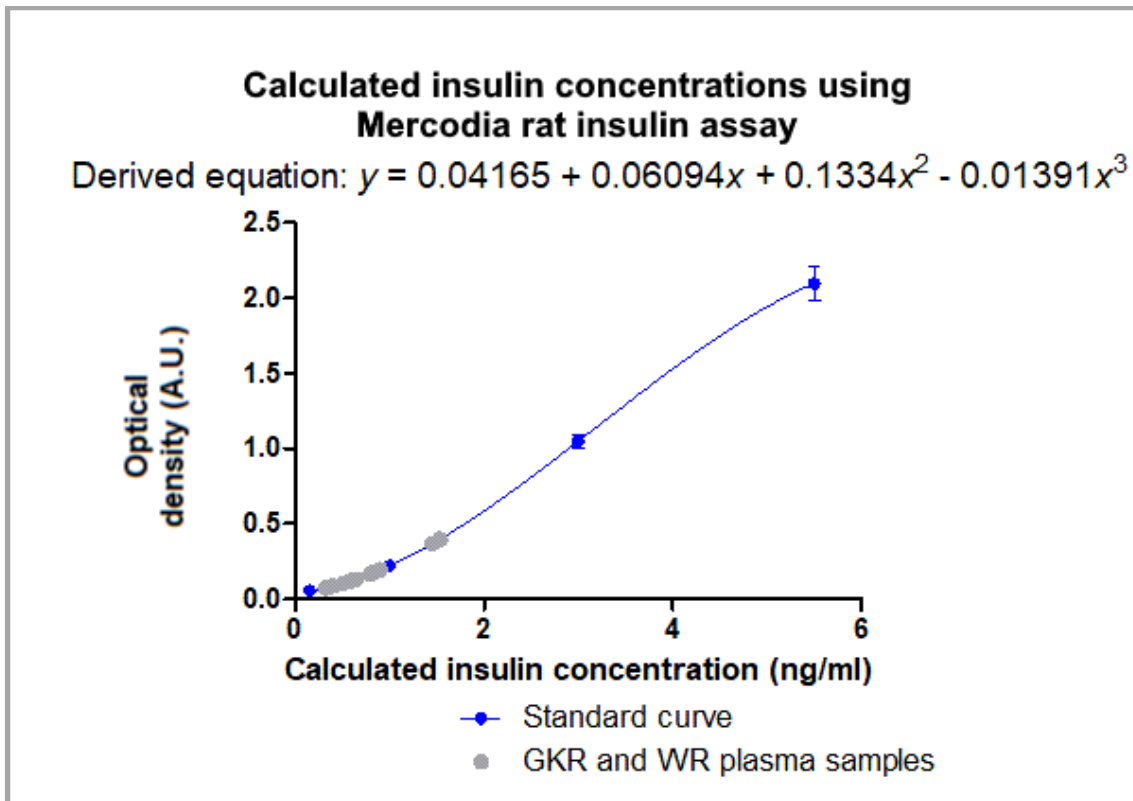


Figure 3.8: Example of calculated insulin concentrations using the Mercodia standard sensitivity rat insulin assay. A.U: arbitrary units. Error bars (where shown) show S.E.M but these are minimal hence omitted for most points; each point is the mean of four experimental runs, in the case of “unknown” (grey) points from two separately stored samples from one animal.

3.2.7.2 Optimised insulin quantification methodology

Having completed the pilot studies described above, subsequent evaluation of blood insulin content was performed on blood plasma, prepared as per section 2.3.3. Plasma insulin content was quantified using the normal sensitivity Mercodia ELISA, and if this revealed an insulin content less than 0.15ng/ml then a second set of stored aliquots was analysed using the ultra-sensitive assay. All analyses were performed on duplicated samples and the results presented are means of at least two experimental runs.

3.2.8 Blood insulin content in two rat strains

Having selected a methodology for quantifying blood insulin content in the rats, samples from WRs and GKR aged 3, 8, 12 and 15 months were processed as per the described method, yielding the results shown in Figure 3.9:

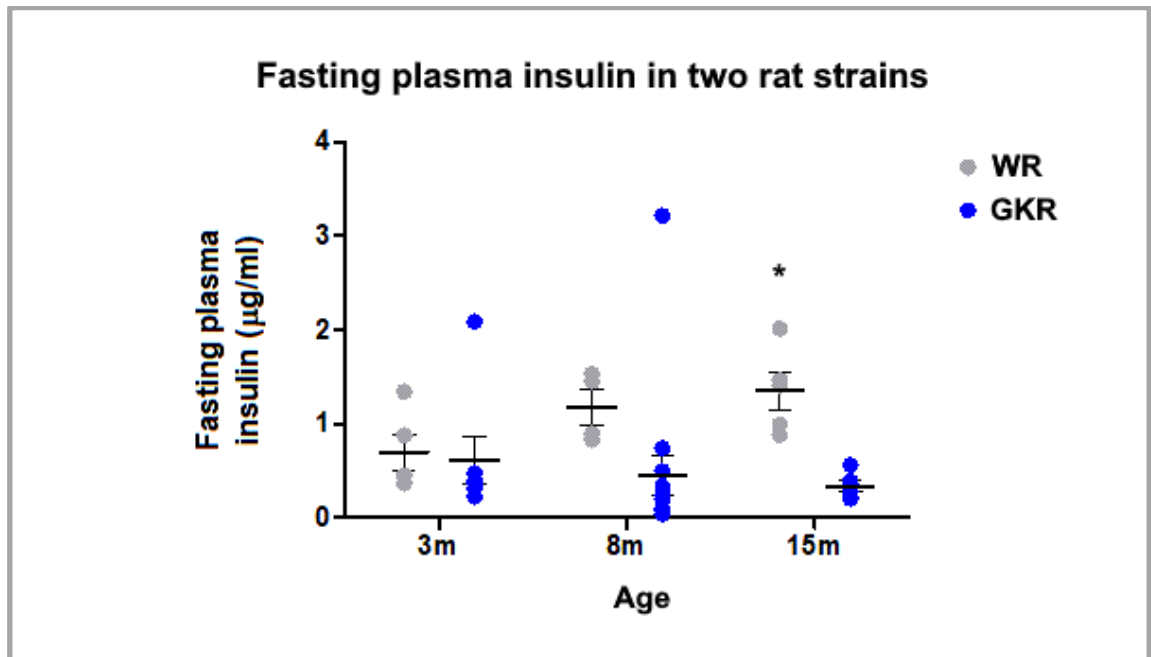


Figure 3.9: Fasting plasma insulin content in two rat strains. Fasting insulin levels were low in the GKR and remained low throughout follow-up, with no statistically significant change with age. This was a distinct pattern from development in the WRs, for whom fasting insulin levels started low and increased with age. Although the upwards trend itself did not reach statistical significance, by the age of 15 months, fasting plasma insulin was significantly higher in WRs than in GKR WR: Wistar rat; GKR: Goto Kakizaki rat. Each point is the mean of four experimental runs from two separately stored samples from one animal. Error bars show S.E.M., *: P<0.05 vs age-matched GKR group.

Fasting insulin levels were low in the GKR and remained low throughout follow-up, with no statistically significant change with age ($0.61 \pm 0.66 \mu\text{g/ml}$ at 3m, $0.45 \pm 0.82 \mu\text{g/ml}$ at 8m and $0.34 \pm 0.13 \mu\text{g/ml}$ at 15m; P=NS for all comparisons). This was a distinct pattern from development in the WRs, for whom fasting insulin levels started low and increased with age ($0.70 \pm 0.41 \mu\text{g/ml}$ at 3m, $1.18 \pm 0.37 \mu\text{g/ml}$ at 8m and $1.35 \pm 0.45 \mu\text{g/ml}$ at 15m; P=NS for all comparisons). Although the upwards trend itself did not reach significance, by the age of 15 months, fasting plasma insulin was significantly higher in WRs than in GKR ($1.35 \pm 0.45 \mu\text{g/ml}$ vs $0.34 \pm 0.13 \mu\text{g/ml}$ at 15m, P<0.05; $1.18 \pm 0.37 \mu\text{g/ml}$ vs 0.45 ± 0.82 at 8m, P=NS).

In summary: using insulin assays that gave reproducible and accurate results across the whole range of results, GKR were shown to have similar fasting levels of insulin to age-matched WRs in all but the 15 month age-group. The emerging difference at 15 month was due to a trend to higher circulating insulin

levels in the WR group, rather than a worsening of insulin deficiency in the GKR group with age.

3.2.9 Insulin resistance

Using fasting glucose and insulin measurements presented above, we calculated insulin resistance statistics using the homeostatic model assessment of diabetes (HOMA), as per Figure 3.10:

$$\text{HOMA-IR} = \frac{\text{Glucose} \times \text{Insulin}}{22.5} \qquad \text{HOMA-}\beta = \frac{20 \times \text{Insulin}}{\text{Glucose} - 3.5} \%$$

Figure 3.10: Calculation of homeostatic model assessment of insulin resistance statistic (HOMA-IR) and homeostatic model assessment of β cell function (HOMA- β). Measurements are fasting; glucose is denominated in mass units (mmol/dL); insulin is denominated in mIU/L.

In total we had 13 complete matched fasting insulin and glucose datapoints in WRs and 21 in GKRs, from among the same 50 animals used above. The HOMA-IR statistics are presented in Figure 3.11.

Differences in the HOMA-IR statistic between these groups are dominated by the large differences in circulating insulin, which outweigh the comparatively small differences in fasting glucose levels between the groups. Thus, Figure 3.11 looks very similar to Figure 3.9 (“Fasting blood insulin content in two rat strains”), and comparisons between the groups yields similar results:

Insulin responsiveness is good in the 3 month GKRs and remained stable throughout follow-up, with no statistically significant change with age (HOMA-IR 0.0063 ± 0.0048 at 3m, 0.0056 ± 0.0096 at 8m and 0.0031 ± 0.0017 at 15m; $P = \text{NS}$ for all comparisons). WRs exhibited a trend towards insulin resistance from 8 months but this only became statistically significant at 15 months (HOMA-IR 0.0055 ± 0.0035 vs 0.0063 ± 0.0048 , $P = \text{NS}$ at 3m; 0.0101 ± 0.0035 vs 0.0056 ± 0.0096 , $P = \text{NS}$ at 8m; 0.0191 ± 0.0105 vs 0.0031 ± 0.0017 , $P < 0.01$ at 15m) due to a trend to increasing insulin resistance with age in the WRs (HOMA-IR 0.0055 ± 0.0035 at 3m; 0.0101 ± 0.0035 at 8m; 0.0191 ± 0.0105 at 15m; $P = \text{NS}$ for all comparisons).

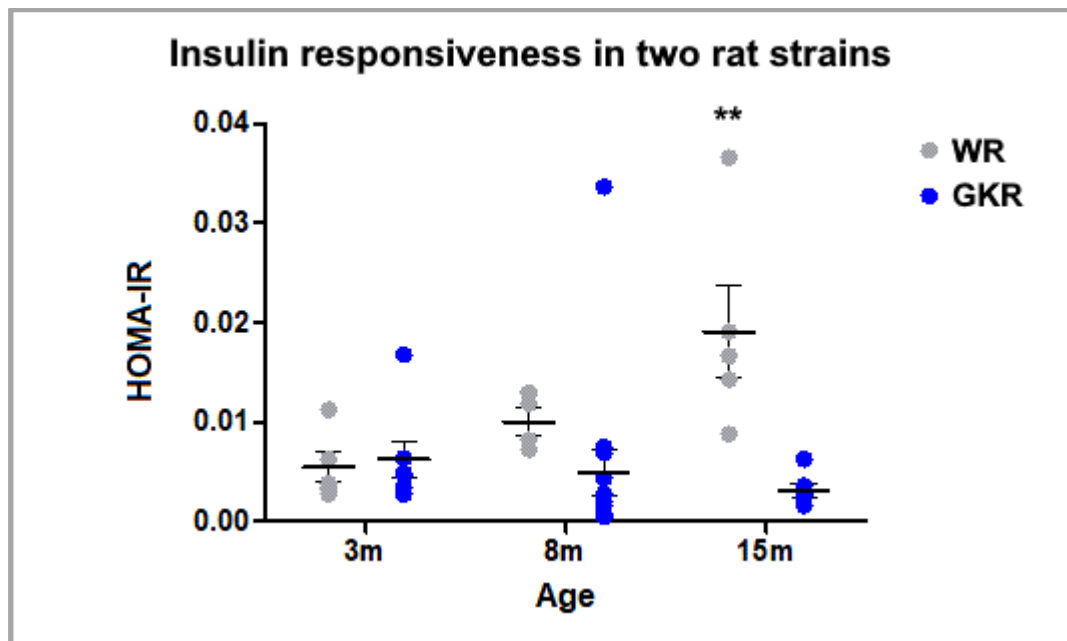


Figure 3.11: Insulin responsiveness in two rat strains as assessed by modelling with the HOMA-IR statistic using fasting plasma glucose and insulin measurements. Insulin responsiveness is high in the 3 month GKR and remained high throughout follow-up, with no statistically significant change with age. WRs exhibited a trend towards insulin resistance from 8 months but this only became statistically significant at 15 months due to a trend to increasing insulin resistance with age in the WRs. WR: Wistar rat; GKR: Goto Kakizaki rat; HOMA-IR: Homeostasis assessment model insulin resistance statistic. Each point is the mean of four experimental runs from two separately stored samples from one animal. Error bars show S.E.M., **: P<0.05 vs age-matched GKR group.

Overall, there was significant variation in insulin resistance according to strain (P=0.0057) i.e. overall WRs had higher HOMA-IR statistics than GKR.

Although age did not independently influence insulin resistance over the full dataset (P=0.19), the interaction between age and strain was statistically significant (P=0.02), i.e. strain had a larger effect on insulin resistance at higher ages.

In summary: HOMA-IR analysis would suggest that compared to wild-type WRs, inbred UCL-GKRs exhibit less whole body insulin resistance throughout life, but this only becomes statistically significant in older animals, as WRs' insulin resistance develops with age, whereas the GKRs remain insulin sensitive.

3.2.10 Insulin secretion

Using fasting glucose and insulin measurements already presented we calculated insulin secretion statistics, reflecting pancreatic beta cell function,

using the homeostatic model assessment of diabetes (HOMA), as per Figure 3.11 (see above). The results are presented in Figure 3.12:

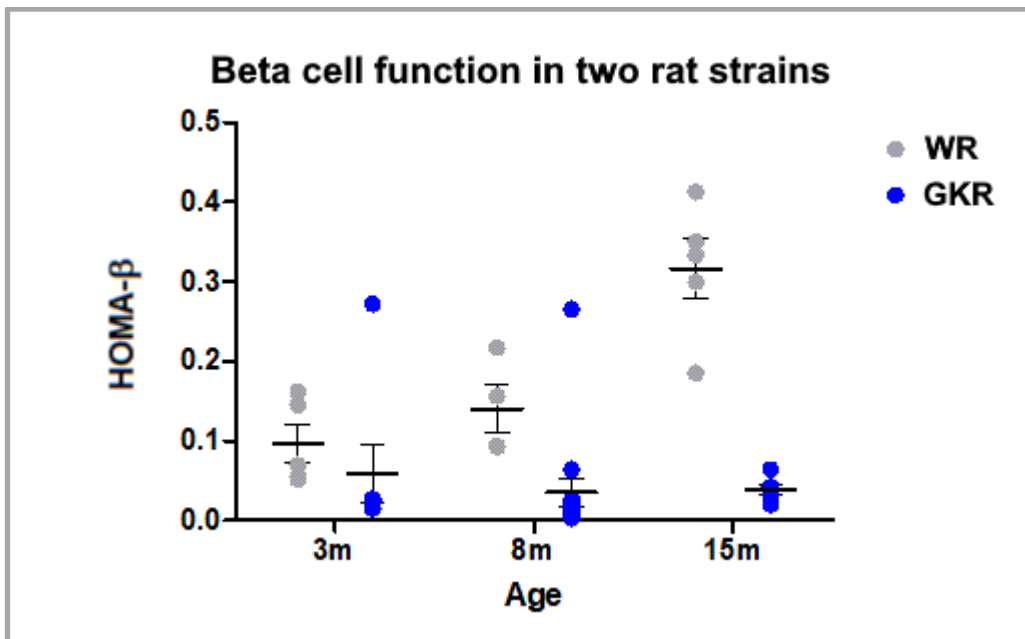


Figure 3.12: Beta cell function in two rat strains. GKRs have lower HOMA- β statistics than WRs at all ages, though this only becomes statistically significant at ages 8 months and 15 months. WRs' beta cell secretory function increases with age and this reaches statistical significance with the change from 8 to 15 months. WR: Wistar rat; GKR: Goto Kakizaki rat. Each point is the mean of four experimental runs on two separately stored samples from one animal. Error bars show S.E.M.

GKRs have lower HOMA- β statistics, i.e. less beta cell secretory function, than WRs at all ages, though this only becomes statistically significant at ages 8 months and 15 months (0.059 ± 0.09 vs 0.097 ± 0.053 at 3m, $P = \text{NS}$; 0.035 ± 0.068 vs 0.140 ± 0.060 at 8m, $P < 0.05$; 0.038 ± 0.015 vs 0.317 ± 0.084 at 15m, $P < 0.001$). WRs' beta cell secretory function increases with age and this reaches statistical significance with the change from 8 to 15 months (0.097 ± 0.053 at 3m vs 0.140 ± 0.060 at 8m, $P = \text{NS}$; 0.035 ± 0.068 at 8m vs 0.317 ± 0.084 at 15m, $P < 0.01$).

Overall, strain has a significant influence on HOMA- β ($P < 0.0001$), i.e. WRs have a significantly higher beta cell secretory response to a given circulating concentration of insulin than do GKs. Age also has a significant influence on beta cell function ($P = 0.025$), which given the divergence of WR and GKR data is more difficult to interpret. There is a significant interaction between age and

strain ($P=0.0006$), i.e. strain has a larger effect on beta cell function in the older ages studied.

3.2.11 Non-fasting blood glucose

Mixed blood was collected from the thoracic cavity after euthanasia by excision of the heart, however, this coagulated so quickly, was of mixed arterial and venous composition, and was collected after administration of substantial amounts of Pentobarbitone anaesthesia. Quantification of blood glucose was attempted, but proved technically unfeasible due to rapid blood coagulation, and given the known interference between anaesthesia and glucose handling³⁴⁹, the measurement was felt to be of limited utility and was abandoned.

3.2.12 Glucose tolerance test

We planned to conduct glucose tolerance tests using oral glucose dosing in conscious animals. However, our failed phlebotomy in non-vasodilated animals meant that to achieve reliable blood sampling after administering the oral glucose load, we would have had to heat a non-fasted animal. The vomiting risk was perceived to be high with this, and moreover, the stress of being heated may have interacted with glucose handling to skew results. This measurement was therefore abandoned.

3.2.13 Mitochondrial function

Mitochondria were isolated from ventricular tissue of eighteen animals aged 3 and 18 months (6 GKR, 6 WR and 6 SDR). Samples were equalised for mitochondrial protein content and underwent oximetry protocols to assess mitochondrial function. ADP-limited, ADP-stimulated, leak and uncoupled states were examined as per Hall's protocol⁴¹⁴. Four isolations failed to yield live mitochondria (i.e. there was no significant oxygen consumption during oximetry) and results from the remaining experiments are given in Figure 3.13.

Health of mitochondria was assessed by the "respiratory control ratio" (the ratio of oxygen consumption in ADP-limited vs ADP-stimulated states). Acceptable values are between six and eight⁴²⁰. Only mitochondria from WRs had respiratory control ratios within this range and the remainder of the results should therefore be interpreted with caution.

ADP-limited respiration (Figure 3.13A) was higher, but not statistically significantly so, in young GKR than in young WR (0.262 vs 0.144nMol/sec/μg; P=NS) and significantly higher than young SDR (0.262 vs 0.079nMol/sec/μg; P<0.01). ADP-limited respiration significantly increased with age in GKRs (0.262 in 3m, increasing to 0.431nMol/sec/μg at 18m; P<0.05). In WRs and SDRs, ADP-limited respiration did not vary with age (P=NS for all comparisons).

ADP-stimulated respiration (Figure 3.13B) did not vary with age in any strain (P=NS for all comparisons) though again the three-month baseline was similar between GKRs and WRs (1.410 vs 1.018nMol/sec/μg; P=NS) and significantly higher than SDRs (1.410 vs 0.405nMol/sec/μg; P<0.01).

Leak respiration in the presence of ETC blockade by oligomycin (Figure 3.13C) was similar in young GKRs and young WRs (0.280 vs 0.212nMol/sec/μg; P=NS) and significantly higher than in young SDRs (0.280 vs 0.076nMol/sec/μg; P<0.001). Leak respiration decreased significantly with age in the GKR (3m: 0.280 vs 18m: 0.056nMol/sec/μg; P<0.001) but not in the other two strains (from 0.212 to 0.171nMol/sec/μg in WRs and from 0.076 to 0.046nMol/sec/μg in SDRs; P=NS for all comparisons).

The maximal rate of uncoupled respiration was significantly higher in young GKRs than in young WRs and young SDRs (1.95 vs 0.709 and 0.338nMol/sec/μg; P<0.05 and P<0.01 respectively). Uncoupled respiration decreased significantly with age in GKRs (3m: 1.95 vs 18m: 0.42nMol/sec/μg; P<0.01) but not in WRs (3m: 0.709 vs 18m: 1.47nMol/sec/μg; P=NS) and SDRs (3m: 0.338 vs 18m: 1.26nMol/sec/μg; P=NS).

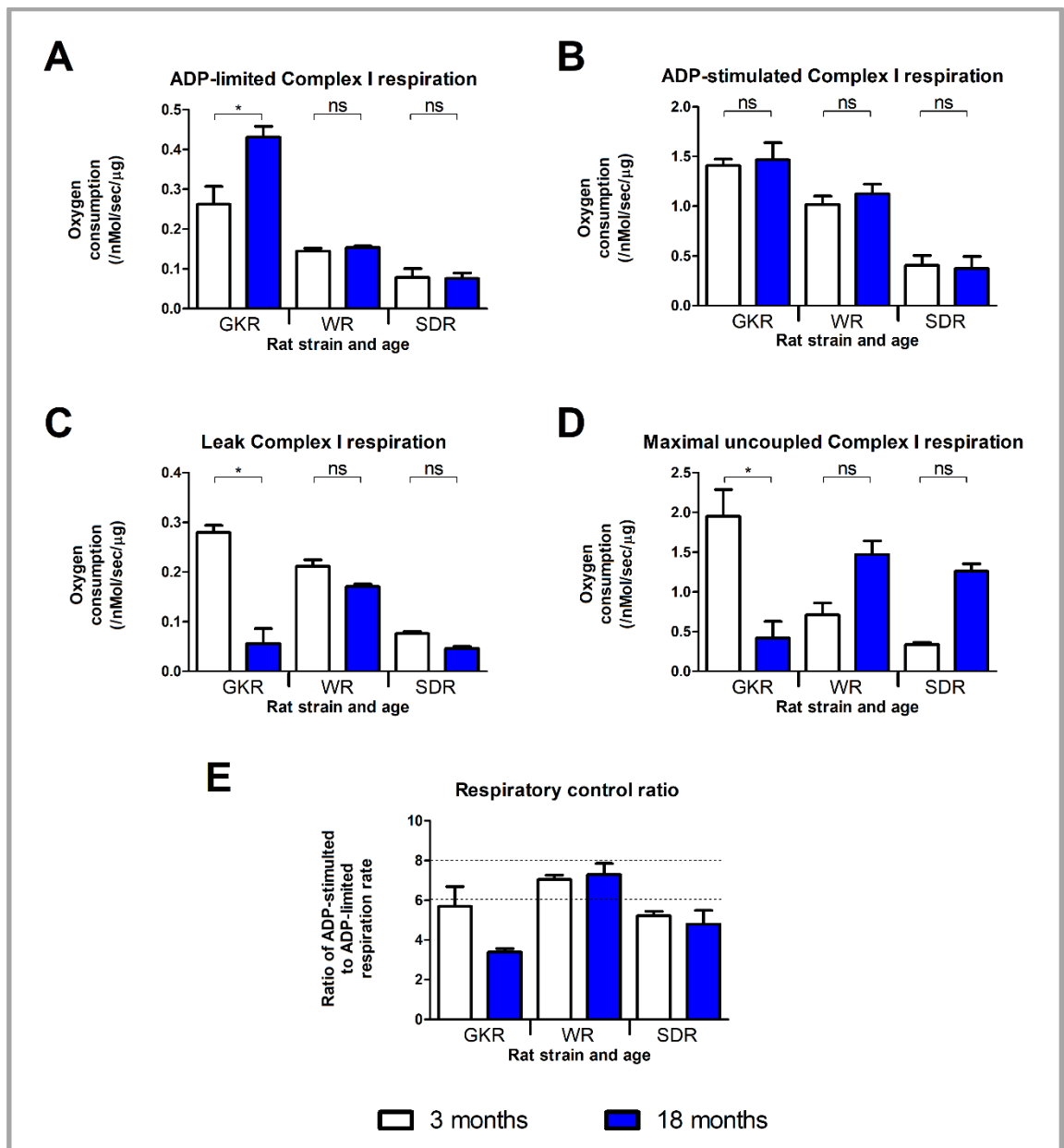


Figure.3.13: Mitochondrial respiration in three rat strains at three and 18 months age. ADP-limited respiration (**A**) was similar in young GKR and young WRs and significantly higher than in young SDRs. ADP-limited respiration significantly increased with age in GKR. In WRs and SDRs, ADP-limited respiration did not vary with age. ADP-stimulated respiration (**B**) did not vary with age in any strain though the three-month baseline in WRs and GKR was significantly higher than in SDRs. Leak respiration in the presence of ETC blockade by oligomycin (**C**) was similar in young GKR and young WRs and significantly higher than in young SDRs. Leak respiration decreased significantly with age in the GKR only. The maximal rate of uncoupled respiration (**D**) was significantly higher in young GKR than in young WRs and young SDRs. Uncoupled respiration decreased significantly with age in GKR but not in WRs and SDRs. GKR: Goto Kakizaki rat; WR: Wistar rat; SDR: Sprague Dawley rat. Error bars show S.E.M. n=4 for each group. *: P<0,.05; ns: not significant.

3.3 Summary of UCL GKR phenotyping studies

In summary, we showed that GKR from the UCL colony are similar to other colonies. Compared to non-diabetic controls (Wistar and Sprague Dawley rats), adult GKR had lower body weight, and stopped gaining weight between three and eight months age. Fasting glucose was elevated in the GKR compared to other strains at all ages except the oldest age assessed (15 months), and no strain showed significant changes in fasting blood glucose over time. Glycated haemoglobin, a measure of circulating glucose over the medium-term, was low in both non-diabetic strains at every age tested but was significantly raised in GKR from eight months onwards. We compared fasting blood insulin content in GKR and WR and found lower circulating levels of insulin in fasting GKR than fasting WR, from eight months age onwards, though statistical significance was only reached at 15 months, due to higher insulin in older WR rather than age-related decline in the GKR.

We used the homeostatic model assessment of diabetes to model insulin secretion and insulin resistance from fasting state blood tests. GKR exhibited less whole-body insulin resistance than WR at each age tested. This only reached statistical significance at older ages due to rising insulin resistance in the WR. GKR secreted less insulin than WR at all ages, becoming statistically significant at eight months onwards. Age, strain and age-strain interaction all contributed statistically significantly to the differences in insulin secretion seen.

Respiration of mitochondria isolated from ventricular tissue of GKR, WR and SDR was examined. Only mitochondria from WR met *a priori* definitions of healthy mitochondria after isolation. Bearing this in mind, leak respiration and ADP-limited respiration was higher in young GKR than other strains. ADP limited respiration increased with age in GKR, whereas leak respiration declined. Uncoupled respiration was higher in young GKR than other strains and declined with age, in contrast to the other two strains.

Critical discussion of these findings is in Chapter 6, "Discussions".

4. EFFECT OF PRECONDITIONING IN THE GOTO KAKIZAKI RAT

4.1 Aims and hypotheses

We aim to clarify the existing contradiction about intrinsic cardioprotective functions in the diabetic heart. Specifically:

1. To clarify activation state of the RISK pathway at baseline and in different states of stimulation in animals with diabetes.
2. To investigate whether the threshold effect seen with direct ischaemic preconditioning in diabetic animals also pertains to remote ischaemic preconditioning.

On the basis of our phenotyping work presented in Chapter 3, we hypothesised that 8-month-old UCL-GKRs would exhibit the features of impaired cardioprotection responses shown by Tsang in a mixed-age population of Taconic GKRs¹⁴⁷. We hypothesised that this would affect not only direct ischaemic preconditioning, but also the more clinically relevant remote ischaemic preconditioning. We further expected inhibition of cardioprotective signalling to be accompanied by tonic activation of cardioprotection pathways in the diabetic state, that heart explantation may be associated with loss of tonic activation of Akt phosphorylation, and that IPC / RIPC may protect against that.

4.2 Results

10 SDRs were used in the infarct size reproducibility study. 83 animals (49 GKRs, 34 SDRs) were used in the infarct size study. A further six GKRs were used in the kinase activation study.

4.2.1 Rat morphology and blood glucose content

Fasting hyperglycaemia was confirmed in the 8 month GKRs and excluded in the 3 month SDRs used in these experiments prior to the terminal procedures being performed. Summary statistics are given in Tables 4.1 & 4.2. Within each rat strain, no statistically significant differences were observed between treatment groups:

	<i>Ex vivo</i> IPC protocols		<i>In vivo</i> RIPC protocols	
	SDR Controls	SDR IPC	SDR Controls	SDR RIPC
Body mass	351±25g	319±38g	315±68g	312±42g

Heart mass	2.18±0.42g	2.37±19g	1.58±0.34g	1.76±0.21g
Fasting blood glucose	7.03 ±0.25mmol/L	6.99 ±0.44mmol/L	7.12 ±0.22mmol/L	7.06 ±0.17mmol/L

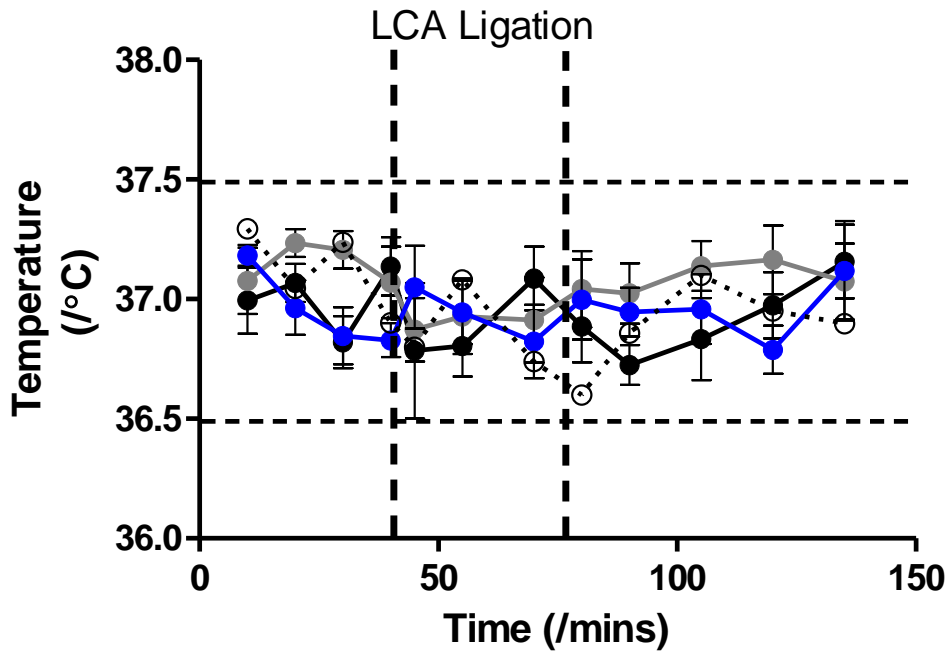
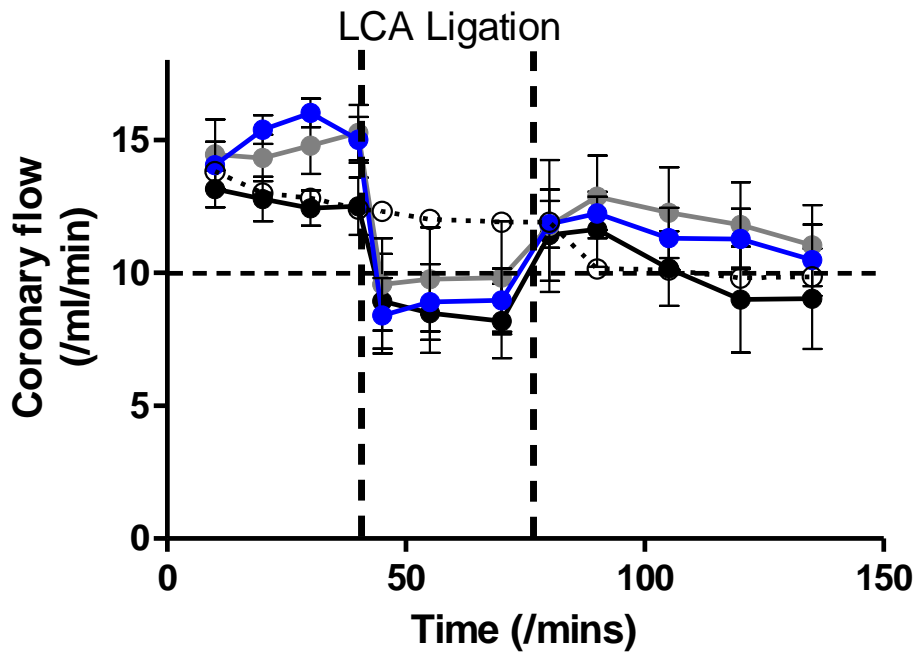
Table 4.1: Morphology and blood glucose content in 3 month Sprague Dawley rats used in direct and remote ischaemic preconditioning protocols. SDR: Sprague Dawley Rat; IPC: ischaemic preconditioning; RIPC: Remote ischaemic preconditioning.

	<i>Ex vivo</i> IPC protocols		<i>In vivo</i> RIPC protocols	
	GKR Controls	GKR IPC	GKR Controls	GKR RIPC
Body mass	415±25g	406±16g	421±25g	405±68g
Heart mass	2.73±0.22g	2.69±0.16g	2.37±0.62g	1.92±0.22g
Fasting blood glucose	11.59 ±2.66mmol/L	13.22 ±3.80mmol/L	12.02 ±2.95mmol/L	12.18 ±3.25mmol/L

Table 4.2: Morphology and blood glucose content in 8 month Goto Kakizaki rats used in direct and remote ischaemic preconditioning protocols. GKR: Goto Kakizaki rat; IPC: ischaemic preconditioning; RIPC: remote ischaemic preconditioning.

4.2.2 Perfusion during *ex vivo* ischaemic preconditioning

All Langendorff perfused hearts were subject to regular monitoring. In total, 15 SDR hearts and 23 GKR hearts completed infarct protocols. In addition, 5 SDR perfusions and 7 GKR perfusions were abandoned due to not meeting *a priori* conditions for a valid Langendorff perfusion (see Chapter 2 “General Methods” for further detail). The most common reasons for abandoned perfusions were inappropriate coronary flow rate (6 perfusions) and poor temperature control (four perfusions). Damage to the heart or prolonged time taken to hang the heart accounted for the other abandoned perfusions. Results from physiological monitoring of the completed perfusions, presented in Figure 4.3 and 4.4, show no significant differences between baseline physiology of the SDR and GKR treatment groups, respectively:

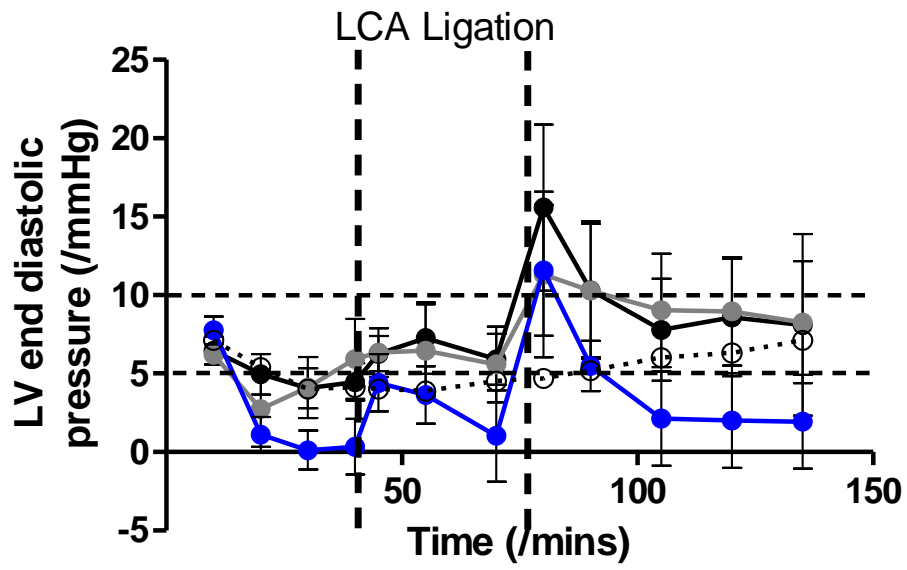
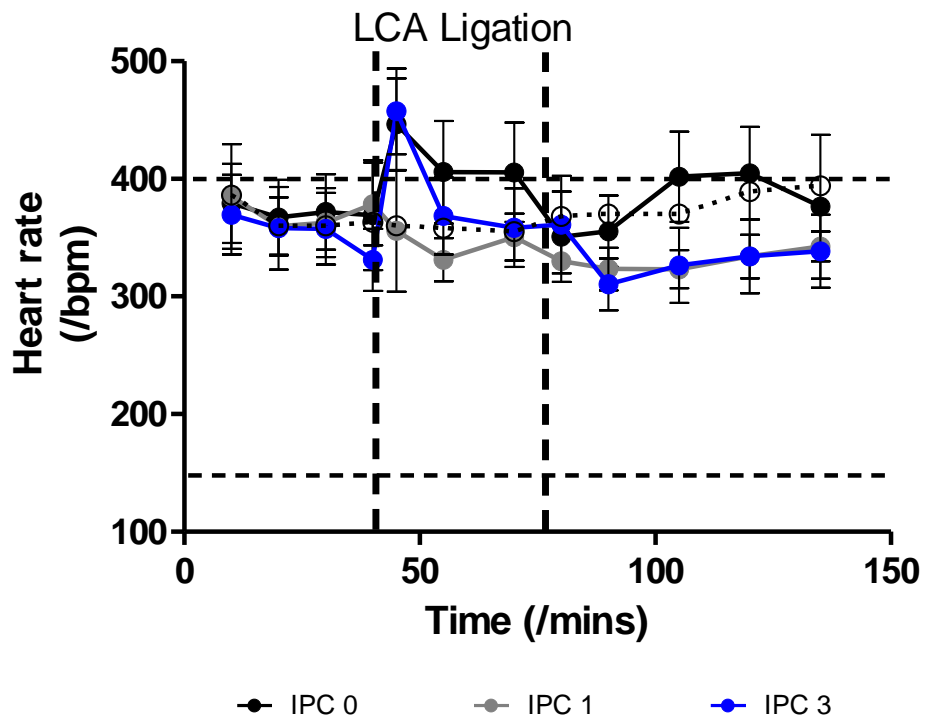
A**Temperature control****B****Coronary flow**

● IPC 0

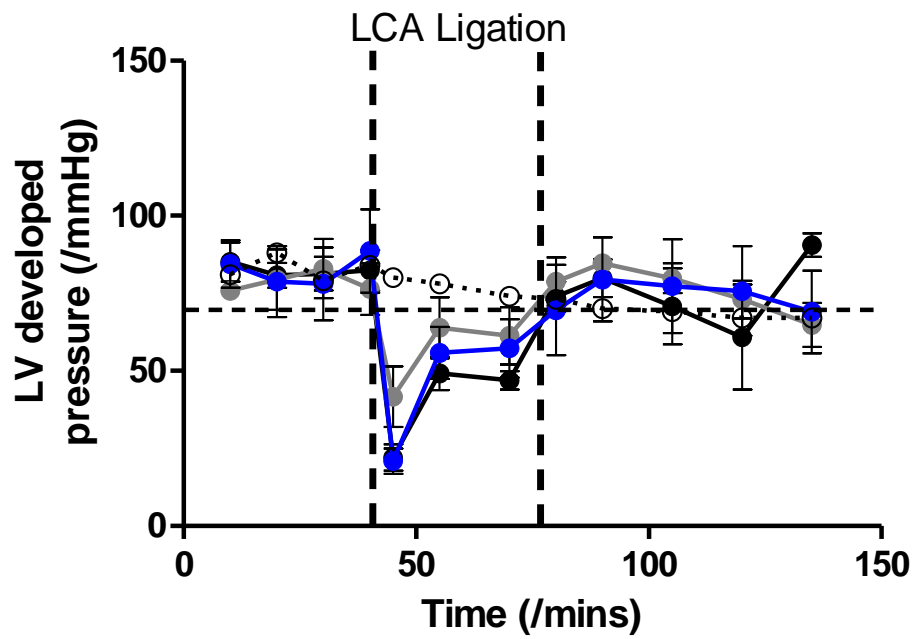
● IPC 1

● IPC 3

○ Sham

C**Left ventricular end diastolic pressure****D****Heart rate**

E Left ventricular developed pressure



F Left ventricular rate-pressure product

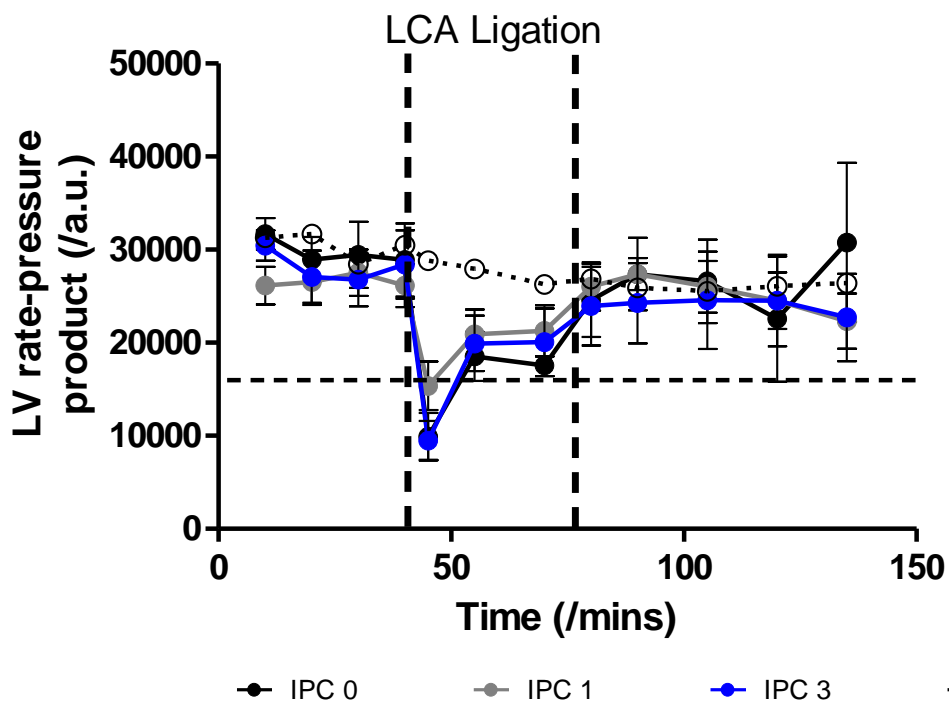
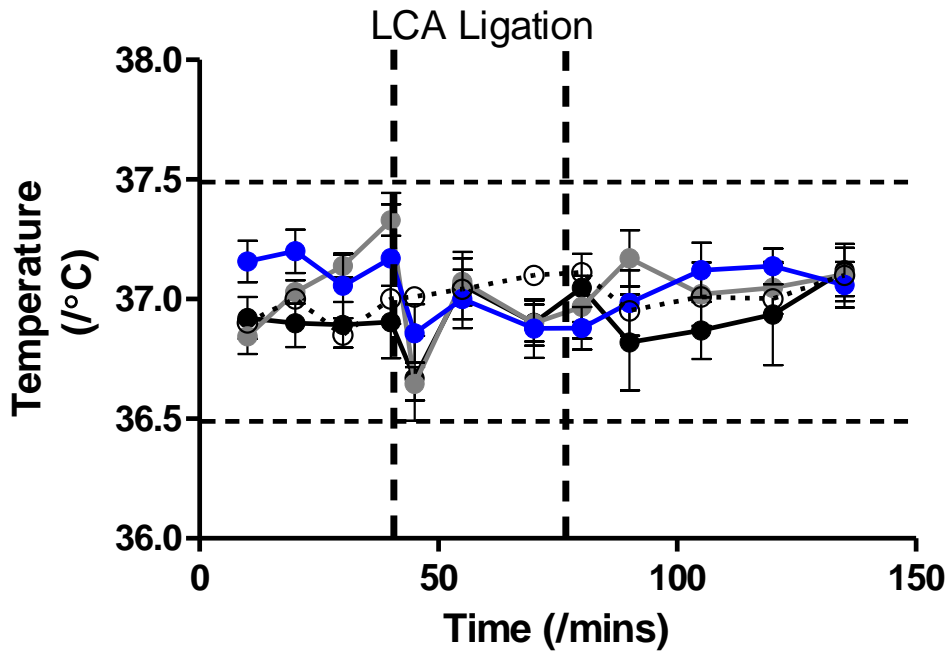
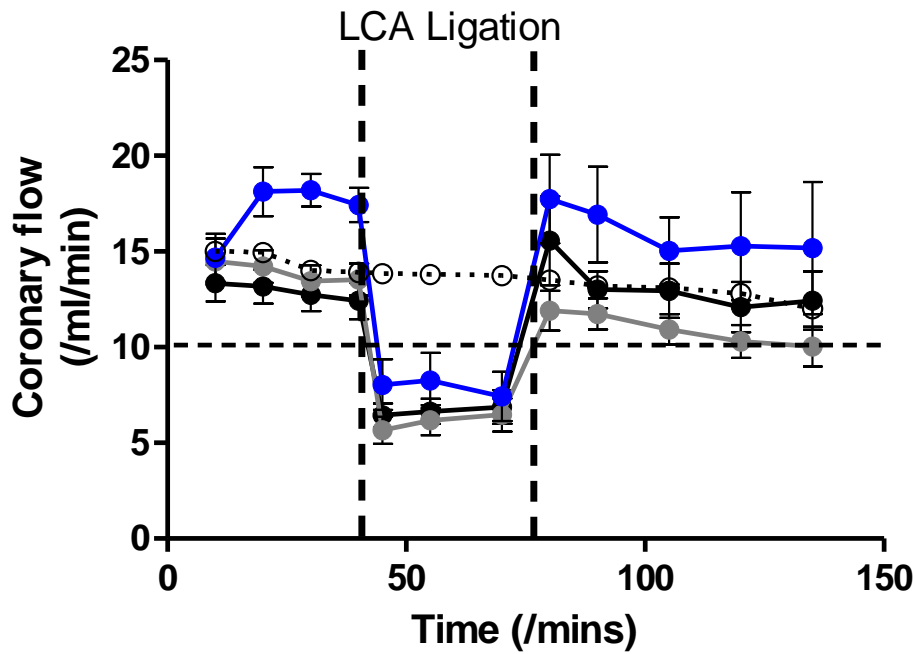


Figure 4.3 (see pages 168-170): Physiological parameters during direct ischaemic preconditioning and *ex vivo* infarction of 3 month Sprague Dawley rat hearts. Independent and dependent variables all met *a priori* criteria of acceptability for valid *ex vivo* perfusion, assessed after 10mins perfusion, and temperature control (**A**) was maintained within the target range for all hearts included in this and other analyses. Coronary flow rate (**B**) and LV developed pressure (**E**) dropped appropriately in all hearts after tightening of the ligature around the left anterior descending coronary artery. Left ventricular end diastolic pressure was adjusted after 10mins perfusion to the target range 5-10mmHg and varied dependent on other variables thereafter (**C**). Heart rate profiles were relatively high compared to the expected reference range (**D**) but with no obviously abnormal outliers. Hearts with persistent arrhythmia were excluded from this and other analyses. No significant differences developed between groups treatment groups in the dependent variables left ventricular end diastolic pressure (**C**), heart rate (**D**), left ventricular developed pressure (**E**), or left ventricular rate-pressure product (**F**). Experimental groups are as follows: IPC 0: no ischaemic preconditioning (IPC); IPC 1: single cycle of 5mins ischaemia and 5mins reperfusion; IPC 3: Three repeated cycles of 5 mins sublethal ischaemia-reperfusion prior to experimental infarction. Error bars show S.E.M; n=5 in each group.

A**Temperature control****B****Coronary flow**

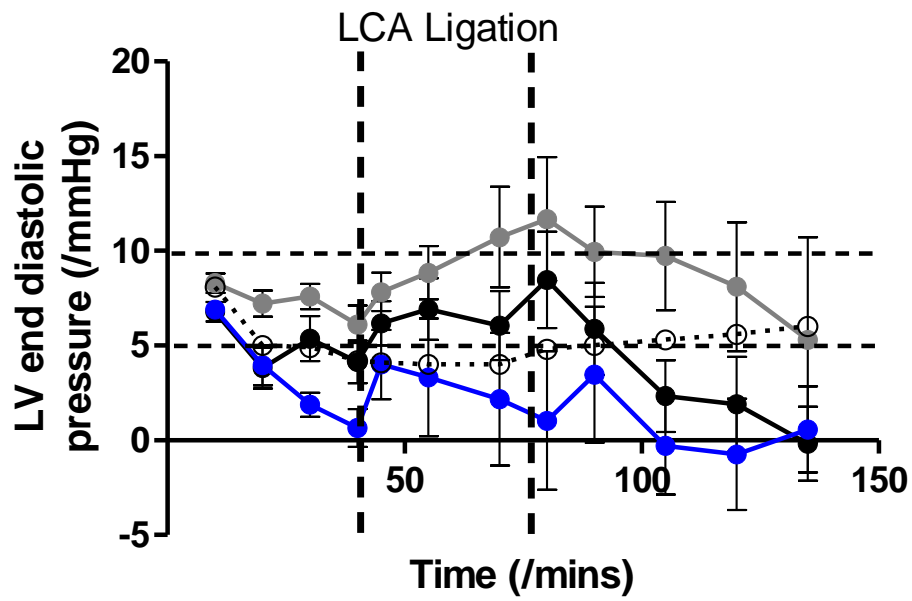
● IPC 0

● IPC 1

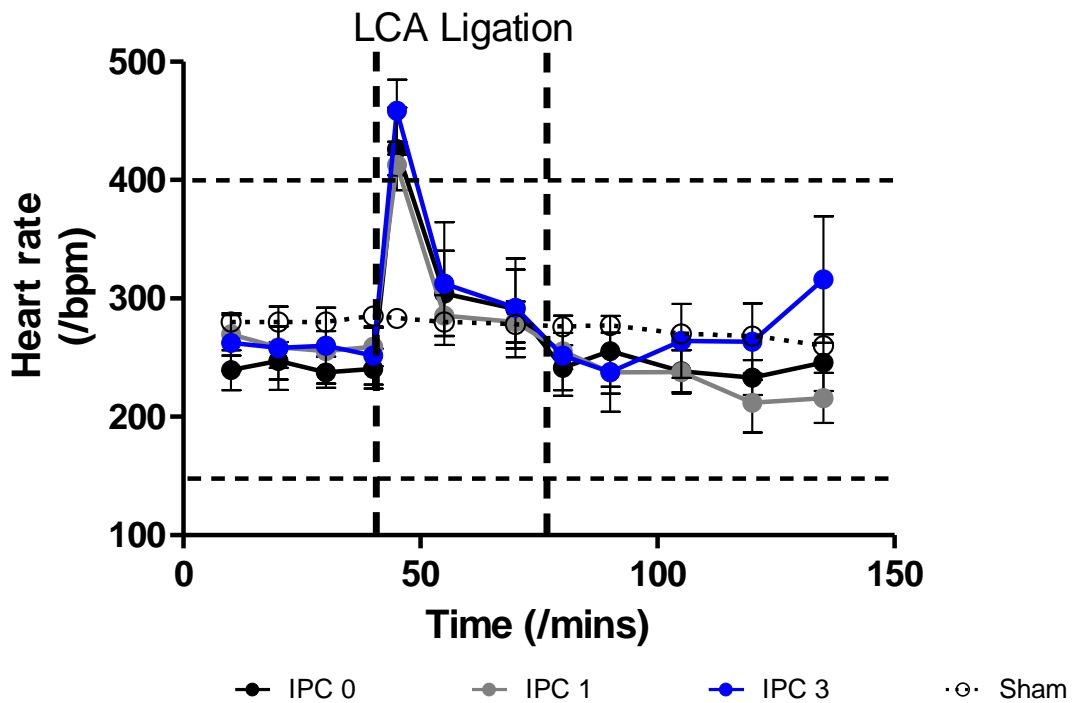
● IPC 3

○ Sham

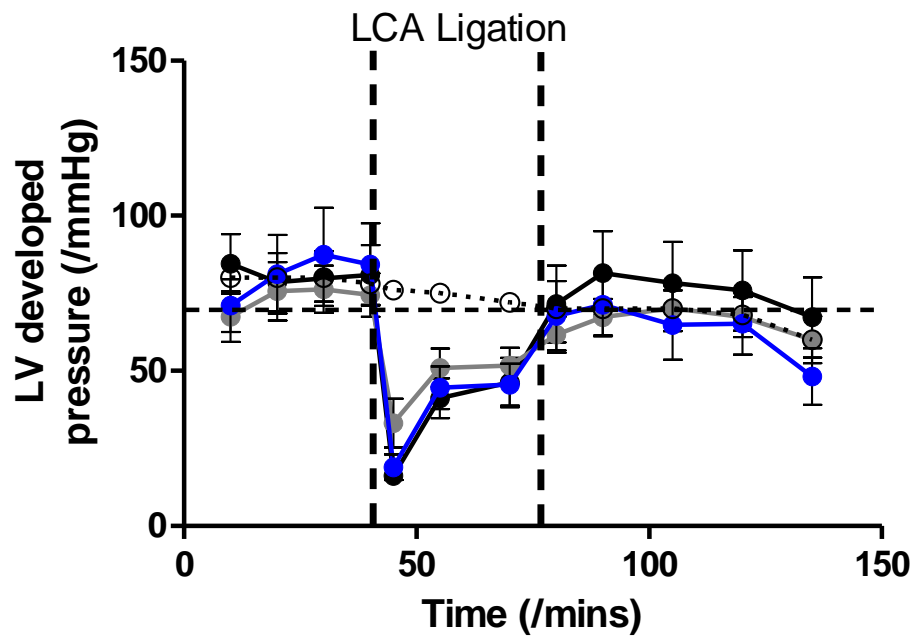
C Left ventricular end diastolic pressure



D Heart rate



E Left ventricular developed pressure



F Left ventricular rate-pressure product

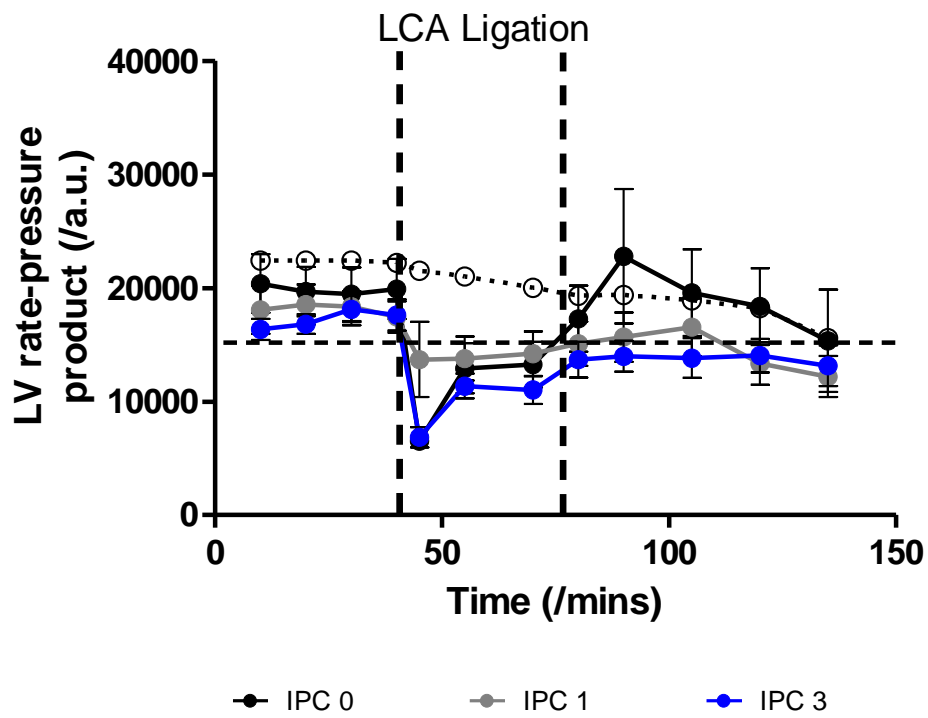


Figure 4.4 (see pages 172-174): Physiological parameters during direct ischaemic preconditioning and *ex vivo* infarction of 8 month Goto Kakizaki rat hearts. Independent and dependent variables all met *a priori* criteria of acceptability for valid *ex vivo* perfusion, assessed after 10mins perfusion, though developed pressure (**E**) was towards the lower end of the acceptable range at the 10min assessment point, with no significant difference between treatment groups. Rate-pressure product (**F**) fell within the expected range. Temperature control (**A**) was maintained within the target range for all hearts included in this and other analyses. Coronary flow rate (**B**) and LV developed pressure (**E**) dropped appropriately in all hearts after tightening of the ligature around the left anterior descending coronary artery. Left ventricular end diastolic pressure was adjusted after 10mins perfusion to the target range 5-10mmHg and varied dependent on other variables thereafter (**C**). Heart rate profiles were relatively high compared to the expected reference range (**D**) but with no obviously abnormal outliers. Hearts with persistent arrhythmia were excluded from this and other analyses. No significant differences developed between groups treatment groups in the dependent variables left ventricular end diastolic pressure (**C**), heart rate (**D**), left ventricular developed pressure (**E**), or left ventricular rate-pressure product (**F**). Experimental groups are as follows: IPC 0: no ischaemic preconditioning (IPC); IPC 1: single cycle of 5mins ischaemia and 5mins reperfusion; IPC 3: Three repeated cycles of 5 mins sublethal ischaemia-reperfusion prior to experimental infarction. Error bars show S.E.M; n=8 in each group.

4.2.2.1 Perfusion parameters in Sprague Dawley rat hearts

A priori definitions of a successful Langendorff perfusion were assessed after 10 min perfusion on the Langendorff rig. Heart temperature, coronary flow, LVEDP, LV developed pressure, and LV rate-pressure product all met the definition of acceptability set by Bell *et al*³⁷¹ and summarised in Table 4.1. In three SDR hearts, baseline heart rate at the 10 min assessment exceeded the proposed maximum acceptable rate of 400bpm (Figure 4.3D). Taking the SDR hearts as a whole, the heart rates were in general towards the upper end of the proposed acceptable range, and thus those with rates above 400bpm were not outliers in the group. We also observed this trend towards higher than expected heart rates during initial validation of the Langendorff rig method using SDR hearts (see Chapter 2, “General Methods”). The potential reasons for this, and our decision to accept higher heart rates are discussed fully in Chapter 2 but in brief we felt it was a marker of success of the Langendorff perfusion method, rather than indicative of a problem. Moreover, we were careful to exclude any heart with prolonged arrhythmia (e.g.: atrial or ventricular fibrillation) from the analysis. Arrhythmia was diagnosed from the LV pressure trace and from visual inspection of the perfused heart, as outlined in Chapter 2. Given the purpose of the heart rate cut-off is to exclude arrhythmic hearts from the analysis, we were satisfied that inclusion of the 3 hearts with starting rates greater than 400bpm was appropriate.

Aside from the assessment of baseline function at 10mins, perfusion temperature and pH was assessed continuously and any heart exiting the acceptable ranges was excluded from this experimental analysis. Poor temperature control accounted for the exclusion of four hearts, which are not included in this or in subsequent analyses. pH was maintained between 7.35 and 7.40 in all hearts throughout.

4.2.2.2 Perfusion parameters in Goto Kakizaki rat hearts

Again, heart performance was assessed against Bell's *a priori* definitions of an acceptable Langendorff perfusion³⁷¹ after 10 minutes stabilisation. Heart temperature, coronary flow, heart rate and LV rate-pressure product were within the pre-specified limits, and LV end-diastolic pressure was set appropriately in all hearts. LV developed pressure was towards the lower end of Bell's specified

range, the lower end of acceptability being set at 70mmHg. Developed pressure in the three study groups were 84.5 ± 25.1 mmHg (IPC 0), 67.4 ± 19.9 mmHg (IPC 1) and 71.1 ± 22.5 mmHg (IPC 3). There was no significant difference between the groups ($P=ns$), and as the same perfusion rig was used as for the SDR hearts, the low DevP could not be indicative of a perfusion or technique problem. The only remaining explanation was that the GKR hearts had impaired systolic function at baseline, and this was supported by the observation that LV rate-pressure product in GKR hearts was lower than in SDR hearts, but reassuringly this did not fall below Bell's proposed cut-off (Figure 4.4F). We decided to accept the perfusions on the basis that a low DevP was a resting feature of GKR hearts in the Langendorff preparation.

4.2.2.3 Verification of LCA occlusion

The expected 30% or greater drop in coronary flow rate and of LV developed pressure³⁷¹ was seen in all hearts included in the analysis. Figure 4.3B shows rapid recovery of coronary flow rate in the SDR group, so that the mean drop in coronary flow between immediately before tightening the LCA snare, to the point five minutes into experimental infarction is $20 \pm 35\%$ in control hearts vs $38 \pm 20\%$ in the IPC1 group and $45 \pm 15\%$ in the IPC3 group ($P=NS$ for all comparisons). The GKR hearts behaved differently, with less rapid recovery of the drop in coronary flow rate (CFR), such that the drop in CFR between immediately before and five minutes after LCA occlusion in GKR hearts was $48 \pm 8\%$ in the GKR controls versus $58 \pm 10\%$ and $54 \pm 19\%$ in the IPC1 and IPC3 groups respectively. Again, there was no statistically significant difference in the scale of CFR drop between the GKR heart treatment groups.

Decreases in developed pressure (DevP) with LCA snare tightening persisted beyond 5 mins ischaemia in both SDR and GKR hearts, such that the mean drop between the measurement taken immediately before snaring and the measurement five minutes later was $69 \pm 13\%$ (IPC0) vs $48 \pm 17\%$ (IPC1) and $77 \pm 4\%$ (IPC3) in the SDR hearts. The drop in DevP was significantly less in the SDR IPC1 group than the IPC3 group ($P < 0.05$); no other comparisons were statistically significant. In the GKR hearts the equivalent drops in DevP were $79 \pm 2\%$ (IPC0) versus $61 \pm 20\%$ (IPC1) and $77 \pm 8\%$ (IPC3). As with the SDR

hearts, the drop in DevP was lowest in the GKR IPC1 group, and this reached statistical significance against the GKR IPC0 group ($P < 0.05$).

In summary, all groups met the prespecified criteria for validation of successful LCA occlusion.

4.2.3 Analytical reproducibility

To demonstrate analytical reproducibility, I repeatedly analysed a panel of 10 hearts, calculating total cross-sectional area, area at risk and infarct size 20 times for each. The order of analysis was varied each time. The results are shown in Figure 4.5 and Table 4.1:

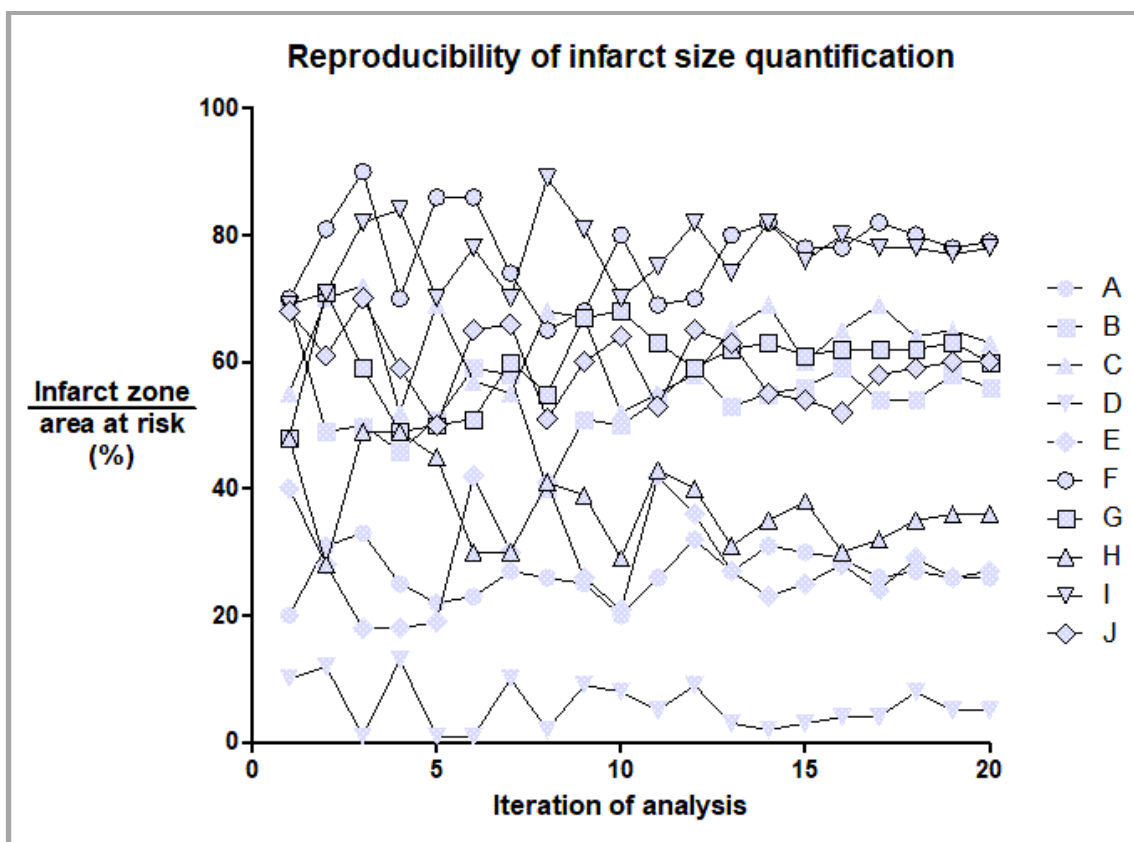


Figure 4.5: Reproducibility of infarct size quantification. Variation in infarct size quantified by semi-automated colorimetry reduces with experience. 200 blinded heart assessments carried out over four days, showing a decrease in the variability of assessment with repeated exposure by the operator.

Over the course of 20 iterations of the same operator examining the same hearts in a different random order each time, the consistency of assessment improved significantly. Standard deviations for the spread of assessed infarct sizes for each set of five iterations are given in Table 4.1.

Variation, as measured by standard deviation, decreases linearly as more iterations of analysis are performed ($P < 0.01$; $R^2 = 0.99$). Comparing the final two iterations of analysis yields a mean variability of only 1.75%.

Iterations	Standard deviation of five assessments			
	1-5	6-10	11-15	16-20
Heart A	5.630	2.775	2.588	1.304
Heart B	9.138	7.635	2.302	2.280
Heart C	9.343	7.259	5.595	2.280
Heart D	5.941	4.183	2.793	1.643
Heart E	9.581	9.247	8.081	1.924
Heart F	9.154	8.591	5.933	1.673
Heart G	9.762	7.396	1.673	1.095
Heart H	8.983	5.718	4.615	2.683
Heart I	7.190	8.019	3.899	1.095
Heart J	7.956	6.140	5.568	3.347
Mean	8.27	6.70	4.31	1.93

Table 4.1: Numerical representation of improving reproducibility of infarct size assessment with increasing assessment experience. Each row is a blinded heart and each figure the standard deviation of five consecutive assessments of the infarct size on that heart. The standard deviations decrease progressively moving from right to left of the table, illustrating there is progressively less variation in the infarct size assessments with more assessment experience.

4.2.4 Infarct size following *ex vivo* ischaemic preconditioning

All hearts completing the ischaemia-reperfusion phase of the experiment were included in the final analyses; no heart was excluded because of an inappropriate area at risk. Infarct sizes are summarised in Figure 4.6:

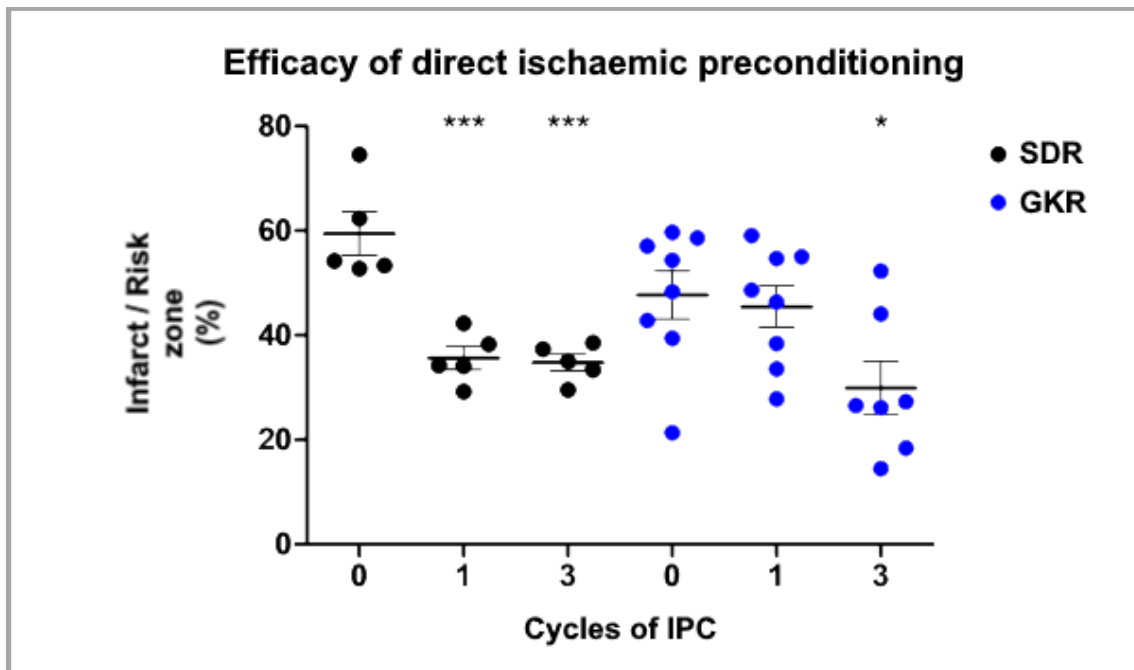


Figure 4.6: Efficacy of direct ischaemic preconditioning in both 3 month Sprague Dawley and 8 month Goto Kakizaki rat hearts subjected to *ex vivo* experimental infarction. A single cycle of IPC produces a significant reduction in infarct size compared to the control infarct size in SDR hearts. Three cycles of IPC had a similar effect. In GKR hearts, a single cycle of IPC produced no change in infarct size compared to control but efficacy of three cycles of IPC was preserved. SDR: Sprague Dawley rat; GKR: Goto Kakizaki; IPC: ischaemic preconditioning. Error bars show S.E.M.; n=5 per group for SDRs; n=7-8 per group for GKR; *: P<0.05 vs strain-matched control (no IPC) group; ***: P<0.001 vs strain-matched control (no IPC) group..

SDR and GKR hearts differ significantly in their responsiveness to IPC.

Baseline infarct size in the SDR hearts is ameliorated significantly with one or three cycles of IPC: In control SDR hearts, infarct size is 59.5±4.2% of the area at risk, vs 35.6±2.2% following IPC1 (P<0.01) and 34.7±1.6% with IPC3 (P<0.01). In GKR hearts, IPC1 does not reduce infarct size (47.7±4.6% vs 45.5±4.0%; P=NS), but IPC3 ameliorates the size significantly from 47.7±4.6% to 29.9±5.1% (P<0.05).

4.2.5 Perfusion during and after *in vivo* remote preconditioning

19 SDR hearts and 26 GKR hearts successfully completed RIPC (RIPC1, RIPC3) or Sham RIPC (RIPC0) protocols. After tracheal intubation, observations were taken *in vivo* every 10 minutes until the heart was transferred *ex vivo* to the Langendorff apparatus, from which point on physiological observations were taken as per the usual *ex vivo* protocol. SDR physiology is summarised in Figure 4.7, and GKR physiology in Figure 4.8.

4.2.5.1 Physiology of Sprague Dawley rats during RIPC

Appropriate core body temperature was maintained throughout RIPC or sham procedure in all SDRs (Figure 4.7A). Heart rate was consistently within the expected range for live rats during the procedure⁴⁰⁰ (Figure 4.7B).

4.2.5.2 Perfusion parameters in Sprague Dawley rat hearts

Performance against *a priori* definitions of successful Langendorff perfusion was assessed after 10 minutes of retrograde perfusion. One SDR heart perfusion was discontinued due to high coronary flow and low developed pressure, suggesting injury to the aortic valve. The remaining perfusions are presented in Figure 4.7 and for these, heart temperature, coronary flow, LVEDP, heart rate, LV developed pressure and rate-pressure product all met Bell's proposed cut-offs for a successful Langendorff preparation³⁷¹.

Heart temperature and pH of the perfusate was maintained within target ranges for the experiment duration in all hearts.

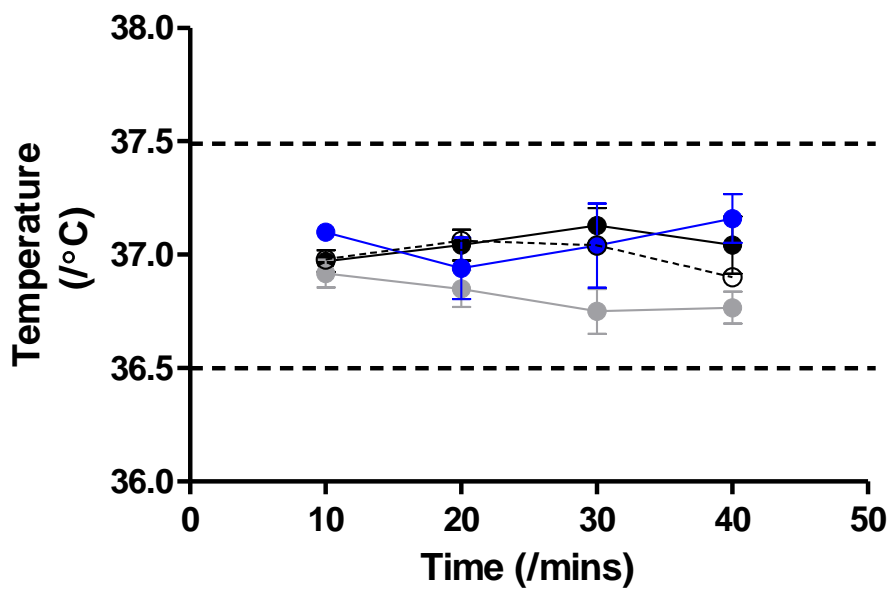
4.2.5.3 Physiology of Goto Kakizaki rats during RIPC

Appropriate core body temperature and heart rates were maintained throughout RIPC or sham procedure in all GKRs (Figure 4.8A-B).

In vivo phase:

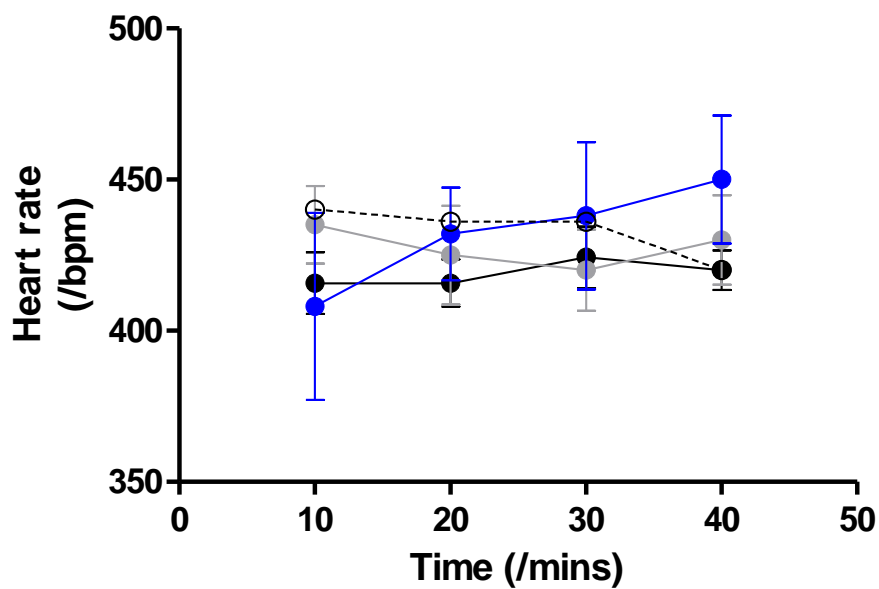
A

Temperature control



B

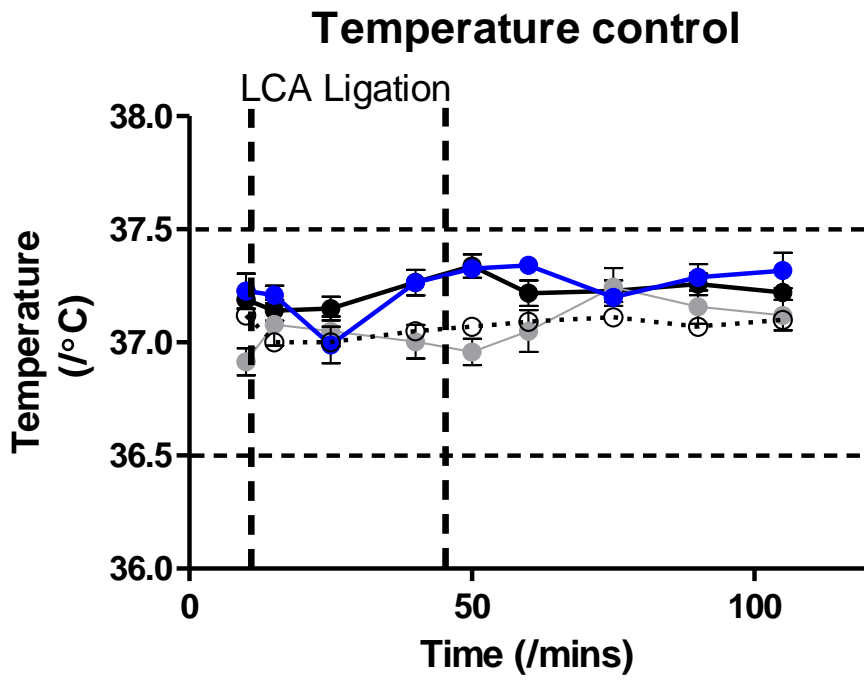
Heart rate



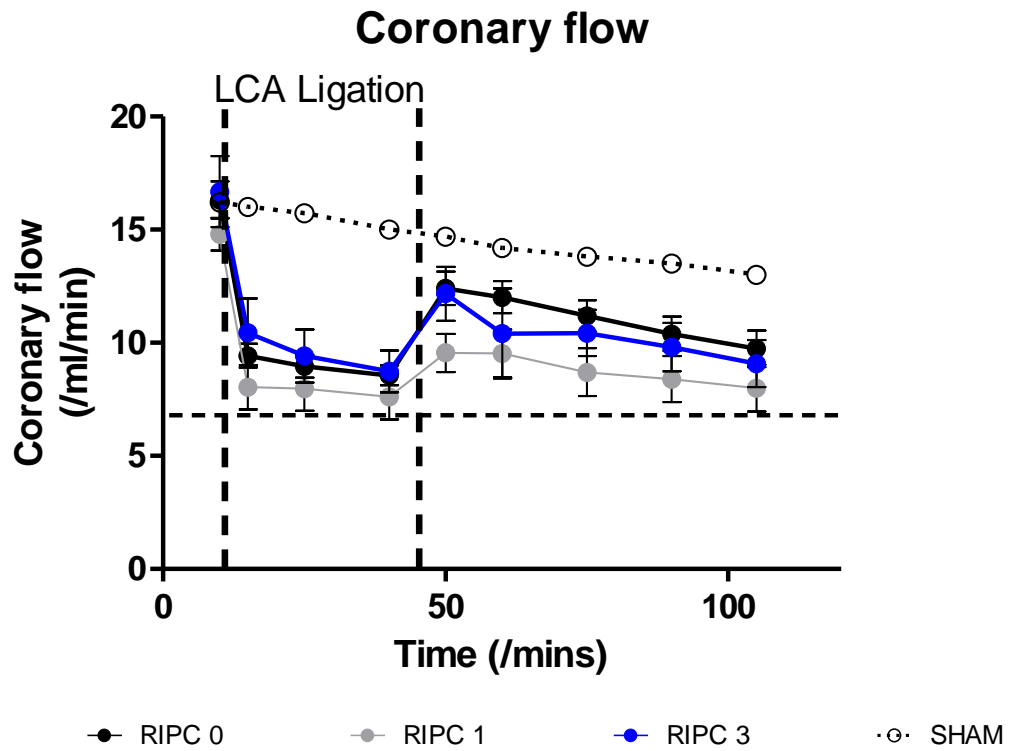
● RIPC 0 ● RIPC 1 ● RIPC 3 ·○· SHAM

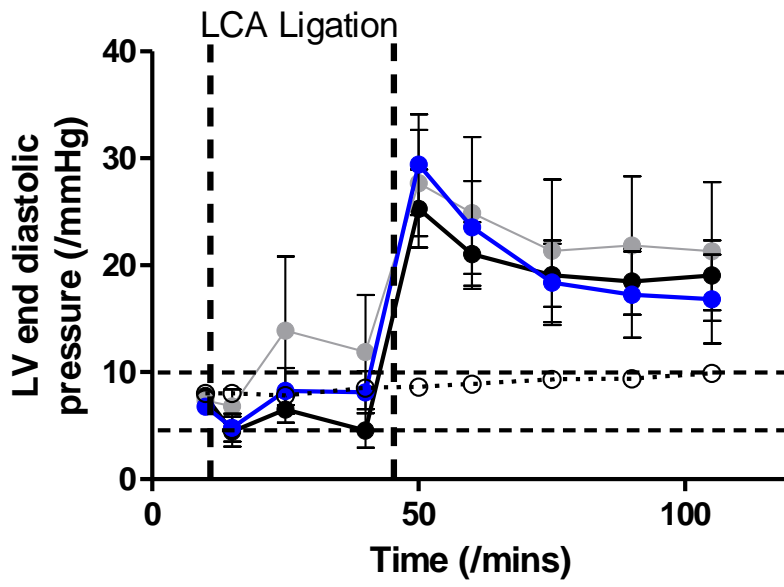
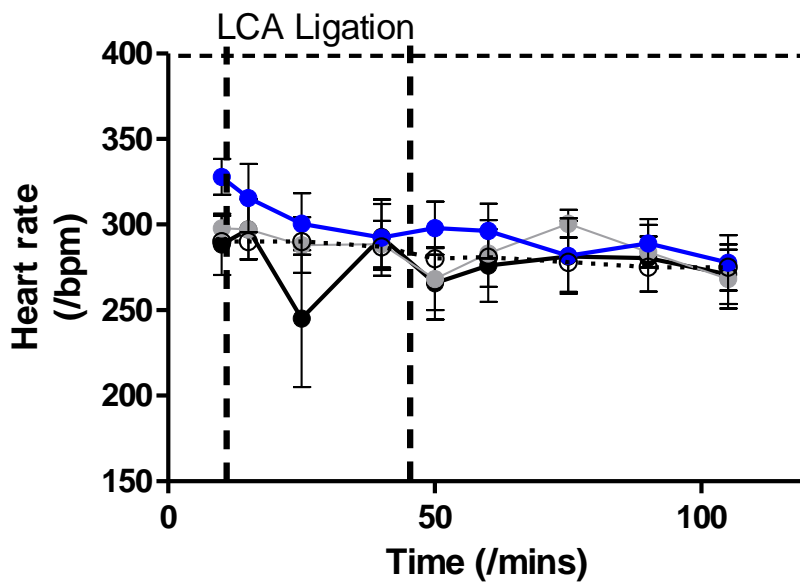
Ex vivo phase:

C



D



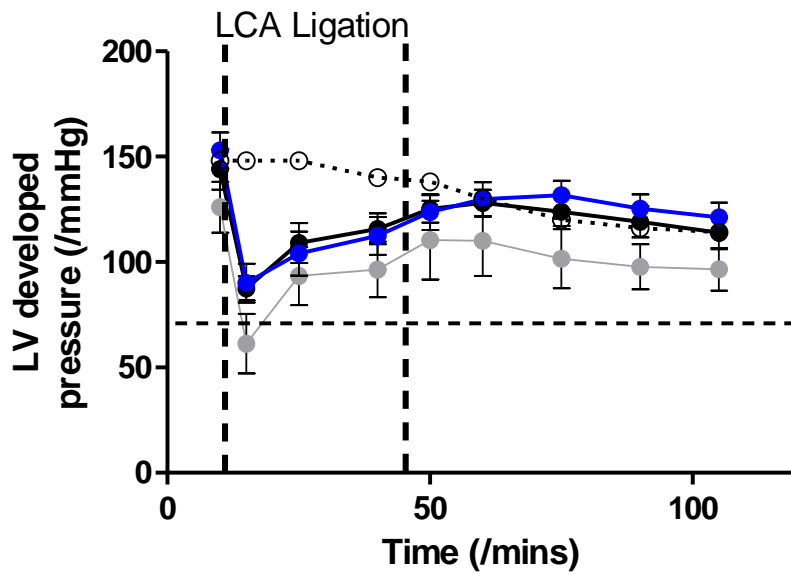
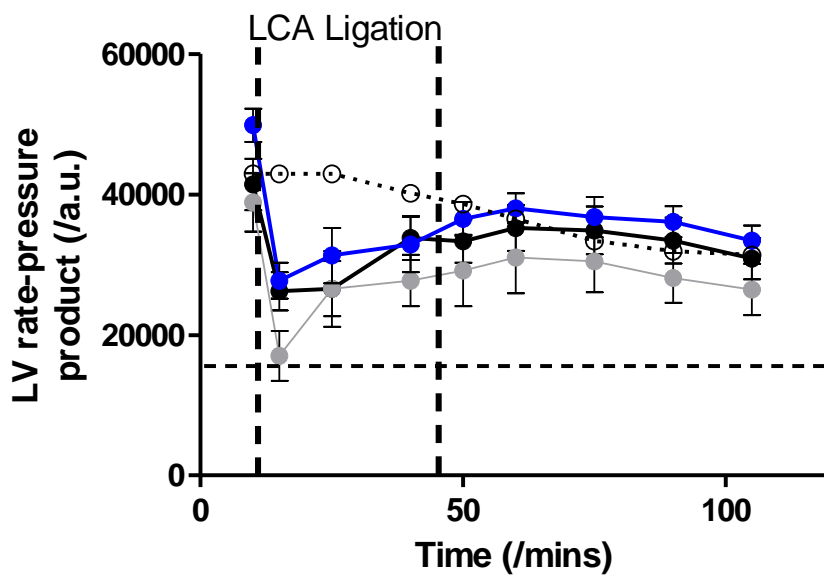
E**Left ventricular end diastolic pressure****F****Heart rate**

● RIPC 0

● RIPC 1

● RIPC 3

● SHAM

G**Left ventricular developed pressure****H****Left ventricular rate-pressure product**

● RIPC 0

● RIPC 1

● RIPC 3

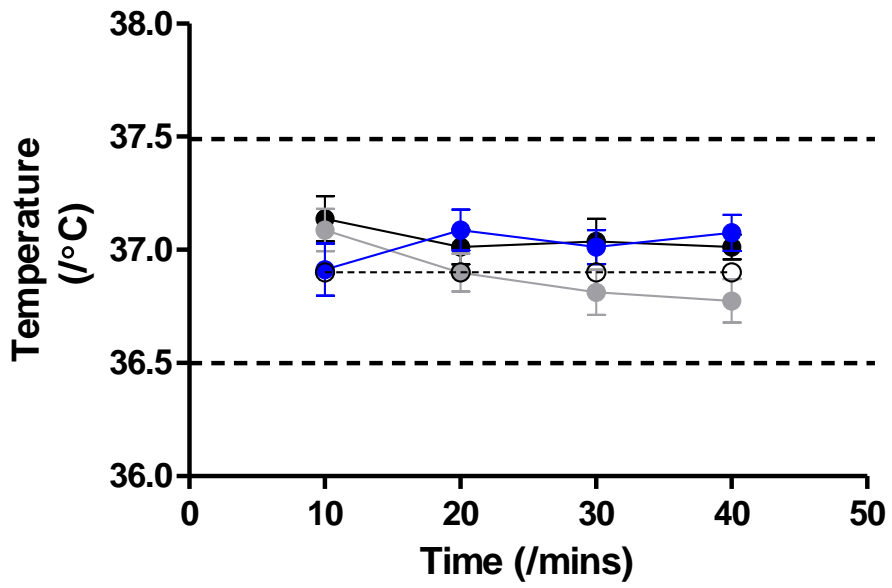
● SHAM

Figure 4.7 (see pages 182-185): Physiological parameters during *in vivo* remote ischaemic preconditioning of 3 month Sprague Dawley rat hearts, followed by *ex vivo* experimental infarction. During the *in vivo* phase, both body temperature (**A**) and heart rate (**B**) were maintained in the expected range for all experiments. After 10mins of *ex vivo* perfusion all hearts included here met *a priori* definitions of a valid Langendorff perfusion for both dependent and independent variables. Coronary flow (**D**) and developed pressure (**G**) fell as expected with occlusion of the left anterior descending coronary artery. No statistically significant differences emerged between treatment groups for any of the dependent variable including end diastolic pressure (**E**), heart rate (**F**), developed pressure (**G**) or rate-pressure product (**H**). Experimental groups are as follows: RIPC0: No remote ischaemic preconditioning (RIPC); RIPC1: single cycle of five minutes sub-lethal limb ischaemia and reperfusion; RIPC3: three similar cycles of limb ischaemia. Error bars show S.E.M.; n≥5 per group.

In vivo phase:

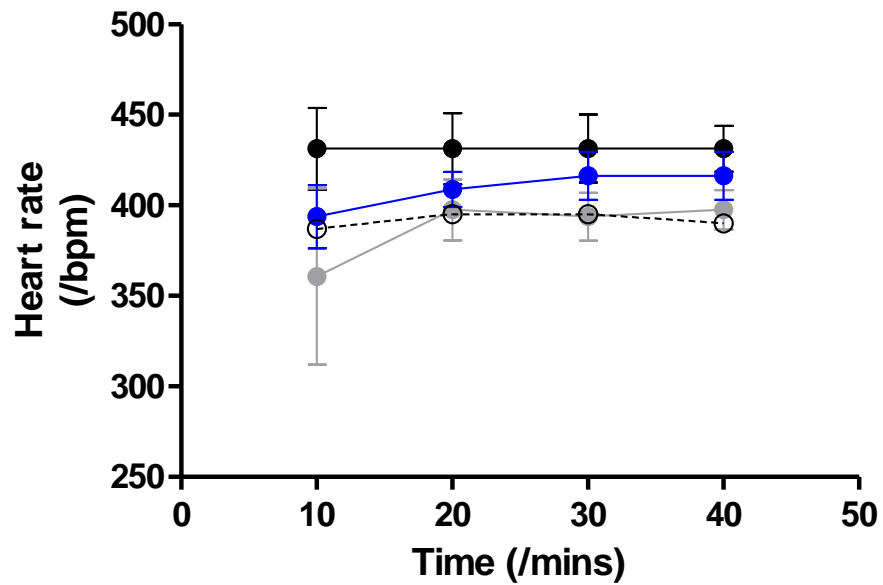
A

Temperature control



B

Heart rate



● RIPC 0

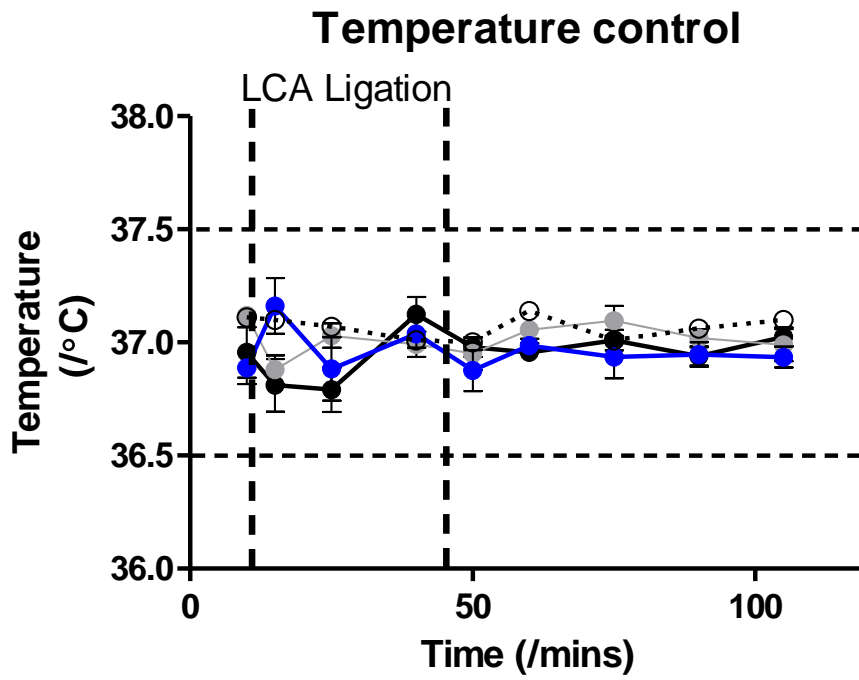
● RIPC 1

● RIPC 3

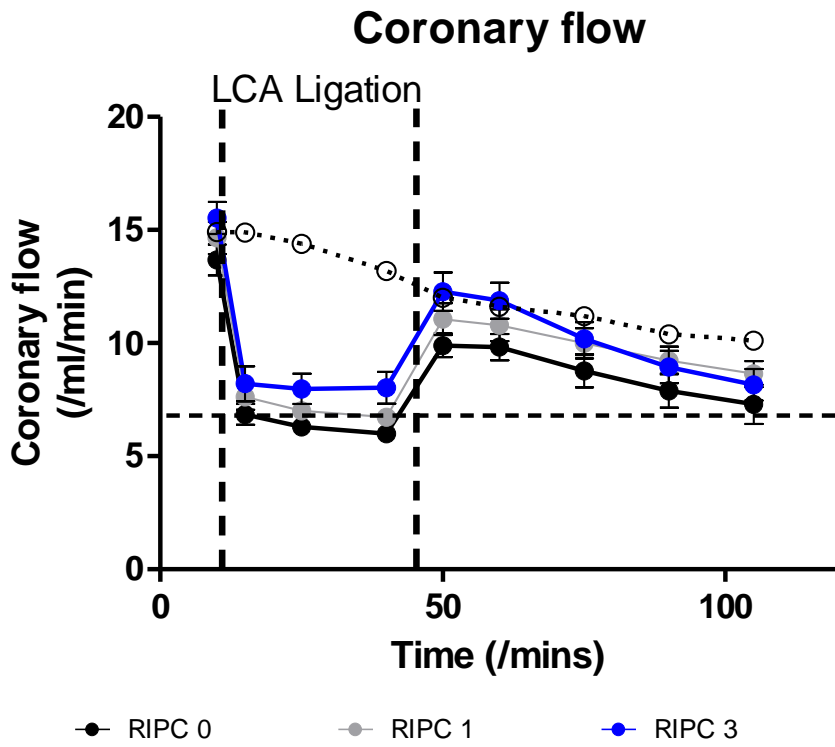
○ SHAM

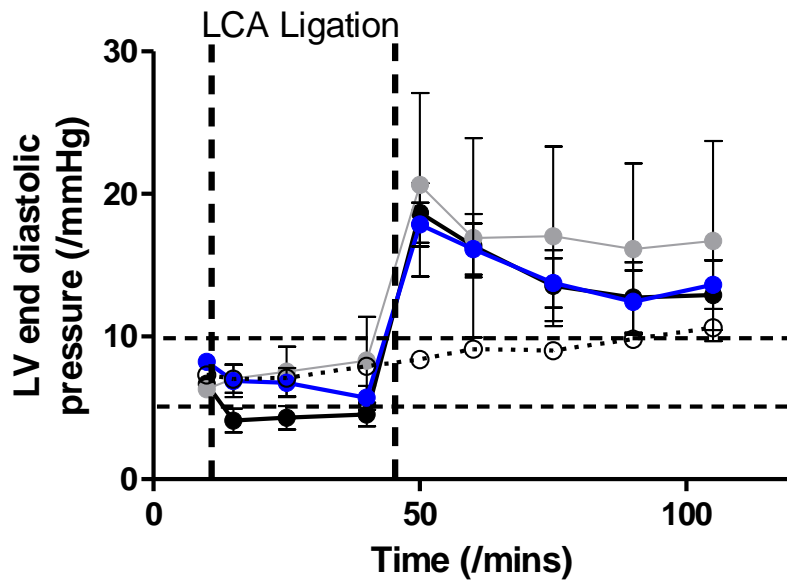
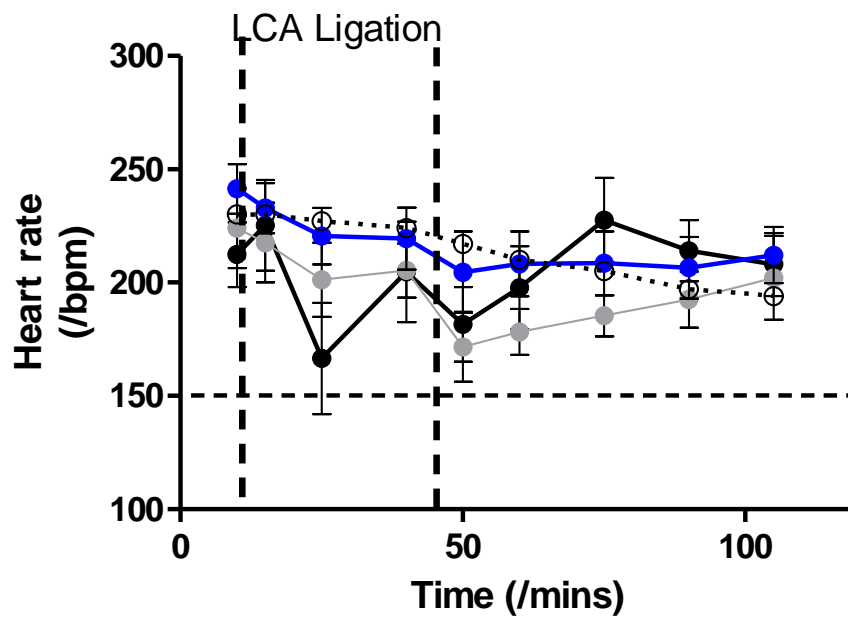
Ex vivo phase:

C



D



E**Left ventricular end diastolic pressure****F****Heart rate**

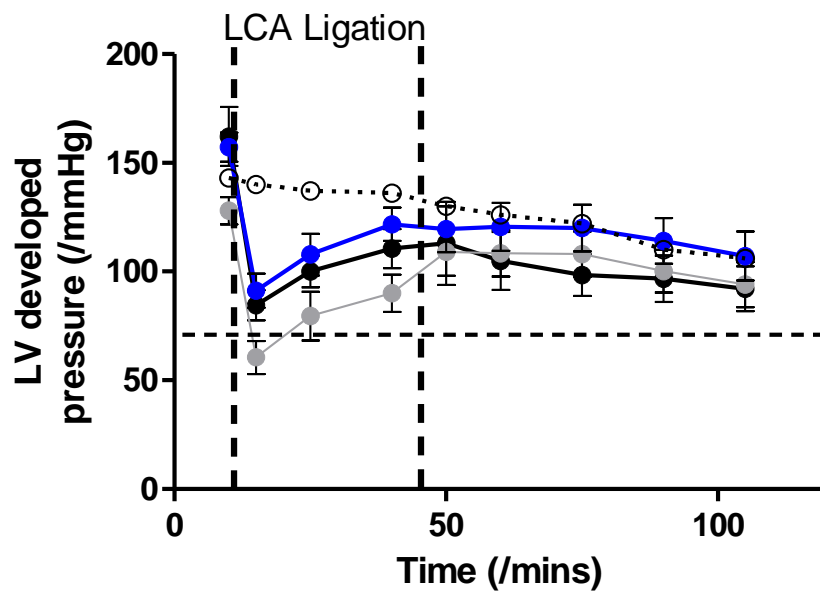
● RIPC 0

● RIPC 1

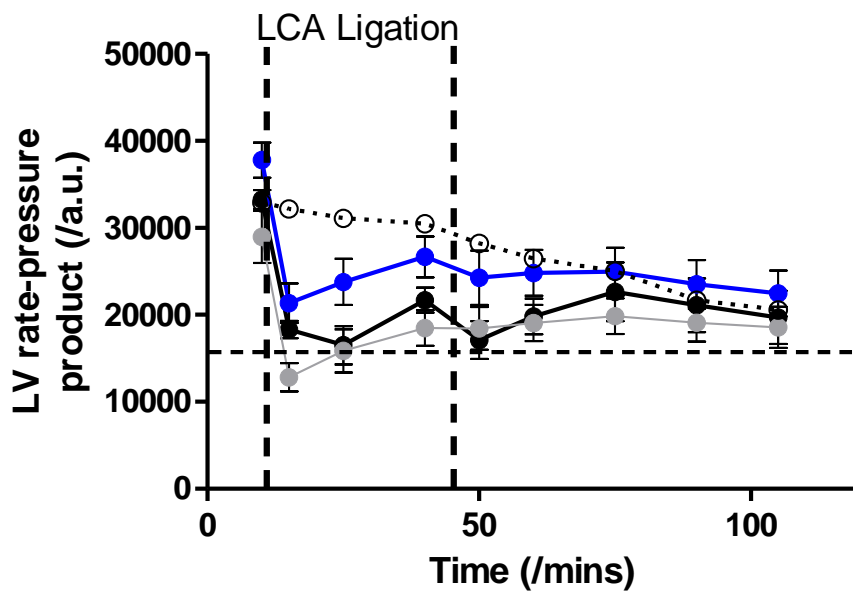
● RIPC 3

● SHAM

G Left ventricular developed pressure



H Left ventricular rate-pressure product



● RIPC 0 ● RIPC 1 ● RIPC 3 ○ SHAM

Figure 4.8 (see pages 187-190): Physiological parameters during *in vivo* remote ischaemic preconditioning of 8 month Goto Kakizaki rat hearts, followed by *ex vivo* experimental infarction. During the *in vivo* phase, both body temperature (**A**) and heart rate (**B**) were maintained in the expected range for all experiments. After 10mins of *ex vivo* perfusion all hearts included here met *a priori* definitions of a valid Langendorff perfusion for both dependent and independent variables. Coronary flow (**D**) and developed pressure (**G**) fell as expected with occlusion of the left anterior descending coronary artery. No statistically significant differences emerged between treatment groups for any of the dependent variable including end diastolic pressure (**E**), heart rate (**F**), developed pressure (**G**) or rate-pressure product (**H**). Experimental groups are as follows: RIPC0: No remote ischaemic preconditioning (RIPC); RIPC1: single cycle of five minutes sub-lethal limb ischaemia and reperfusion; RIPC3: three similar cycles of limb ischaemia. Error bars show S.E.M.; n=8 per group.

4.2.5.4 Perfusion parameters in Goto Kakizaki Rat hearts

Performance against *a priori* definitions of successful Langendorff perfusion was assessed after 10 minutes of retrograde perfusion. Two GKR heart perfusions were discontinued due to developed pressure below the pre-specified cut-off (70mmHg). The remaining hearts all met pre-specified conditions at the 10 minute checkpoint (Figure 4.8C-H). Temperature and perfusate pH remained within target limits for the remainder of all perfusions.

4.2.5.5 Verification of LCA occlusion

In all SDR and all GKR hearts, the expected 30% drop in CFR and LV developed pressure accompanied tightening the LCA snare, consistent with effective LCA occlusion. There was no heterogeneity between the groups with respect to the drop in CFR seen ($P=NS$ for all comparisons). Statistically significant differences were seen in the degree of drop in DevP between the treatment groups. In SDRs, DevP drop in the IPC1 group was $48\pm 9\%$, significantly less than in the IPC3 group ($77\pm 2\%$); $P<0.05$. In GKRs, DevP dropped significantly less in the IPC1 group ($61\pm 9\%$) than the IPC0 group ($79\pm 2\%$); $P<0.05$). No other comparisons reached statistical significance.

In summary, there was no heterogeneity seen in the drop or initial recovery in coronary perfusion between treatment groups which is the most reliable marker of coronary occlusion. Heterogeneity was seen in DevP drops, but this was inconsistent and did not show a trend towards preservation or deleteriousness in the hearts exposed to RIPC.

4.2.6 Infarct size following *in vivo* remote preconditioning

All hearts completing the ischaemia-reperfusion phase of the experiment were included in the final analyses; no heart was excluded because of an inappropriate area at risk. Infarct sizes are summarised in Figure 4.9:

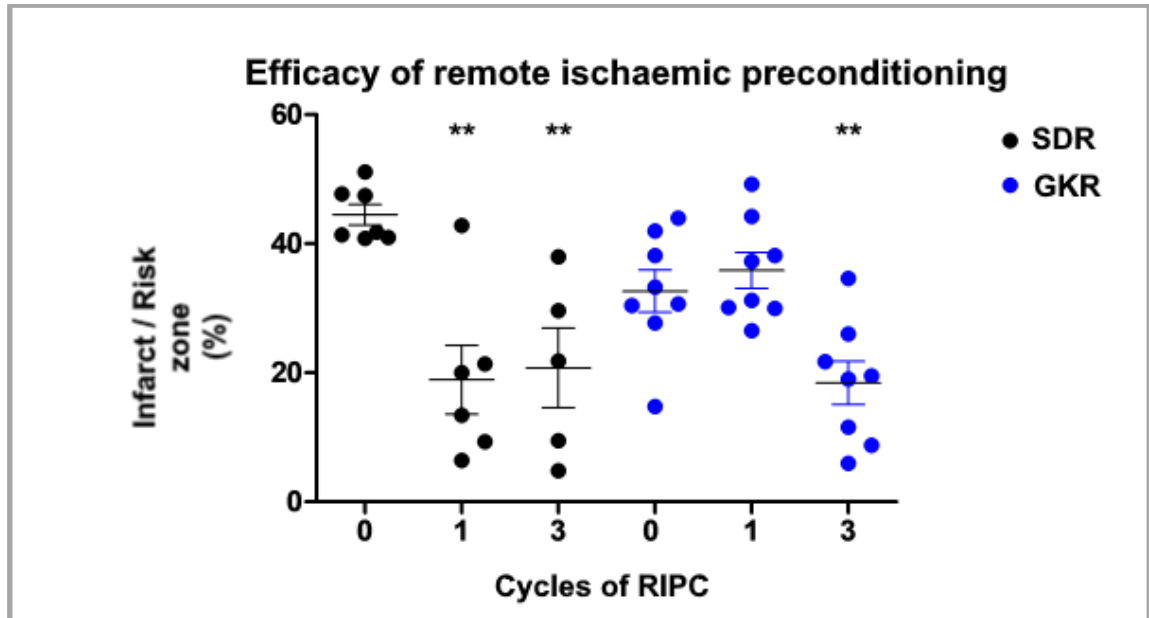


Figure 4.9: Efficacy of remote ischaemic preconditioning in both 3 month Sprague Dawley and 8 month Goto Kakizaki rat hearts subjected to *in vivo* remote ischaemic preconditioning followed by *ex vivo* experimental infarction. A single cycle of RIPC produces a significant reduction in infarct size compared to the control infarct size in SDR hearts. Three cycles of RIPC had a similar effect. In GKR hearts, a single cycle of RIPC produced no change in infarct size compared to control but efficacy of three cycles of RIPC was preserved. SDR: Sprague Dawley rat; GKR: Goto Kakizaki rat; RIPC: Remote ischaemic preconditioning. **= $P < 0.01$. Error bars show S.E.M.; $n \geq 5$ for SDRs; $n = 8$ for GKR.

One and three cycles of remote ischaemic preconditioning were both associated with significantly smaller infarct size than control conditions in Sprague Dawley rat hearts: RIPC0 infarcts comprised $44.5 \pm 1.6\%$ of area at risk vs $18.9 \pm 5.3\%$ in RIPC1 hearts ($P < 0.01$) and $20.8 \pm 6.2\%$ in RIPC3 hearts ($P < 0.01$). In GKR hearts RIPC1 exerted no effect, with baseline infarct size $32.6 \pm 3.7\%$ similar to the $35.9 \pm 2.8\%$ seen in RIPC1 hearts ($P = \text{NS}$). RIPC3 associated with a significant decrease in infarction with infarct size in this group to $18.4 \pm 3.3\%$ ($P < 0.01$). No trend towards smaller infarct size was seen in the GKR RIPC1 group.

4.2.7 Survival kinase activation with preconditioning

Eight GKR hearts from eight-month old animals underwent three cycles of *ex vivo* preconditioning (n=2), three cycles of *in vivo* remote ischaemic preconditioning (n=2), control Langendorff perfusion (n=2) or simple washing (n=2). Ventricular tissue was sampled and blotted for total Akt, Phospho-Akt and Tubulin (loading control). Quantitative densitometry analysis of the blots is presented in Figure 4.10:

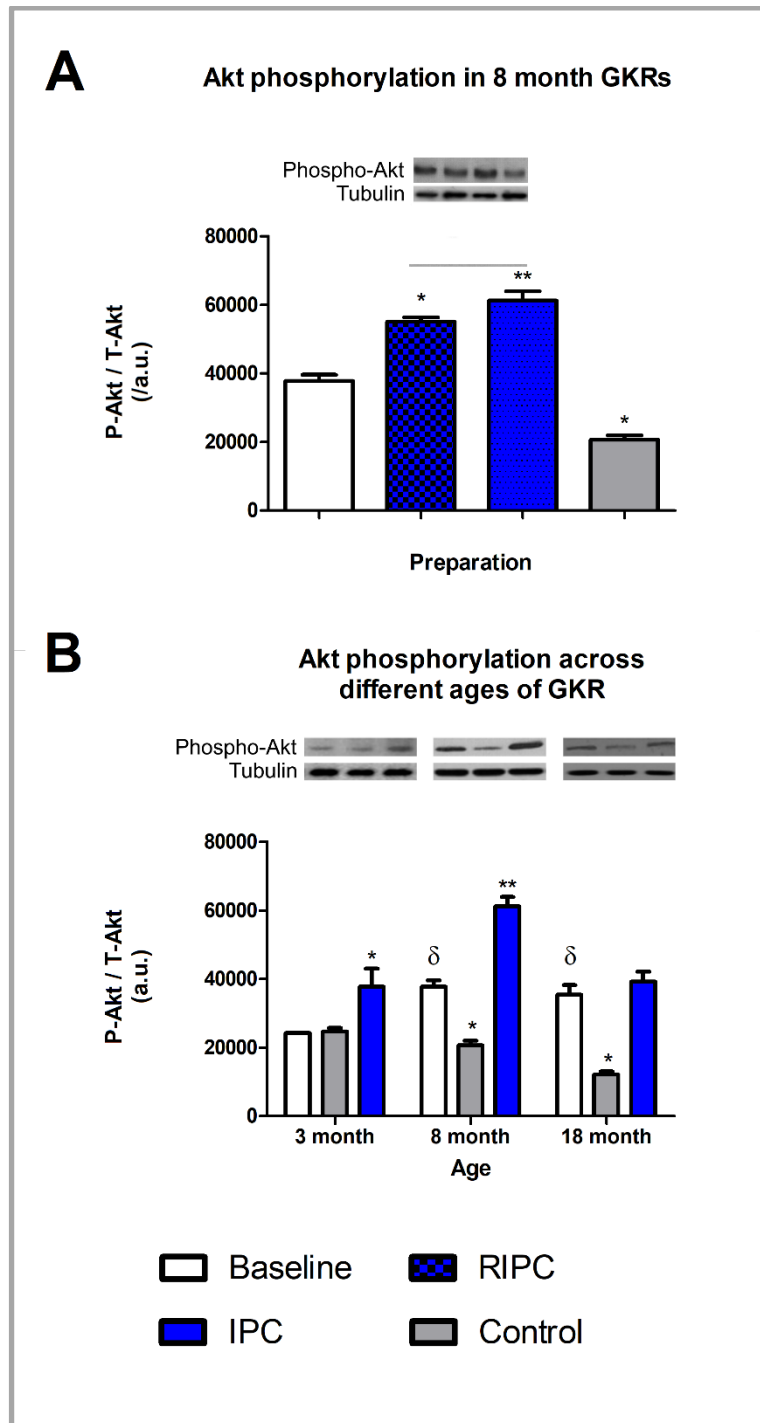


Figure 4.10 (see page 194): Phosphorylation of myocardial Akt in reaction to direct and remote ischaemic preconditioning in 8 month Goto Kakizaki rat myocardium (**A**) and in Goto Kakizaki rats of different ages subjected to IPC (**B**). Both IPC and RIPC produce increases in Akt phosphorylation in 8 month GKR hearts compared to hearts not exposed to IPC or RIPC (**A**). 8 month GKR hearts not exposed to IPC or RIPC but explanted and perfused for 40mins exhibit less Akt phosphorylation than hearts explanted and immediately snap frozen for blotting (**A**). Akt phosphorylation in 3 month GKR hearts is preserved after 40mins *ex vivo* perfusion (**B**) Akt phosphorylation immediately after heart explant is higher in 8 month and 18 month hearts than in 3 month hearts but this additional phosphorylation at baseline is lost during 40mins *ex vivo* perfusion (**B**). IPC only increases Akt phosphorylation above baseline levels in 3 month and 8 month hearts (**B**). Experimental groups are as follows: Baseline: tissue sampled immediately on heart explantation; RIPC: tissue sampled after 3 cycles sub-lethal hindlimb ischaemia; IPC: tissue sampled after 3 cycles sub-lethal myocardial ischaemia; Control: tissue sampled after 10mins continuous retrograde perfusion. *: P<0.05 compared to age-matched Baseline group; **: P<0.01 compared to age-matched Baseline group; δ : P<0.05 compared to 3 month old Baseline group. Error bars show S.E.M; n=4 per group from two rats.

In 8 month GKR, Phospho-Akt increased from 37783 ± 1778 a.u. at baseline after heart explant to 55059 ± 1223 a.u. after RIPC (P<0.05) and to 61175 ± 2708 a.u. after direct IPC (P<0.01). Without either treatment, Phospho-Akt decreased to 20634 ± 1359 a.u. (P<0.01). This pattern of response is modulated by age: in three month animals there is significantly less Akt phosphorylation at baseline (24260 ± 74 a.u. vs 37783 ± 1778 a.u.; P<0.05) and this is not lost after 10mins control Langendorff perfusion (24260 ± 74 a.u. vs 24610 ± 1098 a.u.; P=NS), but is enhanced by three cycles of IPC (24260 ± 74 a.u. vs 37780 ± 5170 a.u.). At 18 months the baseline phosphorylation is no different to 8 months (35380 ± 2855 a.u.) but it is not further enhanced by IPC (35380 ± 2855 a.u. vs 39180 ± 2940 a.u.; P=NS), and it is lost with control perfusion ($12160843 \pm$ a.u. vs 35380 ± 2855 a.u.; P<0.01).

4.3 Summary of preconditioning studies

Experimental *ex vivo* infarction was induced in all hearts included in the final analysis and indirect markers of successful left coronary artery occlusion were consistently met. Areas at risk were comparable across all experimental groups and met *a priori* criteria for inclusion. There were minor differences between GKR and controls in patterns of developed pressure suppression and coronary

flow rate recovery during ischaemia, but nothing to suggest differences in the success of LCA occlusion or depth of ischaemia between experimental groups.

One or three cycles of direct ischaemic preconditioning ameliorated infarct size in non-diabetic hearts: a single cycle produced a statistically significant 40.1% relative reduction in infarct size and three cycles produced a statistically significant 41.7% relative reduction with no significant differences between the preconditioned groups. By contrast, one cycle of IPC did not reduce infarct size in diabetic GKR hearts, but three cycles produced a statistically significant 37.3% relative reduction.

Likewise, one or three cycles of remote ischaemic preconditioning ameliorated infarct size in non-diabetic rat hearts: a single cycle produced a statistically significant 57.5% relative reduction in infarct size and three cycles produced a statistically significant 53.3% relative reduction. By contrast, one cycle of RIPC did not reduce infarct size in the diabetic hearts, but three cycles produced a statistically significant 43.6% relative reduction.

Ventricular tissue lysates from different ages of GKR hearts showed Akt phosphorylation is statistically significantly increased after three cycles of direct or remote preconditioning in eight month animals, and significantly decreased after 10 mins continuous *ex vivo* perfusion. These effects are significantly modulated by age, with Akt phosphorylation sustained in control perfusions in younger (three month) animals, and IPC failing to augment phosphorylation in older (18 month) animals. All results are assessed critically in Chapter 6, "Discussions".

**5. EFFECTS OF GLUCOSE ON THE RESPONSE TO
REPERFUSION INJURY IN A DIABETIC AND A NON-
DIABETIC MODEL**

5.1 Aims and hypotheses

The aims of this work are to:

1. Clarify whether some of the deleterious effect of high blood glucose during MI is the result of exacerbation of tissue death from acute ischaemia-reperfusion
2. Explore whether the effect of blood glucose content on IRI is stronger in patients without diabetes than in patients with diabetes, i.e. whether the relationship mirrors the epidemiological trends seen.
3. To isolate the effect of variable perfusing glucose concentrations on the extent of reperfusion injury in the heart.

Based on the early impact of insulin infusion in patients with diabetes, we hypothesised that some or all of the impact of blood glucose content on myocardial infarction may be seen during acute reperfusion.

We further hypothesised that exposing hearts to variable glucose concentrations during reperfusion after ischaemic injury would modulate the extent of tissue death from a standardised ischaemic insult. Based on the idea that hearts from diabetic animals would have some sort of chronic adaptation to high glucose, we hypothesised that there would be less excess tissue damage in diabetic hearts versus non-diabetic, when exposed to high glucose during reperfusion. The work reported in Chapter 3 (“Testing for evidence of diabetes in UCL’s Goto-Kakizaki Rat colony”) had confirmed significant hyperglycaemia and insulin deficiency in 8 month GKR, suggesting these animals are a model of established insulin deficient (“type 1”) diabetes in man.

We anticipated the greatest burden of cell death in non-diabetic hearts exposed to the highest glucose content during reperfusion, and hypothesised that the site of this extra injury would be within the cardiomyocyte, and hence could be ameliorated by partially blocking basal glucose uptake by the myocardium - i.e. the opposite of the effect of giving insulin, which in the absence of diabetes increases inward glucose flux via GLUT-4 facilitated glucose transporters.

If these experiments were successful, we aimed to use a model of acute oxidative stress in isolated cardiomyocytes to investigate cells' resilience in the settings of various glucose concentrations. We hypothesised that cardiomyocytes' response to oxidative stress would mirror their resilience during ischaemia-reperfusion injury during the whole heart experiments, and that this cellular model could then be used to investigate the mechanism of glucose's deleterious effect, and the protective potential of drugs that reduce cellular glucose uptake.

5.2 Results

Overall, 79 animals (47 SDRs and 32 GKR) were used in the infarct size experiments. Isolated cardiomyocytes were prepared from a further 26 SDRs for use in the sIRI and ROS quantification protocols.

5.2.1 Rat morphology and blood glucose content

Fasting hyperglycaemia was confirmed in the GKR and excluded in the SDRs used in these experiments at least two days prior to the terminal procedures being performed. Summary findings are given in Table 5.1:

	SDRs	GKR
Body mass	358±22g	416±29g
Heart mass	2.25±0.11g	2.08±0.37g
Fasting blood glucose	7.04±0.18mmol/L	12.11±3.03mmol/L

Table 5.1: Baseline characteristics of n=73 8 month Goto Kakizaki (GKR) and n=32 3 month Sprague Dawley (SDR) rats used in variable reperfusion glucose protocols, both whole heart (GKR and SDR) and isolated cardiomyocytes (SDR only).

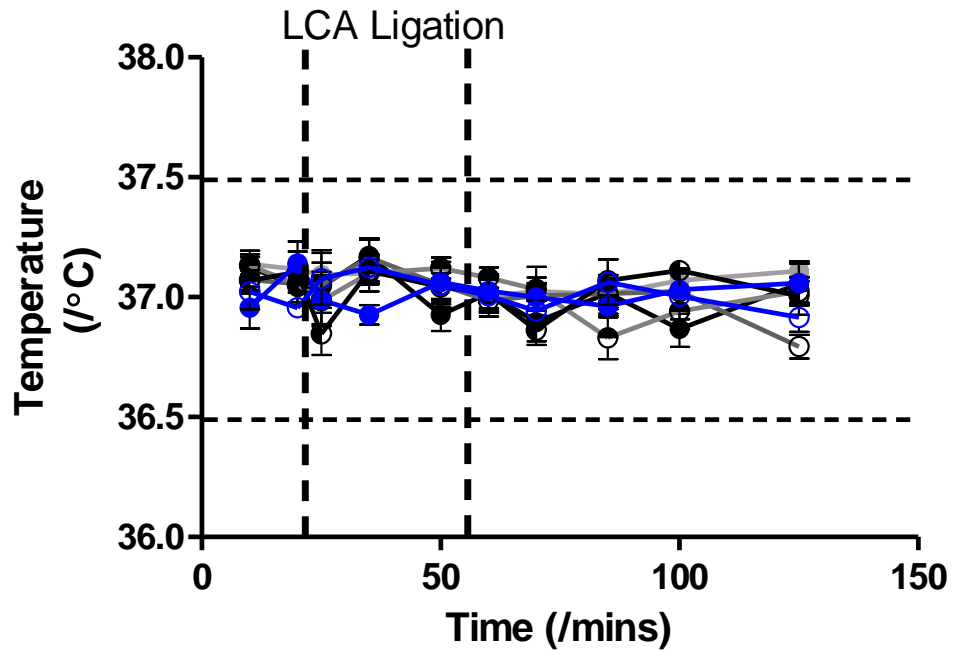
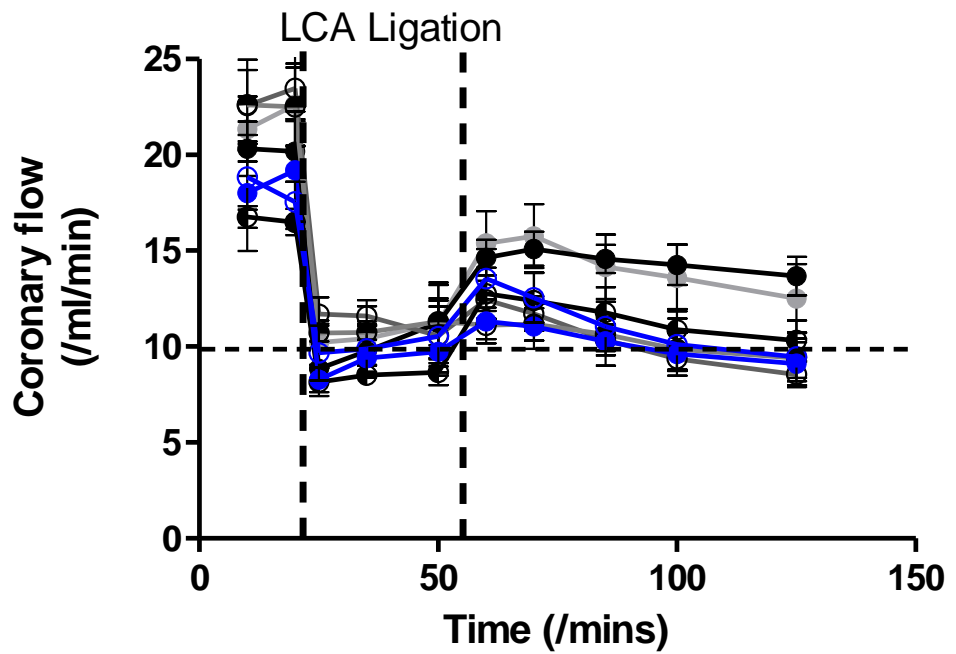
5.2.2 Glucose exposure during reperfusion

In total, 44 SDRs and 32 GKR completed Langendorff retrograde perfusion protocols. Three SDR perfusions were abandoned due to inappropriate coronary flow rates after 10 minutes perfusion, compared to *a priori* definitions of a successful Langendorff perfusion³⁷¹.

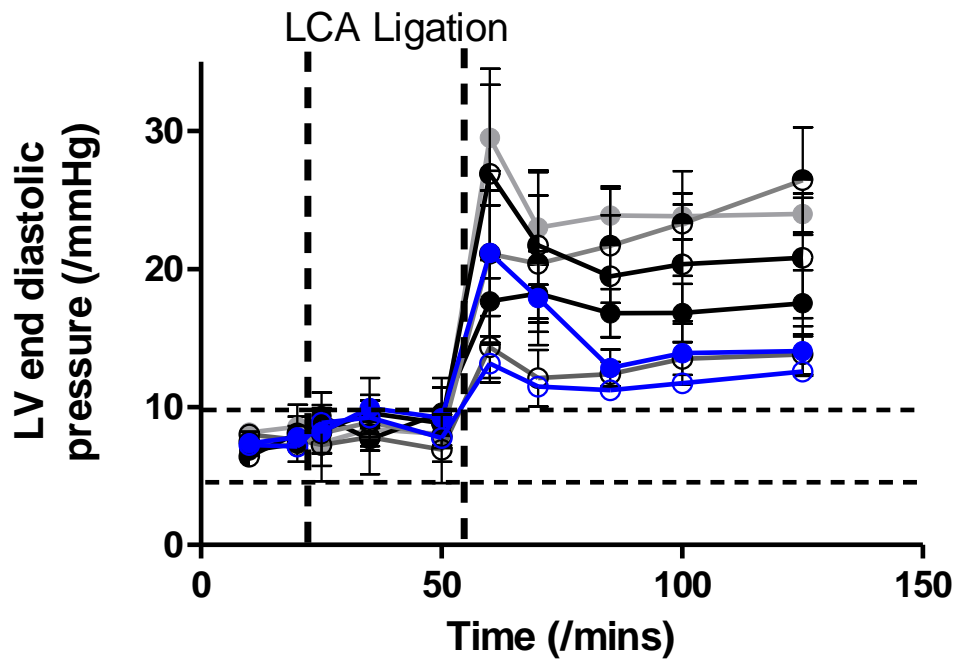
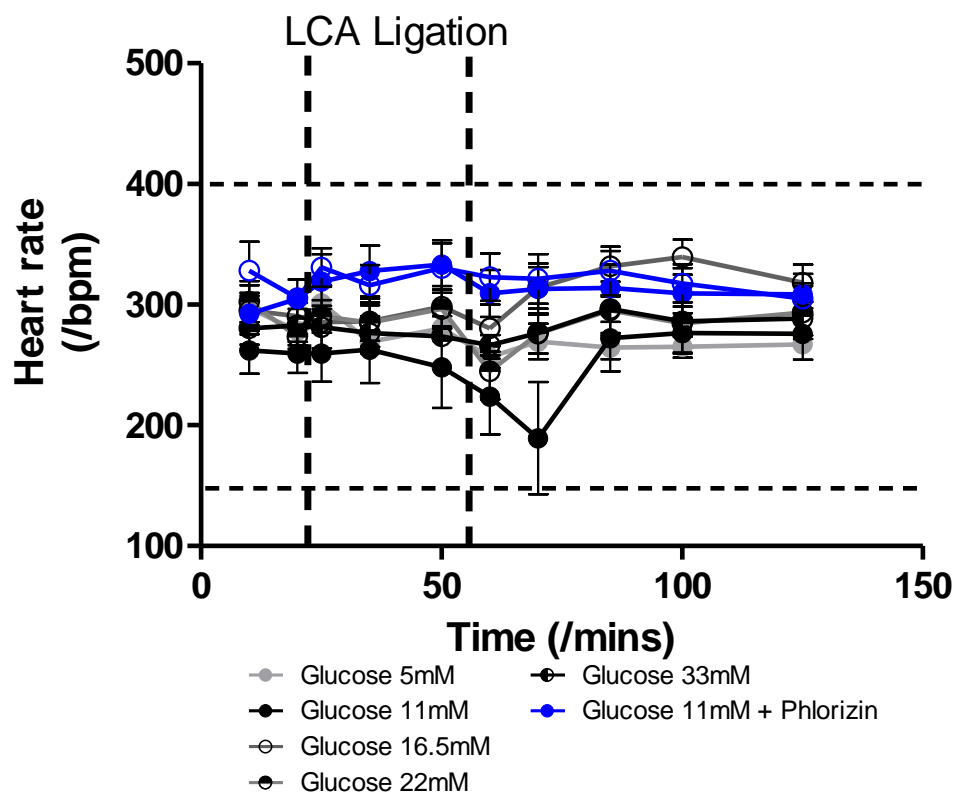
5.2.2.1 Cardiac physiology *ex vivo*

Physiological parameters of the successful Langendorff perfusions were monitored regularly and are shown in Figure 5.1 (SDRs) and 5.2 (GKRs).

Within each strain, there were no statistically significant differences between groups in temperature, coronary flow, LVEDP, heart rate, LVDevP, or LVRPP at baseline or at the onset of ischaemia. Temperature remained within target range throughout all experiments included in the analysis. The expected 30% or more drop in coronary flow and LV developed pressure was seen in all hearts with no heterogeneity for the scale of drop (P=NS for all comparisons).

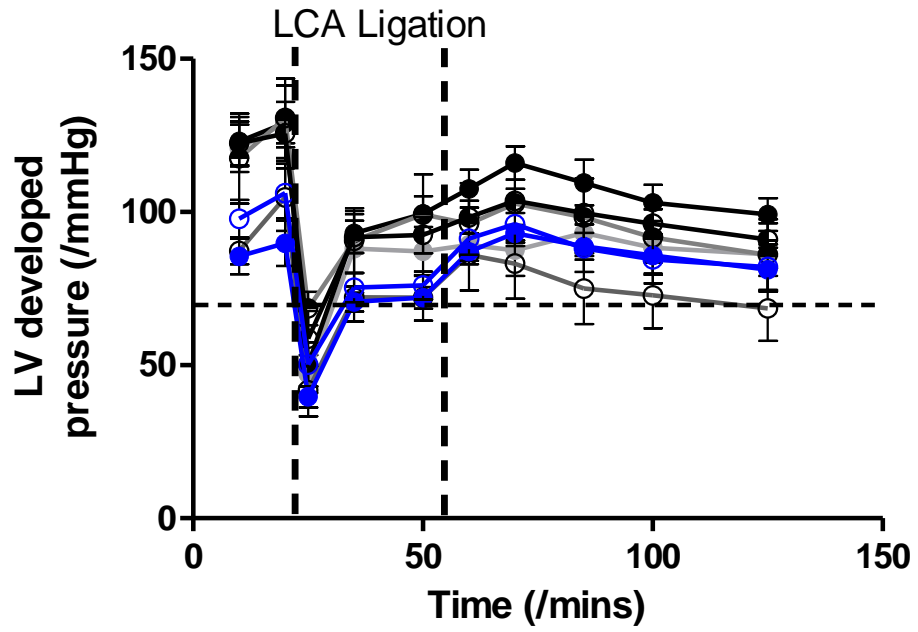
A**Temperature control****B****Coronary flow**

- Glucose 5mM
- Glucose 11mM
- Glucose 16.5mM
- Glucose 22mM
- Glucose 33mM
- Glucose 11mM + Phlorizin

C**Left ventricular end diastolic pressure****D****Heart rate**

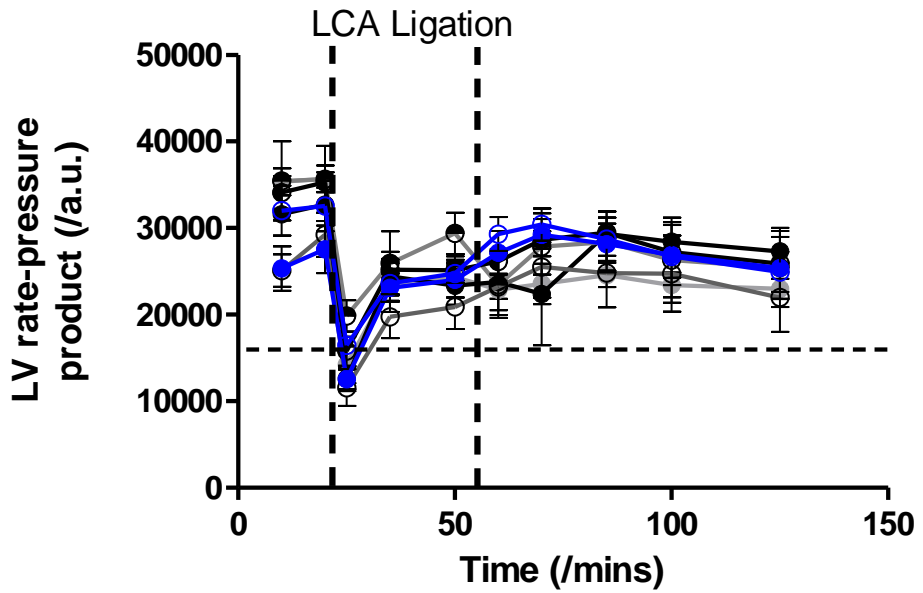
E

Left ventricular developed pressure



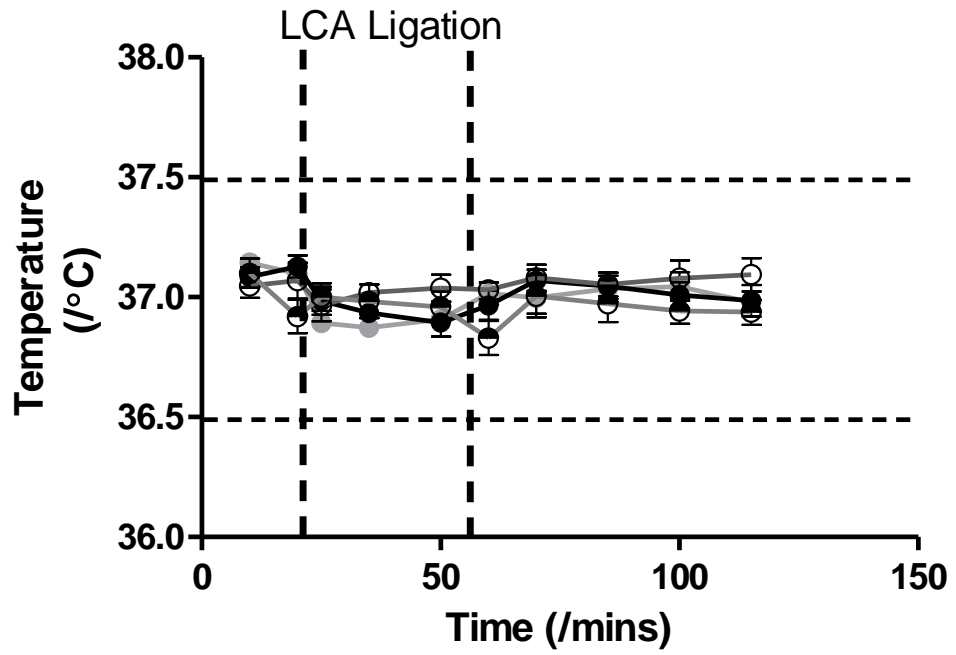
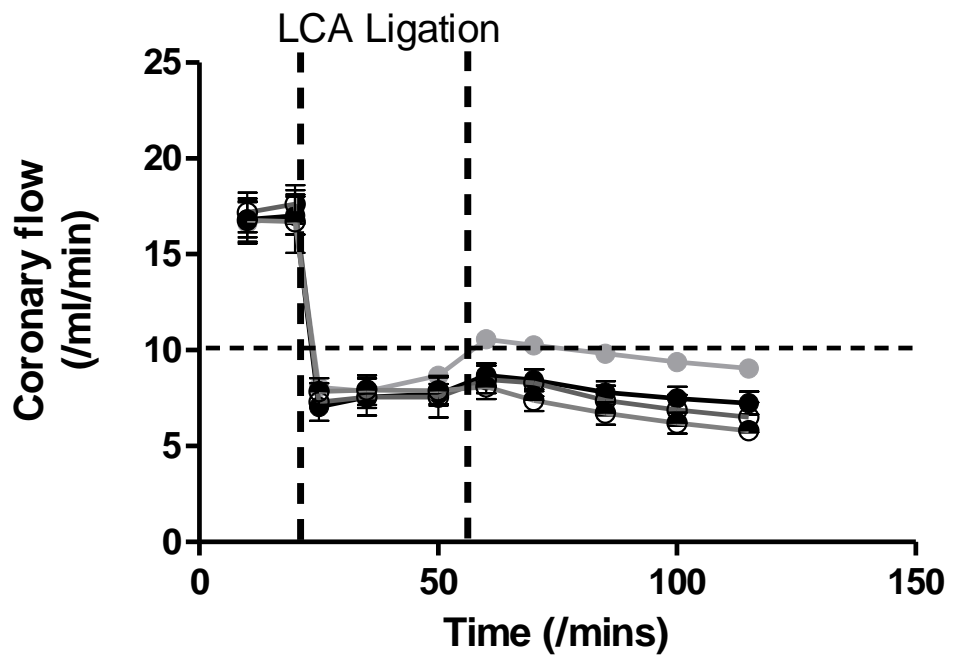
F

Left ventricular rate-pressure product

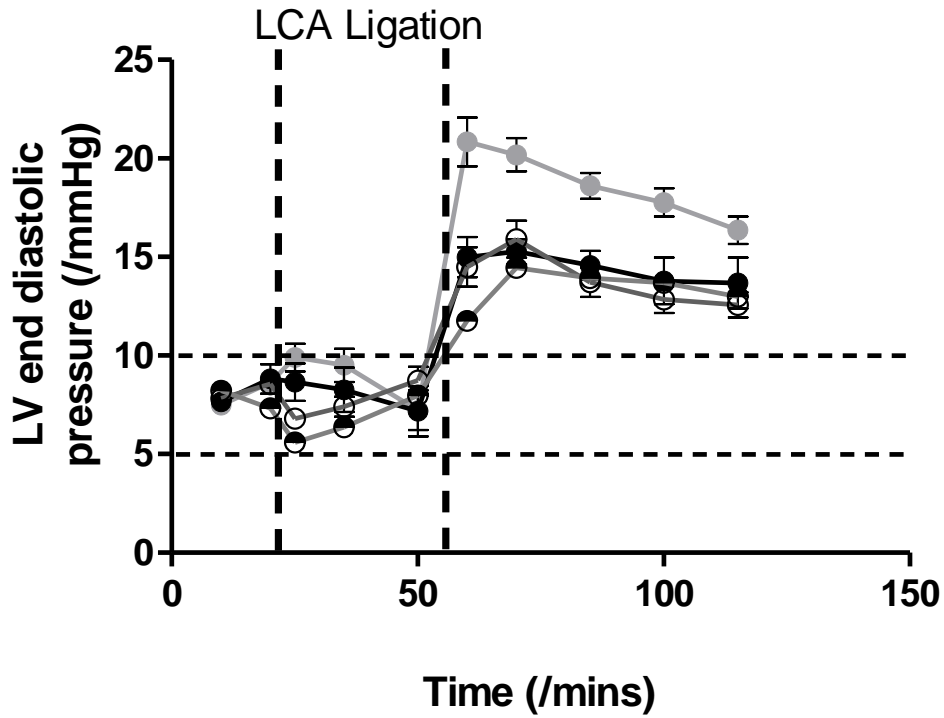
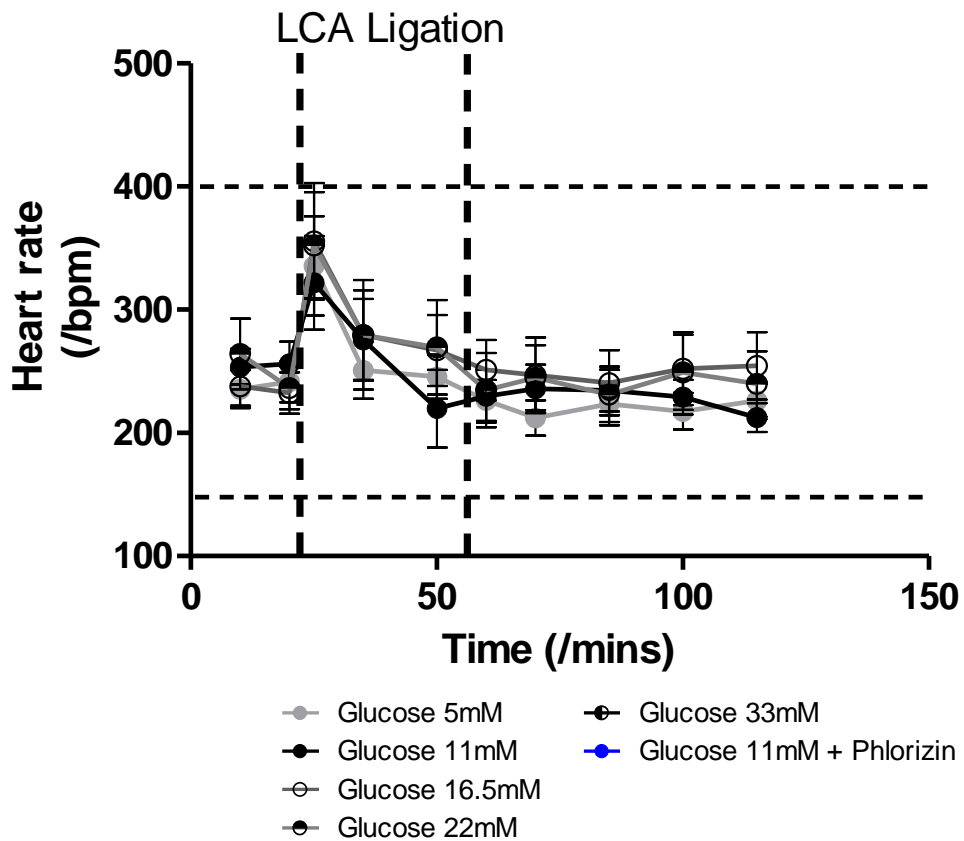


- Glucose 5mM
- Glucose 11mM
- Glucose 16.5mM
- Glucose 22mM
- Glucose 33mM
- Glucose 11mM + Phlorizin

Figure 5.1 (see pages 201-203): Physiological parameters during *ex vivo* ischaemia and reperfusion with varying concentrations of glucose at reperfusion in 3 month Sprague Dawley rat hearts. Temperature control was maintained within the target range throughout (**A**). All dependent and independent variables passed *a priori* criteria of a successful Langendorff perfusion at 10mins. Coronary flow (**B**) and LV developed pressure (**E**) fell in line with expectations when the left anterior descending artery was occluded by a snare. No significant differences developed in the dependent variables LV end diastolic pressure (**C**), heart rate (**D**), LV developed pressure (**E**), or LV rate-pressure product (**F**) between different experimental groups. Experimental groups as per the key. mM = mMol/L. All perfusions either with Phlorizin at a concentration of 3 μ Mol/L in DMSO, or equivalent DMSO vehicle. Error bars show S.E.M.; n=5 per group.

A**Temperature control****B****Coronary flow**

- Glucose 5mM
- Glucose 11mM
- Glucose 16.5mM
- Glucose 22mM
- Glucose 33mM
- Glucose 11mM + Phlorizin

C**Left ventricular end diastolic pressure****D****Heart rate**

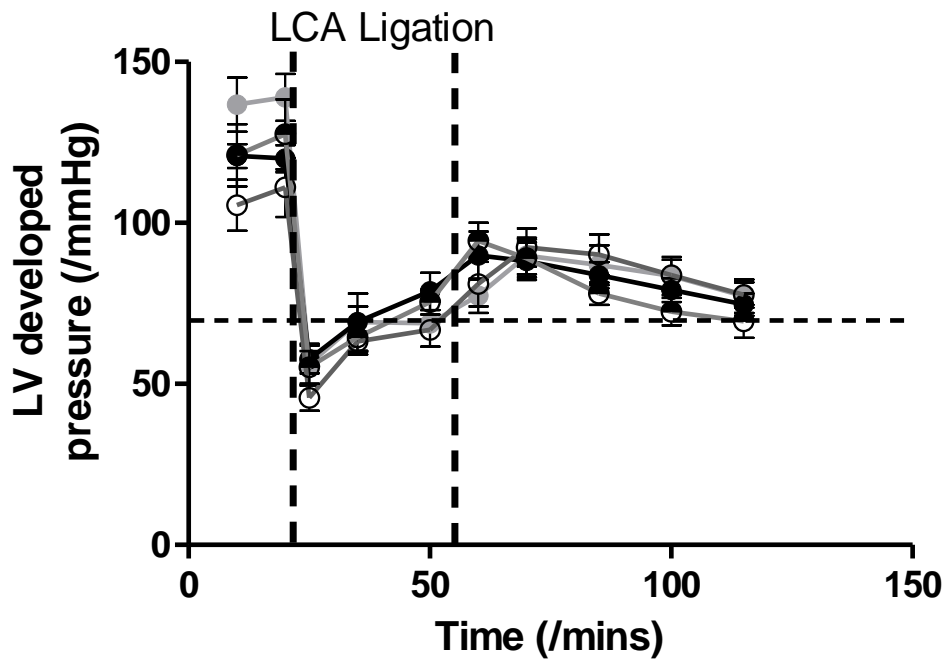
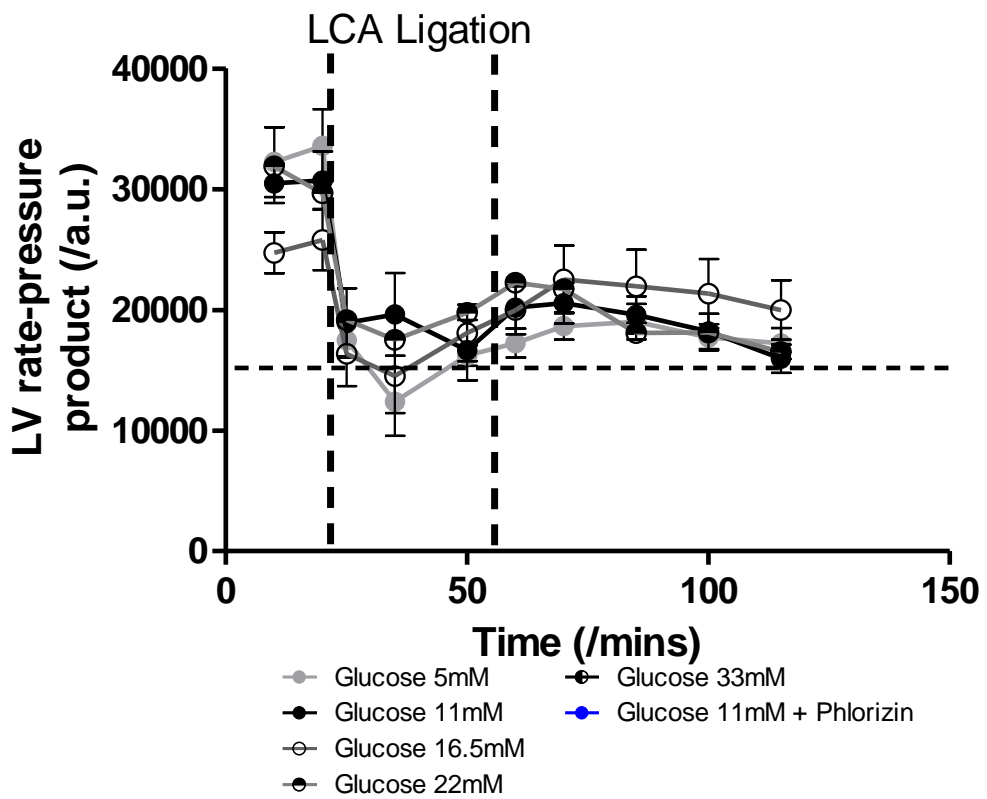
E**Left ventricular developed pressure****F****Left ventricular rate-pressure product**

Figure 5.2 (see pages 205-207): Physiological parameters during *ex vivo* ischaemia and reperfusion with varying concentrations of glucose at reperfusion in 8 month Goto Kakizaki rat hearts. Temperature control was maintained within the target range throughout (**A**). All dependent and independent variables passed a *a priori* criteria of a successful Langendorff perfusion at 10mins. Coronary flow (**B**) and LV developed pressure (**E**) fell in line with expectations when the left anterior descending artery was occluded by a snare. No significant differences developed in the dependent variables LV end diastolic pressure (**C**), heart rate (**D**), LV developed pressure (**E**), or LV rate-pressure product (**F**) between different experimental groups. Experimental groups as per the key. mM = mMol/L. Error bars show S.E.M; n=8 per group.

5.2.2.2 Reperfusion injury with variable glucose

Due to the linear relationship between area at risk and infarct size, hearts are only included in infarct size analysis if the cross-sectional area at risk is between 45% and 65% of LV cross-sectional area. Of the 40 SDR hearts to complete successful Langendorff perfusions, four were discounted from infarct size analysis due to areas at risk falling above the acceptable range. The remaining 36 SDR hearts and all 32 GKR hearts were included in subsequent analysis. No significant differences were seen in AAR between treatment groups ($P=NS$ for all comparisons). Infarct size expressed as a proportion of AAR is shown in Figure 5.3:

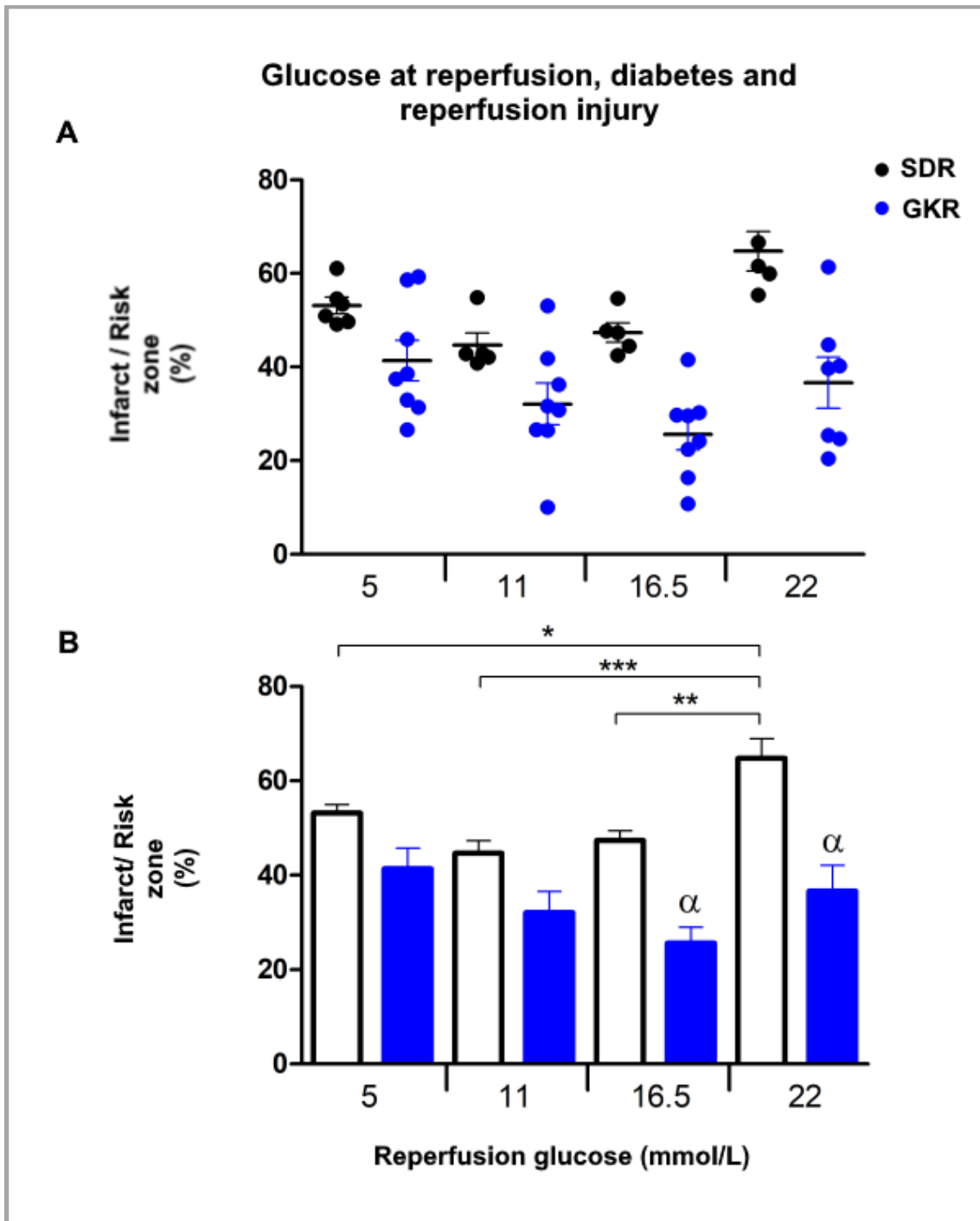


Figure 5.3: Influence of diabetic phenotype and glucose availability at reperfusion on myocardial injury. Both panels show the same data, represented as a scatter graph (**A**) to illustrate data spread and as a summary bar chart (**B**) to show trends in the data clearly and illustrate statistically significant results. Infarcts in the 8 month GKR tend to be smaller at each Glucose concentration than the corresponding 3 month SDR infarcts. The nadir infarct sizes occur at 11mmol Glucose in SDRs and at 16.5mmol Glucose in GKR. Statistically significant differences exist between the SDR groups but not between the GKR groups. There is a J-shaped relationship between reperfusion glucose and infarct size in both strains, shifted to the right in GKR. *, **, ***: p<0.05, p<0.01, p<0.001; α = p<0.01 vs glucose-matched SDR group. Error bars show S.E.M.; n=5 for SDRs; n=8 for GKR.

There are clear differences in the distribution of infarct sizes in the SDRs versus the GKR. The smallest SDR infarcts are seen in the group exposed to 11mmol Glucose ($44.7\pm 2.6\%$), whereas the smallest infarcts in the GKR are seen in the 16.5mmol Glucose group ($25.6\pm 3.4\%$). Infarcts in the GKR tend to be smaller at each Glucose concentration, and this reaches statistical significance in the 16.5mmol ($25.6\pm 3.4\%$ vs $47.4\pm 2.1\%$; $P<0.01$) and 22mmol ($36.7\pm 5.4\%$ vs $64.8\pm 4.2\%$) groups.

The largest infarcts are seen in the SDR 22mmol Glucose group ($64.8\pm 4.2\%$), and these are statistically significantly larger than the infarcts at 16.5mmol ($47.4\pm 2.1\%$; $P<0.01$), 11mmol ($44.7\pm 2.6\%$; $P<0.01$) and 5mmol ($53.2\pm 1.8\%$; $P<0.05$).

There is clearly a J-shaped relationship between reperfusion glucose and infarct size in both strains, but the excess infarction seen in SDRs at 5mmol does not quite reach statistical significance against the nadir infarct seen at 11mmol ($53.2\pm 1.8\%$ vs $44.7\pm 2.6\%$; $P=NS$). The J-shaped relationship is also present in the GKR, shifted to the right, with the nadir infarcts seen in the 16.5mmol Glucose group, but notwithstanding the larger sampling numbers in the GKR experiment, the wider spread of infarct sizes seen in each GKR group means that none of the comparisons within the GKR strain reach statistical significance ($P=NS$ for all comparisons).

5.2.2.3 Impact of reducing of myocardial glucose uptake

To test whether partial blockade of glucose uptake can reduce excess glucose-induced myocardial injury at reperfusion, the non-selective SGLT blocker Phlorizin was added at reperfusion to the SDR groups with the smallest and largest infarct sizes, i.e. 11mmol/L glucose and 22mmol/L glucose, respectively.

The physiological perfusion parameters for these groups are included in Figure 5.1. All perfusions met *a priori* defined characteristics, and successful LCA occlusion was demonstrated in all by a 30% drop in both coronary flow and LV developed pressure. On processing with TTC, all hearts demonstrated areas at risk 45-65% of total cross-sectional area thus none were excluded from infarct size analysis, which is presented in Figure 5.4:

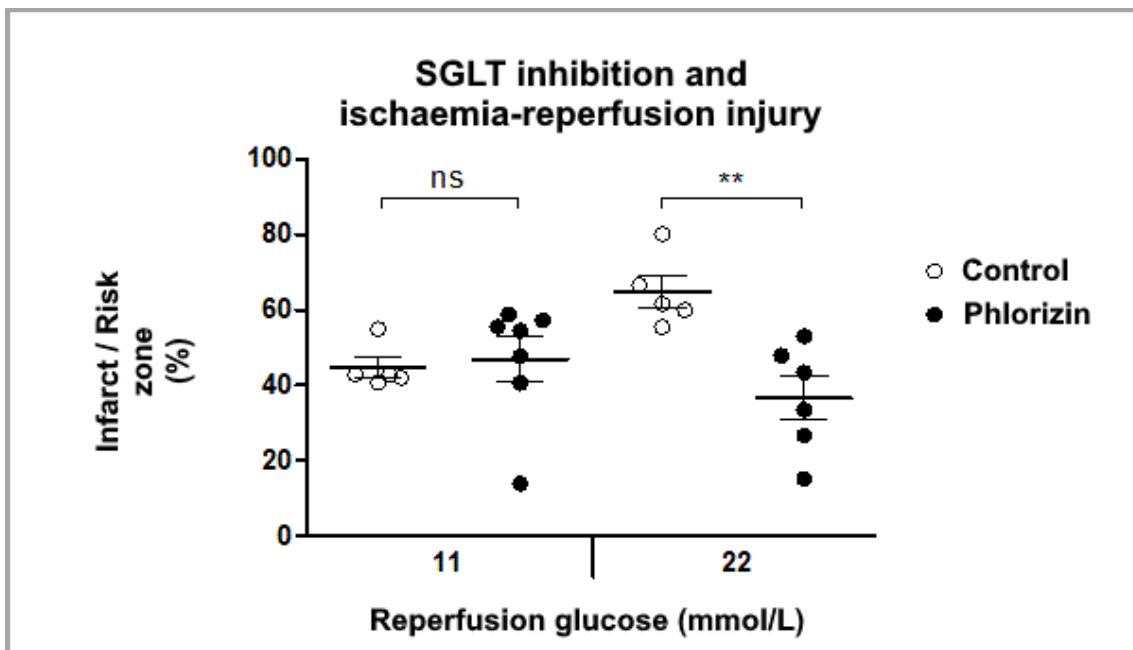


Figure 5.4: Impact of the SGLT inhibitor Phlorizin on glucose-mediated augmentation of reperfusion injury. Phlorizin was added at reperfusion only to the SDR groups with the smallest and largest infarct sizes. At 11mmol Glucose, Phlorizin had no impact on infarct size but at 22mmol Glucose, Phlorizin had the effect of reducing infarct size to roughly the level seen in the 11mmol Glucose group, i.e. abrogating the excess infarction inflicted by high glucose exposure. ns = not significant; ** = $P < 0.01$. Error bars show S.E.M.; $n = 5-7$ per group.

At baseline 11mmol Glucose, Phlorizin had no statistically significant impact on infarct size ($44.7 \pm 2.6\%$ vs $46.9 \pm 5.8\%$; $P = \text{NS}$) but during exposure to high glucose (22mmol) at reperfusion, Phlorizin was associated with a reduction in infarct size ($64.7 \pm 4.2\%$ vs $36.6 \pm 5.8\%$; $P < 0.01$). The Phlorizin-treated 22mmol group was indistinguishable from infarct sizes in the treated and untreated 11mmol groups (36.6 ± 5.8 vs $44.7 \pm 2.6\%$ and $46.9 \pm 5.8\%$; $P = \text{NS}$ for both comparisons).

5.2.2.4 Reactive oxygen species in isolated cardiomyocytes

Hypothesising that glucotoxicity at reperfusion is mediated by excess production of reactive oxygen species, we developed a model of oxidative stress in isolated cardiomyocytes to measure ROS production in myocytes subjected to different glucose concentrations. We first had to optimise our model for ROS-induced-ROS production and detection, as follows:

5.2.2.4.1 Optimisation 1: dye validation

To confirm that the CM-H2DCFDA was appropriately loaded and sensitive to ROS at the quantities present in our cardiomyocytes, we imaged cells after stabilisation at baseline in standard Tyrode's (11mM glucose) and immediately after addition of 100mM H₂O₂. The results are in Figure 5.5 (n=5) and show that the dye, loading conditions and confocal microscope are functioning appropriately to detect the presence of significant concentrations of ROS in the presence of the oxidising agent H₂O₂.

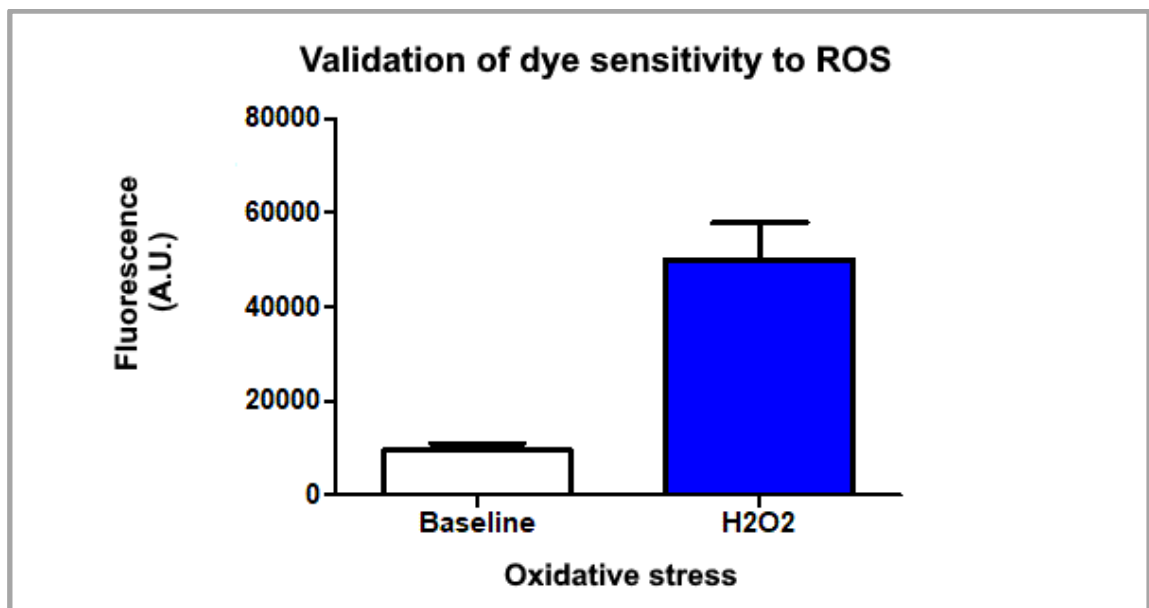


Figure 5.5: CM-H2DCFDA ROS-sensitive fluorescent dye is appropriately activated and detected in our system by exposure to 100mM H₂O₂ with a gross increase in detected ROS after addition of H₂O₂ to the experimental system, indicating successful induction and detection of ROS-induced-ROS in this experimental system. Error bars show S.E.M.; n=5 per group.

5.2.2.4.2 Optimisation 2: timecourse

To elucidate how long we should expose cardiomyocytes to variable levels of glucose for, before imaging for ROS, we undertook a timecourse experiment. Cells were imaged after stabilisation at baseline in standard Tyrode's (11mM glucose) and immediately after substitution with Tyrode's containing glucose 22mM. Imaging was repeated at 30mins, 60mins and 90mins, and then after addition of 100mM H₂O₂ as a positive control. The results are given in Figure 2.23 and show a raised level of ROS developing by 30mins after introduction to high glucose, remaining unchanged thereafter. Addition of H₂O₂ consistently produced a flood of ROS.

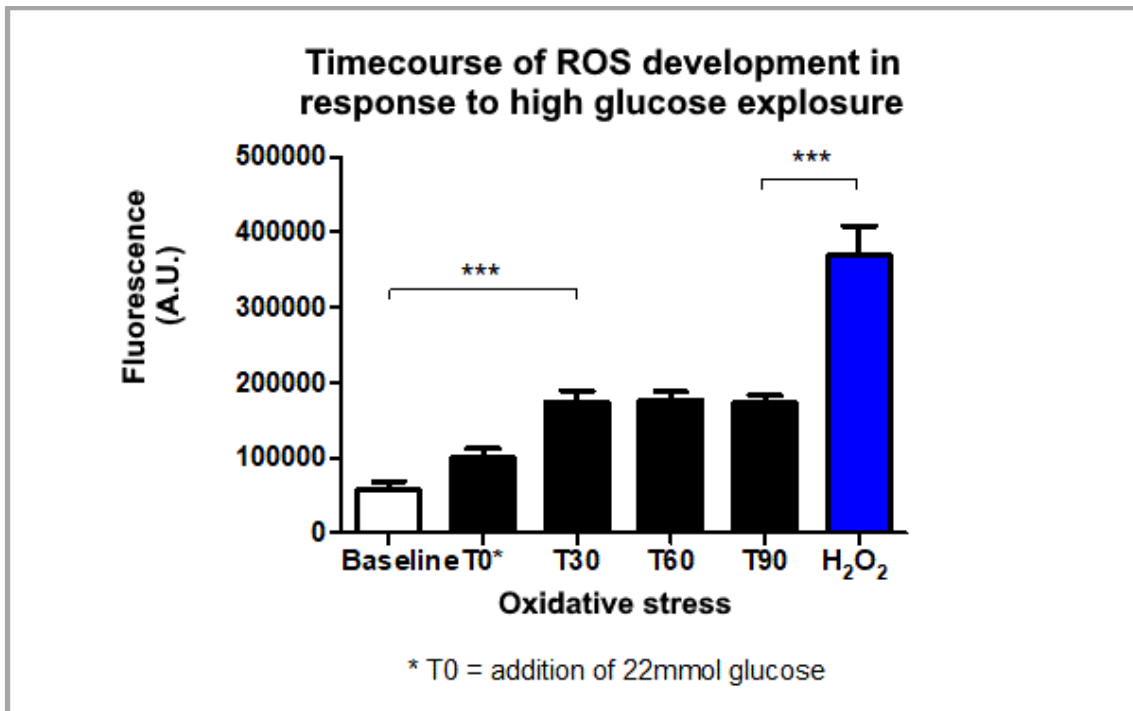


Figure 5.6: Detection of ROS in isolated cardiomyocytes after introduction of high glucose medium. Baseline imaging is in standard Tyrode's buffer (11mM glucose) and shows low ROS detection. At T0, high 22mmol glucose medium is substituted and by 30mins later (T30) ROS production is significantly higher than at baseline. ROS concentration is then stable for up to 90mins exposure with 22mmol glucose (T90). At 90mins, H₂O₂ is added to the system resulting in sudden large-scale augmentation of ROS production, acting as a positive control. Error bars show S.E.M.; n=5 per group.

5.2.2.4.3 Optimisation 3: dose of H₂O₂

Thus far we had used high dose H₂O₂ to produce near-maximal outpouring of ROS in isolated cardiomyocytes acting as a positive control for our ROS detection system. We now sought to optimise use of a lower dose of H₂O₂ to produce measurable ROS production, but allow differentiation between cells at high and low background oxidative stress (i.e. in high and low glucose conditions). We chose two concentrations of H₂O₂ to test at 1mM and 10mM. The results are shown in Figure 5.7. 10mM, as anticipated, triggered higher ROS production in the cardiomyocytes, but surprisingly the production from 1mM H₂O₂ was so low that it could not be readily distinguished from background ROS production.

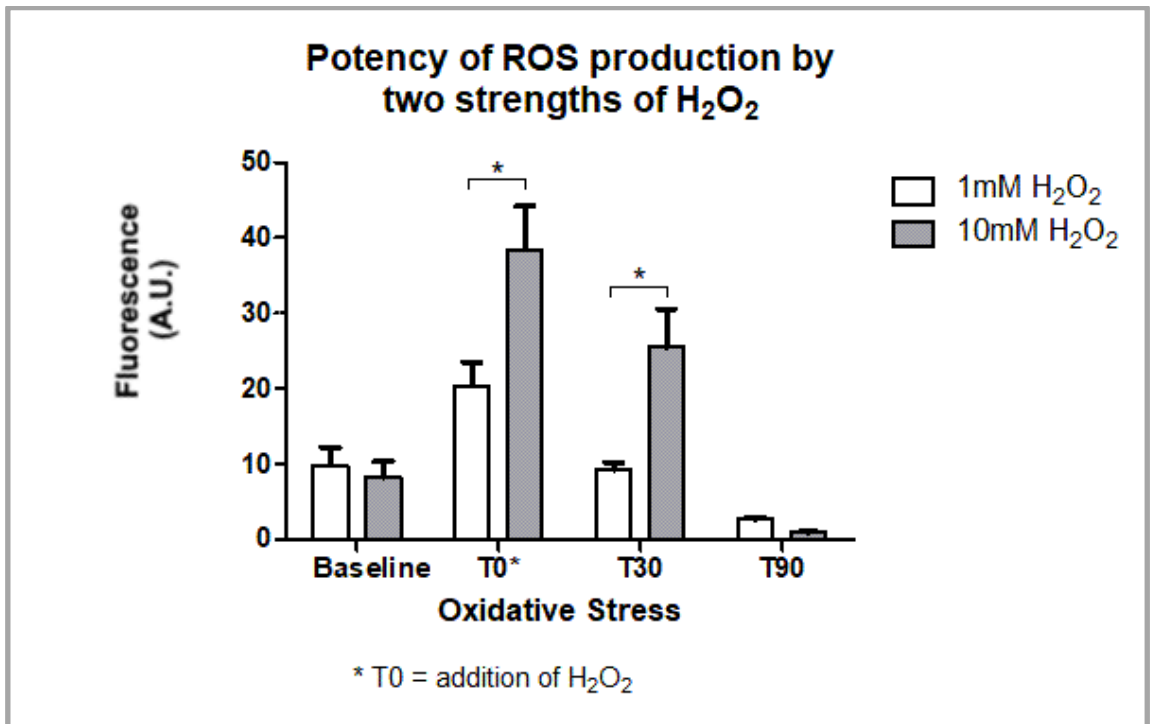


Figure 5.7: ROS-induced-ROS detection following oxidative stress with two strengths of H₂O₂. 10mM H₂O₂ resulted in significantly higher ROS production than 1mM strength. The ROS seen with 1mM strength quickly decayed to baselines levels of ROS, whereas the ROS induced by 10mM remained elevated 30mins after administration of H₂O₂ (T30). Error bars show S.E.M.; n=7 per group.

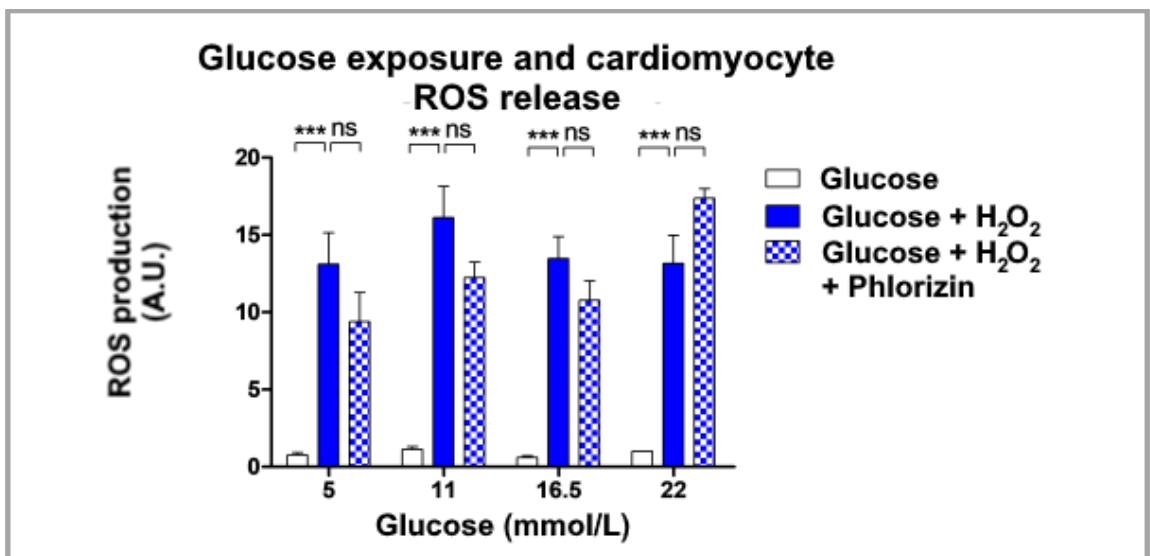


Figure 5.8: Impact of glucose availability on ROS release in isolated cardiomyocytes at rest and under oxidative stress with 10mM H₂O₂ (hydrogen peroxide – i.e. ROS-induced-ROS release). For each glucose concentration, addition of H₂O₂ triggered large scale ROS release, which was not significantly modified by the addition of Phlorizin. No differences were seen in ROS production under different glucose concentrations. Results are normalised across different experimental runs by defining the ROS detected in 22mmol/L glucose as 1 unit. *** = P<0.001; ns = non-significant. Error bars show S.E.M.; n=7 per group.

5.2.2.4.4 ROS production in response to different glucose media

Having optimised this model of ROS-induced-ROS release we applied different concentrations of glucose in Tyrodes solution onto cardiomyocytes and quantified ROS production at baseline, with H₂O₂-induced ROS and with H₂O₂ plus Phlorizin. Results are presented in Figure 5.8 normalised across different experimental runs, with the level of ROS detected in baseline Tyrodes 22mmol/L glucose solution prior to addition of H₂O₂ +/- Phlorizin defined as 1 unit. This method of normalising did not affect statistical outcomes compared to statistical tests carried out on raw data. There were no significant differences between ROS production after 30mins exposure to different concentrations of glucose (5mM 0.76±0.2a.u. vs 11mM 1.1±0.2a.u. vs 16.5mM 0.6±0.1a.u.; P=NS for all comparisons). Likewise, under oxidative stress with 10mM H₂O₂, no differences were seen between groups exposed to different glucose concentrations (5mM 13.1±2.0a.u vs 11mM 16.1±2.0a.u. vs 16.5mM 13.5±1.4a.u. vs 22mM 13.2±1.8a.u.; P=NS for all comparisons). With the SGLT blocker Phlorizin, ROS production was significantly higher with 22mMol glucose than other groups, and this reached statistical significance comparing the 22mM group to the 5mM group (22mM 17.4±0.6a.u. vs 5mM 9.4±1.9a.u., P<0.001; P=NS for all other comparisons).

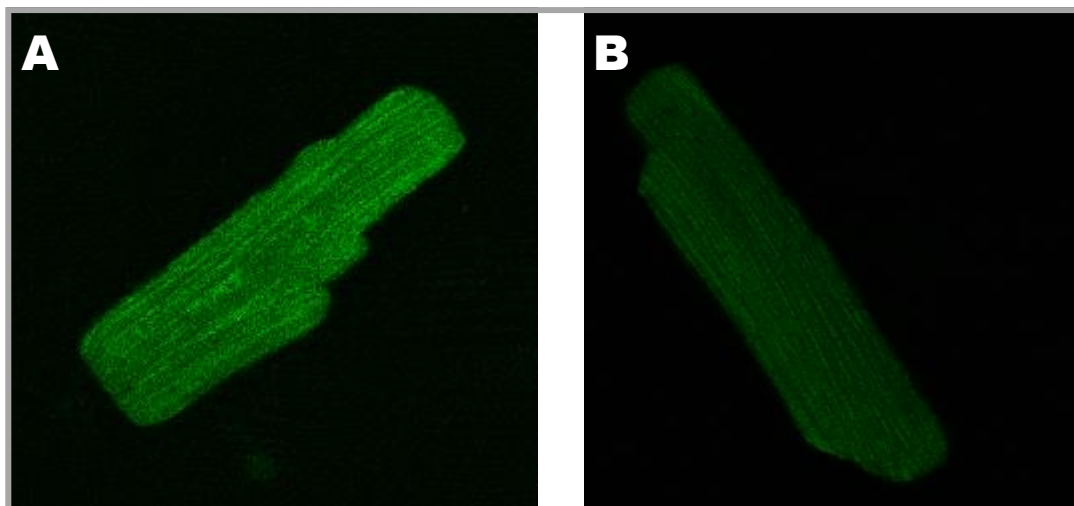


Figure 5.9: Representative examples of ROS imaging with CM-H₂DCFDA ROS-sensitive dye imaged at $\lambda=527\text{nm}$ with excitation at $\lambda=495\text{nm}$. **A:** A cardiomyocyte imaged after 30mins loading with CM-H₂DCFDA, 30mins equilibration to standard Tyrodes buffer and then 30mins in Tyrodes with 22mM glucose, 10mM H₂O₂ and 3 μM Phlorizin. **B:** A cardiomyocyte imaged after 30mins loading with CM-H₂DCFDA, 30mins equilibration to standard Tyrodes buffer and then 30mins in Tyrodes with 5mM glucose, 10mM H₂O₂ and 3 μM Phlorizin. The cardiomyocyte

exposed to 22mM glucose (A) shows more intense fluorescence of the CM-H2DCFDA ROS-sensitive dye than the cardiomyocyte exposed to 5mM glucose (B), indicating presence of more ROS. As shown in Figure 5.8, this difference did not reach statistical significance across n=7.

Overall, ANOVA suggests that glucose concentration contributed only 2.7% of the variance seen in these results, but that this small effect is statistically significant ($P<0.05$). There is interaction between glucose concentration and treatment (glucose vs glucose + H₂O₂ vs glucose + H₂O₂ + Phlorizin) and this accounts for 5.1% of the variance seen ($P<0.05$). Presence of H₂O₂ and/or Phlorizin accounts for 74% of the variance seen and this is highly significant ($P<0.0001$).

5.2.2.5 Simulated ischaemia-reperfusion in cardiomyocytes

To investigate why variable glucose concentrations had failed to modulate ROS production in isolated cardiomyocytes, we recapitulated the earlier infarct size experiment (Figures 5.3 & 5.4) in an isolated cardiomyocyte model. Three experimental runs were excluded from analysis due to cell death exceeding 25% in the normoxic control groups. The remaining results of a cell-based simulated ischaemia-reperfusion model of myocardial infarction are shown in Figure 5.10:

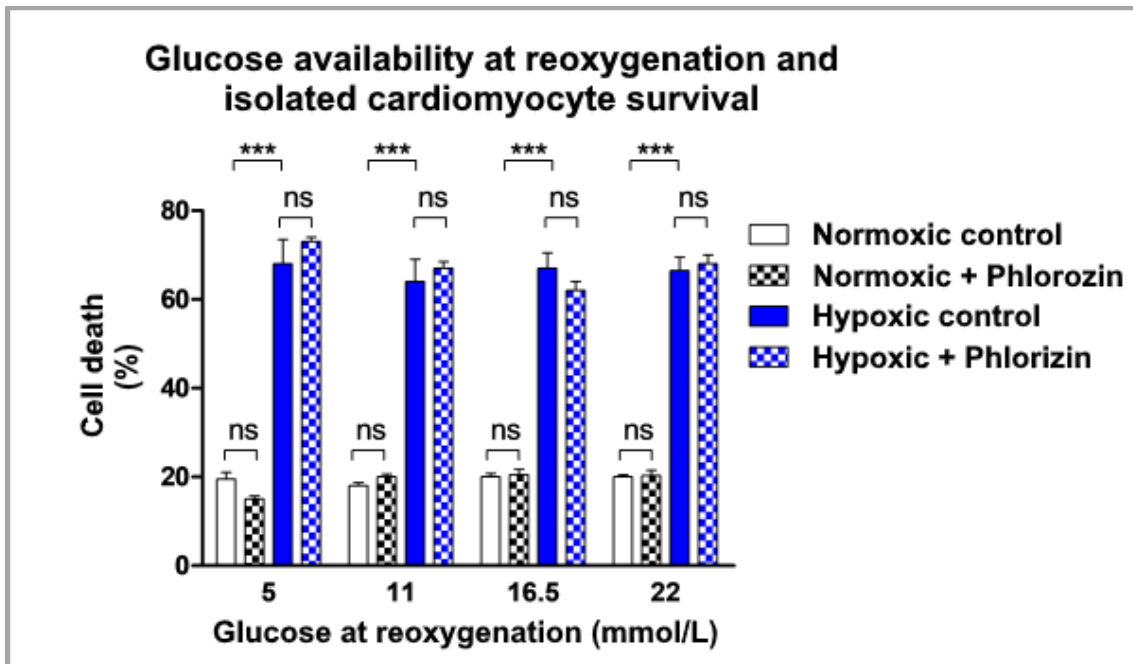


Figure 5.10: Exposure to glucose during reoxygenation phase of simulated ischaemia-reperfusion in isolated cardiomyocytes. At each different glucose concentration, continuous normoxic culture results in less cardiomyocyte death than simulated ischaemia-reperfusion. Exposure to different levels of glucose at reperfusion does not modify cell death and cell death is not affected by addition of Phlorizin to the reperfusion medium. *** = $P < 0.01$; ns = not significant. Error bars show S.E.M.; $n = 7$ per group.

At each different concentration of glucose, the hypox-reox protocol appears effective, achieving 60-70% cell death consistently versus background cell death of around 20% in normoxic negative controls ($P < 0.01$ for all comparisons). In contrast to the results of the whole heart Langendorff model, there is no significant difference in cell death across groups exposed to different concentrations of glucose at reoxygenation (Bonferroni post-tests; $P = NS$ for all comparisons). Phlorizin did not modulate cell death in normoxic controls ($P = NS$ for all comparisons) or in cells undergoing hypoxia ($P = NS$ for all comparisons). Overall, Glucose concentration did not contribute to the variance in results ($P = NS$).

5.3 Summary of reperfusion glucotoxicity studies

Cardiac physiology during *ex vivo* infarction and reperfusion of diabetic and non-diabetic hearts during these studies was not significantly different to that seen in our earlier studies using standard 11mmol/L glucose perfusion. Infarct sizes, however, were modulated by exposure to different concentrations of

glucose during reperfusion. Non-diabetic hearts were more sensitive to changes in glucose than diabetic hearts, with statistically significant differences seen between non-diabetic heart groups, but only trends towards differences seen between diabetic heart groups. Infarcts in diabetic hearts tended to be smaller at each glucose concentration, reaching statistical significance at the higher two glucose concentrations (16.5mmol/L and 22mmol/L). The relationship between reperfusion glucose and infarct size appeared shifted to the right in the diabetic hearts, with nadir infarct sizes were seen in at 11mmol/L in the non-diabetic hearts and 16.5mmol/L in the diabetic hearts.

Excess infarction in the 22mmol/L glucose non-diabetic hearts was rescued by addition of low dose Phlorizin at reperfusion, which returned infarcts to the baseline size seen after perfusion with 11mmol/L glucose with or without Phlorizin.

We then examined ROS production under conditions of glucose and H₂O₂ stress in isolated cardiomyocytes using confocal microscopy and a ROS-sensitive fluorophore. This approach failed to detect differences in ROS production either after stable incubation with glucose, or after spiking with H₂O₂ to induce oxidative stress.

Attempts to reproduce the pattern of glucotoxicity seen in the whole heart also failed in an isolated cardiomyocyte model. Simulated ischaemia-reperfusion protocols reached appropriate quality controls, with low levels of cardiomyocyte death in groups not subjected to sIRI, and high levels of death in cells subjected to control sIRI. However, varying the simulated reperfusion conditions with variable concentrations of glucose with and without Phlorizin did not modulate cell death to a significant degree.

These results are assessed critically in Chapter 6, "Discussions".

6. DISCUSSIONS

6.1 Structure of discussions

This overarching objective of this project was to investigate the extent to which the poor prognosis experienced by diabetic and hyperglycaemic MI patients might be mediated by exacerbation of myocardial reperfusion injury. To that end, we set out to address six individual aims; these are stated at the end of Chapter 1, and re-stated below:

1. To establish and verify rat models of *ex vivo* myocardial infarction, *ex vivo* direct ischaemic preconditioning and *in vivo* remote ischaemic preconditioning.
2. To verify the relevance of a rat model of diabetes in which to investigate further the interplay between diabetic state, hyperglycaemia and infarct size.
3. To demonstrate that our rat model of diabetes exhibits impaired cardioprotection via direct and remote conditioning.
4. To investigate the alterations in RISK signalling that accompany the expected failure of cardioprotection in our rat model of diabetes.
5. To investigate to what extent hyperglycaemia exacerbates reperfusion, as opposed to ischaemic, injury, and how this differs between diabetic versus non-diabetic rat hearts.
6. To investigate the mechanism by which hyperglycaemia exacerbates reperfusion injury in the non-diabetic heart.

Performance against each of these aims is discussed in detail below, with overall conclusions, implications for management of clinical MI, and directions for future research work discussed at the end of this chapter.

6.2 AIM 1: establish and verify models of infarction and direct and remote preconditioning

Success at achieving consistent model performance can be judged by the acuity of control of physiological parameters during *in vivo* remote ischaemic preconditioning and *ex vivo* direct preconditioning and experimental infarction.

6.2.1 *Ex vivo* infarction

Where relevant, *a priori* definitions of a successful Langendorff perfusion were met consistently. Overall the aim here was achieved. Physiological parameters were closely controlled, and coronary occlusion consistently applied during *ex vivo* experimental infarction leading to consistent decreases in coronary flow and LV developed pressure. Consistency of ischaemic burden is also verified by the consistent infarct sizes in control groups.

We have shown that consistency of infarct size analysis by semi-automated planimetry improves with exposure to the technique, and we achieved mean intra-operator variability on repeat analysis of the same hearts of 1.75%..

6.2.2 *In vivo* remote ischaemic preconditioning

The novel method of surgical single hindlimb remote ischaemic preconditioning proved both feasible and effective, producing a mean 57.5% reduction in infarct size in healthy rat hearts, which is a large effect compared to those elicited by other models of RIPC, summarised in Bromage's meta-analysis of animal studies¹³⁶.

The most potent RIPC stimulus previously seen in rat was bilateral hindlimb ischaemia caused by infrarenal aortic ligation, which achieved mean infarct size reduction of 42%⁴²¹. Following infrarenal aortic ligation, subsequent index ischaemia was carried out by *in vivo* coronary ligation, allowing coronary ischaemia to follow hindlimb ischaemia more quickly than in our protocol (5mins vs 17mins). This difference may explain the increased potency of our conditioning protocol, as time between remote reperfusion and onset of index ischaemia modulates the efficacy of RIPC profoundly⁴²¹. Wever's meta-analysis of direct IPC in animals previously showed that time between IPC and index ischaemia is one of the few consistent methodological parameters to have a consistent effect on IPC efficacy¹⁰⁵. It is probable that by allowing time for *in vivo* remote reperfusion, followed by heart explantation and transfer to the Langendorff rig and then 10mins stabilisation, we unwittingly increased the efficacy of our RIPC stimulus.

Success and critique of other models are discussed with the relevant experimental results, below, but in terms of general physiological parameters,

area at risk, control infarct sizes, spread of infarct size and extent of infarct size reduction with direct ischaemic preconditioning were comparable to other studies from our group using similar methodologies^{147,244,422,423}. Spread of infarct sizes was consistently wider in diabetic rat hearts than the control hearts, despite similarly tight physiological control during the experiments and reasons for this are discussed in relation to the individual experimental results.

6.2.3 Limitations

Limitations of this work mainly relate to translation of the results to human MI and preconditioning interventions in humans. We know from earlier studies that *ex vivo* studies of ischaemia reperfusion, and of ischaemic preconditioning in particular have not consistently been reproduced in man⁴²⁴. This phenomenon is discussed in the background chapter and the various theories advanced have been explored there, also. To recap briefly: *Ex vivo* infarction and reperfusion in murine hearts is distanced from clinical MI by species differences and by removal of neurohumoral of inputs to the heart. These are inherent and intractable limitations in the model being used. There is also the issue of cardiac work not being well modelled by the Langendorff preparation, though this does not matter so much for this series of experiments, where haemodynamic endpoints are not so important. Questions of haemodynamics would be better addressed by a working heart model, and questions of chronic cardiac recovery and remodelling would be best addressed by *in vivo* ischaemia-reperfusion techniques.

Ligation of a major epicardial coronary artery reproduces some but not all aspects of STEMI. Those aspects that are missing include the pre-existence of coronary artery plaque, acute plaque disruption, platelet activation and subsequent thrombogenesis and thrombus stabilisation. Likewise, release of the temporary arterial ligation reproduces some, but not all, aspects of acute recanalisation of a clinical culprit artery (either via PPCI or spontaneously). The aspects of recanalisation modelled poorly here include vessel trauma from PPCI, distal dispersal of thrombus, reperfusion arrhythmias (particularly those secondary to profound neurohormal activation) and stent deployment.

Realistically, modelling these aspects of acute myocardial IRI would require a large animal model on which PPCI could be performed.

6.3 AIM 2: verify the UCL GK rat as a relevant model of diabetes in which to study myocardial IRI

We set out to establish whether the UCL-GKR is a suitable model in which to study cardiac ischaemia-reperfusion injury in human diabetic subjects. Cardiac ischaemia is a feature of human diabetes typically after a number of years of imperfect gluco-regulation⁴²⁵, and is a late complication of the diabetic condition. Most human patients with diabetes suffering myocardial injury will have type 2 (insulin resistant) diabetes. Therefore the UCL-GKR should ideally parallel the diabetic phenotype in established human type 2 diabetes.

6.3.1 Comparison to other rats

Diabetes in humans is defined by international consensus guidelines giving precise cut-offs for the transition between normality and disease states in parameters such as fasting blood glucose, response to glucose challenges and insulin sensitivity parameters⁴²⁶. Working in an animal model we do not have the advantage of these *a priori* definitions and must show that our “diabetic” animals exhibit significantly different glucose handling to supposed normal, or wild type, controls.

6.3.1.1 Weight

UCL-GKRs failed to gain weight after age three months in this study and were significantly lighter than age-matched controls in outbred wild type rat strains. This is consistent with their characterisation as a “lean” model of diabetes, and sets them apart from obese models such as the Otsuka Long Evans Tokushima Fatty (OLETF) rat⁴²⁷, the Zucker diabetic fatty (ZDF) rat⁴²⁸ and *db/db* mouse⁴²⁹. Obese animal models of diabetes develop diabetes preceded by peripheral insulin resistance, a period of compensatory hyperinsulinaemia and a late fall in insulin secretion⁴³⁰, i.e. similar to human “type two” diabetes⁴³¹. A lean animal model of diabetes, however, requires more explanation as peripheral insulin resistance due to obesity cannot be inferred.

6.3.1.2 Glucose

We have shown here that UCL-GKRs exhibit hyperglycaemia by age three months, and this persists throughout life compared to two outbred control strains: the wild type Wistar, from which the inbred GKR is derived, and the

Sprague Dawley rat, thought to be distantly derived from a Wistar rat female and a Long-Evans male⁴³². The pattern of hyperglycaemia we see in UCL-GKRs is consistent with the pattern seen in the GKR colony in Paris, in which overt hyperglycaemia is present from 3-4 weeks old, preceded by failure of proliferation and survival of endocrine precursor cells *in utero* and decreased pancreatic beta cell mass compared to Wistar controls^{417,433}.

Adult UCL-GKRs continue throughout adult life to be underweight, with hyperglycaemia compared to outbred controls. Interestingly, glycated haemoglobin only became significantly different from controls at age eight months, whereas fasting hyperglycaemia was evident in venous blood glucose measurements from age three months. This is a novel finding, and potentially runs counter to the general idea that glycated haemoglobin levels reflect mean blood glucose content over the lifespan of the currently circulating haemoglobin and red blood cells. Crucially, however, this separation between immediate measures of blood glucose content and an indirect measure of long-term blood glucose trends reproduces earlier findings from our research group in GKRs obtained from Taconic Ltd²⁴⁴: like us, Whittington found dissociation between HbA1c and fasting glucose but did not explain the mechanism. There are three potential explanations:

Firstly, HbA1c level in three month-old animals may be unrepresentative, due to some unique factor is present in young animals which renders HbA1c non-comparable with the assay at other ages. This error may relate to either high red cell turnover specific to this age group, or selective non-reactivity of the assay with persisting foetal haemoglobins, which are subsequently replaced before the eight-month testing point. Neither of these explanations seems feasible, as rat haemoglobin is known to be exclusively adult-type from day 18 of gestation⁴³⁴, and eight week old WRs' red cell lifespan has been modelled with scintigraphy as 60 days and stable³⁵⁷; regression in red cell behaviour after this age is unlikely.

A third, and more likely explanation is that the assay itself is giving a reliable indication of the level of glycated haemoglobin present, but that overt hyperglycaemia only occurs just prior to age three months, so that the slow process of glycation has not had significant impact by the time the three-month

assay is performed. This illustrates the potential problems with compressing the evolution of a disease that develops over decades in man, into a few months in rat. Some aspects of the disease will inevitably be missing in young animals, and the low HbA1c levels are suggestive of low direct glucotoxicity mechanisms, such as glycation and build-up of advanced glycation end products, in all tissues.

6.3.1.3 Insulin

The UCL-GKR exhibits low levels of circulating insulin in the fasting state compared to WR controls. This is consistent with studies across other GKR colonies³⁴⁵, particularly that the low levels of circulating insulin do not evolve with age⁴¹⁷. This is dissimilar to the finding in our WR controls, in which hyperinsulinaemia developed with advancing age, presumably related to obesity. To elucidate questions of insulin sensitivity and production, we used a non-invasive approach with mathematical modelling based on the Homeostatic Model Assessment developed for use comparing populations of human patients with diabetes. Although the HOMA-IR and HOMA- β statistics were designed for use in human populations they have been validated against gold standard insulin tolerance test measures of insulin metabolism in the Wistar rat⁴³⁵.

The insulin production and response parameters derived from the HOMA model suggest a broad comparability with the GK colony in Paris, where invasive insulin tolerance studies have shown higher endogenous hepatic glucose production, but also increased peripheral insulin action, compared to WR controls⁴¹⁷, so that the overall whole body appears to have increased sensitivity to insulin in the fasting state. However, this data is difficult to interpret due to the presence of high circulating glucose levels, and clarity was only reached in the Paris colony when hyperinsulinaemic-euglycaemic clamp experiments indicated significant insulin resistance and decreased peripheral glucose utilisation. The striking finding here is actually with respect to the WRs, which display a strong trend towards increasing whole body insulin resistance with age, related to increasing fat deposition³⁴⁷. Our results reproduce this.

In summary: our outline study of GKR development is generally reflective of experience with other colonies, including with the best characterised colony worldwide, in Paris. It is important to show parity here, as the UCL-GKR has

been kept for several generations without a specific maintenance breeding programme. Moreover, the close similarities to the Paris colony in particular is reassuring, as Paris GKR mice have been shown to develop classic “late” diabetic complications such as myocardial infarction, stroke and renal failure in middle age, providing the best possible evidence for clinical relevance of the model³⁴⁵.

6.3.1.4 Mitochondrial function

Examination of mitochondrial function was more speculative than the other lines of investigation here. Our experiment is hampered by low experimental numbers (n between two and three for each group) and a failure to consistently meet a quality control standard for mitochondrial function after the isolation protocol. In healthy mitochondria the respiratory control ratio is usually between six and eight. This represents a six-to-eightfold differential between respiration in the absence of metabolic substrate (ADP-limited respiration) – i.e. the “idling” level of function – and respiration in the presence of excess substrate (ADP-stimulated respiration) – i.e. “maxed-out” function. A high RCR implies that the mitochondria have high reserve capacity for substrate oxidation and ATP turnover and low oxygen consumption in the resting state; i.e. they are highly substrate responsive. The principal reason for a low ratio would be presence of high proton leak across the inner mitochondrial membrane, which would raise the consumption of oxygen in the “idling” state. This oxygen consumption would be uncoupled to production of ATP. Low RCR may also represent some limitation on electron flux in the “maxed-out” state⁴³⁶.

The reason for low RCRs varies across our experimental groups. Both age-groups of WRs fall into the expected range. The young GKR mice, and both SDR age-groups, just miss out on the lower bound of the expected range. Perhaps as expected, the 18-month GKR mitochondria have very low RCRs, and this relates to relatively high oxygen consumption in the “idling” (ADP-limited) state, implying a high degree of proton leak across the inner mitochondrial membrane independent of ETC function, with protons being lost without contributing to ATP synthesis. In fact, in the 18-month GKR group, the rate of oxygen consumption is virtually the same in ADP-limited respiration, as when the ETC is poisoned by Oligomycin, and IMM then permeabilised with FCCP. This suggests a very low reserve in uncoupled respiration in these mitochondria, with a minimal potential

to increase uncoupled respiration in response to acute changes in membrane permeability, for example with flickering opening of the mPTP⁶². This may lead to an excess susceptibility to cell death via reduced resilience to the recruitment of the cell-death mediator Bax by flickering opening of the mPTP.

Age-related changes in healthy cardiac mitochondrial function are controversial and seem to relate to the methods used to isolate the mitochondria. Investigators using only mechanical means to isolate cardiac mitochondria have reported consistent oxidative potential across different ages of murine hearts, whereas groups using protease enzymes in their isolation protocol tend to show an age-related decline in function, presumably due to age-related loss of resilience to the protease used in isolation, and loss or damage of outer mitochondrial components⁴³⁷. It is therefore particularly striking that using a non-protease isolation method, we have shown age-related loss of ETC function in the GKR that is not seen in either the WR or SDR. This may contribute to loss of IRI resilience in older GKRs.

6.3.2 Parallels with human diabetes

The Goto Kakizaki rat is widely described as a model of lean type 2 diabetes^{234,345,347,438–440}. This is a problematic description, as human type 2 diabetes rarely occurs in truly lean individuals⁴⁴¹; the vast majority of sufferers have normal or high body mass complicated by tissue insulin resistance, and studies of type 2 diabetics with truly low body mass (i.e. a BMI less than 18.5) have sometimes been flawed in ruling out autoimmune, or type 1, diabetes⁴⁴². Notwithstanding these difficulties, prevalence of truly “lean” diabetes is estimated to contribute only 3.5% at most of human type 2 diabetes, even in populations with a predisposition to this less usual form of the disease (e.g.: in India)⁴⁴³. Limited work has been done to phenotype the truly lean subset of human diabetics, and it remains controversial whether this represents a separate condition.

Progression of type 2 diabetes in man is characterised by deterioration in insulin action, decreased insulin response to a glucose load and non-suppression of endogenous glucose production by insulin⁴⁴⁴. Later in the disease there is commonly failure of pancreatic insulin production to keep up with the increased peripheral need for insulin to overcome resistance, and pancreas tissue from

human patients with type 2 diabetes exhibit inflammation and fibrosis⁴⁴⁵. It is these features of late diabetic disease in man that have prompted previous groups working with the GKR to identify parallels between the low insulin, high glucose GKR and established human type 2 diabetes^{345,347,417,446,447}.

However, our work suggests a much more straightforward parallel.

Our GKRs exhibit low circulating insulin and high blood glucose content from the earliest measurement timepoint, in comparison to age-matched WR controls. On its own, this pattern suggests that failure of insulin secretion, rather than insulin resistance, is the major defect in these animals. This pattern is of course more similar to human “type one” diabetes than “type two”, especially so since this change is established very early on in the animals’ lifespan. “Type one” diabetes in man is a disease of childhood or teenage onset⁴⁴⁸, whereas type two usually follows many decades of deteriorating insulin resistance⁴⁴⁴.

We used the HOMA- β statistic to quantify insulin secretion function in the fasting state and these results also support a secretory defect in the GKRs compared to WR controls.

Interpretation of this pattern is perhaps complicated by the HOMA-IR statistic we used to quantify insulin resistance. Results here suggested whole-body insulin resistance, mimicking findings in other GKR colonies. However, the HOMA-IR statistic is essentially the product of blood insulin and blood glucose concentrations multiplied together; the absolute differences in blood glucose concentrations between WRs and GKRs were very large in our study, but the differences between insulin concentrations were general quite small. The divergence in HOMA-IR statistics between the two strains is therefore driven almost entirely by the large difference in blood glucose concentrations and thus the HOMA-IR statistic cannot add much to the interpretation of this data. It would be a mistake to label the GKR as insulin resistant purely on the basis that it is hyperglycaemic.

Elsewhere in the literature, the GKR is described as a lean model of type 2 diabetes, and a good model for those patients who are predominantly insulin deficient⁴⁴⁹. However, insulin deficiency in that setting is due to massively increased demand for insulin as a result of peripheral insulin resistance, with

subsequent “burn out” of pancreatic insulin production. On the basis of our results, it would seem the GKR is not a model of this situation, but is a fairly good analogue of a sublethal type one diabetic phenotype, with subtotal pancreatic islet loss and therefore some residual level of insulin function.

The applicability of this model to human disease is likely to be limited, mostly because other, better validated models of a mild “type one” diabetes phenotype exist, such as partial pancreatic islet ablation using low-dose streptozotocin³⁴³.

6.3.3 Limitations

Clearly the UCL-GKR is not the model that we anticipated it would be from work in other colonies. A complete description of the diabetic phenotype in these animals is, sadly, beyond the scope of the project presented here. A detailed examination of the metabolic profile and altered insulin metabolism could have consumed this entire PhD project. However, even accepting that this was perhaps not the focus of the current project, some major limitations here are obvious. In particular, the failure to achieve measurements of glucose or insulin concentration in the fed state undermines the credibility of our findings on insulin resistance. The use of mathematical modelling of insulin action based on fasting tests was our attempt to circumvent this limitation but it has produced more troublesome results than it has explained. Clearly any future work with the UCL-GKR would have to take glucose and insulin tolerance testing as a starting point. Methodologically this will be challenging without changes to the project license under which the department operates, but collaboration with a lab experienced in metabolic profiling would be a sensible way forward here.

6.3.4 Summary

We set out to show broad comparability between the UCL-GKR colony, other GKR colonies and established human type two diabetes. In the first aim we have succeeded, and the UCL-GKR has much in common with the best described colony in Paris. However, even our basic examination of insulin metabolism in our colony has exposed inconsistencies in the literature. Far from being a model of human “type two” diabetes, the GKR in our hands seems a better analogue of “type one”, or insulin deficient, diabetes.

6.4 AIM 3: demonstrate impaired cardioprotection in the diabetic model

After phenotyping the UCL-GKR we used eight-month old male animals to study the efficacy of direct and remote ischaemic preconditioning in this rat model of established human diabetes; at this age the animals have established hyperglycaemia and evidence of chronic tissue-glucose interactions. As a positive control, we took young UCL-bred Sprague Dawley rats, which we expected to be fully sensitive to preconditioning stimuli. We had previously demonstrated that comparable differences in age in young and middle-aged non-diabetic rats have no effect on myocardial survival signalling and cardioprotection²⁴⁴. Over the age of 12 months, differences in RISK activation and ischaemic tolerance are seen when comparison is made to young rats near weaning age^{244,450,451}. Senescent animals have been demonstrated to have impaired cardioprotective responses to remote and direct ischaemic preconditioning when compared to juveniles^{450,452,453}. No significant heterogeneity in cardioprotective responses have been demonstrated in non-diabetic rats under 12 months age^{244,451–453} therefore we considered non-diabetic SDRs with a mean age of three months to be adequately matched controls GKR with a mean age of eight months. However, this does add a further layer of complexity and possible confounding to the experimental design. Ideally, precisely age-matched animals would have been used.

6.4.1 Animal diabetes

Blood tests confirmed that our eight-month-old GKRs were indeed diabetic, with fasting hyperglycaemia and evidence of chronic tissue-glucose interactions in the form of elevated HbA1c. The young SDR controls showed neither of these characteristics.

6.4.2 Successful Langendorff perfusions

80 retrograde heart perfusions were performed lasting up to 135 minutes. Temperature control was maintained throughout, and all perfusions passed quality checks according to *a priori* standards 10 minutes into perfusion³⁷¹. GKR hearts were seen to generate slightly less than anticipated developed pressure, and SDR hearts had marginally raised heart rates compared to our initial exclusion criteria, which were revised accordingly. All perfusions exhibited

significant impairment of LV systolic function (as reflected in developed pressure) and a sharp drop in coronary flow rate, in keeping with successful occlusion of the left coronary artery during induction of ischaemia. The scale of coronary flow rate reduction makes persisting low flow down a partially occluded coronary artery less likely, though it is not possible to rule this out entirely. Low flow coronary ischaemia is a valid model of coronary ischaemia and investigators have used it with some success to model some aspects of myocardial infarction⁴⁵⁴. However, low flow ischaemia allows the continuation of oxidative metabolism within the ischaemic myocardium, and thus the “reperfusion” event following low flow ischaemia is both less dramatic and less injurious⁴⁵⁵. Direct ischaemic preconditioning has been shown to completely obviate injury from subsequent low flow ischaemia in the heart⁴⁵⁶, but this is a problematic finding, as “reperfusion injury” as such, does not occur in this setting, and IPC putatively exerts its effects by ameliorating reperfusion injury. It is thought that in this setting, IPC exerts its effect during low-flow ischaemia by preservation of creatine phosphate energy stores. As interesting this phenomenon is, it is not the subject of study here and we sought to avoid low flow ischaemia for this reason. The best marker we have for total ischaemia within the area at risk are profound (>1/3) drops in CFR and DevP at ischaemia induction, and these were consistently achieved. Inability to conclusively rule out low flow down the ligated artery is an insurmountable limitation of the Langendorff regional infarction technique and may contribute to heterogeneity of results.

6.4.3 Cardiac function during *ex vivo* perfusions

The Langendorff isolated heart is not suited to precise assessment of cardiac function, as the heart does not perform work on an external blood pool in this preparation⁴⁵⁷. This lack of fidelity is reflected in our experiments, in which hearts sustaining very different amounts of damage from ischaemia-reperfusion fail to show significant differences in function during the reperfusion phase of the Langendorff perfusions. This limitation of the Langendorff preparation is reflected in other publications from our group, and although Whittington did observe some differences in LV developed pressure recovery comparing animals of different ages, this presumably reflected extremely large differences in LV systolic function, rather than the fine distinctions one is trying to make

between protected vs unprotected hearts in the post-MI phase of isolated heart perfusion²⁴⁴.

6.4.4 Success of direct and remote ischaemic preconditioning

Positive control young SDR hearts proved sensitive to preconditioning stimuli, with a single cycle of five minutes ischaemia and five minutes reperfusion (direct ischaemic preconditioning) achieving a 40% relative reduction in infarcted tissue. Two further cycles of sublethal ischaemia-reperfusion did not modify this response. Likewise, a single cycle of hindlimb ischaemia prior to heart explantation limb ischaemia (remote ischaemic preconditioning) reduced infarct size by 58%, and again increasing the number of cycles did not modify protection. In diabetic hearts, a single cycle of IPC or RIPC proved ineffective at reducing infarct size, and three cycles produced 37% and 53% reductions in infarct size, respectively.

6.4.5 Implications for acute MI in human patients with diabetes

This work has confirmed that intrinsic cardioprotective signalling is impaired in a clinically relevant model of established diabetes. This provides additional support for the idea that impaired outcomes from acute MI in human patients with diabetes stem from augmented cellular injury at the time of infarction, rather than purely due to adverse post-ischaemic remodelling. However, it has never been shown that acute cardioprotective signalling pathways are a predominant influence in clinical MI, and thus it is premature to conclude a definite link between increased threshold to preconditioning and impaired clinical outcomes.

6.4.6 Limitations

Limitations of *ex vivo* coronary artery ligation as a model of clinical MI are discussed above. Within the narrow limits defined in the aim of this work, we have been successful in showing impairment of cardioprotection in this diabetic model. The animal model used is more similar to “type one” human diabetes than “type two” and this limits the direct applicability to human MI; as stated elsewhere, the preponderance of human diabetics undergoing MI are of the “type 2” phenotype. As discussed in section 6.4, above, the age difference between the healthy SDR controls and the animals with diabetes is a confounder in this experimental design, however, published work suggests this scale of age difference in young animals has no effect on cardioprotection and infarct size. However, it is acknowledged that an ideal setup with no financial or

practical constraints would see precisely aged and age-matched groups to avoid concerns regarding age differences, rather diabetes, contributed to the differences seen between the two groups of animals.

6.4.7 Summary

By targeting early established diabetes, this work has provided the first documentation of successful remote ischaemic preconditioning of the diabetic heart. We have also confirmed that there is a threshold effect for cardioprotective interventions in diabetes and that this applies to both direct and remote preconditioning. Failure of intrinsic cardioprotective signalling pathways may underpin increased vulnerability to ischaemia-reperfusion in the human diabetic heart. These conclusions are subject to the significant confounder that different age animals were studied in the two groups, albeit that other published data suggests that this scale of age difference exerts no effect on preconditioning, cell survival signalling or the extent of IRI.

6.5 AIM 4: investigate the alterations in RISK signalling that accompany failure of cardioprotection in diabetes

Using Akt phosphorylation as a readout for activation of the reperfusion injury salvage kinase (RISK) cascade of pro-survival kinases known to mediate both IPC and RIPC, we found significant basal activation of Akt in hearts immediately after removal from the live eight-month diabetic animal. We observed that successful cardioprotective interventions (either IPC or RIPC) acutely increased this phosphorylation, in line with other reports on IPC's cardioprotective mechanism within the heart^{244,458}. Interestingly, in all but three-month animals, control perfusions failed to maintain basal levels of Akt phosphorylation, suggesting a role for continuous neurohormonal input during life in maintaining a "pre-preconditioned" state in the established diabetic. This is a subtly different interpretation from that advanced by Whittington, who observed that acutely increased Akt phosphorylation predicts successful cardioprotection but did not carry out control Langendorff perfusions. Our finding of self-sustaining Akt phosphorylation in three-month that early or pre-diabetes is a transient spontaneously occurring cardioprotected state in some diabetic models, especially those involving insulin resistance^{241,459,460}.

6.5.1 Implications for acute MI in human patients with diabetes

Previously, there was a conflict in data relating cardiac Akt phosphorylation and diabetes: On the one hand, Sivaraman showed that isolated human atrial tissue exhibits an abrogated cardioprotective response to a standard hypoxia-reoxygenation protocol of IPC. He observed reduced Akt phosphorylation in human diabetic atrial tissue compared with patients without diabetes and argued there was reduced activation of the RISK pathway in these patients, and that this accounted for reduced cardioprotection. This runs counter to our subsequent observations in rat, with Whittington, when we observed increased Akt activation associated with resistance to preconditioning.

Our new experiment comparing immediate (“Baseline”) versus delayed (“Control”) assessment of Phospho-Akt provides the missing piece of this jigsaw: it seems likely that Sivaraman’s assessments were performed on atrial tissue only after transfer from the clinical operating theatre into the research lab and perhaps subject to some delay; our data would suggest that without continued stimulation from IPC or RIPC, Phospho-Akt in these samples would rapidly degrade. Conversely, Whittington’s samples were assessed immediately, and hence showed increasing Phospho-Akt with age and diabetes, similar to our “Baseline” samples.

The integrated interpretation of these data is that both humans and rats with established diabetes have tonic activation of myocardial survival signalling, presumably to offset deleterious influences such as increased oxidative stress and mitochondrial electron leakage. This tonic activation is under the influence of extracardiac neurohormonal influences, which are lost in the isolated heart, or in the isolated atrial trabeculae model used by Sivaraman.

However, early in the course of diabetes, (our eight-month animals) the tonic basal Akt activation can be augmented by exposure to IPC or RIPC, leading to effective preconditioning and cardioprotection. In older diabetic animals, and presumably in humans with more longstanding diabetes, other unknown factors may come into play to limit further augmentation of Akt signalling, and thus make the longstanding diabetic heart resistant to ischaemic and remote ischaemic preconditioning. Doubtless this failure of intrinsic cardioprotective pathways also underpins the increased vulnerability to ischaemia-reperfusion

injury and patients with diabetes' poorer outcomes from myocardial infarction, though whether this is mediated primarily by increased tissue death, as suggested by these experiments, remains to be seen.

6.5.2 Limitations

These investigations into the mechanism of the block to IPC and RIC in diabetes are severely limited. Western blotting of the pro-survival RISK cascade is a starting point for investigation rather than a thorough examination and the number of individual animals included in these mechanistic experiments is small and undermines their sensitivity, though statistically significant differences were seen between groups so inadequate statistical power is not a practical limitation here as the measured differences between groups were in the event quite large. Other techniques including PCR could be used to confirm the findings.

Akt is presented here as the only readout for activity of the RISK pathway, though this examines only the signalling state of the proximal pathway. Distal signalling in the RISK pathway is not entirely understood, however, as made clear in Figure 1.4, which makes further interrogation difficult especially when proximal activation follows some counterintuitive trends, as shown in our small study. The role of GSK3 β is particularly controversial with some authors suggesting it does not figure in acute cardioprotective signalling⁴⁶¹. We did attempt to blot for GSK3 β activation status but these blots gave inconsistent results and the low *n* number hampered meaningful interpretation. In one of the better quality blots the activation of GSK3 β seemed decreased in conditions where Akt phosphorylation was increased, but this is a single result and could not be replicated. This does fit, however, with others' suggestions that GSK3 β may be negatively regulated by Akt in RISK signalling. This is not a conclusion I would draw with any weight from this work, however. A useful way forward would be to quantify phosphorylation state of multiple proteins putatively involved in the RISK cascade (Akt, P5076K, GSK3 β , PKC γ for example) with an alternate technique such as PCR.

6.5.3 Summary

Within the limits discussed above, this small experiment has resolved the apparent conflict in previous data concerning the role of acute vs chronic Akt

activation in diabetic animals undergoing heart explant experiments during investigation of ischaemic conditioning.

6.6 AIM 5: investigate if hyperglycaemia exacerbates reperfusion injury and how this differs between diabetic and non-diabetic hearts

Transient hyperglycaemia during acute MI is well described in both diabetic and non-diabetic patients, with contributions from both increased glucose production and decreased peripheral uptake. Increased gluconeogenesis and glycogenolysis are the results of catecholamine and adrenal steroid release, and peripheral insulin resistance is caused by inflammatory cytokines, principally tumour necrosis factor alpha (TNF α)^{260,261}.

Hyperglycaemia is associated with impaired outcome from acute MI in both patients with and without diabetes¹⁵. The effect is far more potent in patients without diabetes than in those with, with a steeper relationship between blood glucose and mortality²⁴⁹. As discussed in Chapter 1, the evidence for benefit of intervention to normalise glucose during acute MI is mixed (see section 1.4.4. Hypoglycaemic agents to reduce infarct size), though our interpretation of large published studies remains that there is an effect in high risk individuals. There may also be important differences in responses to glucose normalisation between patients with, versus those without, diabetes. An alternative interpretation is that hyperglycaemia is an epiphenomenon in patients without diabetes, a marker of how “sick” the patient is, rather than an upstream cause for worsening prognosis via worsening myocardial injury. However, the myocardium itself is among the target organs to develop insulin resistance after acute MI, and this has been experimentally demonstrated to predict a higher risk of developing post-MI heart failure²⁶². Moreover, exposure to moderately high glucose has also been shown to predict larger myocardial infarct size in non-diabetic animals both *in vivo* and in isolated heart models of infarction^{285,287,462}.

We sought to address whether high glucose (HG) has comparable effects in diabetic and non-diabetic hearts, whether the effect is felt during the reperfusion phase of myocardial injury, and by what mechanism.

6.6.1 Osmolality and infarct size

Osmolality is a potential confounder in experiments involving variable glucose.

Pre-infarct osmolality is a key determinate of infarct size. On a Langendorff rat heart model similar to ours, exposure to 600mOsm for 2mins just prior to coronary artery ligation reduced infarct size by roughly half⁴⁶³. An *in vivo* experiment in dog used Raffinose to raise dogs' plasma osmolality moderately from ~300mOsm to ~330mOsm for 65mins just prior to coronary ligation and again reduced infarct size by around half²²⁸. Exposure to osmolar stress can be considered a preconditioning treatment.

Counter to experimental data, observational data from one thousand patients undergoing urgent PCI for acute coronary syndrome suggests that high osmolality at presentation predicts poor outcome from subsequent reperfusion⁴⁶⁴. It is difficult to know how to integrate this into understanding of osmolality, blood glucose content and reperfusion injury, however, given that high glucose is one of the prime drivers of hyperosmolality in man. Clinical data is therefore subject to significant confounding, which multivariate analyses can only partially correct.

Due to the interaction between glucose content and osmolality, we took care to ensure the same osmolality across different treatment groups in our variable glucose experiment.

All hearts in our glucose study were exposed to high osmolality during reperfusion, with osmotic pressure exerted by mixtures of mannitol and glucose in varying proportions; to our knowledge this is the first time such an approach has been used to limit high osmolality to reperfusion. Although a direct comparison is not strictly valid due to minor protocol differences, it is striking that the hearts exposed to 11mmol/L glucose with increased osmolality in reperfusion sustained far smaller infarcts than those seen in control hearts in Chapter 2, when all hearts were exposed to 11mmol/L glucose mKHB throughout, with constant osmolality and no extra mannitol (59.5±4.2% vs 44.7±2.6% for SDRs and 47.7±4.6% vs 32.1±1.1% for GKR).

These observations fit with prior experimental data that high osmolality promotes myocardial survival and suggest that osmotic potential may exert a

real effect even when applied only during the reperfusion phase of myocardial IRI. This is the first suggestion that hyperosmolality may function as a postconditioning intervention, though appropriately controlled experiments are needed to confirm this.

It is interesting to note that if hyperosmolality does indeed activate pro-survival signalling, then to exert an overall deleterious effect, hyperglycaemia must inhibit this signal in addition to any other harmful mechanism. Evidence abounds that hyperglycaemia blocks other conditioning modalities^{14,297,465,466}.

6.6.2 High glucose and reperfusion injury

Peri-infarct HG exacerbates myocardial injury and is associated with poor clinical outcomes. We sought to clarify whether glucose exerts an effect specifically on reperfusion injury and whether the effect is modified by pre-existing diabetes.

Our results confirm that exposure to glucose modulates tissue death during the reperfusion phase of myocardial IRI. Moreover, we have shown different effects in the diabetic versus nondiabetic myocardium, with an overall pattern suggesting tolerance to glucose exposure in the diabetic hearts: infarcts tended to be smaller in heart from rats with diabetes, and the nadir infarct size was at 16.5mmol/L glucose compared to 11mmol/L in the non-diabetic. Whilst in the non-diabetic there was a clear stepwise increase in tissue death from the 11mmol/L to the 16.5mmol/L and 22mmol/L groups.

The experiment was clearly under-powered to detect the scale of differences seen between groups in the diabetic hearts.

6.6.3 Low glucose and reperfusion injury

Observational data in man suggests hypoglycaemia predicts a mildly increased chance of poor outcome from MI in patients with and without diabetes¹⁶. Our results suggest that both these effects may be mediated by worsening reperfusion injury.

Nadir infarct size in patients without diabetes was in the 11mmol/L glucose group. In the 5mmol/L glucose group, a slightly higher degree of cell death was seen, though this did not reach statistical significance. The experiment was

underpowered to detect differences of this scale. *Post hoc* analysis suggests a linear relationship between infarct size and reperfusion glucose ($R^2=0.35$, $P=0.00009$) only when the 5mmol/L group is omitted. A *post hoc* Student's T-test between the 5mmol/L and 11mmol/L groups confirms excess tissue death in the 5mmol/L hearts.

Other investigators have shown excess myocardial damage with HG, but few have examined the nature of the relationship in detail, the most complete description being in dog²²⁸, which showed a linear relationship between blood glucose and *in vivo* infarct size but included only one dog below 6mmol/L. No-one has before reported a J-shaped curve with excess tissue death at both low and high levels of glucose. Recently, Pælestik showed excess myocardial injury with very low levels of glucose (3mmol/L) in the reperfused isolated rat heart⁴⁶⁷ but low glucose was given both during ischaemia and reperfusion, making it impossible to exclude worsening glycopenic injury during ischaemia as the mechanism. Also, this work did not include truly HG groups for comparison, but compared only 3mmol/L to 11mmol/L glucose. In an experiment that is commonly cited to support the idea that glucose does not influence infarct size, Diemar used glucose clamping in pigs during and after coronary artery ligation to maintain low (1.8-2.2mmol/L), "normal" (5-7mmol/L) or high (22-23mmol/L) glucose throughout⁴⁶⁸. Inevitably, the use of variable dose insulin infusion to maintain target levels of glucose interfered with the results, so that no differences in tissue death were seen across the three groups in this experiment.

Thus, our demonstration of the linear relationship between increasing glucose at reperfusion and exacerbation of reperfusion injury in non-diabetic hearts is a plausible novel finding.

6.6.4 Limitations

This is perhaps the most compelling work in the project. Again, the limitations of the Langendorff *ex vivo* IRI preparation with regards to translation into man apply. Another minor point is that the addition of DMSO to perfusate in these experiments (with and without Phlorizin) may also have interfered with results and undermines the speculative comparison between groups of hearts in these experiments versus those in the standard Langendorff preparations in other

chapters. However, this comparison was not a central outcome of the work. As discussed elsewhere in this project, mannitol was used to balance osmolality between samples with different glucose content. Some may criticise this approach, citing historical experiments suggesting mannitol may have a cardioprotective effect⁴⁶⁹, however this is to misunderstand the evidence base. In previous experiments, mannitol has been used to induce a hyperosmolar state, and as discussed above, hyperosmolality rather than mannitol *per se* is cardioprotective.

We examined a relatively low number of different blood glucose concentrations over a conservative range. Whilst there is an argument for including more glucose groups in the experimental design, in practise this would have reduced our statistical power to detect differences between groups with an ANOVA test and this would have worked to our disadvantage. A major criticism of the experiment is that the GKR groups were undersized to detect differences in infarct size in this strain; this is a valid criticism and stems from the fact that we over-estimated the effect that glucose would have on infarct size in diabetic hearts.

6.6.5 Summary

By subjecting isolated hearts to glucose stress during only the reperfusion phase of experimental infarction, we have shown for the first time that glucose modifies myocardial reperfusion injury specifically. This has been previously shown in brain tissue, but not in the heart. The relationship between burden of cell death and glucose availability is very similar to the relationship between glucose levels during MI and impaired clinical outcomes, with excess injury seen at high and low glucose in non-diabetic hearts and the curve shifted to the right in diabetic hearts. This is highly suggestive that impaired outcomes from reperfusion injury may contribute a large part of the poor clinical picture in those patients presenting with hyperglycaemia and acute MI.

6.7 AIM 6: investigate the mechanism by which hyperglycaemia exacerbates reperfusion injury in the non-diabetic heart

Both HG and reperfusion augment ROS production in myocardial cells^{388,470,471}. We hypothesised that HG and reperfusion may act synergistically on ROS production to worsen reperfusion injury in non-diabetic hearts undergoing reperfusion with HG. We tested this by administering Phlorizin, a non-selective SGLT blocker, to block the HG component of ROS production³⁸⁸.

Indeed, in our hands, Phlorizin at very low dose completely abolished the increased reperfusion injury seen with HG, returning infarcts to the baseline size seen with normal glucose reperfusion. Phlorizin had negligible effect on hearts perfused with standard (11mmol/L) glucose content mKHB. This contrasts with other groups' finding that administration of Phlorizin on the Langendorff prior to experimental infarction increases infarct size in mouse³⁴⁰. The two findings are not mutually exclusive, as it is quite possible that when administered prior to ischaemia, Phlorizin decreases vital inward glucose flux during ischaemia, thus worsening the insult to an extent that outweighs its benefit at reperfusion. This theory is given weight by the fact that during chronic ischaemia, SGLT1 expression is increased in the human heart, implying a role as a glucose scavenger in situations of poor glucose supply⁴⁴.

The two-pronged role of different SGLT isoforms in ischaemic brain is well-described. During cerebral ischaemia the glucose sensor SGLT3 is neuron-sparing, such that SGLT3 knockdown mice suffer larger volume tissue loss in an *in vivo* model of middle cerebral artery occlusion. Contrastingly, post-ischaemia, SGLT1 exacerbates neuronal cell death under hyperglycaemic conditions. In the absence of hyperglycaemia, SGLT function is not deleterious to neurons under oxidative stress^{336–338}.

Kashiwagi's work in the heart demonstrated infarct size exacerbation when Phlorizin is given prior to ischaemia³⁴⁰. In combination with our data regarding later Phlorizin administration, this supports the same dual role for SGLT as seen in the brain^{336–338}.

6.7.1 Glucose availability and ROS production

We next attempted to confirm in isolated cardiomyocytes that HG triggers increased ROS production at reperfusion and that Phlorizin blocks this increase. In designing these experiments, we faced practical difficulties in combining the measurement of ROS production via confocal microscopy, with simulated ischaemia-reperfusion using an airtight chamber. Such a model has been used at the Hatter using a relatively resilient immortalised cell line⁴⁷², but not with primary isolated adult cardiomyocytes. Other groups have reported using a similar technique on adult CMs⁴⁷³. Colleagues at the Hatter had little success with replicating this approach, however.

Therefore, we elected to use oxidative stress generated by the addition of hydrogen peroxide as a surrogate for the reperfusion event. This approach has since been used to investigate neuron IRI resilience in the setting of HG, but at the time we designed the experiment it was a novel approach to the problem³³⁸.

Our model allowed cardiomyocytes to stabilise in a high osmolality buffer with variable glucose solution, followed by exposure to oxidative stress by spiking with H₂O₂, with or without Phlorizin at the same concentration employed in whole heart infarct experiments.

During validation of this model, we saw acute increases in ROS on moving CMs from standard Tyrode's (10mmol/L glucose) into variable glucose solutions comprising glucose plus mannitol. However, in contrast to Yamazaki's more recent findings in neurons³³⁸, we saw no difference in ROS generation with exposure to low (5mmol/L), normal (11mmol/L) or high (16.5mmol/L and 22mmol/L) glucose.

Other investigators who have reported increased ROS with HG in CMs have generally cultured the cells in differential glucose concentrations for longer than we did (hours to days – we used minutes)^{388,471,474}. This is because most investigators are interested in the long-term effects of high glucose, their paradigm being that HG is a chronic, low-level stress that may increase the vulnerability of cells to intercurrent insults such as IRI. In our Langendorff setup, the HG itself was the acute insult, and therefore it was appropriate to expose

CMs to HG for only a short time. This is an artificial situation, and we accept that the clinical relevance of acute HG restricted to reperfusion is obscure. However, this work aims to prove the principle that HG exerts a real effect at reperfusion as distinct from during ischaemia.

Introducing oxidative stress produced immediate and sustained high levels of intracellular ROS. Whilst minor differences were seen across different glucose concentrations, no statistically significant differences were seen.

6.7.1.1 Failure to detect differences in ROS

It is possible that the failure to detect significant differences in ROS production on exposure to differential glucose and after oxidative stress is related to problems with our assay, particularly the timing of ROS measurements. It is notable that Balteau detected significant differences in ROS with exposure to low vs high glucose (5mmol/L vs 21mmol/L) in a similar experimental design, but after incubation with glucose for 3 hrs³⁸⁸.

However, successful time-course experiments conducted during the optimisation of this method suggest that our experimental design was appropriate. Moreover, we did detect a trend towards ROS reduction with administration of Phlorizin, which suggests a technically successful assay, even if a greater sample size is needed to reach statistically significant results. Sample size in this experiment was sufficient to detect a difference of one standard deviation with power of 0.93⁴⁷⁵.

6.7.2 Glucose exposure and isolated cardiomyocyte survival

Thus far, we had seen large-scale modulation of infarct size by exposure to variable glucose at reperfusion in the intact heart, but had failed to see those differences reflected in ROS production in an isolated cell model of oxidative stress. We decided to verify whether the toxicity of acute glucose exposure at reperfusion persisted in the isolated cell model.

Despite technically successful simulated ischaemia-reperfusion experiments, with results for control runs in the expected range, we saw no difference in cardiomyocyte death after simulated ischaemia-reperfusion injury with acute exposure to low, normal or high glucose during reperfusion, or with the

administration of the SGLT blocker Phlorizin. We employed an experimental protocol very similar to others who have observed large-scale glucotoxicity³⁸⁸, with the exception that other investigators used glucose exposure prior to and during simulated ischaemia^{285,287}.

This entirely negative result called into question the original results from intact rat heart on the Langendorff rig. Dr Rob Bell therefore repeated the intact heart experiment using mouse heart, and a whole organ ischaemia model. The results produced were very similar to our original results in rat heart, confirming a true difference between the intact heart (both rat and mouse) and isolated cardiomyocytes.

6.7.2.1 Failure to augment cellular injury with glucose

The model of sIRI met *a priori* criteria for a valid experiment, with low (<25%) levels of cell death in normoxic controls and high (>60%) cell death in cells subjected to sIRI. Manipulations of glucose and presence of Phlorizin during reoxygenation, however, failed to have significant effects on the cell death outcome. The experiment was adequately powered to detect a difference in cell death of one standard deviation with over 90% sensitivity, and therefore insufficient sample size and power is unlikely to be the reason for a negative result.

Propidium Iodide tagging is a well-established method to assess cell death. Specifically, PI assesses membrane integrity by binding DNA; as PI may only enter cells and nuclei in settings where membrane integrity is compromised, this is felt to be a specific test of cell viability. However, cell death with preservation of the external cell membrane (eg: during early apoptosis⁴⁷⁶) may be under-detected. The larger potential problem with our cell death assay lies with quantifying the denominator: the total number of potentially live cells present in the sample. Under our protocol, we quantified this by morphological assessment of cells in a field under light microscopy. This method – although widely used – is inherently subjective. Other protocols call for tagging of all cell nuclei with a stain such as 4',6-Diamidine-2'-phenylindole dihydrochloride (DAPI) to more reliably assess the total number of potentially live cells in the sample. For further increased reproducibility we could have used flow cytometry to then assess total vs PI stained cell numbers⁴⁷⁷.

These methodological flaws aside, it is also possible that glucose does not exert a direct deleterious effect on cardiomyocytes over the short time-course that we studied. In our protocol, CMs were reperfused for just one hour before assaying for cell death; other investigators have incubated CMs with glucose for much longer.

Longer-term CM exposure to glucose reduces availability of the oxidative stress buffer thioredoxin²⁸⁷, increases ROS production by cytosolic NADH oxidase(NOX)³⁸⁸ and induces phosphorylation of the Jak/STAT3 (SAFE) cascade of kinases. Interestingly, increased ROS production by NOX is inhibited by SGLT blockade with Phlorizin. The lack of effect from Phlorizin in our experiment would suggest that this is either an effect that evolves over a longer timescale, or that it is counteracted by superimposed sIRI.

6.7.2.2 Contrasts between the whole heart and isolated cell model

In our work, three isolated heart models gave similar results with clear modulation of reperfusion injury by glucose exposure in non-diabetic rat and mouse heart, and trends to statistically significant modulation in diabetic rat heart. Similar experimental protocols in isolated ventricular cardiomyocytes from non-diabetic rat heart failed to show such an effect.

There are broadly two possible explanations for this conflict: either the difference is artefactual and relates to preparation of the cellular model, or it represents a real difference between the effects of glucose in intact ventricular myocardium versus plated cells that have been through an isolation process.

Considering first potential problems with the model: the isolated cardiomyocyte model could have been inappropriately set up with poor choice of hypoxia and reoxygenation times, or poor methodology of acute exposure to variable glucose media at reoxygenation. Timings are unlikely to have been the problem, as both control groups exposed and not exposed to hypoxia had levels of cell death comparable with other successful sIRI experiments⁴⁷⁸. Poor methodology at reoxygenation is a real concern; in the whole heart model, variable glucose medium was supplied at the same instant that oxygen was resupplied to ischaemic myocardium, whereas in the cell model inevitably there was a short

delay between re-exposing cells to oxygen by opening the hypoxic chamber and replenishing their medium with variable glucose media. Such concerns could be overcome by changing to a model with continuous slow-flow perfusion with medium, which could be switched at the same instant as oxygen is restored. However, such a setup would sacrifice depth of simulated ischaemia, as such preparations are inevitably in contact with environmental oxygen to some extent, rather than isolated in a high CO₂ incubator environment.

Secondly, considering reasons why glucose may have different effects in intact myocardium versus isolated cardiomyocytes: the isolation protocol we used has been optimised for harvesting large numbers of viable cardiomyocytes without reference to other significant cell types present in myocardium. Other cell populations known to play important roles in reperfusion injury include inflammatory cell populations, fibroblasts and the endothelial cells of blood vessels^{52,479,480} and these are of course present in the intact heart but may be absent from the cell preparation. This may be relevant.

A prime assumption of using an isolated cell model is that the entire glucose-infarct size relationship is determined within the isolated cardiomyocyte; this may not in fact be correct. The effect of glucose on the cardiomyocyte may be mediated by other cell types and may require intact cell-cell interactions that are disrupted during breakdown of cardiac structure.

With the breakdown of extracellular matrix any signalling reliant on physical cell-cell interaction will be compromised. This may be of relevance to endothelial cells, structured in the intact heart into capillary networks, and in a highly regulated relationship with neighbouring cardiomyocytes.

Co-culture experiments have shown that in some settings, cardiomyocyte cell survival is influenced by paracrine signalling from endothelial cells releasing mediators in response to cytoprotective stimuli⁴⁸¹. Comprehensive identification of mediators is ongoing but nitric oxide is implicated; many micro-RNAs have been shown to increase in preconditioned hearts, but the sites of production and action have yet to be elucidated. Such mediators may be released from

endothelial cells encased in lipid bilayer structures (exosomes), which have been shown to reduce reperfusion cell death⁴⁸².

One potential explanation for the disparity between our intact heart and isolated cardiomyocyte experiments is therefore that glucose sensing is undertaken in one set of cells (e.g. capillary endothelium) and communicated to cardiomyocytes by paracrine signalling, which is disrupted by preparation of the isolated cell model. In support of this explanation, the injurious effect of glucose on isolated cells has been shown to be independent of glucose's participation in cardiomyocyte metabolism³⁸⁸.

However, Van Steenbergen recently published a putative mechanism for glucose sensing and exacerbation of ROS production by NOX all within the single cardiomyocyte cell-type⁴⁸³. It is suggested that the SGLT family members SGLT6 and SMIT1 transport glucose within cardiomyocytes and in so doing, activate NOX2 producing ROS. This runs counter to our experimental results, as one would expect this effect to persist in our isolated cell model, and therefore for glucose to exacerbate cell death in our model. Moreover, as Phlorizin is a potent inhibitor of both SGLT6 and SMIT1⁴⁸⁴, we would expect Phlorizin to rescue the toxicity of high glucose in our isolated cardiomyocytes.

Identifying expression of SGLTs is hampered by poor antibody availability and we have not yet examined cardiomyocytes specifically for SGLT6 and SMIT1. However, in work following up on the experiment discussed above, we have used real time PCR to show that SGLT1 is not expressed in cardiomyocytes but is expressed in other myocardial cell types⁴⁸⁵.

6.7.3 Limitations

The many potential reasons for our cell-based experiments failing to reproduce the results seen in the whole heart experiments are discussed in detail above. In broad terms the potential explanations fall into three groups: artefactual findings due to methodological flaws in the cell work; under-powering of cell-based experiments to detect real differences in cell behaviour; genuine differences in cell behaviour between whole heart and isolated cell models. There is also a possibility that the findings of the whole heart experiments could be incorrect, with the isolated cell work giving a truer picture. There are certainly

many methodological flaws to be corrected in the cell work, particularly with assay methodology for both cell death assessment and ROS quantification. Correcting these and repeating experiments should be the focus of future work in this area.

6.7.4 Summary

The SGLT blocker Phlorizin successfully abrogated excess cell death seen in non-diabetic hearts exposed to glucose-reperfusion injury, which we took to indicate the importance of glucose uptake by cardiomyocytes. However, attempts to reproduce the relationship between glucose exposure and cell death in an isolated cell model failed. We also failed to demonstrate increased ROS in cells exposed acutely to high glucose concentrations with or without coincident oxidative stress.

Further work to explore reasons for these disparate results is discussed in Chapter 7, "Conclusions and future directions".

7. CONCLUSIONS AND FUTURE DIRECTIONS

7.1 Conclusions

The over-arching aim of this work was to elucidate the ways in which diabetes interacts with reperfusion injury within the heart to modulate tissue death during reperfused acute myocardial infarction. We were particularly interested in whether excess complication rates from MI in diabetes and in hyperglycaemia are underpinned by increased sensitivity to reperfusion injury.

We verified a model of established diabetes using the inbred, hyperglycaemic Goto Kakizaki rat colony at University College London, and showed this animal has similar characteristics to other colonies used for similar work elsewhere.

The adult UCL GKR is an insulin deficient, hyperglycaemic animal likely to develop the full range of spontaneous complications of diabetes, though in the lifespans of our animals we observed only poor weight gain, polyuria and cataract as spontaneous complications.

We confirmed that endogenous mechanisms which may limit tissue death in the experimental setting – specifically the RISK pathway – is inhibited in our diabetic model, compared to a younger, fully IPC-sensitive control rat. The experimental design, without age matching of the strains with and without diabetes, introduces a significant potential confounder which is not addressed within the statistical analysis. However, we showed that within the strain with diabetes, inhibition of RISK evolves over time in a pattern that mirrors the failure of endogenous cardioprotection; we established that this inhibition is associated with prior activation of upstream signalling pathways utilised by endogenous cell-survival promotion mechanisms within the myocardial tissue itself.

Subsequently we conducted experiments showing that the failure of endogenous protection involves failure of both remote and direct ischaemic preconditioning. This does not directly prove that failure of cytoprotective mechanisms are the dominant influence on myocardial infarction size and complication rate in human diabetes, but it is very suggestive.

Turning to hyperglycaemic modulation of infarct size, we showed that epidemiological patterns of MI complications seen in man are closely mirrored by trends in infarct size in experimental animals. This is strong circumstantial evidence that the effect of glucose on prognosis following MI is at least partially

mediated by glucose's effect on reperfusion injury. We could not reproduce this pattern in an isolated cell model, however, so further investigation of the mechanisms whereby glucose sensitises to ischaemia-reperfusion injury were unsuccessful.

7.2 Future directions

7.2.1 The Goto Kakizaki rat

Despite our initial success with the Goto Kakizaki rat, including showing for the first time that the diabetic phenotype is preserved despite years of non-selective breeding, I would not recommend continued use of this model for this kind of work. This is a question of balancing advantages vs drawbacks of the model; a decision that hinges for me on the consistency of the effect that we see. Yes, the GKR population is, as a whole, hyperglycaemic, low in body mass and shares many characteristics with human established diabetes. However, ageing animals for eight months before they are suitable to be used, is expensive – not least because the polyuria necessitated smaller caging groups and more intensive husbandry. The long lag between weaning and use at eight months also has ethical implications. Moreover, we saw many times throughout this work that the GKR hearts performed less consistently (i.e. gave a wider spread of results) on the Langendorff rig and in mitochondrial preparations, than controls. This must raise questions about the consistency of the phenotype.

Rather than using an “integrated” model of diabetes, I feel there is more future in using models of individual aspects of the condition to investigate mechanistic questions. The obvious paradigm here is use of genetic modification to perturb insulin sensitivity, in models such as the Brn-3b knockout mouse⁴⁸⁶. Tissue specific knockouts and knockdowns of insulin signalling components could have utility in future studies of IPC and its failure in the comorbid patient.

Development of the endothelium specific mutant insulin receptor (ESMIRO) mouse⁴⁶⁰ is an excellent example of a model well suited to help unpick this issue.

If the GKR has a future as a model it is to answer epidemiological questions about what is common in animals with abnormal glucose metabolism, rather than to untangle issues of pathophysiology: there is simply not enough known

about the pathophysiology of the model itself. A particularly big omission is our lack of understanding of integrin signalling in the GKR and this must be resolved if the model is to be used further.

7.2.2 Cardioprotection in diabetes

Clinical investigation of cardioprotection is at a crossroads. The consensus of clinical preconditioning trials is that this treatment has a negligible clinical effect in its current form; we must take this on board if the field is to move forward⁴⁸⁷. In much the same way as we have had to examine why results in our intact heart model were not reproduced in a cell model, the cardioprotection research community needs to address why findings in laboratory studies are not reproduced in the clinic. Appreciating the impact of diabetes and insulin resistance are important aspects of this analysis, but it also needs to go further. Such analysis may include questioning the basic design of experiments showing efficacious preconditioning in animal models. Typically these experiments have relatively short ischaemic times, predictable reperfusion and assiduous control of other parameters such as temperature and heart rate. It is notable that none of these characteristics are present in the clinic.

It is clear from this and other studies that achieving acute cytoprotection in diabetes is challenging, and there is an increased ischaemic stimulus required. We linked this to *in vivo* high levels of RISK activation, which then declined following heart explantation. Our finding that high levels of phosphorylated Akt were maintained after heart explantation from the three-month prediabetic animal is intriguing and suggests that the prediabetic heart may be spontaneously preconditioned. This could be investigated using prediabetic animals and chronic administration of blockers to cell surface receptors upstream of RISK activation, prior to experimental infarction. It would be interesting to find whether RISK signalling is active in prediabetic human hearts but obtaining live tissue samples would be challenging.

7.2.3 Hyperglycaemia and ischaemia-reperfusion injury

Our results suggest there is a difference between the effect of hyperglycaemia on IRI in diabetic vs non-diabetic hearts. Previous clinical studies investigating the merits of acute glucose control during MI have included patients with diabetes alongside patients with acute stress hyperglycaemia. Our data would

suggest future trials should be adequately powered to detect benefit in one population or the other, and that a trial of acute glucose control specifically in patients without diabetes is needed.

Our finding that partial blockade of glucose uptake during MI is beneficial in the setting of hyperglycaemia suggests that any acute glucose control trials should not use insulin, as driving further glucose into cells may well be detrimental.

There is also further work to be done unpick the mechanism by which SGLT blockade glucose ameliorates myocardial reperfusion injury, and the cell types that are implicated. Recent work by Van Steenbergen suggests that SGLT6 and SGLT1 are important in generation of ROS in steady state high glucose⁴⁸³. A similar mechanism may underlie the deleterious effect of acute glucose at reperfusion, however, findings in our lab on the cardiomyocyte expression of SGLT family members differ Van Steenbergen's important paper and we failed to correlate glucose exposure with cell death in the isolated cell model.

We should first try to reproduce Van Steenbergen's findings, exposing cardiomyocytes to glucose over a longer time course and assessing ROS production. Once we have clearly seen increased ROS and increased cell death with increasing glucose then we should go back to examining SIRT1 superimposed on the glucose insult. It may be that whilst chronic glucose acts directly on the myocyte, acute glucose exposure at reperfusion specifically acts via endothelium-mediated signalling, as we suspect.

8. REFERENCES

1. GBD 2016 Causes of Death Collaborators, M. *et al.* Global, regional, and national age-sex specific mortality for 264 causes of death, 1980-2016: a systematic analysis for the Global Burden of Disease Study 2016. *Lancet (London, England)* **390**, 1151–1210 (2017).
2. Patel, P. A. *et al.* An evaluation of 20-year survival in patients with diabetes mellitus and acute myocardial infarction. *Int. J. Cardiol.* **203**, 141–4 (2016).
3. Lavie, C. J., Milani, R. V. & Ventura, H. O. Obesity and Cardiovascular Disease. *J. Am. Coll. Cardiol.* **53**, 1925–1932 (2009).
4. Hedblad, B., Nilsson, P., Engström, G., Berglund, G. & Janzon, L. Insulin resistance in non-diabetic subjects is associated with increased incidence of myocardial infarction and death. *Diabet. Med.* **19**, 470–475 (2002).
5. Reaven, G. M. Banting lecture 1988. Role of insulin resistance in human disease. *Diabetes* **37**, 1595–1607 (1988).
6. McNeill, A. M. *et al.* The Metabolic Syndrome and 11-Year Risk of Incident Cardiovascular Disease in the Atherosclerosis Risk in Communities Study. *Diabetes Care* **28**, 385–390 (2005).
7. Okwechime, I. O., Roberson, S. & Odoi, A. Prevalence and Predictors of Pre-Diabetes and Diabetes among Adults 18 Years or Older in Florida: A Multinomial Logistic Modeling Approach. *PLoS One* **10**, e0145781 (2015).
8. Iwasaki, K., Matsumoto, T., Aono, H., Furukawa, H. & Samukawa, M. Prevalence of subclinical atherosclerosis in asymptomatic diabetic patients by 64-slice computed tomography. *Coron. Artery Dis.* **19**, 195–201 (2008).
9. Donahoe, S. M. *et al.* Diabetes and mortality following acute coronary syndromes. *JAMA* **298**, 765–75 (2007).
10. Jernberg, T. *et al.* Cardiovascular risk in post-myocardial infarction patients: nationwide real world data demonstrate the importance of a long-term perspective. *Eur. Heart J.* **36**, 1163–1170 (2015).

11. Jacoby, R. M. & Nesto, R. W. Acute myocardial infarction in the diabetic patient: Pathophysiology, clinical course and prognosis. *J. Am. Coll. Cardiol.* **20**, 736–744 (1992).
12. World Health Organization. *Definition and diagnosis of diabetes mellitus and intermediate hyperglycemia: report of a WHO/IDF consultation.* (2006).
13. Kajbaf, F., Mojtahedzadeh, M. & Abdollahi, M. Mechanisms underlying stress-induced hyperglycemia in critically ill patients. *Therapy* **4**, 97–106 (2007).
14. Kehl, F. *et al.* Hyperglycemia prevents isoflurane-induced preconditioning against myocardial infarction. *Anesthesiology* **96**, 183–8 (2002).
15. Capes, S. E., Hunt, D., Malmberg, K. & Gerstein, H. C. Stress hyperglycaemia and increased risk of death after myocardial infarction in patients with and without diabetes: a systematic overview. *Lancet* **355**, 773–778 (2000).
16. Kosiborod, M. *et al.* Glucometrics in Patients Hospitalized With Acute Myocardial Infarction: Defining the Optimal Outcomes-Based Measure of Risk. *Circulation* **117**, 1018–1027 (2008).
17. Stranders, I. *et al.* Admission blood glucose level as risk indicator of death after myocardial infarction in patients with and without diabetes mellitus. *Arch. Intern. Med.* **164**, 982–8 (2004).
18. Stanley, W. C. Myocardial Energy Metabolism During Ischemia and the Mechanisms of Metabolic Therapies. *J. Cardiovasc. Pharmacol. Ther.* **9**, S31–S45 (2004).
19. Meier, P. *et al.* The collateral circulation of the heart. *BMC Med.* **11**, 143 (2013).
20. Messer, J. V. *et al.* PATTERNS OF HUMAN MYOCARDIAL OXYGEN EXTRACTION DURING REST AND EXERCISE*. *J. Clin. Invest.* **41**, 725–742 (1962).

21. Ventura-Clapier, R., Garnier, A., Veksler, V. & Joubert, F. Bioenergetics of the failing heart. *Biochim. Biophys. Acta* **1813**, 1360–72 (2011).
22. Heads, R. J., Latchman, D. S. & Yellon, D. M. The molecular basis of adaptation to ischemia in the heart: the role of stress proteins and antioxidants in the ischemic and reperfused heart. *EXS* **76**, 383–407 (1996).
23. Tahiliani, A. G. & McNeill, J. H. Diabetes-induced abnormalities in the myocardium. *Life Sci.* **38**, 959–74 (1986).
24. Hausenloy, D. J. & Yellon, D. M. Myocardial ischemia-reperfusion injury: a neglected therapeutic target. *J.Clin.Invest* **123**, 92–100 (2013).
25. Bhimji, S., Godin, D. V & McNeill, J. H. Coronary artery ligation and reperfusion in alloxan-diabetic rabbits: ultrastructural and haemodynamic changes. *Br. J. Exp. Pathol.* **67**, 851–63 (1986).
26. Yellon, D. M. & Hausenloy, D. J. Myocardial reperfusion injury. *N. Engl. J. Med.* **357**, 1121–35 (2007).
27. Woodcock, E. A. & Matkovich, S. J. Cardiomyocytes structure, function and associated pathologies. *Int. J. Biochem. Cell Biol.* **37**, 1746–1751 (2005).
28. Di Carlo, S. & Collins, H. Estimating ATP resynthesis during a marathon run: a method to introduce metabolism. *Advan Physiol Educ* **25**, 70–71 (2001).
29. Schramm, M., Klieber, H. G. & Daut, J. The energy expenditure of actomyosin-ATPase, Ca(2+)-ATPase and Na⁺,K(+)-ATPase in guinea-pig cardiac ventricular muscle. *J. Physiol.* **481** (Pt 3, 647–62 (1994).
30. Lopaschuk, G. D., Ussher, J. R., Folmes, C. D. L., Jaswal, J. S. & Stanley, W. C. Myocardial Fatty Acid Metabolism in Health and Disease. *Physiol. Rev.* **90**, 207–258 (2010).
31. *Molecular System Bioenergetics: Energy for Life.* (John Wiley & Sons, 2008).

32. Harvey, R. A. & Ferrier, D. R. *Biochemistry*. (Lippincott Williams & Wilkins, 2011).
33. Pascual, F. & Coleman, R. A. Fuel availability and fate in cardiac metabolism: A tale of two substrates. *Biochim. Biophys. Acta - Mol. Cell Biol. Lipids* **1861**, 1425–1433 (2016).
34. Montessuit, C. & Lerch, R. Regulation and dysregulation of glucose transport in cardiomyocytes. *Biochim. Biophys. Acta - Mol. Cell Res.* **1833**, 848–856 (2013).
35. Wood, I. S. & Trayhurn, P. Glucose transporters (GLUT and SGLT): expanded families of sugar transport proteins. *Br. J. Nutr.* **89**, 3 (2003).
36. Ackerman, S. H. & Tzagoloff, A. Function, Structure, and Biogenesis of Mitochondrial ATP Synthase. in 95–133 (2005). doi:10.1016/S0079-6603(05)80003-0
37. Papa, S. *et al.* The Oxidative Phosphorylation System in Mammalian Mitochondria. in 3–37 (Springer, Dordrecht, 2012). doi:10.1007/978-94-007-2869-1_1
38. MITCHELL, P. Coupling of phosphorylation to electron and hydrogen transfer by a chemi-osmotic type of mechanism. *Nature* **191**, 144–8 (1961).
39. Akhmedov, A. T., Rybin, V. & Marín-García, J. Mitochondrial oxidative metabolism and uncoupling proteins in the failing heart. *Heart Fail. Rev.* **20**, 227–249 (2015).
40. Tait, S. W. G. & Green, D. R. Mitochondria and cell death: outer membrane permeabilization and beyond. *Nat. Rev. Mol. Cell Biol.* **11**, 621–632 (2010).
41. Shamas-Din, A., Kale, J., Leber, B. & Andrews, D. W. Mechanisms of Action of Bcl-2 Family Proteins. *Cold Spring Harb. Perspect. Biol.* **5**, a008714–a008714 (2013).
42. Ponticos, M. *et al.* Dual regulation of the AMP-activated protein kinase

provides a novel mechanism for the control of creatine kinase in skeletal muscle. *EMBO J.* **17**, 1688–99 (1998).

43. Egert, S., Nguyen, N. & Schwaiger, M. Contribution of alpha-adrenergic and beta-adrenergic stimulation to ischemia-induced glucose transporter (GLUT) 4 and GLUT1 translocation in the isolated perfused rat heart. *Circ. Res.* **84**, 1407–15 (1999).
44. Di Franco, A. *et al.* Sodium-dependent glucose transporters (SGLT) in human ischemic heart: A new potential pharmacological target. *Int. J. Cardiol.* **243**, 86–90 (2017).
45. Kalogeris, T., Baines, C. P., Krenz, M. & Korthuis, R. J. Cell biology of ischemia/reperfusion injury. *Int. Rev. Cell Mol. Biol.* **298**, 229–317 (2012).
46. Rouslin, W., Broge, C. W. & Grupp, I. L. ATP depletion and mitochondrial functional loss during ischemia in slow and fast heart-rate hearts. *Am. J. Physiol.* **259**, H1759-66 (1990).
47. Reimer, K. A., Lowe, J. E., Rasmussen, M. M. & Jennings, R. B. The wavefront phenomenon of ischemic cell death. 1. Myocardial infarct size vs duration of coronary occlusion in dogs. *Circulation* **56**, 786–94 (1977).
48. Sinnaeve, P. R. *et al.* Contemporary inter-hospital transfer patterns for the management of acute coronary syndrome patients: Findings from the EPICOR study. *Eur. Hear. J. Acute Cardiovasc. Care* **4**, 254–262 (2015).
49. Zweier, J. L., Flaherty, J. T. & Weisfeldt, M. L. Direct measurement of free radical generation following reperfusion of ischemic myocardium. *Proc. Natl. Acad. Sci. U.S.A* **84**, 1404–1407 (1987).
50. Piper, H. M., García-Dorado, D. & Ovize, M. A fresh look at reperfusion injury. *Cardiovasc. Res.* **38**, 291–300 (1998).
51. Lemasters, J. J. *et al.* The pH paradox in ischemia-reperfusion injury to cardiac myocytes. *EXS* **76**, 99–114 (1996).
52. Vinten-Johansen, J. Involvement of neutrophils in the pathogenesis of lethal myocardial reperfusion injury. *Cardiovasc. Res.* **61**, 481–497

- (2004).
53. Staat, P. *et al.* Postconditioning the human heart. *Circulation* **112**, 2143–8 (2005).
 54. Schäfer, C., Ladilov, Y. V, Siegmund, B. & Piper, H. M. Importance of bicarbonate transport for protection of cardiomyocytes against reoxygenation injury. *Am. J. Physiol. Heart Circ. Physiol.* **278**, H1457-63 (2000).
 55. Murphy, E. & Steenbergen, C. Mechanisms underlying acute protection from cardiac ischemia-reperfusion injury. *Physiol. Rev.* **88**, 581–609 (2008).
 56. Chistiakov, D. A., Sobenin, I. A., Revin, V. V., Orekhov, A. N. & Bobryshev, Y. V. Mitochondrial Aging and Age-Related Dysfunction of Mitochondria. *Biomed Res. Int.* **2014**, 1–7 (2014).
 57. McCord, J. M. & McCord, J. M. Oxygen-derived free radicals in postischemic tissue injury. *N. Engl. J. Med.* **312**, 159–63 (1985).
 58. Guarnieri, C., Flamigni, F. & Caldarera, C. M. Role of oxygen in the cellular damage induced by re-oxygenation of hypoxic heart. *J. Mol. Cell. Cardiol.* **12**, 797–808 (1980).
 59. Schäfer, C. Role of the reverse mode of the Na⁺/Ca²⁺ exchanger in reoxygenation-induced cardiomyocyte injury. *Cardiovasc. Res.* **51**, 241–250 (2001).
 60. Ong, S.-B., Dongworth, R. K., Cabrera-Fuentes, H. A. & Hausenloy, D. J. Role of the MPTP in conditioning the heart - translatability and mechanism. *Br. J. Pharmacol.* **172**, 2074–2084 (2015).
 61. Halestrap, A. P. & Richardson, A. P. The mitochondrial permeability transition: A current perspective on its identity and role in ischaemia/reperfusion injury. *J. Mol. Cell. Cardiol.* **78**, 129–141 (2015).
 62. De Giorgi, F. *et al.* The permeability transition pore signals apoptosis by directing Bax translocation and multimerization. *FASEB J.* **16**, 607–9

(2002).

63. Di Lisa, F. & Bernardi, P. A CaPful of mechanisms regulating the mitochondrial permeability transition. *J. Mol. Cell. Cardiol.* **46**, 775–80 (2009).
64. Bhamra, G. S. *et al.* Metformin protects the ischemic heart by the Akt-mediated inhibition of mitochondrial permeability transition pore opening. *Basic Res. Cardiol.* **103**, 274–84 (2008).
65. Shanmuganathan, S., Hausenloy, D. J., Duchon, M. R. & Yellon, D. M. Mitochondrial permeability transition pore as a target for cardioprotection in the human heart. *Am. J. Physiol. Heart Circ. Physiol.* **289**, H237-42 (2005).
66. Bratton, S. B. & Salvesen, G. S. Regulation of the Apaf-1-caspase-9 apoptosome. *J. Cell Sci.* **123**, 3209–3214 (2010).
67. Salvesen, G. S. & Riedl, S. J. Caspase Mechanisms. in *Advances in experimental medicine and biology* **615**, 13–23 (2008).
68. Green, D. R. & Llambi, F. Cell Death Signaling. *Cold Spring Harb. Perspect. Biol.* **7**, a006080 (2015).
69. Jost, P. J. *et al.* XIAP discriminates between type I and type II FAS-induced apoptosis. *Nature* **460**, 1035–1039 (2009).
70. Galluzzi, L. *et al.* Molecular mechanisms of cell death: recommendations of the Nomenclature Committee on Cell Death 2018. *Cell Death Differ.* **25**, 486–541 (2018).
71. Murphy, J. M. *et al.* The Pseudokinase MLKL Mediates Necroptosis via a Molecular Switch Mechanism. *Immunity* **39**, 443–453 (2013).
72. Murry, C. E., Richard, V. J., Reimer, K. A. & Jennings, R. B. Ischemic preconditioning slows energy metabolism and delays ultrastructural damage during a sustained ischemic episode. *Circ. Res.* **66**, 913–31 (1990).

73. Tan, H. L. *et al.* Ischaemic preconditioning delays ischaemia induced cellular electrical uncoupling in rabbit myocardium by activation of ATP sensitive potassium channels. *Cardiovasc. Res.* **27**, 644–51 (1993).
74. Crestanello, J. A., Lingle, D. M., Kamelgard, J., Millili, J. & Whitman, G. J. R. Ischemic Preconditioning Decreases Oxidative Stress during Reperfusion: A Chemiluminescence Study. *J. Surg. Res.* **65**, 53–58 (1996).
75. Maulik, A., Davidson, S. M., Piotrowska, I., Walker, M. & Yellon, D. M. Ischaemic Preconditioning Protects Cardiomyocytes from Anthracycline-Induced Toxicity via the PI3K Pathway. *Cardiovasc. Drugs Ther.* (2018). doi:10.1007/s10557-018-6793-y
76. Shanmuganathan, S., Hausenloy, D. J., Duchon, M. R. & Yellon, D. M. Mitochondrial permeability transition pore as a target for cardioprotection in the human heart. *AJP Hear. Circ. Physiol.* **289**, H237–H242 (2005).
77. Schulman, D., Latchman, D. S. & Yellon, D. M. Urocortin protects the heart from reperfusion injury via upregulation of p42/p44 MAPK signaling pathway. *Am. J. Physiol. Circ. Physiol.* **283**, H1481–H1488 (2002).
78. Baxter, G. F., Mocanu, M. M., Brar, B. K., Latchman, D. S. & Yellon, D. M. Cardioprotective effects of transforming growth factor-beta1 during early reoxygenation or reperfusion are mediated by p42/p44 MAPK. *J. Cardiovasc. Pharmacol.* **38**, 930–9 (2001).
79. Bell, R. M. & Yellon, D. M. Atorvastatin, administered at the onset of reperfusion, and independent of lipid lowering, protects the myocardium by up-regulating a pro-survival pathway. *J. Am. Coll. Cardiol.* **41**, 508–15 (2003).
80. Jonassen, A. K., Sack, M. N., Mjøs, O. D. & Yellon, D. M. Myocardial protection by insulin at reperfusion requires early administration and is mediated via Akt and p70s6 kinase cell-survival signaling. *Circ. Res.* **89**, 1191–8 (2001).
81. Párrizas, M., Saltiel, A. R. & LeRoith, D. Insulin-like growth factor 1

- inhibits apoptosis using the phosphatidylinositol 3'-kinase and mitogen-activated protein kinase pathways. *J. Biol. Chem.* **272**, 154–61 (1997).
82. Bell, R. M. & Yellon, D. M. Bradykinin limits infarction when administered as an adjunct to reperfusion in mouse heart: the role of PI3K, Akt and eNOS. *J. Mol. Cell. Cardiol.* **35**, 185–93 (2003).
 83. Maddock, H. L., Mocanu, M. M. & Yellon, D. M. Adenosine A₃ receptor activation protects the myocardium from reperfusion/reoxygenation injury. *Am. J. Physiol. Circ. Physiol.* **283**, H1307–H1313 (2002).
 84. Schulte, G. & Fredholm, B. B. Human adenosine A(1), A(2A), A(2B), and A(3) receptors expressed in Chinese hamster ovary cells all mediate the phosphorylation of extracellular-regulated kinase 1/2. *Mol. Pharmacol.* **58**, 477–82 (2000).
 85. Ovize, M. *et al.* Postconditioning and protection from reperfusion injury: where do we stand? Position paper from the Working Group of Cellular Biology of the Heart of the European Society of Cardiology. *Cardiovasc. Res.* **87**, 406–23 (2010).
 86. Hausenloy, D. J. & Yellon, D. M. New directions for protecting the heart against ischaemia-reperfusion injury: targeting the Reperfusion Injury Salvage Kinase (RISK)-pathway. *Cardiovasc. Res.* **61**, 448–60 (2004).
 87. Yamaguchi, H. & Wang, H.-G. The protein kinase PKB/Akt regulates cell survival and apoptosis by inhibiting Bax conformational change. *Oncogene* **20**, 7779–7786 (2001).
 88. Tsuruta, F., Masuyama, N. & Gotoh, Y. The Phosphatidylinositol 3-Kinase (PI3K)-Akt Pathway Suppresses Bax Translocation to Mitochondria. *J. Biol. Chem.* **277**, 14040–14047 (2002).
 89. Lecour, S. *et al.* Pharmacological Preconditioning With Tumor Necrosis Factor- Activates Signal Transducer and Activator of Transcription-3 at Reperfusion Without Involving Classic Prosurvival Kinases (Akt and Extracellular Signal-Regulated Kinase). *Circulation* **112**, 3911–3918 (2005).

90. Tamarelle, S. *et al.* RISK and SAFE signaling pathway interactions in remote limb ischemic preconditioning in combination with local ischemic postconditioning. *Basic Res. Cardiol.* **106**, 1329–39 (2011).
91. Lacerda, L., Somers, S., Opie, L. H. & Lecour, S. Ischaemic postconditioning protects against reperfusion injury via the SAFE pathway. *Cardiovasc. Res.* **84**, 201–208 (2009).
92. Goodman, M. D., Koch, S. E., Fuller-Bicer, G. A. & Butler, K. L. Regulating RISK: a role for JAK-STAT signaling in postconditioning? *Am. J. Physiol. Heart Circ. Physiol.* **295**, H1649-56 (2008).
93. Perrelli, M.-G., Pagliaro, P. & Penna, C. Ischemia/reperfusion injury and cardioprotective mechanisms: Role of mitochondria and reactive oxygen species. *World J. Cardiol.* **3**, 186–200 (2011).
94. Schaper, J. & Schaper, W. Reperfusion Of Ischemic Myocardium: Ultrastructural and Histochemical Aspects. *J AM COLL CARDIOL* **10371**, 1037–46 (1983).
95. Cardone, M. H. *et al.* Regulation of Cell Death Protease Caspase-9 by Phosphorylation. *Science (80-.)*. **282**, 1318–1321 (1998).
96. Datta, S. R. *et al.* Akt phosphorylation of BAD couples survival signals to the cell-intrinsic death machinery. *Cell* **91**, 231–41 (1997).
97. Datta, S. R. *et al.* Survival factor-mediated BAD phosphorylation raises the mitochondrial threshold for apoptosis. *Dev. Cell* **3**, 631–43 (2002).
98. Brunet, A. *et al.* Akt promotes cell survival by phosphorylating and inhibiting a Forkhead transcription factor. *Cell* **96**, 857–68 (1999).
99. Cross, D. A. E., Alessi, D. R., Cohen, P., Andjelkovich, M. & Hemmings, B. A. Inhibition of glycogen synthase kinase-3 by insulin mediated by protein kinase B. *Nature* **378**, 785–789 (1995).
100. Maurer, U., Charvet, C., Wagman, A. S., Dejardin, E. & Green, D. R. Glycogen Synthase Kinase-3 Regulates Mitochondrial Outer Membrane Permeabilization and Apoptosis by Destabilization of MCL-1. *Mol. Cell* **21**,

749–760 (2006).

101. Manning, B. D. & Cantley, L. C. AKT/PKB signaling: navigating downstream. *Cell* **129**, 1261–74 (2007).
102. Tian, Y. *et al.* Postconditioning inhibits myocardial apoptosis during prolonged reperfusion via a JAK2-STAT3-Bcl-2 pathway. *J. Biomed. Sci.* **18**, 53 (2011).
103. La Fortezza, M. *et al.* JAK/STAT signalling mediates cell survival in response to tissue stress. *Development* **143**, 2907–2919 (2016).
104. Murry, C. E., Jennings, R. B. & Reimer, K. A. Preconditioning with ischemia: a delay of lethal cell injury in ischemic myocardium. *Circulation* **74**, 1124–36 (1986).
105. Wever, K. E. *et al.* Determinants of the Efficacy of Cardiac Ischemic Preconditioning: A Systematic Review and Meta-Analysis of Animal Studies. *PLoS One* **10**, e0142021 (2015).
106. Mocanu, M. M., Bell, R. M. & Yellon, D. M. PI3 kinase and not p42/p44 appears to be implicated in the protection conferred by ischemic preconditioning. *J. Mol. Cell. Cardiol.* **34**, 661–8 (2002).
107. Tong, H., Chen, W., Steenbergen, C. & Murphy, E. Ischemic preconditioning activates phosphatidylinositol-3-kinase upstream of protein kinase C. *Circ. Res.* **87**, 309–15 (2000).
108. Hausenloy, D. J., Tsang, A., Mocanu, M. M. & Yellon, D. M. Ischemic preconditioning protects by activating prosurvival kinases at reperfusion. *Am. J. Physiol. Heart Circ. Physiol.* **288**, H971-6 (2005).
109. Kositprapa, C., Ockaili, R. A. & Kukreja, R. C. Bradykinin B2Receptor is Involved in the Late Phase of Preconditioning in Rabbit Heart. *J. Mol. Cell. Cardiol.* **33**, 1355–1362 (2001).
110. Schultz, J. E., Hsu, A. K. & Gross, G. J. Ischemic preconditioning in the intact rat heart is mediated by delta1- but not mu- or kappa-opioid receptors. *Circulation* **97**, 1282–9 (1998).

111. Liu, G. S. *et al.* Evidence that the adenosine A3 receptor may mediate the protection afforded by preconditioning in the isolated rabbit heart. *Cardiovasc. Res.* **28**, 1057–1061 (1994).
112. Liu, G. S. *et al.* Protection against infarction afforded by preconditioning is mediated by A1 adenosine receptors in rabbit heart. *Circulation* **84**, 350–6 (1991).
113. Hausenloy, D., Wynne, A., Duchon, M. & Yellon, D. Transient mitochondrial permeability transition pore opening mediates preconditioning-induced protection. *Circulation* **109**, 1714–7 (2004).
114. Speechly-Dick, M. E., Mocanu, M. M. & Yellon, D. M. Protein kinase C. Its role in ischemic preconditioning in the rat. *Circ. Res.* **75**, 586–90 (1994).
115. Liu, Y. & Downey, J. M. Ischemic preconditioning protects against infarction in rat heart. *Am. J. Physiol.* **263**, H1107-12 (1992).
116. Przyklenk, K., Bauer, B., Ovize, M., Kloner, R. A. & Whittaker, P. Regional ischemic 'preconditioning' protects remote virgin myocardium from subsequent sustained coronary occlusion. *Circulation* **87**, 893–9 (1993).
117. Kharbanda, R. K. *et al.* Transient limb ischemia induces remote ischemic preconditioning in vivo. *Circulation* **106**, 2881–3 (2002).
118. Schmidt, M. R. *et al.* Intermittent peripheral tissue ischemia during coronary ischemia reduces myocardial infarction through a KATP-dependent mechanism: first demonstration of remote ischemic preconditioning. *Am. J. Physiol. Heart Circ. Physiol.* **292**, H1883-90 (2007).
119. Bromage, D. I. *et al.* Remote ischaemic conditioning reduces infarct size in animal in vivo models of ischaemia-reperfusion injury: a systematic review and meta-analysis. *Cardiovasc. Res.* **113**, 288–297 (2017).
120. Gidday, J. M., Fitzgibbons, J. C., Shah, A. R. & Park, T. S. Neuroprotection from ischemic brain injury by hypoxic preconditioning in the neonatal rat. *Neurosci. Lett.* **168**, 221–4 (1994).

121. Kume, M. *et al.* Ischemic preconditioning of the liver in rats: implications of heat shock protein induction to increase tolerance of ischemia-reperfusion injury. *J. Lab. Clin. Med.* **128**, 251–8 (1996).
122. Islam, C. F. *et al.* Ischaemia-reperfusion injury in the rat kidney: the effect of preconditioning. *Br. J. Urol.* **79**, 842–7 (1997).
123. Pang, C. Y. *et al.* Acute ischaemic preconditioning protects against skeletal muscle infarction in the pig. *Cardiovasc. Res.* **29**, 782–8 (1995).
124. Zahir, K. S., Syed, S. A., Zink, J. R., Restifo, R. J. & Thomson, J. G. Ischemic preconditioning improves the survival of skin and myocutaneous flaps in a rat model. *Plast. Reconstr. Surg.* **102**, 140–50; discussion 151-2 (1998).
125. Serejo, F. C., Rodrigues, L. F., da Silva Tavares, K. C., de Carvalho, A. C. C. & Nascimento, J. H. M. Cardioprotective properties of humoral factors released from rat hearts subject to ischemic preconditioning. *J. Cardiovasc. Pharmacol.* **49**, 214–20 (2007).
126. Shimizu, M. *et al.* Transient limb ischaemia remotely preconditions through a humoral mechanism acting directly on the myocardium: evidence suggesting cross-species protection. *Clin. Sci. (Lond).* **117**, 191–200 (2009).
127. Breivik, L., Helgeland, E., Aarnes, E. K., Mrdalj, J. & Jonassen, A. K. Remote postconditioning by humoral factors in effluent from ischemic preconditioned rat hearts is mediated via PI3K/Akt-dependent cell-survival signaling at reperfusion. *Basic Res. Cardiol.* **106**, 135–45 (2011).
128. Pickard, J. M. J., Davidson, S. M., Hausenloy, D. J. & Yellon, D. M. Co-dependence of the neural and humoral pathways in the mechanism of remote ischemic conditioning. *Basic Res. Cardiol.* **111**, 50 (2016).
129. Heusch, G., Bøtker, H. E., Przyklenk, K., Redington, A. & Yellon, D. Remote Ischemic Conditioning. *J. Am. Coll. Cardiol.* **65**, 177–195 (2015).
130. Leung, C. H. *et al.* Remote Cardioprotection by Transfer of Coronary

Effluent from Ischemic Preconditioned Rabbit Heart Preserves Mitochondrial Integrity and Function via Adenosine Receptor Activation. *Cardiovasc. Drugs Ther.* **28**, 7–17 (2014).

131. Surendra, H. *et al.* Interaction of δ and κ opioid receptors with adenosine A1 receptors mediates cardioprotection by remote ischemic preconditioning. *J. Mol. Cell. Cardiol.* **60**, 142–150 (2013).
132. Davidson, S. M. *et al.* Remote ischaemic preconditioning involves signalling through the SDF-1alpha/CXCR4 signalling axis. *Basic Res. Cardiol.* **108**, 377 (2013).
133. Jones, W. K. *et al.* Peripheral nociception associated with surgical incision elicits remote nonischemic cardioprotection via neurogenic activation of protein kinase C signaling. *Circulation* **120**, S1-9 (2009).
134. Hausenloy, D. J. *et al.* Investigating the Signal Transduction Pathways Underlying Remote Ischemic Conditioning in the Porcine Heart. *Cardiovasc. Drugs Ther.* **26**, 87–93 (2012).
135. Xin, P. *et al.* Combined local ischemic postconditioning and remote preconditioning recapitulate cardioprotective effects of local ischemic preconditioning. *Am. J. Physiol. Circ. Physiol.* **298**, H1819–H1831 (2010).
136. Bromage, D. I. *et al.* Remote ischaemic conditioning reduces infarct size in animal *in vivo* models of ischaemia-reperfusion injury: a systematic review and meta-analysis. *Cardiovasc. Res.* **113**, cvw219 (2016).
137. Le Page, S., Bejan-Angoulvant, T., Angoulvant, D. & Prunier, F. Remote ischemic conditioning and cardioprotection: a systematic review and meta-analysis of randomized clinical trials. *Basic Res. Cardiol.* **110**, 11 (2015).
138. Brevoord, D. *et al.* Remote ischemic conditioning to protect against ischemia-reperfusion injury: a systematic review and meta-analysis. *PLoS One* **7**, e42179 (2012).
139. Blusztein, D. I., Brooks, M. J. & Andrews, D. T. A systematic review and

- meta-analysis evaluating ischemic conditioning during percutaneous coronary intervention. *Future Cardiol.* **13**, 579–592 (2017).
140. Eitel, I. *et al.* Cardioprotection by combined intrahospital remote ischaemic preconditioning and postconditioning in ST-elevation myocardial infarction: the randomized LIPSIA CONDITIONING trial. *Eur. Heart J.* **36**, 3049–3057 (2015).
141. Touboul, C. *et al.* Ischaemic postconditioning reduces infarct size: Systematic review and meta-analysis of randomized controlled trials. *Arch. Cardiovasc. Dis.* **108**, 39–49 (2015).
142. Hausenloy, D. J. *et al.* Effect of remote ischemic preconditioning on clinical outcomes in patients undergoing coronary artery bypass graft surgery (ERICCA): rationale and study design of a multi-centre randomized double-blinded controlled clinical trial. *Clin. Res. Cardiol.* **101**, 339–348 (2012).
143. White, S. K. *et al.* Remote Ischemic Conditioning Reduces Myocardial Infarct Size and Edema in Patients With ST-Segment Elevation Myocardial Infarction. *JACC Cardiovasc. Interv.* **8**, 178–188 (2015).
144. Whittaker, P. & Przyklenk, K. Reduction of infarct size in vivo with ischemic preconditioning: mathematical evidence for protection via non-ischemic tissue. *Basic Res. Cardiol.* **89**, 6–15 (1994).
145. Przyklenk, K. Ischaemic conditioning: pitfalls on the path to clinical translation. *Br. J. Pharmacol.* **172**, 1961–73 (2015).
146. Schulman, D., Latchman, D. S. & Yellon, D. M. Effect of aging on the ability of preconditioning to protect rat hearts from ischemia-reperfusion injury. *Am. J. Physiol. Circ. Physiol.* **281**, H1630–H1636 (2001).
147. Tsang, A., Hausenloy, D. J., Mocanu, M. M., Carr, R. D. & Yellon, D. M. Preconditioning the diabetic heart: the importance of Akt phosphorylation. *Diabetes* **54**, 2360–2364 (2005).
148. Wider, J. & Przyklenk, K. Ischemic conditioning: the challenge of

- protecting the diabetic heart. *Cardiovasc. Diagn. Ther.* **4**, 383–96 (2014).
149. Qazi, M. U. & Malik, S. Diabetes and Cardiovascular Disease: Original Insights from the Framingham Heart Study. *Glob. Heart* **8**, 43–48 (2013).
 150. Kannel, W. B. & McGee, D. L. Diabetes and cardiovascular disease. The Framingham study. *JAMA* **241**, 2035–8 (1979).
 151. MacDonald, M. R. *et al.* Impact of diabetes on outcomes in patients with low and preserved ejection fraction heart failure: An analysis of the Candesartan in Heart failure: Assessment of Reduction in Mortality and morbidity (CHARM) programme. *Eur. Heart J.* **29**, 1377–1385 (2008).
 152. Nesto, R. W. & Singh, P. P. Diabetes and residual risk of coronary heart disease. *Nat. Clin. Pract. Endocrinol. Metab.* **3**, 71–71 (2007).
 153. Lewis, G. F., Carpentier, A., Adeli, K. & Giacca, A. Disordered Fat Storage and Mobilization in the Pathogenesis of Insulin Resistance and Type 2 Diabetes. *Endocr. Rev.* **23**, 201–229 (2002).
 154. Bayeva, M., Sawicki, K. T. & Ardehali, H. Taking diabetes to heart--deregulation of myocardial lipid metabolism in diabetic cardiomyopathy. *J. Am. Heart Assoc.* **2**, e000433 (2013).
 155. Rijzewijk, L. J. *et al.* Altered Myocardial Substrate Metabolism and Decreased Diastolic Function in Nonischemic Human Diabetic Cardiomyopathy. *J. Am. Coll. Cardiol.* **54**, 1524–1532 (2009).
 156. Ferré, P. The biology of peroxisome proliferator-activated receptors: relationship with lipid metabolism and insulin sensitivity. *Diabetes* **53 Suppl 1**, S43-50 (2004).
 157. Cha, D. R. *et al.* Peroxisome proliferator-activated receptor-alpha deficiency protects aged mice from insulin resistance induced by high-fat diet. *Am. J. Nephrol.* **27**, 479–82 (2007).
 158. Amaral, N. & Okonko, D. O. Metabolic abnormalities of the heart in type II diabetes. *Diabetes Vasc. Dis. Res.* **12**, 239–248 (2015).

159. Newsholme, P. *et al.* Diabetes associated cell stress and dysfunction: role of mitochondrial and non-mitochondrial ROS production and activity. *J. Physiol.* **583**, 9–24 (2007).
160. Utriainen, T. *et al.* Insulin resistance characterizes glucose uptake in skeletal muscle but not in the heart in NIDDM. *Diabetologia* **41**, 555–559 (1998).
161. Ma, H. *et al.* Advanced glycation endproduct (AGE) accumulation and AGE receptor (RAGE) up-regulation contribute to the onset of diabetic cardiomyopathy. *J. Cell. Mol. Med.* **13**, 1751–1764 (2009).
162. Boudina, S. *et al.* Mitochondrial energetics in the heart in obesity-related diabetes: direct evidence for increased uncoupled respiration and activation of uncoupling proteins. *Diabetes* **56**, 2457–66 (2007).
163. Croston, T. L. *et al.* Functional deficiencies of subsarcolemmal mitochondria in the type 2 diabetic human heart. *Am. J. Physiol. Heart Circ. Physiol.* **307**, H54-65 (2014).
164. How, O.-J. *et al.* Increased myocardial oxygen consumption reduces cardiac efficiency in diabetic mice. *Diabetes* **55**, 466–73 (2006).
165. Russo, I. & Frangogiannis, N. G. Diabetes-associated cardiac fibrosis: Cellular effectors, molecular mechanisms and therapeutic opportunities. *J. Mol. Cell. Cardiol.* **90**, 84–93 (2016).
166. Regan, T. J. *et al.* Evidence for Cardiomyopathy in Familial Diabetes Mellitus. *J. Clin. Invest.* **60**, 885–899 (1977).
167. Candido, R. *et al.* A breaker of advanced glycation end products attenuates diabetes-induced myocardial structural changes. *Circ. Res.* **92**, 785–92 (2003).
168. Kim, R. J. *et al.* Relationship of MRI delayed contrast enhancement to irreversible injury, infarct age, and contractile function. *Circulation* **100**, 1992–2002 (1999).
169. Jellis, C., Martin, J., Narula, J. & Marwick, T. H. Assessment of

- Nonischemic Myocardial Fibrosis. *J. Am. Coll. Cardiol.* **56**, 89–97 (2010).
170. Sutherland, C. G. *et al.* Endomyocardial biopsy pathology in insulin-dependent diabetic patients with abnormal ventricular function. *Histopathology* **14**, 593–602 (1989).
171. Fein, F. S. & Sonnenblick, E. H. Diabetic cardiomyopathy. *Prog. Cardiovasc. Dis.* **27**, 255–70 (1985).
172. Sedgwick, B. *et al.* Investigating inherent functional differences between human cardiac fibroblasts cultured from nondiabetic and Type 2 diabetic donors. *Cardiovasc. Pathol.* **23**, 204–210 (2014).
173. Hutchinson, K. R., Lord, C. K., West, T. A. & Stewart, J. A. Cardiac Fibroblast-Dependent Extracellular Matrix Accumulation Is Associated with Diastolic Stiffness in Type 2 Diabetes. *PLoS One* **8**, e72080 (2013).
174. Fowlkes, V. *et al.* Type II diabetes promotes a myofibroblast phenotype in cardiac fibroblasts. *Life Sci.* **92**, 669–676 (2013).
175. Singh, V. P., Baker, K. M. & Kumar, R. Activation of the intracellular renin-angiotensin system in cardiac fibroblasts by high glucose: role in extracellular matrix production. *AJP Hear. Circ. Physiol.* **294**, H1675–H1684 (2008).
176. Fiaschi, T. *et al.* Hyperglycemia and angiotensin II cooperate to enhance collagen I deposition by cardiac fibroblasts through a ROS-STAT3-dependent mechanism. *Biochim. Biophys. Acta - Mol. Cell Res.* **1843**, 2603–2610 (2014).
177. Tang, M. *et al.* High glucose promotes the production of collagen types I and III by cardiac fibroblasts through a pathway dependent on extracellular-signal-regulated kinase 1/2. *Mol. Cell. Biochem.* **301**, 109–114 (2007).
178. Han, D. C., Isono, M., Hoffman, B. B. & Ziyadeh, F. N. High glucose stimulates proliferation and collagen type I synthesis in renal cortical fibroblasts: mediation by autocrine activation of TGF-beta. *J. Am. Soc.*

Nephrol. **10**, 1891–9 (1999).

179. Zorzano, A., Liesa, M. & Palacín, M. Role of mitochondrial dynamics proteins in the pathophysiology of obesity and type 2 diabetes. *Int. J. Biochem. Cell Biol.* **41**, 1846–54 (2009).
180. Nunes, S., Rolo, A. P., Palmeira, C. M. & Reis, F. Diabetic Cardiomyopathy: Focus on Oxidative Stress, Mitochondrial Dysfunction and Inflammation. in *Cardiomyopathies - Types and Treatments* (InTech, 2017). doi:10.5772/65915
181. Poirier, P., Bogaty, P., Garneau, C., Marois, L. & Dumesnil, J. G. Diastolic dysfunction in normotensive men with well-controlled type 2 diabetes: importance of maneuvers in echocardiographic screening for preclinical diabetic cardiomyopathy. *Diabetes Care* **24**, 5–10 (2001).
182. Mathew, P., John, L., Jose, J. & Krishnaswami, S. Assessment of left ventricular diastolic function in young diabetics--a two dimensional echo Doppler study. *Indian Heart J.* **44**, 29–32 (1992).
183. Petrova, R. *et al.* Advanced glycation endproduct-induced calcium handling impairment in mouse cardiac myocytes. *J. Mol. Cell. Cardiol.* **34**, 1425–31 (2002).
184. Brownlee, M. Advanced protein glycosylation in diabetes and aging. *Annu. Rev. Med.* **46**, 223–34 (1995).
185. Astorri, E. *et al.* Isolated and preclinical impairment of left ventricular filling in insulin-dependent and non-insulin-dependent diabetic patients. *Clin. Cardiol.* **20**, 536–40 (1997).
186. Fang, Z. Y. *et al.* Echocardiographic detection of early diabetic myocardial disease. *J. Am. Coll. Cardiol.* **41**, 611–7 (2003).
187. Friedman, N. E. *et al.* Echocardiographic evidence for impaired myocardial performance in children with type I diabetes mellitus. *Am. J. Med.* **73**, 846–50 (1982).
188. Baum, V. C., Levitsky, L. L. & Englander, R. M. Abnormal cardiac function

- after exercise in insulin-dependent diabetic children and adolescents. *Diabetes Care* **10**, 319–23 (1987).
189. Vered, A. *et al.* Exercise-induced left ventricular dysfunction in young men with asymptomatic diabetes mellitus (diabetic cardiomyopathy). *Am. J. Cardiol.* **54**, 633–7 (1984).
190. Scognamiglio, R., Casara, D. & Avogaro, A. Myocardial dysfunction and adrenergic innervation in patients with Type 1 diabetes mellitus. *Diabetes. Nutr. Metab.* **13**, 346–9 (2000).
191. Fang, Z. Y., Prins, J. B. & Marwick, T. H. Diabetic cardiomyopathy: evidence, mechanisms, and therapeutic implications. *Endocr.Rev.* **25**, 543–567 (2004).
192. Yaras, N. *et al.* Effects of diabetes on ryanodine receptor Ca release channel (RyR2) and Ca²⁺ homeostasis in rat heart. *Diabetes* **54**, 3082–8 (2005).
193. Tian, C. *et al.* Reactive carbonyl species and their roles in sarcoplasmic reticulum Ca²⁺ cycling defect in the diabetic heart. *Heart Fail. Rev.* **19**, 101–112 (2014).
194. Vinik, A. I. & Ziegler, D. Diabetic Cardiovascular Autonomic Neuropathy. *Circulation* **115**, 387–397 (2007).
195. Pop-Busui, R. *et al.* Sympathetic dysfunction in type 1 diabetes. *J. Am. Coll. Cardiol.* **44**, 2368–2374 (2004).
196. Stevens, M. J. *et al.* Cardiac sympathetic dysinnervation in diabetes: implications for enhanced cardiovascular risk. *Circulation* **98**, 961–8 (1998).
197. Balcioğlu, A. S. & Müderrisoğlu, H. Diabetes and cardiac autonomic neuropathy: Clinical manifestations, cardiovascular consequences, diagnosis and treatment. *World J. Diabetes* **6**, 80–91 (2015).
198. Cardoso, C. R. L., Salles, G. F. & Deccache, W. Prognostic value of QT interval parameters in type 2 diabetes mellitus: results of a long-term

follow-up prospective study. *J. Diabetes Complications* **17**, 169–78 (2003).

199. Megherbi, S.-E. *et al.* Association between diabetes and stroke subtype on survival and functional outcome 3 months after stroke: data from the European BIOMED Stroke Project. *Stroke* **34**, 688–94 (2003).
200. Freisinger, E., Malyar, N. M., Reinecke, H. & Lawall, H. Impact of diabetes on outcome in critical limb ischemia with tissue loss: a large-scaled routine data analysis. *Cardiovasc. Diabetol.* **16**, 41 (2017).
201. De Luca, G. *et al.* Effect of diabetes on scintigraphic infarct size in STEMI patients undergoing primary angioplasty. *Diabetes. Metab. Res. Rev.* **31**, 322–328 (2015).
202. Marso, S. P. *et al.* Comparison of Myocardial Reperfusion in Patients Undergoing Percutaneous Coronary Intervention in ST-Segment Elevation Acute Myocardial Infarction With Versus Without Diabetes Mellitus (from the EMERALD Trial). *Am. J. Cardiol.* **100**, 206–210 (2007).
203. Alegria, J. R. *et al.* Infarct size, ejection fraction, and mortality in diabetic patients with acute myocardial infarction treated with thrombolytic therapy. *Am. Heart J.* **154**, 743–750 (2007).
204. Mather, A. N. *et al.* Relationship of dysglycemia to acute myocardial infarct size and cardiovascular outcome as determined by cardiovascular magnetic resonance. *J. Cardiovasc. Magn. Reson.* **12**, 61 (2010).
205. LEHTO, S. *et al.* Myocardial infarct size and mortality in patients with non-insulin-dependent diabetes mellitus. *J. Intern. Med.* **236**, 291–297 (1994).
206. Cubbon, R. M. *et al.* Diabetes Mellitus and Mortality after Acute Coronary Syndrome as a First or Recurrent Cardiovascular Event. *PLoS One* **3**, e3483 (2008).
207. Prasad, A. *et al.* Impact of diabetes mellitus on myocardial perfusion after primary angioplasty in patients with acute myocardial infarction. *J. Am. Coll. Cardiol.* **45**, 508–514 (2005).

208. Malviya, A. & Mishra, A. Coronary intervention in diabetes: is it different. *Heart Asia* **7**, 9–14 (2015).
209. Jensen, L. O. *et al.* Influence of Diabetes Mellitus on Clinical Outcomes Following Primary Percutaneous Coronary Intervention in Patients With ST-Segment Elevation Myocardial Infarction. *Am. J. Cardiol.* **109**, 629–635 (2012).
210. Harjai, K. J. *et al.* Comparison of outcomes of diabetic and nondiabetic patients undergoing primary angioplasty for acute myocardial infarction. *Am. J. Cardiol.* **91**, 1041–5 (2003).
211. Angeja, B. G. *et al.* Impact of diabetes mellitus on epicardial and microvascular flow after fibrinolytic therapy. *Am. Heart J.* **144**, 649–56 (2002).
212. Frangogiannis, N. G. The inflammatory response in myocardial injury, repair, and remodelling. *Nat. Rev. Cardiol.* **11**, 255–65 (2014).
213. Andrassy, M. *et al.* High-Mobility Group Box-1 in Ischemia-Reperfusion Injury of the Heart. *Circulation* **117**, 3216–3226 (2008).
214. Fullerton, J. N., O'Brien, A. J. & Gilroy, D. W. Pathways mediating resolution of inflammation: when enough is too much. *J. Pathol.* **231**, 8–20 (2013).
215. Libby, P., Nahrendorf, M. & Swirski, F. K. Monocyte heterogeneity in cardiovascular disease. *Semin. Immunopathol.* **35**, 553–562 (2013).
216. Frangogiannis, N. G. The Reparative Function of Cardiomyocytes in the Infarcted Myocardium. *Cell Metab.* **21**, 797–798 (2015).
217. de Lemos, J. A. *et al.* Serial Measurement of Monocyte Chemoattractant Protein-1 After Acute Coronary Syndromes. *J. Am. Coll. Cardiol.* **50**, 2117–2124 (2007).
218. Tschöpe, C. *et al.* Transgenic activation of the kallikrein-kinin system inhibits intramyocardial inflammation, endothelial dysfunction and oxidative stress in experimental diabetic cardiomyopathy. *FASEB J.* **19**,

2057–2059 (2005).

219. Rajesh, M., Mukhopadhyay, P., ... S. B.-J. of cellular & 2009, undefined. Xanthine oxidase inhibitor allopurinol attenuates the development of diabetic cardiomyopathy. *Wiley Online Libr.*
220. Rajesh, M., Bátkai, S., Kechrid, M., Diabetes, P. M.- & 2012, undefined. Cannabinoid 1 receptor promotes cardiac dysfunction, oxidative stress, inflammation, and fibrosis in diabetic cardiomyopathy. *Am Diabetes Assoc*
221. Rajesh, M., Mukhopadhyay, P., ... S. B.-J. of the & 2010, undefined. Cannabidiol attenuates cardiac dysfunction, oxidative stress, fibrosis, and inflammatory and cell death signaling pathways in diabetic cardiomyopathy. *onlinejacc.org*
222. Hsueh, W. A., Lyon, C. J. & Quiñones, M. J. Insulin resistance and the endothelium. *Am. J. Med.* **117**, 109–17 (2004).
223. Moberly, S. P. *et al.* Impaired cardiometabolic responses to glucagon-like peptide 1 in obesity and type 2 diabetes mellitus. *Basic Res. Cardiol.* **108**, 365 (2013).
224. Muniyappa, R., Montagnani, M., Koh, K. K. & Quon, M. J. Cardiovascular Actions of Insulin. *Endocr. Rev.* **28**, 463–491 (2007).
225. Cho, Y. M., Fujita, Y. & Kieffer, T. J. Glucagon-like peptide-1: glucose homeostasis and beyond. *Annu. Rev. Physiol.* **76**, 535–59 (2014).
226. Ebel, D. *et al.* Effect of acute hyperglycaemia and diabetes mellitus with and without short-term insulin treatment on myocardial ischaemic late preconditioning in the rabbit heart in vivo. *Pflügers Arch. - Eur. J. Physiol.* **446**, 175–182 (2003).
227. Hadour, G. *et al.* Improved Myocardial Tolerance to Ischaemia in the Diabetic Rabbit. *J. Mol. Cell. Cardiol.* **30**, 1869–1875 (1998).
228. Kersten, J. R., Toller, W. G., Gross, E. R., Pagel, P. S. & Wartier, D. C. Diabetes abolishes ischemic preconditioning: role of glucose, insulin, and osmolality. *Am. J. Physiol. Heart Circ. Physiol.* **278**, H1218-24 (2000).

229. Lefer, D. J. *et al.* HMG-CoA reductase inhibition protects the diabetic myocardium from ischemia-reperfusion injury. *FASEB J.* **15**, 1454–6 (2001).
230. Marfella, R. *et al.* Myocardial infarction in diabetic rats: role of hyperglycaemia on infarct size and early expression of hypoxia-inducible factor 1. *Diabetologia* **45**, 1172–81 (2002).
231. Nawata, T. *et al.* Cardioprotection by streptozotocin-induced diabetes and insulin against ischemia/reperfusion injury in rats. *J. Cardiovasc. Pharmacol.* **40**, 491–500 (2002).
232. Ravingerová, T., Neckár, J. & Kolár, F. Ischemic tolerance of rat hearts in acute and chronic phases of experimental diabetes. *Mol. Cell. Biochem.* **249**, 167–74 (2003).
233. Tanaka, K. *et al.* Isoflurane-induced preconditioning is attenuated by diabetes. *Am. J. Physiol. Heart Circ. Physiol.* **282**, H2018-23 (2002).
234. Oliveira, P. J. *et al.* Decreased susceptibility of heart mitochondria from diabetic GK rats to mitochondrial permeability transition induced by calcium phosphate. *Biosci. Rep.* **21**, 45–53 (2001).
235. Desrois, M. *et al.* Upregulation of eNOS and unchanged energy metabolism in increased susceptibility of the aging type 2 diabetic GK rat heart to ischemic injury. *AJP Hear. Circ. Physiol.* **299**, H1679–H1686 (2010).
236. Jones, S. P., Girod, W. G., Granger, D. N., Palazzo, A. J. & Lefer, D. J. Reperfusion injury is not affected by blockade of P-selectin in the diabetic mouse heart. *Am. J. Physiol.* **277**, H763-9 (1999).
237. Kristiansen, S. B. *et al.* Ischaemic preconditioning does not protect the heart in obese and lean animal models of Type 2 diabetes. *Diabetologia* **47**, 1716–1721 (2004).
238. Bulhak, A. A. *et al.* PPAR-alpha activation protects the type 2 diabetic myocardium against ischemia-reperfusion injury: involvement of the PI3-

Kinase/Akt and NO pathway. *Am.J.Physiol Hear. Circ.Physiol* **296**, H719–H727 (2009).

239. Matsumoto, S. *et al.* Pharmacological Preconditioning in Type 2 Diabetic Rat Hearts: The Roles of Mitochondrial ATP-Sensitive Potassium Channels and the Phosphatidylinositol 3-Kinase-Akt Pathway. *Cardiovasc. Drugs Ther.* **23**, 263–270 (2009).
240. Korkmaz-Icöz, S. *et al.* Mild Type 2 Diabetes Mellitus Reduces the Susceptibility of the Heart to Ischemia/Reperfusion Injury: Identification of Underlying Gene Expression Changes. *J. Diabetes Res.* **2015**, 1–16 (2015).
241. Whittington, H. J., Babu, G. G., Mocanu, M. M., Yellon, D. M. & Hausenloy, D. J. The diabetic heart: too sweet for its own good? *Cardiol. Res. Pract.* **2012**, 845698 (2012).
242. Desrois, M. *et al.* Upregulation of eNOS and unchanged energy metabolism in increased susceptibility of the aging type 2 diabetic GK rat heart to ischemic injury. *Am. J. Physiol. Circ. Physiol.* **299**, H1679–H1686 (2010).
243. Sivaraman, V., Hausenloy, D. J., Wynne, A. M. & Yellon, D. M. Preconditioning the diabetic human myocardium. *J. Cell. Mol. Med.* **14**, 1740–1746 (2009).
244. Whittington, H. J. *et al.* Cardioprotection in the aging, diabetic heart: The loss of protective Akt signalling. *Cardiovasc. Res.* **99**, 694–704 (2013).
245. Jaffe, A. S. *et al.* Increased congestive heart failure after myocardial infarction of modest extent in patients with diabetes mellitus. *Am. Heart J.* **108**, 31–37 (1984).
246. Lamblin, N., Fertin, M., de Groote, P. & Bauters, C. Cardiac remodeling and heart failure after a first anterior myocardial infarction in patients with diabetes mellitus. *J. Cardiovasc. Med.* **13**, 353–359 (2012).
247. Shah, A. M. *et al.* Left ventricular systolic and diastolic function,

- remodelling, and clinical outcomes among patients with diabetes following myocardial infarction and the influence of direct renin inhibition with aliskiren. *Eur. J. Heart Fail.* **14**, 185–192 (2012).
248. Vahtola, E. *et al.* Sirtuin1-p53, forkhead box O3a, p38 and post-infarct cardiac remodeling in the spontaneously diabetic Goto-Kakizaki rat. *Cardiovasc. Diabetol.* **9**, 5 (2010).
249. Kosiborod, M. *et al.* Glucometrics in patients hospitalized with acute myocardial infarction: defining the optimal outcomes-based measure of risk. *Circulation* **117**, 1018–27 (2008).
250. Oswald, G. A., Smith, C. C., Betteridge, D. J. & Yudkin, J. S. Determinants and importance of stress hyperglycaemia in non-diabetic patients with myocardial infarction. *Br. Med. J. (Clin. Res. Ed)*. **293**, 917–22 (1986).
251. Wei, C. H. & Litwin, S. E. Hyperglycemia and adverse outcomes in acute coronary syndromes: is serum glucose the provocateur or innocent bystander? *Diabetes* **63**, 2209–12 (2014).
252. Cruickshank, N. CORONARY THROMBOSIS AND MYOCARDIAL INFARCTION, WITH GLYCOSURIA. *Br. Med. J.* **1**, 618–9 (1931).
253. Stanley, W., Lopaschuk, G. D., Hall, J. L. & McCormack, J. G. Regulation of myocardial carbohydrate metabolism under normal and ischaemic conditions Potential for pharmacological interventions. *Cardiovasc. Res.* **33**, 243–257 (1997).
254. Bing, R. *et al.* Metabolic studies on the human heart in vivo: I. Studies on carbohydrate metabolism of the human heart. *Am. J. Med.* **15**, 284–296 (1953).
255. Bertrand, L., Horman, S., Beauloye, C. & Vanoverschelde, J.-L. Insulin signalling in the heart. *Cardiovasc. Res.* **79**, 238–48 (2008).
256. Barrett, E. J., Schwartz, R. G., Francis, C. K. & Zaret, B. L. Regulation by insulin of myocardial glucose and fatty acid metabolism in the conscious

- dog. *J. Clin. Invest.* **74**, 1073–9 (1984).
257. du Toit, E. F. & Donner, D. G. Myocardial Insulin Resistance: An Overview of Its Causes, Effects, and Potential Therapy. in *Insulin Resistance* (InTech, 2012). doi:10.5772/50619
258. Monti, L. D. *et al.* Myocardial glucose uptake evaluated by positron emission tomography and fluorodeoxyglucose during hyperglycemic clamp in IDDM patients. Role of free fatty acid and insulin levels. *Diabetes* **44**, 537–42 (1995).
259. Wisneski, J. A., Stanley, W. C., Neese, R. A. & Gertz, E. W. Effects of acute hyperglycemia on myocardial glycolytic activity in humans. *J. Clin. Invest.* **85**, 1648–56 (1990).
260. Marik, P. E. & Bellomo, R. Stress hyperglycemia: an essential survival response! *Crit. Care* **17**, 305 (2013).
261. Kanety, H., Feinstein, R., Papa, M. Z., Hemi, R. & Karasik, A. Tumor necrosis factor alpha-induced phosphorylation of insulin receptor substrate-1 (IRS-1). Possible mechanism for suppression of insulin-stimulated tyrosine phosphorylation of IRS-1. *J. Biol. Chem.* **270**, 23780–4 (1995).
262. MURRAY, A. *et al.* Insulin resistance, abnormal energy metabolism and increased ischemic damage in the chronically infarcted rat heart. *Cardiovasc. Res.* **71**, 149–157 (2006).
263. Ding, H.-S. *et al.* The HMGB1–TLR4 axis contributes to myocardial ischemia/reperfusion injury via regulation of cardiomyocyte apoptosis. *Gene* **527**, 389–393 (2013).
264. Yong, M. & Kaste, M. Dynamic of hyperglycemia as a predictor of stroke outcome in the ECASS-II trial. *Stroke* **39**, 2749–55 (2008).
265. Wahab, N. N. *et al.* Is blood glucose an independent predictor of mortality in acute myocardial infarction in the thrombolytic era? *J. Am. Coll. Cardiol.* **40**, 1748–54 (2002).

266. Wong, V. W., Ross, D. L., Park, K., Boyages, S. C. & Cheung, N. W. Hyperglycemia: still an important predictor of adverse outcomes following AMI in the reperfusion era. *Diabetes Res. Clin. Pract.* **64**, 85–91 (2004).
267. Oswald, G. A., Corcoran, S. & Yudkin, J. S. Prevalence and risks of hyperglycaemia and undiagnosed diabetes in patients with acute myocardial infarction. *Lancet (London, England)* **1**, 1264–7 (1984).
268. Lakhdar, A., Stromberg, P. & McAlpine, S. G. Prognostic importance of hyperglycaemia induced by stress after acute myocardial infarction. *Br. Med. J. (Clin. Res. Ed)*. **288**, 288 (1984).
269. Yudkin, J. S. & Oswald, G. A. Stress hyperglycemia and cause of death in non-diabetic patients with myocardial infarction. *Br. Med. J. (Clin. Res. Ed)*. **294**, 773 (1987).
270. O'Sullivan, J. J., Conroy, R. M., Robinson, K., Hickey, N. & Mulcahy, R. In-hospital prognosis of patients with fasting hyperglycemia after first myocardial infarction. *Diabetes Care* **14**, 758–60 (1991).
271. Soler, N. G. & Frank, S. Value of glycosylated hemoglobin measurements after acute myocardial infarction. *JAMA* **246**, 1690–3 (1981).
272. Lewandowicz, J., Komorowski, J. M. & Goźliński, H. Metabolic disorders in myocardial infarction. Changes in blood serum zinc, growth hormone, insulin and glucose concentration in patients with acute myocardial infarction. *Cor Vasa* **21**, 305–16 (1979).
273. Ravid, M., Berkowicz, M. & Sohar, E. Hyperglycemia during acute myocardial infarction. A six-year follow-up study. *JAMA* **233**, 807–9 (1975).
274. Bellodi, G. *et al.* Hyperglycemia and prognosis of acute myocardial infarction in patients without diabetes mellitus. *Am. J. Cardiol.* **64**, 885–8 (1989).
275. Sewdarsen, M., Vythilingum, S., Jialal, I. & Becker, P. J. Prognostic importance of admission plasma glucose in diabetic and non-diabetic

- patients with acute myocardial infarction. *Q. J. Med.* **71**, 461–6 (1989).
276. Lynch, M., Gammage, M. D., Lamb, P., Nattrass, M. & Pentecost, B. L. Acute myocardial infarction in diabetic patients in the thrombolytic era. *Diabet. Med.* **11**, 162–5 (1994).
277. Gwilt, D. J., Petri, M., Lamb, P., Nattrass, M. & Pentecost, B. L. Effect of intravenous insulin infusion on mortality among diabetic patients after myocardial infarction. *Br. Heart J.* **51**, 626–30 (1984).
278. Leor, J., Goldbourt, U., Reicher-Reiss, H., Kaplinsky, E. & Behar, S. Cardiogenic shock complicating acute myocardial infarction in patients without heart failure on admission: incidence, risk factors, and outcome. SPRINT Study Group. *Am. J. Med.* **94**, 265–73 (1993).
279. Marenzi, G. *et al.* Acute hyperglycemia and contrast-induced nephropathy in primary percutaneous coronary intervention. *Am. Heart J.* **160**, 1170–1177 (2010).
280. Shacham, Y. *et al.* Admission Glucose Levels and the Risk of Acute Kidney Injury in Nondiabetic ST Segment Elevation Myocardial Infarction Patients Undergoing Primary Percutaneous Coronary Intervention. *Cardiorenal Med.* **5**, 191–8 (2015).
281. Okumura, S. *et al.* AS-253: Is Acute Hyperglycemia a Predictor of Contrast-induced Nephropathy in Acute Myocardial Infarction Patients Undergoing Primary Percutaneous Coronary Intervention? *Am. J. Cardiol.* **109**, S124 (2012).
282. Iwakura, K. *et al.* Association between hyperglycemia and the no-reflow phenomenon in patients with acute myocardial infarction. *J. Am. Coll. Cardiol.* **41**, 1–7 (2003).
283. Eitel, I. *et al.* Prognostic impact of hyperglycemia in nondiabetic and diabetic patients with ST-elevation myocardial infarction: insights from contrast-enhanced magnetic resonance imaging. *Circ. Cardiovasc. Imaging* **5**, 708–18 (2012).

284. Jensen, C. J. *et al.* Impact of hyperglycemia at admission in patients with acute ST-segment elevation myocardial infarction as assessed by contrast-enhanced MRI. *Clin. Res. Cardiol.* **100**, 649–659 (2011).
285. Su, H. *et al.* Acute hyperglycemia exacerbates myocardial ischemia/reperfusion injury and blunts cardioprotective effect of GIK. *AJP Endocrinol. Metab.* **293**, E629–E635 (2007).
286. Yang, Z. *et al.* Acute hyperglycemia abolishes ischemic preconditioning by inhibiting Akt phosphorylation: normalizing blood glucose before ischemia restores ischemic preconditioning. *Oxid. Med. Cell. Longev.* **2013**, 329183 (2013).
287. Luan, R. *et al.* High glucose sensitizes adult cardiomyocytes to ischaemia/reperfusion injury through nitrative thioredoxin inactivation. *Cardiovasc. Res.* **83**, 294–302 (2009).
288. Ottani, F. *et al.* Prodromal angina limits infarct size. A role for ischemic preconditioning. *Circulation* **91**, 291–7 (1995).
289. Masci, P. G. *et al.* Prodromal angina is associated with myocardial salvage in acute ST-segment elevation myocardial infarction. *Eur. Hear. J. - Cardiovasc. Imaging* **14**, 1041–1048 (2013).
290. Mladenovic, Z. T. *et al.* The cardioprotective role of preinfarction angina as shown in outcomes of patients after first myocardial infarction. *Texas Hear. Inst. J.* **35**, 413–8 (2008).
291. Ishihara, M. *et al.* Effect of acute hyperglycemia on the ischemic preconditioning effect of prodromal angina pectoris in patients with a first anterior wall acute myocardial infarction. *Am. J. Cardiol.* **92**, 288–291 (2003).
292. Kim, H. S., Kim, S. Y., Kwak, Y. L., Hwang, K. C. & Shim, Y. H. Hyperglycemia Attenuates Myocardial Preconditioning of Remifentanyl. *J. Surg. Res.* **174**, 231–237 (2012).
293. Zálešák, M. *et al.* Severity of lethal ischemia/reperfusion injury in rat

hearts subjected to ischemic preconditioning is increased under conditions of simulated hyperglycemia. *Physiol. Res.* **63**, 577–85 (2014).

294. Canfield, S. G. *et al.* Marked Hyperglycemia Attenuates Anesthetic Preconditioning in Human-induced Pluripotent Stem Cell-derived Cardiomyocytes. *Anesthesiology* **117**, 735–744 (2012).
295. Vladoic, N. *et al.* Decreased tetrahydrobiopterin and disrupted association of Hsp90 with eNOS by hyperglycemia impair myocardial ischemic preconditioning. *Am. J. Physiol. Heart Circ. Physiol.* **301**, H2130-9 (2011).
296. Ge, Z.-D. *et al.* Cardiac-specific overexpression of GTP cyclohydrolase 1 restores ischaemic preconditioning during hyperglycaemia. *Cardiovasc. Res.* **91**, 340–349 (2011).
297. Kersten, J. R., Schmeling, T. J., Orth, K. G., Pagel, P. S. & Warltier, D. C. Acute hyperglycemia abolishes ischemic preconditioning in vivo. *Am. J. Physiol. - Hear. Circ. Physiol.* **275**, H721–H725 (1998).
298. Gu, W. *et al.* Simvastatin Restores Ischemic Preconditioning in the Presence of Hyperglycemia through a Nitric Oxide-mediated Mechanism. *Anesthesiology* **108**, 634–642 (2008).
299. Amour, J. *et al.* Hyperglycemia adversely modulates endothelial nitric oxide synthase during anesthetic preconditioning through tetrahydrobiopterin- and heat shock protein 90-mediated mechanisms. *Anesthesiology* **112**, 576–85 (2010).
300. Baotic, I. *et al.* Apolipoprotein A-1 mimetic D-4F enhances isoflurane-induced eNOS signaling and cardioprotection during acute hyperglycemia. *Am. J. Physiol. Circ. Physiol.* **305**, H219–H227 (2013).
301. Kehl, F. *et al.* N-acetylcysteine restores isoflurane-induced preconditioning against myocardial infarction during hyperglycemia. *Anesthesiology* **98**, 1384–90 (2003).
302. Chen, L. *et al.* Hyperglycemia attenuates remifentanyl postconditioning-induced cardioprotection against hypoxia/reoxygenation injury

- in H9c2 cardiomyoblasts. *J. Surg. Res.* **203**, 483–490 (2016).
303. Raphael, J., Gozal, Y., Navot, N. & Zuo, Z. Hyperglycemia Inhibits Anesthetic-induced Postconditioning in the Rabbit Heart via Modulation of Phosphatidylinositol-3-kinase/Akt and Endothelial Nitric Oxide Synthase Signaling. *J. Cardiovasc. Pharmacol.* **55**, 348–357 (2010).
304. Ichinomiya, T. *et al.* High-dose fasudil preserves postconditioning against myocardial infarction under hyperglycemia in rats: role of mitochondrial KATP channels. *Cardiovasc. Diabetol.* **11**, 28 (2012).
305. Weber, N. C. *et al.* Blockade of anaesthetic-induced preconditioning in the hyperglycaemic myocardium. *Eur. J. Pharmacol.* **592**, 48–54 (2008).
306. Huhn, R. *et al.* Hyperglycaemia blocks sevoflurane-induced postconditioning in the rat heart in vivo : cardioprotection can be restored by blocking the mitochondrial permeability transition pore. *Br. J. Anaesth.* **100**, 465–471 (2008).
307. Matsumoto, S. *et al.* Hyperglycemia raises the threshold of levosimendan- but not milrinone-induced postconditioning in rat hearts. *Cardiovasc. Diabetol.* **11**, 4 (2012).
308. Raphael, J., Gozal, Y., Navot, N. & Zuo, Z. Activation of Adenosine Triphosphate–regulated Potassium Channels during Reperfusion Restores Isoflurane Postconditioning-induced Cardiac Protection in Acutely Hyperglycemic Rabbits. *Anesthesiology* **122**, 1299–1311 (2015).
309. Yu, J. *et al.* High glucose concentration abrogates sevoflurane post-conditioning cardioprotection by advancing mitochondrial fission but dynamin-related protein 1 inhibitor restores these effects. *Acta Physiol.* **220**, 83–98 (2017).
310. Hausenloy, D. J. *et al.* Dipeptidyl peptidase-4 inhibitors and GLP-1 reduce myocardial infarct size in a glucose-dependent manner. *Cardiovasc. Diabetol.* **12**, 154 (2013).
311. Jonassen, A. K. *et al.* Insulin Administered at Reoxygenation Exerts a

Cardioprotective Effect in Myocytes by a Possible Anti-Apoptotic Mechanism. *J. Mol. Cell. Cardiol.* **32**, 757–764 (2000).

312. Gao, F. *et al.* Nitric oxide mediates the antiapoptotic effect of insulin in myocardial ischemia-reperfusion: the roles of PI3-kinase, Akt, and endothelial nitric oxide synthase phosphorylation. *Circulation* **105**, 1497–502 (2002).
313. Malmberg, K. *et al.* Randomized trial of insulin-glucose infusion followed by subcutaneous insulin treatment in diabetic patients with acute myocardial infarction (DIGAMI study): effects on mortality at 1 year. *J. Am. Coll. Cardiol.* **26**, 57–65 (1995).
314. Malmberg, K. *et al.* Intense metabolic control by means of insulin in patients with diabetes mellitus and acute myocardial infarction (DIGAMI 2): effects on mortality and morbidity. *Eur. Heart J.* **26**, 650–661 (2005).
315. National Institute for Health and Care Excellence. *Hyperglycaemia in acute coronary syndromes.* (2011).
316. Jonassen, A. K., Aasum, E., Riemersma, R. A., Mjøs, O. D. & Larsen, T. S. Glucose-insulin-potassium reduces infarct size when administered during reperfusion. *Cardiovasc. drugs Ther.* **14**, 615–23 (2000).
317. Fath-Ordoubadi, F. & Beatt, K. J. Glucose-insulin-potassium therapy for treatment of acute myocardial infarction: an overview of randomized placebo-controlled trials. *Circulation* **96**, 1152–6 (1997).
318. Díaz, R. *et al.* Metabolic modulation of acute myocardial infarction. The ECLA (Estudios Cardiológicos Latinoamérica) Collaborative Group. *Circulation* **98**, 2227–34 (1998).
319. van der Horst, I. C. C. *et al.* Glucose-insulin-potassium infusion in patients treated with primary angioplasty for acute myocardial infarction: the glucose-insulin-potassium study: a randomized trial. *J. Am. Coll. Cardiol.* **42**, 784–91 (2003).
320. Mehta, S. R. *et al.* Effect of glucose-insulin-potassium infusion on

- mortality in patients with acute ST-segment elevation myocardial infarction: the CREATE-ECLA randomized controlled trial. *JAMA* **293**, 437–46 (2005).
321. Timmer, J. R. *et al.* Glucose-insulin-potassium infusion in patients with acute myocardial infarction without signs of heart failure: the Glucose-Insulin-Potassium Study (GIPS)-II. *J. Am. Coll. Cardiol.* **47**, 1730–1 (2006).
322. Bryant, N. J., Govers, R. & James, D. E. Regulated transport of the glucose transporter GLUT4. *Nat. Rev. Mol. Cell Biol.* **3**, 267–277 (2002).
323. Deng, D. & Yan, N. GLUT, SGLT, and SWEET: Structural and mechanistic investigations of the glucose transporters. *Protein Sci.* **25**, 546–58 (2016).
324. Rieg, T. & Vallon, V. Development of SGLT1 and SGLT2 inhibitors. *Diabetologia* **61**, 2079–2086 (2018).
325. Komoroski, B. *et al.* Dapagliflozin, a Novel, Selective SGLT2 Inhibitor, Improved Glycemic Control Over 2 Weeks in Patients With Type 2 Diabetes Mellitus. *Clin. Pharmacol. Ther.* **85**, 513–519 (2009).
326. Nauck, M. A. *et al.* Dapagliflozin Versus Glipizide as Add-on Therapy in Patients With Type 2 Diabetes Who Have Inadequate Glycemic Control With Metformin: A randomized, 52-week, double-blind, active-controlled noninferiority trial. *Diabetes Care* **34**, 2015–2022 (2011).
327. Devineni, D. *et al.* Canagliflozin improves glycaemic control over 28 days in subjects with type 2 diabetes not optimally controlled on insulin. *Diabetes, Obes. Metab.* **14**, 539–545 (2012).
328. Dobbins, R. L. *et al.* Remogliflozin etabonate, a selective inhibitor of the sodium-dependent transporter 2 reduces serum glucose in type 2 diabetes mellitus patients. *Diabetes, Obes. Metab.* **14**, 15–22 (2012).
329. Food and Drug Administration. *Guidance for industry: Diabetes Mellitus - Evaluating cardiovascular risk in new antidiabetic therapies to treat type 2*

diabetes. (2008).

330. Zinman, B. *et al.* Empagliflozin, Cardiovascular Outcomes, and Mortality in Type 2 Diabetes. *N. Engl. J. Med.* **373**, 2117–2128 (2015).
331. Ferrannini, E., Mark, M. & Mayoux, E. CV Protection in the EMPA-REG OUTCOME Trial: A ‘Thriftly Substrate’ Hypothesis. *Diabetes Care* **39**, 1108–14 (2016).
332. Turnbull, F. M. *et al.* Intensive glucose control and macrovascular outcomes in type 2 diabetes. *Diabetologia* **52**, 2288–2298 (2009).
333. Neal, B. *et al.* Canagliflozin and Cardiovascular and Renal Events in Type 2 Diabetes. *N. Engl. J. Med.* **377**, 644–657 (2017).
334. Neal, B. *et al.* Optimizing the analysis strategy for the CANVAS Program: A prespecified plan for the integrated analyses of the CANVAS and CANVAS-R trials. *Diabetes. Obes. Metab.* **19**, 926–935 (2017).
335. AstraZeneca PLC. Farxiga achieved a positive result in the Phase III DECLARE-TIMI 58 trial, a large cardiovascular outcomes trial in 17,000 patients with type-2 diabetes. (2018). Available at: <https://www.astrazeneca.com/media-centre/press-releases/2018/farxiga-achieved-a-positive-result-in-the-phase-iii-declare-timi-58-trial-a-large-cardiovascular-outcomes-trial-in-17000-patients-with-type-2-diabetes-24092018.html>. (Accessed: 4th November 2018)
336. Yamazaki, Y., Ogihara, S., Harada, S. & Tokuyama, S. Activation of cerebral sodium-glucose transporter type 1 function mediated by post-ischemic hyperglycemia exacerbates the development of cerebral ischemia. *Neuroscience* **310**, 674–685 (2015).
337. Yamazaki, Y., Harada, S. & Tokuyama, S. Post-ischemic hyperglycemia exacerbates the development of cerebral ischemic neuronal damage through the cerebral sodium-glucose transporter. *Brain Res.* **1489**, 113–120 (2012).
338. Yamazaki, Y., Harada, S. & Tokuyama, S. Relationship between cerebral

- sodium–glucose transporter and hyperglycemia in cerebral ischemia. *Neurosci. Lett.* **604**, 134–139 (2015).
339. Di Franco, A. *et al.* Sodium-dependent glucose transporters (SGLT) in human ischemic heart: A new potential pharmacological target. *Int. J. Cardiol.* **243**, 86–90 (2017).
340. Kashiwagi, Y. *et al.* Expression of SGLT1 in Human Hearts and Impairment of Cardiac Glucose Uptake by Phlorizin during Ischemia-Reperfusion Injury in Mice. *PLoS One* **10**, e0130605 (2015).
341. HMSO. *Animals (Scientific Procedures) Act, Ch 14.* (HMSO, 1986).
342. Liu, Y. H. *et al.* Chronic heart failure induced by coronary artery ligation in Lewis inbred rats. *Am. J. Physiol.* **272**, H722-7 (1997).
343. Islam, M. S. & Wilson, R. D. *Experimentally induced rodent models of type 2 diabetes. Methods in molecular biology (Clifton, N.J.)* **933**, (2012).
344. Levin, B. E., Dunn-Meynell, A. A., Balkan, B. & Keeseey, R. E. Selective breeding for diet-induced obesity and resistance in Sprague-Dawley rats. *Am. J. Physiol.* **273**, R725-30 (1997).
345. Portha, B., Giroix, M. H., Turrel-Cuzin, C., Le-Stunff, H. & Movassat, J. The GK rat: a prototype for the study of non-overweight type 2 diabetes. *Methods Mol.Biol.* **933**, 125–159 (2012).
346. Portha, B. *et al.* Beta-cell insensitivity to glucose in the GK rat, a spontaneous nonobese model for type II diabetes. *Diabetes* **40**, 486–91 (1991).
347. Berthelie, C., Kergoat, M. & Portha, B. Lack of deterioration of insulin action with aging in the GK rat: A contrasted adaptation as compared with nondiabetic rats. *Metabolism* **46**, 890–896 (1997).
348. Desrois, M. *et al.* Initial steps of insulin signaling and glucose transport are defective in the type 2 diabetic rat heart. *Cardiovasc. Res.* **61**, 288–96 (2004).

349. Aynsley-Green, A., Biebuyck, J. F. & Alberti, K. G. Anaesthesia and insulin secretion: the effects of diethyl ether, halothane, pentobarbitone sodium and ketamine hydrochloride on intravenous glucose tolerance and insulin secretion in the rat. *Diabetologia* **9**, 274–81 (1973).
350. Lee, G. & Goosens, K. A. Sampling blood from the lateral tail vein of the rat. *J. Vis. Exp.* e52766 (2015). doi:10.3791/52766
351. Brownlee, M., Vlassara, H. & Cerami, A. Nonenzymatic glycosylation and the pathogenesis of diabetic complications. *Ann.Intern.Med.* **101**, 527–537 (1984).
352. Weykamp, C. HbA1c: a review of analytical and clinical aspects. *Ann. Lab. Med.* **33**, 393–400 (2013).
353. Jiang, F. *et al.* Assessment of the performance of A1CNow(+) and development of an error grid analysis graph for comparative hemoglobin A1c measurements. *Diabetes Technol. Ther.* **16**, 363–9 (2014).
354. Schnedl, W. J., Liebming, A., Roller, R. E., Lipp, R. W. & Krejs, G. J. Hemoglobin variants and determination of glycated hemoglobin (HbA1c). *Diabetes Metab Res.Rev.* **17**, 94–98 (2001).
355. Gao, W., Bihorel, S., DuBois, D. C., Almon, R. R. & Jusko, W. J. Mechanism-based disease progression modeling of type 2 diabetes in Goto-Kakizaki rats. *J.Pharmacokinet.Pharmacodyn.* **38**, 143–162 (2011).
356. Cohen, R. M. *et al.* Red cell life span heterogeneity in hematologically normal people is sufficient to alter HbA1c. *Blood* **112**, 4284–91 (2008).
357. Derelanko, M. J. Determination of erythrocyte life span in F-344, Wistar, and Sprague-Dawley rats using a modification of the [³H]diisopropylfluorophosphate ([³H]DFP) method. *Fundam. Appl. Toxicol.* **9**, 271–6 (1987).
358. Zimmer, H.-G. The Isolated Perfused Heart and Its Pioneers. *News Physiol. Sci.* **13**, 203–210 (1998).
359. Ikeda, T., Xia, X. Y., Xia, Y. X. & Ikenoue, T. Hyperthermic

- preconditioning prevents blood-brain barrier disruption produced by hypoxia-ischemia in newborn rat. *Brain Res. Dev. Brain Res.* **117**, 53–8 (1999).
360. Yellon, D. M. & Marber, M. S. Hsp70 in myocardial ischaemia. *Experientia* **50**, 1075–84 (1994).
361. Piriou, V. *et al.* Pharmacological preconditioning: comparison of desflurane, sevoflurane, isoflurane and halothane in rabbit myocardium. *Br. J. Anaesth.* **89**, 486–91 (2002).
362. Wang, Q. *et al.* Optimal intervention time of vagal stimulation attenuating myocardial ischemia/reperfusion injury in rats. *Inflamm. Res.* **63**, 987–999 (2014).
363. Dorsch, M. *et al.* Morphine-Induced Preconditioning: Involvement of Protein Kinase A and Mitochondrial Permeability Transition Pore. *PLoS One* **11**, e0151025 (2016).
364. Haessler, R. *et al.* Anaesthetics alter the magnitude of infarct limitation by ischaemic preconditioning. *Cardiovasc. Res.* **28**, 1574–80 (1994).
365. Morita, Y. *et al.* KATPChannels Contribute to the Cardioprotection of Preconditioning Independent of Anaesthetics in Rabbit Hearts. *J. Mol. Cell. Cardiol.* **29**, 1267–1276 (1997).
366. Behmenburg, F. *et al.* Impact of Anesthetic Regimen on Remote Ischemic Preconditioning in the Rat Heart In Vivo. *Anesth. Analg.* **1** (2017).
doi:10.1213/ANE.0000000000002563
367. Lange, M. *et al.* Role of the beta1-adrenergic pathway in anesthetic and ischemic preconditioning against myocardial infarction in the rabbit heart in vivo. *Anesthesiology* **105**, 503–10 (2006).
368. Awan, M. M., Taunyane, C., Aitchison, K. A., Yellon, D. M. & Opie, L. H. Normothermic transfer times up to 3 min will not precondition the isolated rat heart. *J. Mol. Cell. Cardiol.* **31**, 503–11 (1999).
369. Minhaz, U., Koide, S., Shohtsu, A., Fujishima, M. & Nakazawa, H.

- Perfusion delay causes unintentional ischemic preconditioning in isolated heart preparation. *Basic Res. Cardiol.* **90**, 418–23 (1995).
370. Broadley, K. J. The Langendorff Heart Preparation-Reappraisal of its Role as a Research and Teaching Model for Coronary Vasoactive Drugs. *J. Pharmacol. Methods* **2**, 143–156 (1979).
371. Bell, R. M. *et al.* Retrograde heart perfusion: the Langendorff technique of isolated heart perfusion. *J. Mol. Cell. Cardiol.* **50**, 940–50 (2011).
372. Hale, S. L., Dave, R. H. & Kloner, R. A. Regional hypothermia reduces myocardial necrosis even when instituted after the onset of ischemia. *Basic Res. Cardiol.* **92**, 351–7 (1997).
373. Chien, G. L., Wolff, R. A., Davis, R. F. & van Winkle, D. M. “Normothermic range” temperature affects myocardial infarct size. *Cardiovasc. Res.* **28**, 1014–7 (1994).
374. Yellon, D. M. *et al.* The protective role of heat stress in the ischaemic and reperfused rabbit myocardium. *J. Mol. Cell. Cardiol.* **24**, 895–907 (1992).
375. Carrick, D. *et al.* Pathophysiology of LV Remodeling in Survivors of STEMI. *JACC Cardiovasc. Imaging* **8**, 779–789 (2015).
376. Bloor, C. M., Leon, A. S. & Pitt, B. The inheritance of coronary artery anatomic patterns in rats. *Circulation* **36**, 771–6 (1967).
377. Bell, R. M., Mocanu, M. M. & Yellon, D. M. Retrograde heart perfusion: the Langendorff technique of isolated heart perfusion. *J.Mol.Cell Cardiol.* **50**, 940–950 (2011).
378. Murry, C. E., Jennings, R. B. & Reimer, K. A. Preconditioning with ischemia: a delay of lethal cell injury in ischemic myocardium. *Circulation* **74**, 1124–1136 (1986).
379. Alkhulaifi, A. M., Pugsley, W. B. & Yellon, D. M. The influence of the time period between preconditioning ischemia and prolonged ischemia on myocardial protection. *Cardioscience* **4**, 163–9 (1993).

380. Cohen, M. V & Downey, J. M. Ischaemic preconditioning: can the protection be bottled? *Lancet (London, England)* **342**, 6 (1993).
381. Schmatz, D. M. The mannitol cycle--a new metabolic pathway in the Coccidia. *Parasitol. Today* **5**, 205–8 (1989).
382. Walters, H. L. *et al.* The response to ischemia in blood perfused vs. crystalloid perfused isolated rat heart preparations. *J. Mol. Cell. Cardiol.* **24**, 1063–77 (1992).
383. Abel, E. D. Glucose transport in the heart. *Front. Biosci.* **9**, 201–15 (2004).
384. Ojeda, P. *et al.* Noncompetitive blocking of human GLUT1 hexose transporter by methylxanthines reveals an exofacial regulatory binding site. *Am. J. Physiol. Cell Physiol.* **303**, C530-9 (2012).
385. Gilbert, R. E. SGLT2 inhibitors: β blockers for the kidney? *Lancet Diabetes Endocrinol.* **4**, 814 (2016).
386. Frasch, W., Frohnert, P. P., Bode, F., Baumann, K. & Kinne, R. Competitive inhibition of phlorizin binding by D-glucose and the influence of sodium: a study on isolated brush border membrane of rat kidney. *Pflugers Arch.* **320**, 265–84 (1970).
387. Raja, M. & Kinne, R. K. H. Identification of phlorizin binding domains in sodium-glucose cotransporter family: SGLT1 as a unique model system. *Biochimie* **115**, 187–193 (2015).
388. Balteau, M. *et al.* NADPH oxidase activation by hyperglycaemia in cardiomyocytes is independent of glucose metabolism but requires SGLT1. *Cardiovasc. Res.* **92**, 237–246 (2011).
389. Kanwal, A. *et al.* Inhibition of SGLT1 abrogates preconditioning-induced cardioprotection against ischemia-reperfusion injury. *Biochem. Biophys. Res. Commun.* **472**, 392–398 (2016).
390. Ohgaki, R. *et al.* Interaction of the Sodium/Glucose Cotransporter (SGLT) 2 inhibitor Canagliflozin with SGLT1 and SGLT2. *J. Pharmacol. Exp.*

Ther. **358**, 94–102 (2016).

391. Hummel, C. S. *et al.* Structural selectivity of human SGLT inhibitors. *Am. J. Physiol. Cell Physiol.* **302**, C373-82 (2012).
392. Krogstrup, N. V *et al.* Remote ischaemic conditioning on recipients of deceased renal transplants, effect on immediate and extended kidney graft function: a multicentre, randomised controlled trial protocol (CONTEXT). *BMJ Open* **5**, e007941 (2015).
393. Hu, S. *et al.* Effects of Remote Ischemic Preconditioning on Biochemical Markers and Neurologic Outcomes in Patients Undergoing Elective Cervical Decompression Surgery. *J. Neurosurg. Anesthesiol.* **22**, 46–52 (2010).
394. Botker, H. E. *et al.* Remote ischaemic conditioning before hospital admission, as a complement to angioplasty, and effect on myocardial salvage in patients with acute myocardial infarction: a randomised trial. *Lancet* **375**, 727–734 (2010).
395. Thielmann, M. *et al.* Remote ischemic preconditioning reduces myocardial injury after coronary artery bypass surgery with crystalloid cardioplegic arrest. *Basic Res. Cardiol.* **105**, 657–664 (2010).
396. Venugopal, V. *et al.* Remote ischaemic preconditioning reduces myocardial injury in patients undergoing cardiac surgery with cold-blood cardioplegia: a randomised controlled trial. *Heart* **95**, 1567–1571 (2009).
397. Hausenloy, D. J. *et al.* Effect of remote ischaemic preconditioning on myocardial injury in patients undergoing coronary artery bypass graft surgery: a randomised controlled trial. *Lancet* **370**, 575–579 (2007).
398. GÜNAYDIN, B. *et al.* DOES REMOTE ORGAN ISCHAEMIA TRIGGER CARDIAC PRECONDITIONING DURING CORONARY ARTERY SURGERY? *Pharmacol. Res.* **41**, 493–496 (2000).
399. Hoole, S. P. *et al.* Cardiac Remote Ischemic Preconditioning in Coronary Stenting (CRISP Stent) Study: A Prospective, Randomized Control Trial.

- Circulation* **119**, 820–827 (2009).
400. Azar, T., Sharp, J. & Lawson, D. Heart rates of male and female Sprague-Dawley and spontaneously hypertensive rats housed singly or in groups. *J. Am. Assoc. Lab. Anim. Sci.* **50**, 175–84 (2011).
 401. Shahid, M., Tauseef, M., Sharma, K. K. & Fahim, M. Brief femoral artery ischaemia provides protection against myocardial ischaemia-reperfusion injury in rats: the possible mechanisms. *Exp. Physiol.* **93**, 954–968 (2008).
 402. Zennadi, R. *et al.* Erythrocyte plasma membrane-bound ERK1/2 activation promotes ICAM-4-mediated sickle red cell adhesion to endothelium. *Blood* **119**, 1217–27 (2012).
 403. Shapiro, A. L., Viñuela, E. & Maizel, J. V. Molecular weight estimation of polypeptide chains by electrophoresis in SDS-polyacrylamide gels. *Biochem. Biophys. Res. Commun.* **28**, 815–20 (1967).
 404. Kurien, B. T. & Scofield, R. H. Western Blotting: An Introduction. in *Methods in molecular biology (Clifton, N.J.)* **1312**, 17–30 (2015).
 405. A rapid technique for the isolation and purification of adult cardiac muscle cells having respiratory control and a tolerance to calcium. *Biochem. Biophys. Res. Commun.* **72**, 327–333 (1976).
 406. Siddall, H. K. *et al.* Loss of PINK1 increases the heart's vulnerability to ischemia-reperfusion injury. *PLoS One* **8**, e62400 (2013).
 407. DIAZ, R. & WILSON, G. Studying ischemic preconditioning in isolated cardiomyocyte models. *Cardiovasc. Res.* **70**, 286–296 (2006).
 408. Oparka, M. *et al.* Quantifying ROS levels using CM-H 2 DCFDA and HyPer. *Methods* **109**, 3–11 (2016).
 409. Oldenburg, O. *et al.* Bradykinin induces mitochondrial ROS generation via NO, cGMP, PKG, and mitoKATP channel opening and leads to cardioprotection. *AJP Hear. Circ. Physiol.* **286**, 468H – 476 (2003).

410. Das, D. K. & Maulik, N. Preconditioning potentiates redox signaling and converts death signal into survival signal. *Arch. Biochem. Biophys.* **420**, 305–11 (2003).
411. Xu, Z., Ji, X. & Boysen, P. G. Exogenous nitric oxide generates ROS and induces cardioprotection: involvement of PKG, mitochondrial KATP channels, and ERK. *AJP Hear. Circ. Physiol.* **286**, H1433–H1440 (2003).
412. BRENNAN, J. *et al.* Mitochondrial uncoupling, with low concentration FCCP, induces ROS-dependent cardioprotection independent of KATP channel activation. *Cardiovasc. Res.* **72**, 313–321 (2006).
413. Palmer, J. W., Tandler, B. & Hoppel, C. L. Biochemical properties of subsarcolemmal and interfibrillar mitochondria isolated from rat cardiac muscle. *J. Biol. Chem.* **252**, 8731–9 (1977).
414. Hall, A. R. & Hausenloy, D. J. Mitochondrial respiratory inhibition by 2,3-butanedione monoxime (BDM): implications for culturing isolated mouse ventricular cardiomyocytes. *Physiol. Rep.* **4**, (2016).
415. CLARK, L. C., WOLF, R., GRANGER, D. & TAYLOR, Z. Continuous recording of blood oxygen tensions by polarography. *J. Appl. Physiol.* **6**, 189–93 (1953).
416. Pravdic, D. *et al.* Complex I and ATP synthase mediate membrane depolarization and matrix acidification by isoflurane in mitochondria. *Eur. J. Pharmacol.* **690**, 149–157 (2012).
417. Movassat, J. *et al.* Follow-up of GK rats during prediabetes highlights increased insulin action and fat deposition despite low insulin secretion. *Am. J. Physiol. Endocrinol. Metab.* **294**, E168-75 (2008).
418. EMD Millipore. *Rat / Mouse Insulin 96 Well Plate Assay Cat. # EZRMI-13K . Directions for use.* (2012).
419. Rutter, G. A. Personal communication. (2013).
420. Silva, A. M. & Oliveira, P. J. Evaluation of Respiration with Clark Type Electrode in Isolated Mitochondria and Permeabilized Animal Cells. in

Methods in molecular biology (Clifton, N.J.) **810**, 7–24 (2012).

421. Weinbrenner, C., Nelles, M., Herzog, N., Sárváry, L. & Strasser, R. H. Remote preconditioning by infrarenal occlusion of the aorta protects the heart from infarction: a newly identified non-neuronal but PKC-dependent pathway. *Cardiovasc. Res.* **55**, 590–601 (2002).
422. Davidson, S. M. *et al.* Remote ischaemic preconditioning involves signalling through the SDF-1 α /CXCR4 signalling axis. *Basic Res. Cardiol.* **108**, 377 (2013).
423. Pickard, J. M. J., Davidson, S. M., Hausenloy, D. J. & Yellon, D. M. Co-dependence of the neural and humoral pathways in the mechanism of remote ischemic conditioning. *Basic Res. Cardiol.* **111**, 50 (2016).
424. Hausenloy, D. J. *et al.* Translating novel strategies for cardioprotection: the Hatter Workshop Recommendations. *Basic Res. Cardiol.* **105**, 677–686 (2010).
425. Fox, C. S., Sullivan, L., D'Agostino, R. B., Wilson, P. W. F. & Framingham Heart Study. The significant effect of diabetes duration on coronary heart disease mortality: the Framingham Heart Study. *Diabetes Care* **27**, 704–8 (2004).
426. World Health Organisation. WHO diabetes programme www.who.int/diabetes/en. (2014).
427. Kawano, K. *et al.* Spontaneous long-term hyperglycemic rat with diabetic complications. Otsuka Long-Evans Tokushima Fatty (OLETF) strain. *Diabetes* **41**, 1422–8 (1992).
428. Leonard, B. L., Watson, R. N., Loomes, K. M., Phillips, A. R. J. & Cooper, G. J. Insulin resistance in the Zucker diabetic fatty rat: a metabolic characterisation of obese and lean phenotypes. *Acta Diabetol.* **42**, 162–170 (2005).
429. Kobayashi, K. *et al.* The db/db mouse, a model for diabetic dyslipidemia: molecular characterization and effects of Western diet feeding.

Metabolism. **49**, 22–31 (2000).

430. Coleman, D. L. Diabetes-obesity syndromes in mice. *Diabetes* **31**, 1–6 (1982).
431. Cavaghan, M. K., Ehrmann, D. A. & Polonsky, K. S. Interactions between insulin resistance and insulin secretion in the development of glucose intolerance. *J. Clin. Invest.* **106**, 329–33 (2000).
432. Brower, M., Grace, M., Kotz, C. M. & Koya, V. Comparative analysis of growth characteristics of Sprague Dawley rats obtained from different sources. *Lab. Anim. Res.* **31**, 166–73 (2015).
433. Movassat J, Saulnier C, S. P. Impaired development of pancreatic beta-cell mass is a primary event during the progression to diabetes in the GK rat. *Diabetologia* **40**, 916–945 (1997).
434. Iwahara, S. I., Abe, Y. & Okazaki, T. Identification of five embryonic hemoglobins of rat and ontogeny of their constituent globins during fetal development. *J. Biochem.* **119**, 360–6 (1996).
435. Antunes, L. C., Elkfury, J. L., Jornada, M. N., Foletto, K. C. & Bertoluci, M. C. Validation of HOMA-IR in a model of insulin-resistance induced by a high-fat diet in Wistar rats. *Arch. Endocrinol. Metab.* **60**, 138–42 (2016).
436. Brand, M. D. & Nicholls, D. G. Assessing mitochondrial dysfunction in cells. *Biochem. J.* **435**, 297–312 (2011).
437. Lesnefsky, E. J. & Hoppel, C. L. Ischemia–reperfusion injury in the aged heart: role of mitochondria. *Arch. Biochem. Biophys.* **420**, 287–297 (2003).
438. Akash, M. S., Rehman, K. & Chen, S. Goto-Kakizaki rats: its suitability as non-obese diabetic animal model for spontaneous type 2 diabetes mellitus. *Curr. Diabetes Rev.* **9**, 387–96 (2013).
439. Kojima, N. *et al.* Comparison of the Development Diabetic Induced Renal Disease in Strains of Goto-Kakizaki Rats. *J.Diabetes Metab Suppl* **9**, (2013).

440. DESROIS, M. *et al.* Gender differences in hypertrophy, insulin resistance and ischemic injury in the aging type 2Bdiabetic rat heart. *J. Mol. Cell. Cardiol.* **37**, 547–555 (2004).
441. George, A. M., Jacob, A. G. & Fogelfeld, L. Lean diabetes mellitus: An emerging entity in the era of obesity. *World J. Diabetes* **6**, 613–20 (2015).
442. Sutjahjo, A., Taniguchi, H., Hendromartono, Tjokroprawiro, A. & Baba, S. High frequency of autonomic as well as peripheral neuropathy in patients with malnutrition-related diabetes mellitus. *Diabetes Res. Clin. Pract.* **5**, 197–200 (1988).
443. Mohan, V. *et al.* Clinical profile of lean NIDDM in South India. *Diabetes Res. Clin. Pract.* **38**, 101–8 (1997).
444. Weyer, C., Bogardus, C., Mott, D. M. & Pratley, R. E. The natural history of insulin secretory dysfunction and insulin resistance in the pathogenesis of type 2 diabetes mellitus. *J. Clin. Invest.* **104**, 787–94 (1999).
445. Donath, M. Y., Böni-Schnetzler, M., Ellingsgaard, H. & Ehses, J. A. Islet Inflammation Impairs the Pancreatic β -Cell in Type 2 Diabetes. *Physiology* **24**, 325–331 (2009).
446. Serradas, P., Gangnerau, M. N., Giroix, M. H., Saulnier, C. & Portha, B. Impaired pancreatic beta cell function in the fetal GK rat. Impact of diabetic inheritance. *J.Clin.Invest* **101**, 899–904 (1998).
447. Homo-Delarche, F. *et al.* Islet Inflammation and Fibrosis in a Spontaneous Model of Type 2 Diabetes, the GK Rat. *Diabetes* **55**, 1625–1633 (2006).
448. Svensson, M., Eriksson, J. W. & Dahlquist, G. Early glycemic control, age at onset, and development of microvascular complications in childhood-onset type 1 diabetes: a population-based study in northern Sweden. *Diabetes Care* **27**, 955–62 (2004).
449. American Diabetes Association, A. D. Diagnosis and classification of diabetes mellitus. *Diabetes Care* **32 Suppl 1**, S62-7 (2009).

450. Abete, P. *et al.* Preconditioning does not prevent postischemic dysfunction in aging heart. *J. Am. Coll. Cardiol.* **27**, 1777–1786 (1996).
451. Calabrese, E. J. Pre- and post-conditioning hormesis in elderly mice, rats, and humans: its loss and restoration. *Biogerontology* **17**, 681–702 (2016).
452. Behmenburg, F., Heinen, A., Bruch, L. vom, Hollmann, M. W. & Huhn, R. Cardioprotection by Remote Ischemic Preconditioning is Blocked in the Aged Rat Heart in Vivo. *J. Cardiothorac. Vasc. Anesth.* **31**, 1223–1226 (2017).
453. Zheng, H., Guo, H., Hong, Y., Zheng, F. & Wang, J. The effects of age and resveratrol on the hypoxic preconditioning protection against hypoxia–reperfusion injury: studies in rat hearts and human cardiomyocytes. *Eur. J. Cardio-Thoracic Surg.* **48**, 375–381 (2015).
454. Camacho, S. A., Brandes, R., Figueredo, V. M. & Weiner, M. W. Ca²⁺ transient decline and myocardial relaxation are slowed during low flow ischemia in rat hearts. *J. Clin. Invest.* **93**, 951–957 (1994).
455. Göрге, G., Chatelain, P., Schaper, J. & Lerch, R. Effect of increasing degrees of ischemic injury on myocardial oxidative metabolism early after reperfusion in isolated rat hearts. *Circ. Res.* **68**, 1681–92 (1991).
456. Ferrari, R. *et al.* Metabolic Adaptation During a Sequence of No-Flow and Low-Flow Ischemia. *Circulation* **94**, (1996).
457. Leiris, J., Harding, D. P. & Pestre, S. The isolated perfused rat heart: A model for studying myocardial hypoxia or ischaemia. *Basic Res. Cardiol.* **79**, 313–321 (1984).
458. Kunuthur, S. P., Mocanu, M. M., Hemmings, B. A., Hausenloy, D. J. & Yellon, D. M. The Akt1 isoform is an essential mediator of ischaemic preconditioning. *J. Cell. Mol. Med.* **16**, 1739–1749 (2012).
459. Povlsen, J. A. *et al.* Protection against Myocardial Ischemia-Reperfusion Injury at Onset of Type 2 Diabetes in Zucker Diabetic Fatty Rats Is Associated with Altered Glucose Oxidation. *PLoS One* **8**, e64093 (2013).

460. Sharma, V., Kearney, M. T., Davidson, S. M. & Yellon, D. M. Endothelial Insulin Resistance Protects the Heart Against Prolonged Ischemia–Reperfusion Injury But Does Not Prevent Insulin Transport Across the Endothelium in a Mouse Langendorff Model. *J. Cardiovasc. Pharmacol. Ther.* **19**, 586–591 (2014).
461. Nishino, Y. *et al.* Glycogen Synthase Kinase-3 Inactivation Is Not Required for Ischemic Preconditioning or Postconditioning in the Mouse. *Circ. Res.* **103**, 307–314 (2008).
462. Yang, Z. *et al.* Acute Hyperglycemia Abolishes Ischemic Preconditioning by Inhibiting Akt Phosphorylation: Normalizing Blood Glucose before Ischemia Restores Ischemic Preconditioning. *Oxid. Med. Cell. Longev.* **2013**, 1–8 (2013).
463. Falck, G., Schjott, J. & Jynge, P. Hyperosmotic pretreatment reduces infarct size in the rat heart. *Physiol. Res.* **48**, 331–40 (1999).
464. Rohla, M. *et al.* P252 Plasma osmolality predicts clinical outcome in patients with acute coronary syndrome undergoing percutaneous coronary intervention. *Cardiovasc. Res.* **103**, S45.2-S45 (2014).
465. Nakadate, Y. *et al.* Glycemia and the cardioprotective effects of insulin pre-conditioning in the isolated rat heart. *Cardiovasc. Diabetol.* **16**, 43 (2017).
466. Yang, Z. *et al.* Acute hyperglycemia abolishes ischemic preconditioning by inhibiting Akt phosphorylation: normalizing blood glucose before ischemia restores ischemic preconditioning. *Oxid. Med. Cell. Longev.* **2013**, 329183 (2013).
467. Pælestik, K. B. *et al.* Effects of hypoglycemia on myocardial susceptibility to ischemia-reperfusion injury and preconditioning in hearts from rats with and without type 2 diabetes. *Cardiovasc. Diabetol.* **16**, 148 (2017).
468. Diemar, S. S. *et al.* Influence of acute glycaemic level on measures of myocardial infarction in non-diabetic pigs. *Scand. Cardiovasc. J.* **49**, 376–82 (2015).

469. Kloner, R. A., Reimer, K. A., Willerson, J. T. & Jennings, R. B. Reduction of Experimental Myocardial Infarct Size with Hyperosmolar Mannitol. *Exp. Biol. Med.* **151**, 677–683 (1976).
470. Joseph, D., Kimar, C., Symington, B., Milne, R. & Faadiel Essop, M. The detrimental effects of acute hyperglycemia on myocardial glucose uptake. *Life Sci.* **105**, 31–42 (2014).
471. Balteau, M. *et al.* AMPK activation by glucagon-like peptide-1 prevents NADPH oxidase activation induced by hyperglycemia in adult cardiomyocytes. *AJP Hear. Circ. Physiol.* **307**, H1120–H1133 (2014).
472. Ong, S.-B. *et al.* Inhibiting mitochondrial fission protects the heart against ischemia/reperfusion injury. *Circulation* **121**, 2012–22 (2010).
473. Abdallah, Y. *et al.* Interplay between Ca²⁺ cycling and mitochondrial permeability transition pores promotes reperfusion-induced injury of cardiac myocytes. *J. Cell. Mol. Med.* **15**, 2478–2485 (2011).
474. He, Y. *et al.* Exogenous spermine ameliorates high glucose-induced cardiomyocytic apoptosis via decreasing reactive oxygen species accumulation through inhibiting p38/JNK and JAK2 pathways. *Int. J. Clin. Exp. Pathol.* **8**, 15537–49 (2015).
475. QFAB bioinformatics. Power Calculator - ANOVA - Statistical Decision Tree. Available at: <https://www.anzmtg.org/stats/PowerCalculator/PowerANOVA>. (Accessed: 13th December 2017)
476. Lemasters, J. J. *et al.* Mitochondrial dysfunction in the pathogenesis of necrotic and apoptotic cell death. *J. Bioenerg. Biomembr.* **31**, 305–19 (1999).
477. Cummings, B. S., Schnellmann, R. G. & Schnellmann, R. G. Measurement of cell death in mammalian cells. *Curr. Protoc. Pharmacol.* **Chapter 12**, Unit 12.8 (2004).
478. Vicencio, J. M. *et al.* Plasma Exosomes Protect the Myocardium From

- Ischemia-Reperfusion Injury. *J. Am. Coll. Cardiol.* **65**, 1525–1536 (2015).
479. Chen, W. & Frangogiannis, N. G. Fibroblasts in post-infarction inflammation and cardiac repair. *Biochim. Biophys. Acta - Mol. Cell Res.* **1833**, 945–953 (2013).
480. Lefer, A. M., Tsao, P. S., Lefer, D. J. & Ma, X. L. Role of endothelial dysfunction in the pathogenesis of reperfusion injury after myocardial ischemia. *FASEB J.* **5**, 2029–34 (1991).
481. Leucker, T. M. *et al.* Endothelial-cardiomyocyte crosstalk enhances pharmacological cardioprotection. *J. Mol. Cell. Cardiol.* **51**, 803–11 (2011).
482. Zheng, Y., Vicencio, J. M., Yellon, D. M. & Davidson, S. M. 27 Exosomes Released from Endothelial Cells are Cardioprotective. *Heart* **100 Suppl**, A10 (2014).
483. Van Steenbergen, A. *et al.* Sodium-myoinositol cotransporter-1, SMIT1, mediates the production of reactive oxygen species induced by hyperglycemia in the heart. *Sci. Rep.* **7**, 41166 (2017).
484. Sasseville, L. J., Longpré, J.-P., Wallendorff, B. & Lapointe, J.-Y. The transport mechanism of the human sodium/myo-inositol transporter 2 (SMIT2/SGLT6), a member of the LeuT structural family. *Am. J. Physiol. Cell Physiol.* **307**, C431-41 (2014).
485. Bell, R. *et al.* T1 High glucose and myocardial ischaemia/reperfusion injury: the role of the sodium/glucose transporter, SGLT1. *Heart* **102**, A1–A1 (2016).
486. Bitsi, S. *et al.* Profound hyperglycemia in knockout mutant mice identifies novel function for POU4F2/Brn-3b in regulating metabolic processes. *Am. J. Physiol. Endocrinol. Metab.* **310**, E303-12 (2016).
487. Heusch, G. & Rassaf, T. Time to Give Up on Cardioprotection? *Circ. Res.* **119**, 676–695 (2016).